

Reliability of Vibration-based Nondestructive Inspection Methods for Damage Detection in Structural Engineering

DISSERTATION

Zur Erlangung des akademischen Grades

Dr.-Ing.
(Doktor-Ingenieur)

an der Fakultät Bauingenieurwesen der
Bauhaus-Universität Weimar

Vorgelegt von

Maher Deeb

Geboren am 06.09.1984
in Tartous, Syrien
(Interner Doktorand)

Mentor: Prof. Dr.-Ing. habil. Carsten Könke

Weimar, Juni 2017

Tag der Disputation: 31.05.2018

Die Ehrenwörtliche Erklärung

Ich erkläre hiermit ehrenwörtlich, dass ich die vorliegende Arbeit ohne unzulässige Hilfe Dritter und ohne Benutzung anderer als der angegebenen Hilfsmittel angefertigt habe. Die aus anderen Quellen direkt oder indirekt übernommenen Daten und Konzepte sind unter Angabe der Quelle gekennzeichnet.

Weitere Personen waren an der inhaltlich-materiellen Erstellung der vorliegenden Arbeit nicht beteiligt. Insbesondere habe ich hierfür nicht die entgeltliche Hilfe von Vermittlungs- bzw. Beratungsdiensten (Promotionsberater oder anderer Personen) in Anspruch genommen. Niemand hat von mir unmittelbar oder mittelbar geldwerte Leistungen für Arbeiten erhalten, die im Zusammenhang mit dem Inhalt der vorgelegten Dissertation stehen.

Die Arbeit wurde bisher weder im In- noch im Ausland in gleicher oder ähnlicher Form einer anderen Prüfungsbehörde vorgelegt.

Ich versichere ehrenwörtlich dass ich nach bestem Wissen die reine Wahrheit gesagt und nichts verschwiegen habe.

Weimar, den 27. Januar 2017

Maher Deeb

Acknowledgments

The present work was developed in the years 2011 to 2017 during and after my work as a research associate with the Research Training Group 1462 "Bewertung gekoppelter numerischer und experimenteller Partialmodelle im konstruktiven Ingenieurbau" at the Bauhaus- Universität Weimar and during my abroad stay at the University of Leuven - KU Leuven. I would like to take this opportunity to express my gratitude to the German Research Foundation DFG for its financial support.

I would like to express my special appreciation and thanks to my supervisors in Weimar Prof. Dr.-Ing. habil. Carsten Könke and Dr. Volkmar Zabel for their unlimited scientific and personal support during my Master and promotion study. Their support through providing me with their theoretical and experimental knowledge and experience in engineering together with constructive discussions brought a significant improvement of the quality of this work. I highly appreciate Their time they spent revising my thesis, conference and journal papers.

I would like to extend my gratitude to Prof. Dr. Geert Lombaert for his guidance, encouragement and support during my beneficial and pleasant stay in Leuven. His valuable knowledge and experience in Bayesian Theory provided great material for this work. Beside that, His support to overcome my health problem is unforgettable.

I would like to express my sincere thanks to the applicants and the members of the Research Training Group 1462 especially Prof. Dr.-Ing. habil. Carsten Könke and Prof. Dr.-Ing. habil. Frank Werner for giving me the chance to join the research team and for their scientific support and discussion within the framework of our research group during those important three years of my life. I am also grateful to Prof. Dr. rer. nat. Tom Lahmer for his great scientific and personal support and invaluable discussion and inputs which make this work successful. I would like to thank it to, Dr. -Ing. Holger Keitel, Idna Wudtke, Dr.-Ing. Maximilian Huber, Dr.-Ing. Lars Abrahamczyk and Dr.-Ing. Hossein Talebi for their great support during my employment time in GRK 1462. I am also grateful to Univ. Prof. Dr. rer. nat. habil. Klaus Gürlebeck for his support through spending time reviewing my work.

I would like to thanks EDAC team headed by Dr. Jochen Schwarz for their scientific and personal support on every level of my Master and Promotion study. My great thanks is to my colleagues for those three wonderful years full of discussion, scientific and personal support

and working together at the office or at the construction site. Special thanks to Ingmar Stade, Frank Scheiber, Peter Olney, Sharmistha Chowdhury, Martin Roskopf and Jakob Taraben. I would like to extend my gratitude to my colleagues in KU Leuven for their great help during my stay in Leuven. It is important to mention that this research would not have been possible without the support of Versuchstechnische Einrichtung (VTE) members. I wish to express my sincere thanks and love to my parents and my brothers in Syria and Russia who are the reason and the motivation for every successful step in my life. Great thanks to my friends everywhere especially Yuko and Wassim who are beside me every time. I also place on record, my sense of gratitude to one and all, who directly or indirectly, have lent their hand in this work.

Maher Deeb

Weimar 2017

Zusammenfassung

Die Bewertung von schwingungsbasierten Prüfmethode n zur Zustandsbewertung von Tragwerken sollte unter minimalem Eingriff in bestehende Konstruktionen erfolgen. Deshalb wird eine Bewertung üblicherweise durch ein numerisches Modell realisiert. Im Bereich des Bauingenieurwesens werden von Fall zu Fall für gewöhnlich Vereinfachungen getroffen, welche die Qualität des numerischen Modells und der Beurteilung der Prüfmethode beeinflussen können. Die Kriterien des Nachweises der Zuverlässigkeit einer schwingungsbasierten Prüfmethode in Verbindung mit einem abstrahierten numerischen Modell des zu untersuchenden Bauwerks beinhaltet Typ, Maße und Position eines Schadensbildes, eine geeignete Anordnung von Sensoren, zum Beispiel Beschleunigungssensoren, zur Aufzeichnung von Daten des aktuellen Zustands des Bauwerks und die Kalibrierung des numerischen Modells unter Zuhilfenahme der aufgenommenen Daten. Dadurch ist die Zuverlässigkeit einer solchen Prüfmethode von der Qualität des numerischen Modells, des gewählten Versuchsaufbaus und der Qualität der gemessenen Daten abhängig. Ein Verfahren, welches den Einfluss dieser verschiedenen Faktoren auf die Zuverlässigkeit einer schwingungsbasierten Prüfmethode zur Untersuchung der Schadensbildung an Bauwerken ermittelt, ist zur Zeit nicht vorhanden. Ziel dieser Arbeit ist die Untersuchung der Beziehung zwischen der Qualität der gewählten numerischen Modelle, des Versuchsaufbaus, der zugehörigen Messwerte und der Leistungsfähigkeit von schwingungsbasierten Prüfmethode n zur Schadensidentifikation an Bauwerken. Aufbauend auf den oben genannten Untersuchung ist das weitere Ziel dieser Forschungsarbeit ein praxisfähiges Framework, das den Prozess der Bewertung der Leistungsfähigkeit schwingungsbasierter Prüfverfahren zur Schadensdetektion von Bauwerken ordnet und standardisiert. Das Framework soll Anwendung im Vergleich verschiedenartiger Anpassungen des Prüfverfahrens und der Auswahl jener Parameter, welche die höchste Wahrscheinlichkeit einer Schadensdetektion liefern, finden. Das Framework soll mit Hilfe vorhandener Anwendungen und Beispielen aus der Literatur validiert werden. Die Ergebnisse sollen als statistische Datenbank dokumentiert und für weitere Forschung und Entwicklung verwendet werden.

Im Bauingenieurwesen werden sowohl datenbasierte, als auch modellbasierte Prüfmethode n zur Untersuchung der Schadensbildung angewandt. Eine datenbasierte Prüfmethode vergleicht das gemessene Antwortsignal eines schadhafte n Tragwerks mit dem gemessenen Antwortsignal des unbeschädigte n Tragwerks. Eine modellbasierte Prüfmethode vergleicht das gemessene

Antwortsignal eines Tragwerks mit dem im numerischen Modell berechneten Antwortsignal des unbeschädigten Tragwerks. In einigen Bereichen des Ingenieurwesens, beispielsweise der Luft- und Raumfahrttechnik oder des Maschinenbaus, wird die Zuverlässigkeit von Prüfmethode an der Erfassungswahrscheinlichkeit der Schadensbildung gemessen. Dafür ist die statistische Auswertung großer Testreihen nötig, die zum Beispiel an Flugzeug- oder Automobilteilen aufgenommen wurden. Die Literatur stellt eine Reihe von Studien, statistischen Datenbanken und Standards bereit, die zur Evaluierung von Prüfmethode zur Schadensdetektion in den entsprechenden Bereichen des Ingenieurwesens genutzt werden. Speziell im Bauingenieurwesen werden numerische Modelle als Alternative zu physischen Modellen oder Bestandsbauwerken angewandt, um die Beschränkungen statistischer Auswertungsmethode zu umgehen. Dennoch sind bestimmte Standards oder statistische Datenbanken zur Bewertung der Zuverlässigkeit von schwingungsbasierten Prüfmethode unter Verwendung von numerischen Modellen noch nicht vorhanden. Obwohl verschiedene allgemeine Modelleigenschaften, wie beispielsweise Sensitivität, Komplexität, Unsicherheit etc., bereits als Kriterien zur Modellqualitätsanalyse verwendet werden, ist es notwendig weiter nach einer eindeutigen Klassifikation der Resultate zu forschen. Siehe GRK1462 „Bewertung gekoppelter numerischer und experimenteller Partialmodelle im Konstruktiven Ingenieurbau“. Unsicherheiten können in zwei Kategorien unterteilt werden: aleatorische und epistemische Unsicherheiten. Eine aleatorische Unsicherheit gilt als unvermeidbare Unsicherheit, weil sie die inhärente Variation und die Einzigartigkeit eines Systems beschreibt. Eine epistemische Unsicherheit gilt als vermeidbare Unsicherheit, die aufgrund von Informations- und Wissensmangel z. B. aufgrund von unvollständigen Messdaten, einer Nichtberücksichtigung von wichtigen Systemparametern in einem mathematischen Modell oder fehlendem Fachwissen entstanden ist. Die Zuverlässigkeit von Monitoring Systemen kann durch probabilistische oder deterministische Verfahren beurteilt werden. Im Bauingenieurwesen sind noch immer deterministische Methoden vorherrschend, welche meist nur aleatorische Unsicherheiten berücksichtigen. Es gibt nur sehr wenige Studien, die einen probabilistischen Ansatz verfolgen, indem verschiedene Unsicherheitsfaktoren betrachtet werden. Dennoch ist die praktische Anwendbarkeit solcher Methoden noch stark begrenzt. Die probabilistischen Verfahren beruhen auf dem Grundsatz, dass eine Prüfmethode als zuverlässig betrachtet wird, welche eine hohe Erfassungswahrscheinlichkeit vorhandener Schäden und eine niedrige Wahrscheinlichkeit einer Fehldetektion bei Schadensfreien Konstruktionen aufweist.

Es wurde ein modellbasiertes Framework entwickelt, welches den probabilistischen Ansatz zur Bewertung der Zuverlässigkeit von Methoden zur Schadensdetektion nutzt. Bisherigen Arbeiten ist zu entnehmen, dass dieser Ansatz, im Gegensatz zu deterministischen Methoden, eine genaue Bestimmung der Unsicherheiten liefert und eine zuverlässigere Zustandsbewertung ermöglicht. Das Framework vereint ausgewählte und in mehreren Fachrichtungen anwendbare Methoden und Konzepte, wie Sensitivitätsanalysen, Modellpflege (Model Updating), etc. Die Ergebnisse des entwickelten Frameworks können mit Beispielen aus bisherigen Veröffentlichungen verglichen und validiert werden. Der Bewertungsprozess hierfür kann standardisiert und für weitere

Forschung verwendet werden. Zur experimentellen Untersuchung wurden Positionierung und Anzahl der Sensoren, sowie die Eigenschaften der Anregung, welche zur Ermittlung des Tragwerksverhaltens genutzt wurden, variiert. Die Anordnung wurde basierend auf vordefinierten Positionen der Schadensbildung und dynamischen Eigenschaften des Tragwerks (Eigenfrequenzen und -formen) ausgewählt. Im Bereich des Bauingenieurwesens werden von Fall zu Fall für gewöhnlich Vereinfachungen getroffen, um den Rechenaufwand zu reduzieren. Zur Bewertung der Qualität des vereinfachten Modells, wurde untersucht, mit welcher Genauigkeit die zu detektierenden Schadensgrößen abgeschätzt werden können. Zur Quantifizierung der Qualität wurde ein korrelationsbasierter Indikator Q_V eingeführt, welcher das Verhältnis des Strukturverhaltens des vereinfachten Modells zum Strukturverhalten des Referenzmodells bezogen auf verschiedene Schadensgrößen beschreibt. Der Einfluss epistemischer Unsicherheiten auf die Schadensdetektion, welche aus Vereinfachungen des Modells resultieren können, wurde unter Verwendung einer globalen Sensitivitätsanalyse untersucht. Die modellbezogenen epistemischen Unsicherheiten wurden durch die Festlegung eines Parameterbereiches simuliert. Die möglichen Bereichsgrenzen jeden Parameters wurden Beispielen aus bisherigen Veröffentlichungen entnommen. Die Qualität des Versuchsaufbaus wurde bezüglich der Sensitivität des simulierten Strukturverhaltens auf Schadensbildung beurteilt. Die Qualität wurde mittels des sensitivitätsbasierten Indikators Q_{DOE} quantifiziert, welcher sich aus dem Bezug der Ergebnisse der globalen Sensitivitätsanalyse zum simulierten Strukturverhalten ergibt. Für die numerische Untersuchung wurden Experimente unter Berücksichtigung normalverteilter aleatorischer Unsicherheiten simuliert. Im experimentellen Beispiel wurden Versuche mehrfach wiederholt, um eindeutige aleatorische Unsicherheiten im Strukturverhalten erfassen zu können. Die Messwerte aus vorangegangenen Experimenten werden mittels Bayesian Model Updating bewertet und auf die vorhandenen Modellinformationen bezogen, um dadurch die epistemischen Unsicherheiten der Eingangsparameter zu reduzieren. Der Bewertungsprozess wird durch den Indikator Q_M quantifiziert, der die Verringerung der epistemischen Unsicherheit nach der Modellanpassung ausdrückt. Die Zuverlässigkeit der Prüfmethode wird durch die Wahrscheinlichkeit einer Schadensdetektion und die Wahrscheinlichkeit einer Fehldetektion beschrieben. Beide Werte werden im Indikator Q_D berücksichtigt. Die Indikatoren Q_V , Q_{DOE} , Q_M und Q_D , können Werte zwischen 0 (schlechteste Qualität) und 1 (beste Qualität) annehmen, normalisieren die entsprechenden Bezugswerte und können in einer umfassenden Datenbank für unterschiedliche bautechnische Strukturen gespeichert werden. Die detaillierte Anwendungsbeschreibung jeden Schrittes des entwickelten Frameworks wird durch zwei numerische Beispiele unterstützt. Ein Einfeldrahmen in Stahlbauweise und ein Kragbalken wurden für Experimente unter Laborbedingungen genutzt, um die Ergebnisse der numerischen Untersuchungen zu validieren. 26 identische Masten für In-situ-Messungen wurden zur Validierung des entwickelten Frameworks genutzt und bilden die Basis für eine statistische Datenbank, welche den Zusammenhang zwischen Q_{DOE} , Q_M und Q_D dokumentiert und als Richtlinie zur Bestimmung der Zuverlässigkeit von Prüfmethoden genutzt

werden kann.

Die Ergebnisse zeigen, dass der Einfluss der Vereinfachung eines numerischen Modells auf die Genauigkeit der Abschätzung einer Schadensgröße von der Anordnung des Versuchs abhängt, welche zur Berechnung des Tragwerksverhaltens genutzt wird. Im Beispielerperiment betrug $Q_V=0,2$ bei einer harmonischen Anregung des Einfeldrahmens in Stahlbauweise von 20 Hz. Aus einer harmonischen Anregung des identischen Systems von 60 Hz resultierte $Q_V=0,7$, was bedeutet, dass sich der Fehler im Gegensatz zur Anregung mit 20 Hz verringert. Die experimentelle Untersuchung unter Laborbedingungen zeigte die mögliche Größenordnung eines Fehlers bei der Abschätzung der Schadstelle infolge einer fehlerhaften Vereinfachung. Am Beispiel des Kragbalkens lässt sich zeigen, dass ein nicht geeignetes Schadensmodell zum Indikator $Q_V=0,7$ führte und somit der Schaden im numerischen Modell 30 % größer ist, als im Versuch unter Laborbedingungen. Die Untersuchungen zeigen, dass die Betrachtung dynamischer Eigenschaften eines Tragwerks die Sensitivität einer Schadensdetektion beeinflusst. Am Beispiel lässt sich zeigen, dass eine Verringerung der Steifigkeit unter harmonischer Anregung mit einer Frequenz kleiner der 1. Eigenfrequenz des Systems zum Indikator $Q_{DOE}=0,95$ und somit zu $Q_D \approx 1$ führt. Wird das System mit einem Vielfachen der 1. Eigenfrequenz angeregt, nimmt $Q_{DOE}=0,01$ und $Q_D \approx 0$ an. Die Untersuchungen zeigen, dass die Betrachtung von zusätzlichen Messungen von Vorteil ist, wenn ein Schaden unter einem bestimmten Wert detektiert werden muss. Die Ergebnisse der Arbeit zeigen eine Verringerung der Steifigkeit von 15 % ohne Berücksichtigung zusätzlicher Messungen ($Q_M=0$) führte zu $Q_D \approx 0,6$. Wurden zusätzliche Messungen in $Q_M=0,9$ berücksichtigt, resultierte $Q_D \approx 0,97$. Dieser Effekt ist jedoch nicht bei der Detektion einer Verringerung der Steifigkeit um 25 % zu beobachten, wobei $Q_D=1$ für beide Fälle gilt. Die entwickelte Datenbank, welche auf den zwei Experimenten und In-situ-Messungen an 26 identischen Masten basiert, wurde tabellarisch und graphisch ausgewertet. Die Ergebnisse zeigen einen definierten Bereich zuverlässiger Prüfmethode ($Q_D=1$) im Bezug auf Q_{DOE} und Q_M . Diese Datenbank, welche die erste ihrer Art im Bereich schwingungsbasierter Prüfmethode ist, kann als Referenz für weitere Messungen und zum gezielten Design von Experimenten zur Schadensdetektion dienen. Das Framework wurde unter Zuhilfenahme von dokumentierten Experimenten, welche ausreichend Daten für eine entsprechende Bewertung liefern, entwickelt. Weitere Forschung könnte in der Anwendung des Frameworks auf bereits veröffentlichte Experimente liegen. Die daraus entstehenden Ergebnisse können als Erweiterung der erarbeiteten Datenbank dienen und für die Erstellung eines Standards für die Beurteilung von schwingungsbasierten Prüfmethode des Bauingenieurwesens. Die Untersuchungen können auch auf andersartige Prüfmethode erweitert werden, solange eine entsprechende numerische Simulation möglich ist.

Abstract

This work aims to present a model-based strategy to investigate the reliability of an inspection method for damage detection considering model quality. The developed strategy is a probabilistic framework which combines several methods and approaches, such as sensitivity analysis, model updating, etc., that can be used in various disciplines.

Accomplishing the reliability assessment of an inspection method requires a precise definition of damage in a specific structure. An appropriate design of the experiment should be arranged to distinguish between the variation of the outputs due to the uncertainty of the selected input parameters and due to damage. Evaluating the validity of the chosen design of the experiment can be achieved by performing a sensitivity analysis. Based on the results of the performed sensitivity analysis, the important parameters which influence the studied outputs significantly are selected. The uncertainty of the important parameters is updated by a Bayesian inference approach. A Meta-Modeling approach can be followed to reduce the computational effort. Damage indicators are developed based on the target damage size and the response of the studied structure considering obtained posterior density functions of the updated input parameters. The damage indicators are combined with a probability of detection method to estimate the probability of detection curve. In this work, a method was developed and presented to compute the probability of detection curves. The reliability of an inspection method is assessed using the probability of detecting the predefined target damage size associated with a chosen probability of false alarm.

The described procedure was used to investigate the relationship between the reliability of a chosen inspection method for damage detection and the quality of the chosen models. In this work, four essential partial models were considered. They are the numerical model, the design of the experiment, measurements and damage indicator. Since global vibration-based methods have been often used in civil engineering for system identification and damage detection, the developed framework was applied to evaluate the performance of a chosen vibration-based inspection method for damage detection.

The developed strategy was illustrated by evaluating the performance of the inspection method to detect damage in a single degree of freedom system. The results show that choosing appropriate excitation properties can lead to a structural response which is sensitive to the

studied damage model. Moreover, model updating reduced the uncertainty of the input parameters associated with damage and improved the reliability of the inspection method.

The strategy was applied to a three degrees of freedom system to evaluate the performance of the chosen inspection method including several multi-damage and damage locations scenarios. Four damage cases were studied. In the first case, the damage was considered at the top floor of the structure. In the second case, the damage was considered in the middle floor, and the third case damage was at the bottom floor. In the fourth cases, the damage was considered in all the floors. A concept of damage patterns, which represent the relationship between the structural response and the studied damage model, was introduced to consider damage location and damage classification. The results show that the reliability of the inspection method depends on damage location and damage scenario. Moreover, damage patterns can help to reduce the probability of false alarm.

The performance of a chosen inspection method to detect damage in a steel frame structure was evaluated using the developed strategy considering the different design of the experiment. Damage was introduced in the physical model by releasing the hinges located at both ends of the beam. Five damage cases were studied. The undamaged case was considered if both hinges were fixed. In the fifth damage case, both hinges were completely released. Since experimental results show that damage increases the damping of the frame, empirical damping models were proposed and introduced in results of the numerical model to represent the development of damage. The results show that the reliability of the inspection method depends on the design of the experiment model including the number of sensors and the excitation properties. Moreover, it may be possible to improve the quality of the numerical model without considering complex phenomena (damping influence due to damage) if the boundary conditions (excitation properties in this example) are optimized to minimize the influence of those complex phenomena on the studied structural response.

The reliability of an inspection method for damage detection was evaluated in case of a cantilever with an extension which includes two rubber bands fixed to the top of the cantilever and two weights suspended at the second ends of the bands to generate pretension forces that change the support conditions of the system. The undamaged case was considered if both weights were at their maximum which provide tension forces at the end of the cantilever. Damage was developed by reducing the masses on both sides equally. The experimental results show that if damage was increased, the damping of the structure decreases. Two different numerical models were developed to describe the structure and damage. In the first model, the damage was introduced into the structure by reducing the stiffness of the cables attached to the cantilever. In the second model, the influence of the damping effect due to the cables was considered. The results show that the reliability of the inspection method was improved if the damping was included. Also, it was important to consider the imperfection of the structure in the numerical model to obtain agreement between the numerical and experimental models

considering damage.

The experimental study shows that performing a prior modal test and applying system identification to obtain modal parameters can help to understand the structural behavior and to develop appropriate numerical models which lead to an accurate inspection method assessment. However, if an agreement is obtained between the structural response calculated using the developed numerical model and the structural response measured using the physical model before considering damage, it is not necessary that this agreement would remain after considering damage. Therefore, the quality of the numerical model should be evaluated after considering damage to ensure an accurate evaluation of the chosen inspection method.

In many engineering disciplines, such as mechanical engineering, producing large amounts of standardized products provides the opportunity to apply a well-defined reliability assessment procedure which is based on inspecting a large number of samples that emulate a real structure or a part of it. Strict statistical restrictions related to the test conditions, for example, number of samples, damage size interval, number of repetition can be followed. In the civil engineering discipline, each structure is a unique product. Therefore, in most cases applying a traditional reliability assessment procedure is not possible. However, there are some rare cases where civil engineering standardized products are produced in large amounts. In this work, one of these rare cases is presented. The relationship between the reliability of the inspection method and the experimental models were investigated in the case of 26 identical structures (poles) considering two different setups. Two numerical models were developed. In the first numerical model, which was considered as a reference model, cables were modeled to consider the influence of their mass and stiffness on the studied structural response. In the second numerical model, the cables were replaced by a point mass, and their stiffness was ignored. The second model reduced the computational time by 40%. The damping influence was included in both models. The results show that the stiffness of the cables has a local effect. Measurements show that cables increase the modal damping of the first two mode shapes significantly. Therefore, the damage was introduced in the models by reducing the mass of the cables and their damping influence. The experimental data of the 26 poles was used separately to update the model and calculate the probability of damage detection. It was concluded that the reliability of the inspection method was improved if the dynamic test under impulse excitations activated the damping effect of the cables.

The results show that the reliability of an inspection method for damage detection depends on the chosen models. Neglecting important phenomena that describe the studied structure and/or the studied damage can lead to the wrong diagnosis of the reliability of the chosen inspection method. Moreover, a damage indicator that is sensitive to parameters that are not related to damage increases the probability of false alarm. The reliability of the studied inspection method depends on the studied damage scenario, damage location, number of sensors, location of the sensors, excitation properties, input parameters uncertainty and measurement uncertainty.

Keywords: Damage; Model quality; Reliability of inspection methods; Vibration-based; Probability of detection

Content

Die Ehrenwörtliche Erklärung	ii
Acknowledgments	iii
Zusammenfassung	v
Abstract	ix
Content	xvii
List of Symbols	xviii
List of figures	xxix
List of tables	1
1 Introduction	2
1.1 Motivation	2
1.2 Methodology	4
1.3 Outline	6
2 State of the Art	8
2.1 Damage	8
2.1.1 Damage and damage identification	8
2.1.2 Types of damage	9
2.1.3 Damage modeling	11
2.1.4 Damage detection inspection methods	18

2.2	The reliability of an inspection method	26
2.2.1	Reliability	26
2.2.2	Design of experiments	26
2.2.3	Probability of detection	29
2.3	Model quality	30
2.3.1	Models	30
2.3.2	Uncertainty	31
2.3.3	Model quality assessment methods	33
2.4	Conclusion	35
3	Strategy for Reliability Assessment	37
3.1	Overview	37
3.2	Problem definition	39
3.3	Design of Experiment	42
3.4	Sensitivity analysis	50
3.4.1	DOE based on numerical model quality and sensitivity analysis	51
3.4.2	Meta-Modeling	54
3.4.3	Choosing the terms of a Meta-model	55
3.4.4	Meta-Model for Sensitivity analysis	57
3.5	Model Updating	62
3.5.1	Bayesian inference	63
3.5.2	Prior density function	64
3.5.3	Likelihood function	65
3.5.4	Posterior density function	69
3.6	The reliability of an inspection method	74
3.6.1	Damage indicator	75
3.6.2	Probability of damage detection	75
3.7	Model quality and inspection method reliability	80
4	Numerical Study: Three degrees of freedom frame like structure	82

4.1	Introduction	82
4.2	Problem definition	82
4.3	Design of Experiments	84
4.4	Sensitivity analysis results	86
4.5	Model updating results	92
4.6	Reliability of the inspection method	92
4.6.1	Damage indicator	92
4.6.2	Damage location	94
4.6.3	Probability of detection curves	95
5	Experimental Study	98
5.1	Steel frame structure	98
5.1.1	Introduction	98
5.1.2	Problem definition and experimental test setup	98
5.1.3	Modal parameters	103
5.1.4	Results under harmonic excitations	105
5.1.5	Numerical study	114
5.1.6	Design of Experiments	130
5.1.7	Sensitivity analysis	131
5.1.8	Model updating	132
5.1.9	Assessment of the inspection method	132
5.1.10	Conclusion	139
5.2	Cantilever	140
5.2.1	Introduction	140
5.2.2	Problem definition and test setup	140
5.2.3	Test results	143
5.2.4	Numerical model	155
5.2.5	Design of Experiments	169
5.2.6	Sensitivity analysis	171
5.2.7	Model updating	171

5.2.8	Assessment of the inspection method	173
5.2.9	Conclusion	177
6	Reference Object: Pole	178
6.1	Introduction	178
6.2	Problem definition and test setup	178
6.3	Test results	182
6.4	Numerical model	183
6.5	Design of experiments	190
6.6	Sensitivity analysis	201
6.7	Model updating	203
6.8	Assessment of the inspection method	205
6.9	Conclusion	214
7	Discussion	215
7.1	Introduction	215
7.2	Quality assessment: Limitation and improvement	216
7.2.1	Assessment procedure	216
7.2.2	Assessment results	216
7.3	Conclusion	222
8	Conclusion and Outlook	225
	References	240
A	MATLAB Implementations	241
A.1	Bayesian Model updating	241
A.2	Sampling from a uniform distribution function	246
A.3	Sampling from any distribution function using the inverse method	247
A.4	Probability of detection	247
A.5	Developing Meta-models and selecting their terms	249

B	Finite Element models (LS DYNA reduced input)	254
B.1	Steel frame structure	254
B.2	Cantilever PVC with cables	267
B.3	Cantilever PVC with dampers	273
B.4	Pole	281
C	System identification	290
C.1	System identification by applying the Stochastic subspace identification (SSI) method using MACEC	290

List of Symbols

Functions and operations

$argmax$	argument of the maximum
$C(n, k)$	The number of k -combinations from a given set A of n elements
$n!$	the factorial of a non-negative integer n
$A \subseteq B$	Subset: every element of A is also an element of B
$x \in A$	x is an element of the set A
$x \propto y$	x is proportional to y
$x \equiv y$	x is congruent to y
$\prod x$	Product over x
$\log x$	Natural logarithm (to base e) of x
$exp(x)$	natural exponential function e^x
$\sin x$	Sine function of x
$\cos x$	Cosine function of x
$\{\cdot\}$	Column vector
$\{\cdot\}^T$	Row vector
$[\cdot]^{-1}$	Inverse of a Matrix
$\partial^2 y / \partial x^2$	Second order of partial derivative of y with respect to x
H_o	Null hypothesis

Fixed symbols

G_M	Numerical model
G_E	Experimental model
G_{MR}	Reference numerical model
g	Gravitational acceleration
$\epsilon_{d\theta}$	Variation of the chosen response due to the variation of the considered inputs

$\epsilon_{\bar{d}}$	Measurement uncertainty
ϵ	Total uncertainty
β	Regression coefficients
$\hat{\beta}$	Regression coefficients for a Meta-model used in model updating
Q_V	Index quantifies the quality of a solving numerical model and analyzing a computed structural response
Q_{DOE}	Index quantifies the quality of a design of experiment
Q_M	Index quantifies the quality of a set of measurements for model updating
Q_D	Index quantifies the quality of a chosen inspection method for detecting a certain damage size θ^g
k	Stiffness
E	Elastic modulus
ν	Poisson's ratio
m	Mass
R^2	Coefficient of determination
c	Damping
C_d	Damping constant
f_n	Natural frequency [Hz]
\Re	The set of real numbers
\ddot{x}	Second order time derivative of x , acceleration
\dot{x}	First order time derivative of x , velocity
x	Displacement
x^g	Damage location
d	A chosen structural response
\bar{d}	A set of experimental data
d^*	Set of true response of a structure
\hat{d}	Response of a structure obtained using a Meta-model
d_c	Threshold associated with a structural response d
\underline{d}	Response of a structure obtained using a Meta-model
N_{Θ}	Number of the terms in a Meta-model
$N_{\hat{\theta}}$	Number of desired parameters (number of unknown inputs)
n_{θ}	number of elements in a set used to obtain terms for a Meta-model
t	Time
t_e	Time when a signal ends

t_0	Time when a signal starts
Δt	Time step
Δf	Frequency rate
sT	Total-effect index
$F(t)$	Excitation as a function of time
F_a	Amplitude of an excitation
ω	Angular frequency of an excitation
ω_n	Natural angular frequency of a system
ω_d	Damped natural angular frequency of a system
ψ_θ	Degree of mixed terms in a Meta-model
Δk	Stiffness degradation damage type
θ^g	Damage that should be detected
θ	A studied input parameter
ρ	Density
ζ	Damping ratio
η	Ratio of angular frequency of an excitation to a natural angular frequency of system
δ	Uncertainty due to the approximation of a numerical model by a Meta-model

Probability theory

$\sigma_{\bar{d}}$	Standard deviation of a set of experimental data
σ_ϵ	Standard deviation of the total uncertainty
σ_θ	Standard deviation of the model uncertainty due to the inputs' variation
σ_δ	Standard deviation of the model uncertainty due to the approximation of a numerical model by a Meta-model
$P(\cdot)$	Probability
$P(A B)$	Conditional probability of event A given event B
$P(A \cap B)$	Joint probability for events A and B
$p(\theta)$	probability density function of θ
$L(\cdot)$	Likelihood function
$\mathcal{N}(\mu, \sigma^2)$	Normal distribution with parameters μ and σ^2
$\theta \sim P(\theta)$	A random variable θ has the probability distribution $p(\theta)$
$E(\cdot)$	Expected value of a random variable

Acronyms

COV	Coefficient of variance
DOE	Design of experiment
DP	Damage pattern
FE	Finite elements
FFT	Fast Fourier transform
NDE	Nondestructive evaluation
NDT	Nondestructive testing
PFA	Probability of false alarm
PFP	Probability of false positive
POD	Probability of detection
SDOF	Single degree of freedom
SHM	Structural health monitoring
Var	Variance

List of Figures

3.1	Developed strategy to investigate the relationship between the quality of the models and the reliability of an inspection method	38
3.2	A stiffness-mass-damping system excited by a force $F(t)$	41
3.3	The chosen harmonic excitation $F(t)$ (a) and its $ \text{FFT} $ (b)	43
3.4	Structural response $\ddot{x}(t)$ (a), cumulative signal energy $d(t)$ (b), and FFT of the acceleration signal using the mean values, table 3.2, (c)	45
3.5	Structural response $\ddot{x}(t)$ (a) under the contaminated excitation, cumulative signal energy $d(t)$ (b), and FFT of the acceleration signal using the mean values, table 3.2, (c)	47
3.6	The relationship between the input parameters and the output parameter without considering the ambient vibration excitation	48
3.7	The relationship between the input parameters and the output parameter considering white noise ambient vibration excitation	49
3.8	A histogram shows the cumulative signal energy $d(t_e)$ variation due to the inputs $\{\theta\}$ uncertainty using $N = 100$ samples	50
3.9	The relationship between the angular frequency of the excitation and the Total-effect index sT of the input parameters	53
3.10	The relationship between the amplitude of the excitation and the Total-effect index sT of the input parameters	54
3.11	A Strategy to select the terms of a Meta-model	56
3.12	Statistical properties assessment of the residuals	60
3.13	The Total-effect index sT calculated using the numerical model G_M and the Meta-model \underline{d} using 10000 samples. Good agreement is observed	61
3.14	The Total-effect index sT using different excitation types	62

3.15	Statistical properties of the cumulative signal energy $\bar{d}(t)$ considering the variation of the initial conditions.	67
3.16	Investigating the influence of the noise level γ_F on $\bar{d}_t - d^*$	69
3.17	Developed Meta-model for model updating	71
3.18	Statistical properties assessment of the residuals	72
3.19	Prior and posterior density functions of the uncertainty of the stiffness k obtained using the numerical model G_M , the Meta-model for sensitivity analysis \underline{d} and the Meta-model for model updating	73
3.20	Prior and posterior density functions of the uncertainty of the mass m obtained using the numerical model G_M and the Meta-model for sensitivity analysis \underline{d}	73
3.21	Prior and posterior density functions of the uncertainty of damping ratio ζ obtained using the numerical model G_M and the Meta-model for sensitivity analysis \underline{d}	74
3.22	Results of developed POD method	79
4.1	Three degrees of freedom frame structure excited by a force $F(t)$ at x_1	84
4.2	Time series and Fourier transforms of the excitation forces applied at x_1 and used to simulate the modal tests	87
4.3	Time series and Fourier transforms of the structural response of the studied structure at x_1	88
4.4	Posterior density functions $p(\{\theta\} \{\bar{d}\})$ of the input parameters computed using Bayesian updating method. ζ_3 was calculated following the eq.(4.7)	93
4.5	Damage pattern $DP(\theta^g)$ for different damage cases	96
4.6	Probability of detection for different damage scenarios including model updating	97
5.1	Studied single-span one-story steel frame structure and its elements	99
5.2	Sensors locations in each test setup	100
5.3	Hinge and cube elements used to construct the frame and introducing damage in the physical model	102
5.4	The impulse excitation $F(t)$ (a) applied at cube number 6 and its FFT (b)	104
5.5	The response of structure recorded at cube 14 (reference No. 2) (a) and its FFT (b)	105

5.6	Mode shapes $[\phi_E]$ from 1 to 6: case 1 (black), case 2 (red), case 3 (green), case 4 (blue), case 5 (pink)	107
5.7	Mode shapes $[\phi_E]$ from 7 to 12: case 1 (black), case 2 (red), case 3 (green), case 4 (blue), case 5 (pink)	108
5.8	The acceleration output signal recorded using an accelerometer placed at the shaker (a) and its FFT (b)	109
5.9	Examples of the recorded structural response under harmonic excitations	111
5.10	Fourier transform of the response \ddot{y} at cube 12 (middle of the beam) under the applied lateral harmonic excitations	112
5.11	$\sum \bar{d}_{t,min,si} / \bar{d}_{F,si}$ computed based on initial conditions and eq. (5.4) for all the $si = 1 \cdots 11$ sensors	113
5.12	$\sum \bar{d}_{t,min,si} / \bar{d}_{F,si}$ computed based on eq. (5.3) and eq. (5.4) for all the $si = 1 \cdots 11$ sensors	114
5.13	Models of the elements that form the global shell element model of the steel frame	115
5.14	Numerical model of the studied frame using shell elements	115
5.15	Rayleigh damping model included in the numerical model of the frame. Red points represents the damping ratios of undamaged structure obtained from measurements $\{\zeta_E\}$ and black line represents Rayleigh damping model, eq.(5.5) .	116
5.16	Mode shapes from 1 to 12: case 1	119
5.17	Modal Assurance Criterion values (MAC) $MAC(\phi_{E,ri}, \phi_{S,rj})$. $ri = 1 \cdots 12$ and $rj = 1 \cdots 12$ refers to the mode order	121
5.18	The structural response and its FFT under the harmonic excitations applied in y direction	122
5.19	The structural response and its FFT under the harmonic excitations applied in x direction	123
5.20	$\sum d_{t,si}$ computed based on eq. (5.3) for all sensors $si = 1, 2, \cdots, 11$	124
5.21	$\sum d_{t,si}$ computed based on eq. (5.3) for all sensors $si = 1, 2, \cdots, 11$	125
5.22	Correlation coefficient between the time histories of the computed and measured structural response for all studied damage cases under 20 Hz excitation	126
5.23	Correlation coefficient between the time histories of the computed and measured structural response for all studied damage cases under 30 Hz excitation	126
5.24	Correlation coefficient between the time histories of the computed and measured structural response for all studied damage cases under 30 Hz excitation	127

5.25	Correlation coefficient between the time histories of the computed and measured structural response for all studied damage cases under 30 Hz excitation	127
5.26	Comparison between the simulated and measured structural response under different excitations after normalizing the amplitude to 1	128
5.27	Empirical damping models illustrate the influence of damage on the damping of the structural response of the studied frame	130
5.28	Total-effect index $sT_{i,j}$ calculated for all chosen design of experiments models given in table 5.11. Channel numbers from 1 to 11 are in x direction, 12 to 22 are in y direction and 23 to 33 are in z direction, table 5.6.	133
5.29	Posterior density functions of the updated input parameters using $\{\bar{d} DOE_1\}$. .	134
5.30	Posterior density functions of the updated input parameters using $\{\bar{d} DOE_2\}$. .	135
5.31	Posterior density functions of the updated input parameters using $\{\bar{d} DOE_3\}$. .	135
5.32	Posterior density functions of the updated input parameters using $\{\bar{d} DOE_4\}$. .	135
5.33	Posterior density functions of the updated input parameters using $\{\bar{d} DOE_5\}$. .	136
5.34	Posterior density functions of the updated input parameters using $\{\bar{d} DOE_6\}$. .	136
5.35	Probability of damage detection of the studied damage type using different designs of experiment and different damping models. The sensors of each <i>DOE</i> are defined in the tables 5.1 and 5.11.	138
5.36	Studied PVC cantilever	141
5.37	Test setup of the studied PVC cantilever of the dynamic modal test	142
5.38	Introducing damage model in the studied PVC structure	143
5.39	A sketch of damage modeling in the physical model	144
5.40	FFT of input excitations in all studied damage cases	145
5.41	Time histories and FFT of an input excitation	146
5.42	Structural response at the top of the cantilever under the excitation in figure 5.41, case 1	146
5.43	The structure is shifted in y direction due to the added weights and the asymmetry	147
5.44	Mode shapes 1 and 2 scaled to unit modal displacement extracted from experimental data , θ_1^g :black, θ_2^g :red, θ_3^g :green, θ_4^g :blue	148
5.45	Mode shapes 3 and 4 scaled to unit modal displacement extracted from experimental data, θ_1^g :black, θ_2^g :red, θ_3^g :green, θ_4^g :blue	149

5.46	Mode shapes 5 and 6 scaled to unit modal displacement extracted from experimental data, θ_1^g :black, θ_2^g :red, θ_3^g :green, θ_4^g :blue	150
5.47	MAC value computed between damage case 1 and other damage cases	151
5.48	The statistical results of $\bar{d}_t(y)$ normalized to d_F for all studied damage cases . . .	152
5.49	The statistical results of $\bar{d}_t(z)$ normalized to d_F for all studied damage cases . . .	153
5.50	The mean value of \bar{d}_t/d_F	153
5.51	Chosen excitations and their FFT from conducted experiments in order to calculate the response of the studied models for each damage case	154
5.52	\bar{d}_t/d_F under similar impulses	154
5.53	Numerical models considered for evaluating the performance of the studied inspection method	156
5.54	The contribution of the mass of the structure in the Rayleigh damping model during performing transient analysis	158
5.55	Rayleigh damping model included in the cantilever numerical models	159
5.56	Simulated dynamic structural response at the top of the cantilever due to the excitation in figure 5.51, case 1, using the numerical model $G_{M,1}$	160
5.57	Simulated dynamic structural response at the top of the cantilever due to the excitation in figure 5.51, case 1, using the numerical model $G_{M,2}$	160
5.58	Mode shapes 1 and 2 and scaled to unit modal displacement obtained using the numerical model $G_{M,1}$ by analyzing numerical response using the SSI method. θ_1^g : black, θ_2^g : red, θ_3^g : green, θ_4^g : blue	162
5.59	Mode shapes 3 and 4 and scaled to unit modal displacement obtained using the numerical model $G_{M,1}$ by analyzing numerical response using the SSI method. θ_1^g : black, θ_2^g : red, θ_3^g : green, θ_4^g : blue	163
5.60	Mode shapes 5 and 6 and scaled to unit modal displacement obtained using the numerical model $G_{M,1}$ by analyzing numerical response using the SSI method. θ_1^g : black, θ_2^g : red, θ_3^g : green, θ_4^g : blue	164
5.61	Mode shapes 1 and 2 and scaled to unit modal displacement obtained using the numerical model $G_{M,2}$ by analyzing numerical response using the SSI method. θ_1^g : black, θ_2^g : red, θ_3^g : green, θ_4^g : blue	165
5.62	Mode shapes 3 and 4 and scaled to unit modal displacement obtained using the numerical model $G_{M,2}$ by analyzing numerical response using the SSI method. θ_1^g : black, θ_2^g : red, θ_3^g : green, θ_4^g : blue	166

5.63	Mode shapes 5 and 6 and scaled to unit modal displacement obtained using the numerical model $G_{M,2}$ by analyzing numerical response using the SSI method. θ_1^g : black, θ_2^g : red, θ_3^g : green, θ_4^g : blue	167
5.64	d_t/d_F under the same excitation using the first model $G_{M,1}$	169
5.65	d_t/d_F under the same excitation using the second model $G_{M,2}$	169
5.66	Total-effect index $sT_{i,j}$ calculated using the numerical models $G_{M,1}$ and $G_{M,2}$. Channel numbers from 1 to 5 are in y direction, and 6 to 10 are in z direction.	172
5.67	Posterior density functions of the updated input parameters using $\{\bar{d}, G_{M,1}\}$	174
5.68	Posterior density functions of the updated input parameters using $\{\bar{d}, G_{M,2}\}$	174
5.69	$POD(\theta^g)$ curve using $G_{M,1}$	175
5.70	$POD(\theta^g)$ curve using $G_{M,2}$	176
5.71	Comparison between $POD(\theta^g)$ curves obtained G_E , $G_{M,1}$ and $G_{M,1}$	176
6.1	One of the studied pole structure and a sketch shows cross sections	179
6.2	Top view of the sensor location	180
6.3	Developed test system used to perform dynamic measurements on the studied structure	181
6.4	Structural response at the top of the pole Nr.262-28 under an impulse excitation	182
6.5	Mode shapes 1 and 2 extracted from experimental data	184
6.6	Mode shapes 3 and 4 extracted from experimental data	185
6.7	Mode shapes 5 and 6 extracted from experimental data	186
6.8	Mode shapes 7 and 8 extracted from experimental data	187
6.9	\bar{d}_t under 30 impulse excitation setup 1, pole Nr.262-28	188
6.10	\bar{d}_t under 30 impulse excitation setup 2, pole Nr.262-28	188
6.11	Numerical models developed for evaluating the performance of the studied inspection method	189
6.12	The contribution of the mass of the structure in the Rayleigh damping model during performing transient analysis	191
6.13	Rayleigh damping model included in the pole numerical models	191
6.14	Simulated dynamic structural response at the top of the pole due to the excitation in figure 5.51, damage case 1, using the numerical model G_{MR}	192

6.15	Simulated dynamic structural response at the top of the pole due to the excitation in figure 5.51, damage case 1, using the numerical model G_M	192
6.16	Mode shapes 3 and 4 extracted from the simulated test using G_{MR}	193
6.17	Mode shapes 5 and 6 extracted from the simulated test using G_{MR}	194
6.18	Mode shapes 7 and 8 extracted from the simulated test using G_{MR}	195
6.19	Mode shape 4 extracted from the simulated test using G_M	196
6.20	Mode shapes 5 and 6 extracted from the simulated test using G_M	197
6.21	Mode shapes 7 and 8 extracted from the simulated test using G_M	198
6.22	d_t under the same excitation using the reference model G_{MR}	200
6.23	d_t under the same excitation using the model G_M	200
6.24	Total-effect index $sT_{i,j}$ calculated for the two setups given in table 6.1. Channel numbers from 1 to 11 are in x direction, 12 to 22 are in y direction. 11 is x reference and 22 is y reference at the top of the pole	202
6.25	Estimation of the noise energy d_γ in an impulse response d_t	204
6.26	Acceleration signal time history with about 10% noise	204
6.27	Acceleration signal time history with about 2% noise	205
6.28	Posterior density functions of the updated input parameters using \bar{d} from pole Nr. 9 (239-25), Setup S_1	208
6.29	Posterior density functions of the updated input parameters using \bar{d} from pole Nr. 9 (239-25), Setup S_2	209
6.30	Posterior density functions of the updated impulse excitation amplitudes in x and y directions, S_1	210
6.31	Posterior density functions of the updated impulse excitation amplitudes in x and y directions, S_2	211
6.32	$POD(\theta^g)$ using G_M and different 26 pole experimental model, S_1 . Red: maximum and minimum curves value	212
6.33	$POD(\theta^g)$ using G_M and different 26 pole experimental model, S_2 . Red: maximum and minimum curves value	213
7.1	Partial models quality of the SDOF system example (red: with model updating, blue: without model updating)	218
7.2	Partial models quality of the 3DOFs system example: red line is if damage was at the top k_1 or middle story k_2 and blue line if damage was at the ground story k_3	219

7.3	Partial models quality of the studied one span steel frame structure considering different DOE models and damping models (red: no damping influence, blue: linear damping model, green: slow damping changes (parabolic), orange: fast damping model changes (parabolic) (covered by blue in some figures))	221
7.4	Partial models quality of the PVC cantilever example: red line is if the numerical model $G_{M,1}$ was chosen and blue line is if the numerical model $G_{M,2}$ was chosen	222
7.5	Partial models quality of the studied pole structure considering two test setups and and 26 experimental model G_E . The histograms show the distribution of the 26 pole samples based on Q_D . Red: the minimum values of the quality indexes, blue: the maximum values of the quality indexes	223
C.1	Graphic user interface of MACEC	290
C.2	Creating the grid file of the pole's geometry	291
C.3	Creating the slave file to fix the node 0 at z=0 m	291
C.4	Creating the beam file to link the measurement points	292
C.5	Processing the acceleration signal	292
C.6	Assigning the channels to their relevant degrees of freedom and directions	293
C.7	Applying SSI methods	293
C.8	Estimating the real order of the system by checking the singular value figure . .	294
C.9	Performing modal analysis	294
C.10	Plotting mode shapes	295

List of Tables

2.1	Studies on damage in concrete/steel/Composite structures	11
2.2	Damage modeling in numerical models	14
2.3	Damage modeling in physical models	17
2.4	Damage detection inspection methods part 1	24
2.5	Damage detection inspection methods part 2	25
3.1	True values assumed for the studied input parameters $\{\theta\}$	44
3.2	Mean values $\{\mu\}$, minimum and maximum values of the studied parameters $\{\theta\}$ and their coefficients of variation COV	46
3.3	Evaluation the inspection method for detecting 15% stiffness degradation with and without model updating using Q_D	79
3.4	Partial models assessment procedures and the reliability of an inspection method	81
4.1	Applied excitations used to simulate the tests	85
4.2	True values of the studied input parameters. ζ_3 was calculated following the eq.(4.7)	85
4.3	The statistical properties of the stiffness, masses and damping ratios of the studied structure. ζ_3 was calculated following the eq.(4.7)	86
4.4	Total-effect index sT values calculated for all excitations, input parameters $\{\theta\}$ and computed response $\{\underline{d}\}$	90
4.5	The quality of the DOE considering the excitation type and the sensor position .	91
4.6	The statistical properties of the posterior density functions of the input parameters. ζ_3 was calculated following the eq.(4.7)	92
4.7	The quality of the measurements based on damage scenario	93
4.8	Damage patterns $DP(\theta^g)$ for the first damage scenario $\theta^g = \Delta k_1$	95

4.9	Damage patterns $DP(\theta^g)$ for the second damage scenario $\theta^g = \Delta k_2$	95
4.10	Damage patterns $DP(\theta^g)$ for the third damage scenario $\theta^g = \Delta k_3$	95
4.11	Damage patterns $DP(\theta^g)$ for the fourth damage scenario $\theta^g = \Delta k_1 + \Delta k_2 + \Delta k_3$	95
4.12	Reliability of the inspection method for detecting 5% stiffness degradation for different damage scenarios based on Q_D including model updating	96
5.1	Sensors locations for each test setup	101
5.2	Studied damage cases	101
5.3	Natural frequencies $f_{n,E}$ [Hz] of the frame for the studied damage cases	105
5.4	Damping ratios ζ_E [%] of the frame for the studied damage cases	106
5.5	The description of the mode shapes	106
5.6	Arrangement of channels used to record the response and the corresponded cubes number where the sensors were placed	110
5.7	Natural frequencies of the numerical model $f_{n,S}$ [Hz] of the frame for studied damage cases and relative error between $f_{n,E}$ and $f_{n,S}$	118
5.8	Modal Assurance Criterion values (MAC) $MAC(\phi_{E,ri}, \phi_{S,rj})$	120
5.9	Quality of the numerical model compared to the physical model for different DOE given that d is the signal energy. Red values indicate an agreement between the response of the physical model and the numerical model considering the studied damage model	129
5.10	Mean values $\{\mu\}$, minimum and maximum values of the studied parameters $\{\theta\}$ and their coefficients of variation COV	131
5.11	Chosen design of experiments models to detect the studied damage θ^g	131
5.12	The quality of the chosen design of experiments models to detect the studied damage θ^g	132
5.13	The statistical properties of the posterior density functions of the input parameters	134
5.14	The quality of the chosen measurements to detect the studied damage θ^g	134
5.15	$\theta^g POD(\theta^g = 95\%, d_{mi,j}(\theta^g \zeta_{\theta^g}))$ in mm where, $mi = 1, \dots, 4$ is the damping model	137
5.16	Q_D calculated considering $\theta^g = 0.09$ mm	137
5.17	Natural frequencies and damping ratios extracted from measurements for the studied damage cases	145

5.18	Natural frequencies and damping ratios obtained using the numerical model $G_{M,1}$ by analyzing numerical response using the SSI method	161
5.19	Natural frequencies and damping ratios obtained using the numerical model $G_{M,2}$ by analyzing numerical response using the SSI method	161
5.20	The input parameters of $G_{M,1}$ used to calculate Q_V	168
5.21	The input parameters of $G_{M,2}$ used to calculate Q_V	168
5.22	The quality of the numerical model $G_{M,1}$ compared to the experimental model G_E	168
5.23	The quality of the numerical model $G_{M,2}$ compared to the experimental model G_E	168
5.24	The statistical properties of the prior density functions of the input parameters of the developed numerical model $G_{M,1}$	170
5.25	The statistical properties of the prior density functions of the input parameters of the developed numerical model $G_{M,2}$. $C_{d,y,1}$, $C_{d,y,2}$, $C_{d,z,1}$ and $C_{d,z,2}$ are given in $N \times s/mm$	170
5.26	The statistical properties of the posterior density functions of the input parameters calculated using $G_{M,1}$	173
5.27	The statistical properties of the posterior density functions of the input parameters calculated using $G_{M,2}$	173
6.1	Sensor locations for each test setup measured from the base of the pole	181
6.2	Statistical properties of the natural frequencies and modal damping ratios extracted from measurements obtained from 16 poles	183
6.3	The natural frequencies and modal damping ratios extracted from the simulated test using G_{MR}	191
6.4	The natural frequencies and modal damping ratios extracted from the simulated test using G_M	192
6.5	The input parameters of G_{MR} used to calculate Q_V	199
6.6	The input parameters of G_M used to calculate Q_V	199
6.7	The quality of the numerical model G_M compared to the reference model G_{MR} .	199
6.8	The statistical properties of the prior density functions of the input parameters of the developed numerical model G_M	201
6.9	The statistical properties of the posterior density functions of the common input parameters. Pole 1–13. $C_{d,1}$ and $C_{d,2}$ are given in $[N \times s/mm]$	206

6.10 The statistical properties of the posterior density functions of the common input parameters. Pole 14–26. $C_{d,1}$ and $C_{d,2}$ are given in [N×s/mm] 207

6.11 The minimum damage size that can be missed based on the problem definition in eq. (6.1) 212

6.12 The index Q_D computed based on eq. (3.61) for $\theta^g = 0.002$ [t] or $\theta^g = 2$ kg . . . 213

7.1 An overview of the comparison of the studied partial model in each example . . 217

7.2 Quality of the numerical model compared to the physical model for different DOE given that d is the signal energy after applying eq. (7.4) 220

C.1 The obtained frequencies and damping ratios from the experimental data applying SSI 295

Chapter 1

Introduction

1.1 Motivation

The safety and the functionality of engineering structures under many types of random loads have been one of the major concerns in engineering disciplines. This is because of the high risk caused by damage, especially in the case of lifeline structures. For example, damage in dams, gas stations, the nuclear power plant can lead not only to local but also to global disasters, Faber [2007]. Therefore, maintenance is an essential part that should be considered for these important structures. However, the lack of knowledge about the current state of the concerned structure can result in an expensive maintenance plan if damage progresses slower than expected. On the other hand, the maintenance plan cannot be sufficient if the development of damage is rapid.

Modern maintenance plans have been designed based on information that can be acquired about structural damage. For this reason, damage should be identified in the early phase by a well-designed structural health monitoring system. Choosing a monitoring system depends on the structure properties, damage type, budget, etc. One of the most important elements of a well-designed monitoring system is a reliable inspection method for damage detection. The reliability of an inspection method implies that if there is damage, the monitoring system should identify it with a high probability of success. Moreover, if there is no damage, the probability of a false alarm should not exceed a certain level. Also, a designed monitoring system should fulfill two important requirements. First, the integrated inspection method must be nondestructive. The second is that the operation of the structure should not be interrupted.

Structural health monitoring has been developed in many engineering disciplines. For instance, in aerospace engineering, different inspection methods have been utilized for detecting various types of cracks and notches in airframes. Several procedures have been developed to prove the reliability of a chosen inspection method. A traditional reliability assessment is based

on inspecting a large the number of samples that emulate a real structure or a part of it. Several damage sizes should be introduced to the samples, Georgiou [2006]. Strict statistical restrictions related to the test conditions have to be followed, for example, number of samples, damage size interval, number of repetition, etc. Then, the probability of detection (POD) and the probability of false positive (PFP) which is also named as the probability of false alarm (PFA) should be estimated for each damage size. The reliability of the tested inspection method is evaluated by a damage size that should be detected with a chosen probability. However, for civil engineering structures, producing physical samples for statistical tests is not realistic. Moreover, the uniqueness and the complexity of the studied structure can be a serious problem which makes the following statistical restrictions difficult or even impossible.

To overcome the application limits of statistical assessment methods, numerical models have been used as an alternative to physical models and real structures. The importance of the numerical models increases rapidly because of the significant development of computational effort and economical requirements. However, it is still difficult to represent what is called *reality* in a single model. As a result, abstractions should be taken into account when a numerical model has to be chosen. Therefore, model developers should use their experience and knowledge to answer the following questions:

- How far can the model be developed?;
- How far need the model to be developed?;
- How far should the results of the model be trusted?;
- What are the consequences of using a wrong model?.

Answering the questions raised leads to several classes of numerical models which describe a certain phenomenon. Several results may be obtained if different numerical models are used to assess the reliability of an inspection method for damage detection. Therefore, choosing the best model requires following an approach which provides a subjective and reliable comparison between models under consideration. Although several general model properties, such as sensitivity, complexity, uncertainty, etc., have been used to establish criteria for model quality evaluation, an explicit meaning of the results obtained from such criteria still requires more research.

Most of the previous studies investigated damage detection in civil engineering by following a general procedure. This procedure is based on developing a model for a nondamaged structure as a first step and then introducing a damage target size to the model. Many damage indicators and inspection methods have been developed to monitor the variation of a chosen structural response due to several damage types, Doebling et al. [1996], Sinou [2009]. However, in most cases, the variation of the structural response due to other input parameters uncertainty was not

considered. As a result, false alarm observed by the variation of the material and geometrical properties of the studied structure that leads to a structural response similar to what damage produces were not often investigated. This raises the question of the validity of such a procedure to assess the reliability of a chosen inspection method.

Investigating the latent relationship between the quality of the chosen models and the reliability of an inspection method for damage detection considering the influence of different types of uncertainty is the aim of this work.

1.2 Methodology

Since the reliability of an inspection method for damage detection is influenced by many factors, the studied problem was decoupled into several parts. In this work, these parts were named *Partial Models*. Generally, a large number of partial models can be obtained. However, the decoupling procedure was based on classifying models in specific categories. The first partial model G_M includes a numerical model of a studied structure with input parameters $\{\theta\}$ and a chosen damage model θ^g . Numerical models can be analytical or approximated models based on a discretization method such as the Finite Element method. As a result, the model can be implemented and solved by an available computational effort to obtain a response d .

$$G_M : \{\theta\}, \theta^g \rightarrow d(\theta^g, \{\theta\}) \quad (1.1)$$

The second partial model is the design of experiment (DOE) which includes a process that maximizes the probability of reaching the objectives of the performed tests by acquiring information about the important input parameters $\{\hat{\theta}\}$ if a structural response is measured. The design of experiment model should give all necessary information required to simulate or conduct the desired nondestructive test, for example, excitations F , structural response quantities such as the chosen response type, sensor locations $[U] = [X, Y, Z]$, etc.

$$DOE : \{\hat{\theta}\} \subseteq \{\theta\} \rightarrow F, [U], \dots \quad (1.2)$$

The third partial model is the measurement g_E . It contains the results of the performed tests and measurement uncertainty $\epsilon_{\bar{d}}$ obtained from a physical model G_E taking into account the quality of the sensors and the influence of the surrounding environment such as ambient vibration γ_F . Experiments should be performed based on a design of experiment partial model including the experimental damage model θ_E^g .

$$g_E : G_E, DOE, \gamma_F, \theta_E^g \rightarrow \bar{d} \quad (1.3)$$

The fourth partial model includes damage-response relationships which are usually named as damage indicators. It represents the variation of a chosen structural response due to damage θ^g in a studied structure considering different types of uncertainty ϵ .

$$f : \theta^g \rightarrow d(\theta^g, \epsilon) \quad (1.4)$$

The developed strategy starts by combining the numerical and the design of experiment partial models. The coupling is achieved statistically. This means, probabilistic models are chosen to represent the uncertainty of the input parameters then a sampling method is used to generate samples. A sample contains a combination of input parameters values based on the assigned probabilistic models. The numerical model is solved for each sample. As a result, the response of the studied structure is obtained for each sample. In the second step, the coupled models are combined with measurements by a Bayesian updating approach. The resulting posterior probability density functions of the inputs are used to obtain the structural response and its uncertainty due to damage produced using the chosen damage model. In this step, the calculated response, which performs as a damage indicator, is used to evaluate the reliability of the chosen inspection method.

Assessment procedures have been applied to evaluate the chosen coupled partial models. A studied numerical model was evaluated by investigating the agreement between the structural response computed using a numerical model G_M and measured from an experimental model G_E due to a damage model θ^g and θ_E^g . A design of experiment model is verified by performing a sensitivity analysis. The design is considered optimal if the variation of a chosen structural response is sensitive to the desired input parameters and insensitive to unwanted input parameters. The quality of the measurements for model updating is evaluated by their information content that should lead to less uncertainty. The probability of detection curve and the probability of false alarm are used to evaluate the damage-response relationship model and to assess the reliability of the inspection method for detecting the required damage target size.

The procedure described above represents a model-based strategy for assessing and improving the reliability of an inspection method for damage detection using the probability of detection curves. The developed strategy is a probabilistic framework which combines several methods and approaches, for example, sensitivity analysis, model updating, etc., that can be used in various disciplines.

1.3 Outline

To answer the research question raised in this work, the following problems are pointed out:

- The quality of models for damage detection in civil engineering.
- The possibility of combining several available methods in a probabilistic framework to assess a chosen inspection method for damage detection.
- The advantage of applying Meta-models to improve the performance of the developed probabilistic framework.
- The influence of available measurements on the reliability of an inspection method for damage detection.

The highlighted problems are discussed in 8 chapters. The first chapter gives the motivation and presents the challenges related to the assessment of inspection methods for damage detection. Also, the necessity of replacing physical models with numerical models is illustrated. The principles of the developed methodology that have been used to solve the research question are introduced.

The second chapter reports the state of the art related to damage types and damage detection. An overview about damage simulation in numerical and physical models is given. Available tools for reliability assessment of inspection methods to detect damage are introduced. Methods for uncertainty quantification and model quality assessment existing in literature are mentioned.

The third chapter illustrates the proposed framework of the developed strategy. At first, the problem definition as an essential step that leads to a proper application of the strategy is presented. Then, the principles of designing experiments used in this work to detect damage are demonstrated. A sensitivity analysis is pointed out as a quality assessment method for a chosen design of the experiment. Considering the information provided by a measured response to a developed framework using a Bayesian probabilistic approach is presented. A probability of detection method will be presented as a global assessment tool of a chosen inspection method. Also, the application of Meta-models to improve the efficiency of the strategy is demonstrated. Moreover, the assessment of a vibration-based method for damage detection in a single degree of freedom system is given. The example illustrates the application of each step of the developed strategy in detail.

In the fourth chapter, a numerical application to a vibration-based inspection method for damage detection is presented. Three degrees of freedom frame structure illustrates the application of the strategy considering a multi-damage scenario and the influence of damage location.

In the fifth chapter experimental studies are presented. The first example includes a one span steel frame structure which is excited by several harmonic excitations. Releasing the hinges at the ends of the beam are used as damage. The influence of considering different damping models in the damage indicator on the reliability of the inspection method is investigated. The second example presents a cantilever. The reliability of the inspection method is investigated taking into account two different numerical models to represent the structure and the studied damage.

In the sixth chapter, the strategy will be applied to a reference object as a real structure. The reference object, which is one of the research training group (*GRK1462*) Bauhaus-Universität Weimar research projects, contains a series of poles that will be used to carry the catenary system of a new railway line. The poles were designed and manufactured to be identical. The main objective of this example is to investigate the performance of a vibration-based inspection method in case of detecting damage in identical civil engineering structures.

In the seventh chapter, the findings of the applications in chapters 4, 5 and 6 will be discussed. The advantage and the limitation of the developed strategy are pointed out. Suggestions to improve the obtained results are given.

In the eighth chapter, a summary of the work and general conclusions will be given. A proposal for future topics is addressed.

Chapter 2

State of the Art

2.1 Damage

2.1.1 Damage and damage identification

Since damage is a general term that may refer to several meanings based on the discipline where it is used, it is necessary to distinguish between damage in different engineering fields. Damage in structural and mechanical systems is defined as changes to the material and/or geometric properties of a studied structure including changes to the boundary conditions and system connectivity, which adversely affect the system's performance, for example, causing undesirable stresses, displacements or vibrations, in present or future and influence its safety, Kiremidjian et al. [1997], Di [2004], Rao and Ratnama [2010], Golubović-Bugarski and Blagojević [2010], Inocente-junior and Mechbal [2010], Dackermann [2010], Stepinski et al. [2013].

Generally, damage detection was defined as an inverse problem that should be solved to identify damage and its characteristics. Four damage identification levels were defined based on the amount of information which a chosen inspection method provides. The damage identification levels are given based on Rytter [1993] and Sinou [2009] as follows:

- Level 1: the determination of the presence of damage in the structure;
- Level 2: the determination of the damage location in the structure;
- Level 3: the quantification of the severity of the damage;
- Level 4: the prognosis of the remaining service life of the damaged structure;

Many previous studies considered damage classification (information about the damage type) as an additional identification level.

On the other hand, Stepinski et al. [2013] defined damage in structural health monitoring as an imperfection, defect or failing which impairs functional and working conditions of engineering structures. Using system analysis, where structures can be modeled as systems with input excitations and output measurable signals, damage can be considered as an additional excitation that results in energy flow and transformation, leading to modifications of output signals. Basseville [2009] used words deviation, change, fault, and damage to reflect a change in the parameter factor of a model of the monitored structure or system.

Generally, there are many challenges that should be considered in case of damage detection in civil engineering structures, Sohn [1998], Sohn and Law [2000], for example, complicated geometry and material properties, large size, which requires instrumentation with a large number of sensors, and the influence of uncertainty due to environmental effects such as temperature, traffic loading, humidity, etc.

2.1.2 Types of damage

Damage in civil engineering structures varies based on the structure type, applied forces, material properties, surrounding environmental conditions, etc. In literature, many types of damage have been investigated to introduce them in numerical or physical models. As a result, the verification and validation of the developed damage detection methods could be accomplished.

Shih [2009] presented an overview of some types of damage in bridges and possible loads that cause damage. It was mentioned that damage in reinforced concrete (RC) structures could be micro-cracking and concrete crushing, reinforcement bars yielding and bond deterioration at the steel-concrete interfaces. On the other hand, cracks, loose bolts, broken welds, corrosion, fatigue, aging, etc., can be possible damage types in steel structures. Yao et al. [2011] mentioned that strong earthquakes could cause welding cracks in steel nodes in spatial steel structures. Also, other local damages because of material corrosion, construction technology, etc., were always easily ignored if the safety of the structures were evaluated. Zhou et al. [2010] investigated stiffness reduction due to shear fractured fibers and delamination of a Carbon-fiber-reinforced polymer (CFRP) damage types in a composite fuel tank. Di [2004] presented examples related to linear and non-linear damage. The classification was based on a response of a structure after damage. A crack that subsequently opens and closes under operating vibration environment was given as an example of non-linear damage. It is mentioned that most of the publications in the damage detection field were focusing on linear damage. The focus of Argatov and Butcher [2011] was on bolted joints damage which could be caused by self-loosening, shaking apart slippage, stress cracking of fatigue, and breaking because of corrosion. Mattson and Pandit [2006] indicated that stiffness degradation could be due structural damage such as cracks, loosened connections, corrosion, etc. Yan and Golinval [2006] investigated

damage types related to loosening of connecting bolts of an airplane wing and fatigue in a street-lighting device. Lam and Ng [2008] mentioned that many detection methods were developed to detect damage such as cracks in beams, reduction in stiffness of structural members and degradation of materials. Ng et al. [2011] mentioned that corrosion, crack, and delamination can influence the guided waves if they are used in engineering structures to detect damage. Fang and Perera [2011] pointed out that cracks in civil engineering structures influence the moment of inertia (I) directly, but only minor changes in material properties such as the modulus of elasticity (E) are expected. Meruane and Heylen [2010] studied multi-crack damage type that can occur in a beam structure due to a static load. Park et al. [2010] used lamb wave to detect surface cracks in a beam structure. Transportation Research Board [2006] gave an overview of several types of cracks that can occur before and after hardening in concrete structures. The cracks have been classified into different groups based on form, primary cause and the time of appearance. For example, plastic settlement of concrete appears after 10 minutes to 3 hours of casting, but sulfate attack needs between 1 to 5 years to appear. In composite materials, transverse matrix cracking, fiber fracture, and delamination damage types can be observed. It was mentioned that delamination is one of the most common types of damage in laminated fiber-reinforced composites, Turon et al. [2006]. Transverse cracks are a characteristic damage state caused by micro delaminations, Wittel et al. [2006]. Jimbo et al. [2012] indicated that typical damage in bridges could be the failure or even damage in shear connectors in composite structure elements due to corrosion, fatigue or unexpected overloading. Hegenderfer et al. [2012] introduced loosening of bolts at a base connection of one column as a damage form. He and Zhu [2011] mentioned that corrosion, cracks, fatigue, and loosening of bolted joints cause stiffness reduction. In Golubović-Bugarški and Blagojević [2010], it was mentioned that damage in a structure could be due to cracks, loose bolts, broken welds, corrosion, fatigue, etc. Marder [1989] mentioned that creep defects cause the majority of failures in power plant components operating under stress and thermal load. Wood [1989] distinguished between two types of flaws, volumetric flaws which can be described by three dimensions and planar flaws which have two main dimensions and the third dimension is neglected. For example, porosity, shrinkage, holes and voids, corrosion thinning and corrosion pitting were considered as volumetric flaws. On the other hand, plating cracks, fatigue cracks, stress-corrosion cracks and welding cracks were considered as planar flaws. Wang [2010] indicated that honeycomb spaces or void type of damage are commonly found in reinforced concrete structures. Honeycomb spaces in concrete are spaces where concrete could not reach during and after casting in the structural elements (for example beams and columns). An overview about the common damage type in structures is presented in table 2.1.

Table 2.1: Studies on damage in concrete/steel/Composite structures

Damage description	Concrete	Steel	Composite (excluding concrete)
Micro-cracking	x	x	x
Concrete crushing	x		
Reinforcement bars yielding	x		
Bond deterioration at the steel concrete interfaces	x		
Loose bolts		x	
Broken welds		x	
Shear fractured fibers and delamination of a Carbon-fiber-reinforced polymer (CFRB)			x
Delamination			x
Creep	x		x
Volumetric flaws (porosity, shrinkage, holes and voids, corrosion thinning and corrosion pitting)	x	x	x
Planar flaws (plating cracks, fatigue cracks, stress-corrosion cracks and welding cracks were considered as planar flaws)	x	x	x
Honeycomb or void	x		

2.1.3 Damage modeling

Damage modeling in numerical models

To utilize numerical models for damage detection, many numerical damage models have been developed. Stepinski et al. [2013] mentioned that damage modeling could be classified analogously to multiscale modeling methods as single and multiscale models. It was mentioned that in the first group, structural damage could be caused by the material's degradation or other phenomena causing the material to lose its load-carrying capabilities. However, multiscale damage modeling concerns the evaluation of microstructural changes and up-scaling their influence on the macro scale which allows for more precise results. Worden and Friswell [2009] mentioned that modeling cracks fall into three main categories: local stiffness reduction, discrete spring models, and complex models in two or three dimensions

The most popular damage models are based on modifying the initial values of the material properties or geometry to represent an equivalent impact of a chosen damage type. For example, a crack in a beam structure was modeled by a non-dimensional flexibility parameter which depends on the depth of a simulated crack. The damage parameter was introduced in one of the boundary conditions of a Bernoulli Euler beam structure, Lam and Ng [2008]. In Ng et al. [2011] damage was introduced in a semi-infinite beam structure by reducing the cross-sectional

area of an element where damage was located. Reducing the elastic modulus value of beam elements has been used to model a damage type in a lightning mast numerical model in He and Zhu [2011]. In the same work, another damage type was modeled by reducing the shear moduli of solid cylinders corresponding to loosened bolted connections in a space frame structure. Fang and Perera [2011] reduced section inertia of damaged elements to model a damage type in a beam element. In Nair et al. [2006] and Krishnan Nair and Kiremidjian [2007] removing braces which had no flexural stiffness was used to simulate damage in a benchmark frame structure. In Wu and Li [2006] changing cross-section areas of braces was used as a damage model in a benchmark steel structure. A damage model based on reducing Young's modulus value of beam material to reduce the stiffness was proposed by Chandrashekhara and Ganguli [2009]. In Zabel [2002] damage was simulated by reducing a stiffness parameter together with an increase of a damping parameter of a 5 degree of freedom studied system. In Yao and Pakzad [2012] damage was simulated by reducing the stiffness of a spring in a 4 degrees of freedom mass-spring-damper studied system. Zhang et al. [2011] assumed that local structural damage is attributed to a change of structural stiffness parameters. In Fang et al. [2005] structural damage was simulated as stiffness loss in one or multiple elements. A damage type was modeled in a carbon fiber reinforced rectangular epoxy plate by reducing the stiffness of some elements. Perera et al. [2009] assumed that no alteration in mass occurred before and after the damage was observed. Therefore, the parametrization of damage has been represented by a reduction factor or damage index of an element bending stiffness. Kranock [2000] indicated that a linear damage type was modeled as an additive change in stiffness matrix. However, it was mentioned that damage influences a member ability to resist deformation under a load, but it should not change the joints that a member was connected to, nor the way that member was connected to those joints. To model nonlinear damage, a stress-strain curve was modified together with changing stiffness. Reddy and Swarnamani [2012] simulated damage in a studied plate by reducing the thickness of one element. Agosto [1997] investigated damage modeling in mathematical models of a cantilever and a simply supported beam by comparing results from a single and multi-degree of freedom systems.

Another type of damage models is based on using spatial elements to represent the influence of a damage type. For example, in Hegenderfer et al. [2012] a rotational spring was used to model the characteristics of a damaged beam, and damage was described using two parameters: location and magnitude. A similar model has been used by Yao et al. [2011] to simulate damaged supports, which were modeled as elastic elements, by reducing rotation stiffness. Linear damage functions, defined in the same way as shape functions were used in finite element theory, have been used by Perera and Ruiz [2008]. Zhang [2007] emulated damage by adding a zero-length element between two connected elements, where assumed damage is located. The vertical bending stiffness of the zero-length element was reduced to represent damage. Wittel et al. [2006] discussed discrete element approach models for various composite materials and demonstrated their capabilities to describe the damage and multiple failures. Di [2004]

proposed damage-detection-oriented models for two typical damage patterns in a plate-like structure which are crack and delamination. Ostachowicz and Krawczuk [2009] reviewed the existing models used for analyses of the influence of fatigue cracks and delaminations on changes in dynamic characteristics of structural elements. Continuous, discrete-continuous, and discrete models were presented.

To develop more accurate damage models, complex numerical models of a studied structure are required. As a result, only simple or limited parts of structures have to be modeled to avoid expensive computational effort. For example, Kögl et al. [2004] employed quarter-point elements placed circularly around the crack tip to model a simple rectangular slab with a single crack of a specific orientation. A generic mesh has been used to model straight interior cracks of arbitrary orientation in 2D slabs of arbitrary geometry. Dackermann [2010] modeled a saw-cut in a three dimensions steel beam by rectangular openings from the soffit of the beam. The mesh density was refined in the vicinity of the defect. Most and Bucher [2007] modeled growing crack discontinuities in concrete by combining a meshless interpolation scheme with finite elements to reduce computational cost. An overview about modeling a crack damage type in reinforced concrete beams was provided by Wang [2010]. Moreover, more complex damage models can be developed using multi-scale modeling approaches. More examples can be found in Worden and Friswell [2009]. An overview about the common damage models in numerical models is presented in table 2.2.

Table 2.2: Damage modeling in numerical models

Model description	Damage	Global model	Example
Modifying the cross-sectional area	Cracks, saw-cut	Beam, plate	Worden and Friswell [2009], Ng et al. [2011]
Reducing the elastic modulus value	Loosened bolted connections	Mast, frame, beam	He and Zhu [2011], Chandrashekhar and Ganguli [2009]
Changing of structural stiffness parameters	local damages, linear damage type	Cantilever, beam, plate	Zhang et al. [2011], Fang et al. [2005]
Reducing a stiffness together with increasing damping		5 degree of freedom system	Zabel [2002]
Reducing the stiffness of a spring	Cracks	4 degrees of freedom mass-spring-damper system, beam, supports	Yao and Pakzad [2012], Worden and Friswell [2009]
Removing braces	Loss of stiffness	Frame structure	Nair et al. [2006], Krishnan Nair and Kiremidjian [2007]
Modifying stress-strain curve with changing stiffness	Nonlinear damage		Kranock [2000]
Non-dimensional flexibility parameter	Cracks	Beam	Lam and Ng [2008]
Linear damage functions similar to shape functions			Perera and Ruiz [2008]
Adding zero-length element and reducing its vertical bending stiffness	Loss of stiffness	A three-span continuous girder bridge	Zhang [2007]
Damage-detection-oriented models	Crack and delamination	Plate-like structure	Di [2004]
Continuous, discrete-continuous, and Descartes models	Fatigue cracks and delaminations		Ostachowicz and Krawczuk [2009], Wittel et al. [2006]
A generic mesh has been used to model straight interior cracks	single crack of specific orientation	A simple rectangular slab	Kögl et al. [2004]
Multiscale, complex models in two or three dimensions, combining a meshless interpolation scheme with finite elements	Micro-structural changes, growing cracks, discontinuities in concrete	Beam	Stepinski et al. [2013], Worden and Friswell [2009], Most and Bucher [2007]

Damage modeling in physical models

Many physical damage models have been developed and introduced in global physical models of the structures. As in numerical models, most of those artificial damage models were intended to represent the influence of a chosen damage on a studied structure.

Cutting process has been often used to represent damage in physical models. For example, He and Zhu [2011] introduced damage in a scaled lightning mast by machining cross-sections that represent the corresponding stiffness reduction where damage was located. Choi et al. [2007] modeled damage as a rectangular opening with certain dimensions from the soffit of a timber beam to reduce the moment of inertia. Ratcliffe [1997] modeled damage in a flat steel beam by cutting a through-thickness slot in the middle, across approximately half the width which introduced a stiffness change, with minimal effect on the mass of the plate. Rao and Ratnama [2010] introduced damage by cutting a slot in the weld of two welded plates. The slot was done by an electrical discharge machining. Golubović-Bugarski and Blagojević [2010] simulated damage in a beam by a cut at a certain location. The propagation of damage was represented by deepening the cut by 1 mm at every level. Similarly, a cut has been used as a damage model in an aluminum beam by Inocente-junior and Mechbal [2010]. Zhang et al. [2011] modeled local artificial damages of a studied frame by replacing three intact steel tubes with damaged ones. Two types of damage were considered. The type-1 was a perforated slot cut in the central length of a tube, and the type-2 was a removal of a layer of material from a surface of a tube. In Zabel [2002] a local structural damage type was simulated by cutting the beam's lower flange of a steel beam five times at two positions. Jimbo et al. [2012] referenced to experiments where damage corresponds to a symmetric notch of increasing depth induced by saw-cutting one end-connector of a composite beam. Kumar et al. [2012] introduced several damage levels in a lightly reinforced concrete beam by first cutting off a beam up to the cover, then cutting up to neutral axis without cutting the reinforcement in tension portion and finally cutting of the reinforcement also in tension portion. In the SIMCES project (System identification to Monitor Civil Engineering Structures) several damage scenarios were introduced in the full-scale Z24 bridge in Switzerland such as pier settlement, Maeck and De Roeck [1999], Basseville et al. [2007].

Other damage models based on removing some parts from a studied physical model have been used. For example, in He and Zhu [2011], a space frame structure was damaged by loosening an upper bolted connection of a diagonal beam. Yan and Golinval [2006] and Meruane and Heylen [2010] created damage by removing connecting bolts on the right-hand side of the wing of an airplane model. Similar damage model was used by Hegenderfer et al. [2012] where bolts at the base connection of one column were removed. In Nair et al. [2006], damage in a benchmark frame structure was simulated by removing braces in various combinations, resulting in a loss of stiffness. Similar damage model was used by Wu and Li [2006] in a benchmark steel structure.

Indirect damage modeling using external loads has been used to introduce cracks in reinforced concrete structures. For example, Fang and Perera [2011] studied a crack damage type which caused by applying a static load at the middle of a beam of a frame structure. In Zabel [2002], structural damage in a simply supported reinforced concrete beam was caused by incrementally increased static loading. Meruane and Heylen [2010] applied a similar criterion to produce two different damaged zones at non-symmetrical locations in a concrete beam. Similarly, Perera et al. [2009] modeled damage in a one-story and one-bay RC frame structure by increasing static concentrated load at the midspan of a beam to gradually introduce cracks into the specimens.

Other special damage models can be found in the literature. For example, Mattson and Pandit [2006] tested a damage detection method on data sets obtained from a test using a LANL (which stands for Los Alamos National Laboratory) damage-simulation test-bed where a damage type such as open-close crack was introduced by installing bumpers that limit the relative motion between two adjacent masses of the device. Uchida et al. [1992] induced fatigue damage experimentally by constant strain cyclic deformation. In a spatial steel structure scaled model studied by Yao et al. [2011], damaged supports were created using a seismic simulation shaking table. In Yao and Pakzad [2012] two 20.4 kg disks were added to the mid-span of a truss structure to approximate a loss of stiffness in a studied system. In the same work, a two-span reinforced concrete bridge model was progressively damaged during various low-to-high amplitude level earthquake excitation tests, all of which were from the 90 degrees and 180 degrees components of the Century City Country Club North record from the 1994 Northridge, California earthquake. Kranock [2000] inflicted damage on a four-bay truss via a device called a Variable Stiffness Truss Member (VSTM), designed by the University of Colorado. By this device, it was possible to reduce the stiffness of the member by one-sixth each time one of the rods was melted, without applying any unmeasured external forces to the truss. Basseville et al. [2003] introduced damage in a reticular structure containing six cylindrical bars connected in 4 spherical joints through screwed bolts at the laboratory by unscrewing one of the joints to generate several levels of stress before simulating a total collapse by completely unscrewing a joint. Dackermann [2010] introduced damage in a two-story steel frame by modifying the connection condition of a beam-column joint. Another damage scenario was investigated by adding masses to crossbeams in different locations. An overview of the common damage models in physical models is presented in table 2.3.

Table 2.3: Damage modeling in physical models

Model description	Damage	Global model	Examples
Modification of the cross section by cutting a slot	Stiffness reduction, local damage, notch, pier settlement	Beam, frame structure, plates, bridge (concrete, steel, timber, composite)	He and Zhu [2011], Choi et al. [2007], Rao and Ratnama [2010], Golubović-Bugarski and Blagojević [2010]
Removing connecting bolts	Loosening bolted connection, loss of stiffness	Beam, wing of an airplane model, base connection	He and Zhu [2011], Yan and Golinval [2006], Meruane and Heylen [2010], Hegenderfer et al. [2012]
Applying a static load	Crack	Beam, frame structure (concrete)	Fang and Perera [2011], Perera et al. [2009], Zabel [2002], Meruane and Heylen [2010]
Installing bumpers that limit the relative motion between two adjacent masses	Open-close crack	Eight-degree of freedom damage simulation test-bed,	Mattson and Pandit [2006]
Constant strain cyclic deformation	Fatigue	SA508 and Type 304 steel	Uchida et al. [1992]
Seismic simulation shaking table	Damaged supports	Reinforced concrete bridge model	Yao et al. [2011], Yao and Pakzad [2012]
Adding masses	Loss of stiffness	Truss structure	Yao and Pakzad [2012], Dackermann [2010]
A device called a Variable Stiffness Truss Member	Reduce the stiffness	Four-bay truss	Kranock [2000]
Unscrewing one of the joints	Several levels of stress	6 cylindrical bars connected in 4 spherical joints	Basseville et al. [2003]
Modifying the connection condition of a beam-column joint	Boundary condition changes	Two-story steel frame	Dackermann [2010]

2.1.4 Damage detection inspection methods

To detect damage and identify its characteristics, an inspection method should be chosen. Many inspection methods have been developed for damage detection in engineering structures. Inspection methods can be classified based on several criteria. For example, global and local, model-based methods and data-based methods (Signal-based), vibration-based traditional and modern (non-traditional) methods, or real-time and non-real-time methods.

Global inspection methods attempt to simultaneously assess the condition of the whole structure, especially large and complicated structures, whereas local methods focus on non-destructive evaluation tools on specific structural components. Vibration-based global methods assess the variation of vibrational characteristics under specific loads.

Local inspection methods monitor a small area of the structure surrounding the sensor (sensors) using measurements of structural response to certain applied excitation, Stepinski et al. [2013]. However, for large and complicated structures in the invisible or closed environment, it is complicated to detect damage using a local damage detection method, because they can only be used to inspect some special and accessible components of a structure. Moreover, they require prior knowledge about damage location.

Vibration-based traditional inspection methods refer to methods that utilize some characteristics of a structure to detect damage, for example, natural frequencies, modal damping, modal strain energy or mode shapes, etc. However, modern inspection methods have been used for structural damage based on online measured response signals of structures in service. These methods use modern signal-processing techniques and artificial intelligence such as wavelet analysis and neural network as analysis tools.

In model-based methods, a mathematical model is developed to understand the structural behavior and to establish correlations between specific damage conditions and changes in structural response. Shih [2009] indicated that the main disadvantage of model-based methods lies in the fact that the physical parameters obtained from an updating procedure may be unrelated to the actual damage scenarios. With non-model-based methods, it could be possible to detect damage without prior knowledge of the model of a structure. Yuen [2010] mentioned that most existing global structural health monitoring methods use dynamic model updating to determine local loss of stiffness by minimizing an objective function between experiments and a FE model.

Many factors influence the result of an inspection method such as damage type, structure type, experimental setup, post-processing outcomes by means of different damage indicators, etc. More information about different inspection methods and their classifications can be found in Rytter [1993], Doebling et al. [1996], Kiremidjian et al. [1997], Kranock [2000], Di [2004], Fang et al. [2005], Yan et al. [2007], Sinou [2009], Shih [2009], Golubović-Bugarški and Blagojević [2010], Wang [2010], Haghighi [2010], Dackermann [2010], Stepinski et al. [2013].

Most of the developed inspection methods have been employing damage indicators based on the modal parameters of a studied structure. For example, Ratcliffe [1997] developed a technique which required applying a finite difference approximation of Laplace differential operator to mode shapes of a damaged structure. No a priori knowledge of the undamaged structure was required. Maeck and De Roeck [1999] developed a damage detection and quantification method based on the direct determination of stiffness based on mode shape curvatures. The method was intended to be an alternative to damage identification by updating a numerical model of a studied structure. Ahmadian et al. [2000] developed two damage indicators based on mode shapes to localize damage. The undamaged substructure was identified based on an idea that higher modes will not participate in the deflections of undamaged substructures. The proposed method used measured displacements from a structure and predictions from a mathematical model. Khiem [2006] applied an inverse problem method to detect a crack in a structure. The method was based on constructing a dynamic stiffness model of a cracked frame structure. Natural frequencies, obtained from a modal test, were formulated and solved using a nonlinear programming method. Perera and Ruiz [2008] developed a multistage scheme for damage detection for large structures. The scheme based on experimental modal data gained by accelerometers and on finite element model updating methods. An objective function was based on modal flexibility, and another objective function depended on mode shapes and frequencies, combined to be depended on damage location, was formulated.

Shih [2009] developed a multi-criteria procedure for damage assessment of structures by combining natural frequencies, modal flexibility and modal strain energy between healthy and damaged structures. Perera et al. [2009] presented an identification algorithm for assessing structural damage considering differences between frequencies and mode shapes before and after damage. The algorithm was based on a finite element updating procedure and took a modeling error into account. Wang [2010] proposed a new modal strain energy based damage detection method based on the assumption that most damage will result in an equivalent stiffness change, other than the geometric property changes. The improvement was made by normalizing mode shapes curvature. The method was developed mainly for reinforced concrete structures. Tomaszewska [2010] studied the influence of a modal identification error on damage detection using damage indicators based on modal curvature and structural flexibility. He and Zhu [2011] investigated forward and inverse problems in damage detection and localization using natural frequencies' variation as a damage indicator. Fang and Perera [2011] presented a damage identification method based on a response surface based model updating. The response surface was developed using D-optimal designs, which are experimental designs generated from a computer algorithm, which require a minimum number of numerical samples. Physical properties such as Young's modulus and section inertia were chosen as inputs and modal frequency as an output. Jimbo et al. [2012] proposed an inverse problem-based method for damage detection based on finite spectral data associated with a given set of boundary conditions. A cost function which includes eigenvalue data and transversal displacements

of eigenfunctions have been used. The procedure was tested on a composite beam with different damage scenarios. Di [2004] combined both damage indices formulated based on modal flexibility and its derivatives with a model-based updating method to improve the efficiency and the reliability of damage detection. More information related to inspection methods based on the dynamic properties of a studied structure can be found in Worden and Friswell [2009].

Many inspection methods based on frequency response functions properties have been used as a damage indicator. For example, Araújo dos Santos et al. [2005] presented a frequency response functions' sensitivities based technique for damage detection. It was mentioned that better identification results were obtained in lower frequency ranges. Fang et al. [2005] developed a methodology for structural health monitoring to determine the location and the severity of crack damage by establishing an input-output relation between frequency response function characteristics of both an intact and a damaged structure, and damage location and severity using a neural network. Golubović-Bugarski and Blagojević [2010] present a method which uses frequency response functions as characteristics of the dynamic response of a mechanical system to detect damage. Dackermann [2010] proposed two artificial neural network vibration-based damage detection methods. The first was based on a damage index and the second was based on directly measured frequency response functions data. Reddy and Swarnamani [2012] investigated the effectiveness of a frequency response function curvature energy damage index to detect and localize damage.

Instead of studying changes in the frequency domain to detect damage, both frequency and time domains can be investigated by using wavelet transformations. Taha [2006] presented the state of the art of the application of wavelet transformations into structural health monitoring. Zabel [2002] investigated the sensitivity of a wavelet-based first level damage indicator for damage detection in reinforced concrete structures considering impulse response wavelet coefficients' energy components. Zhu et al. [2011] analyzed accelerations of a structure under impact loads and developed a novel damage indicator based on wavelet packet transform.

Other methods based on state space representation have been used. Basseville et al. [2003] proposed a damage detection method based on a residual generated from a subspace-based covariance-driven identification method and on the local statistical approach. Basseville et al. [2007] presented an overview of the theory and the practice of damage identification methods based on input/output and output-only subspace identification algorithms. Inocente-junior and Mechbal [2010] presented a methodology for structural health monitoring based on subspace identification and residue generation.

Statistical approaches were used to develop damage indicators based on statistical properties of measured time histories. For example, Worden and Manson [2000] utilized a Kernel Discriminant Analysis (KDA), which was based on a statistical technique, to classify acceleration data recorded from a ball bearing in five different states: a healthy condition and four distinct damage states. Fugate et al. [2001] used residual errors, which were

obtained after using an auto-regressive model to fit measured acceleration-time histories from an undamaged structure, as a damage indicator. Yan et al. [2005] presented a principal component analysis based method for damage detection during the monitoring of a structure. A residual error was used as a statistical damage indicator. Mattson and Pandit [2006] proposed that an estimate of an auto-regressive model residual series standard deviation together with a repeatable threshold level can be used to identify and localize damage without explicit knowledge of an undamaged structure. Yan and Golinval [2006] presented a method based on subspace identification concepts and statistical process techniques to detect small-sized structural damages. The influence of artificial or environmental vibrations on output-only acceleration time histories was considered. Zhang [2007] presented a 4-step statistical damage identification scheme for bridge health monitoring using acceleration as a structural response. Krishnan Nair and Kiremidjian [2007] modeled acceleration time histories using auto-regressive moving average (ARMA) processes. As a result, a feature vector was obtained and modeled using Gaussian Mixture Models. The Mahalanobis distance between the mixture in a damaged and a baseline (undamaged) was used as an indicator of damage extent. Rao and Ratnama [2010] demonstrated an approach for health monitoring of structures to identify damage using acceleration-time data obtained from piezoelectric accelerometers by combining time series autoregressive models and exponentially weighted moving average (EWMA) control charts. de Lautour and Omenzetter [2010] used an Artificial Neural Network to classify damage cases or estimate remaining structural stiffness by training it using the coefficients of auto-regressive models used to fit acceleration time histories. Haghighi [2010] proposed a multivariate auto-regressive models based method to extract damage features from vibration responses measured at multiple sensor locations. Yao and Pakzad [2012] proposed to use model spectra and a residual auto-correlation, together with resampling-based threshold construction methods to improve the performance of statistical methods based on using auto-regressive models. The statistical models have been used to represent simulated and real acceleration data. More information about statistical based inspection methods can be found in Basseville [2009]

Probabilistic approaches have been used to develop damage detection frameworks. For example, Sohn [1998] developed a probability-based framework using a Bayesian probabilistic approach for global damage detection in case of continuous monitoring of a structure. The most probable damage event was obtained by comparing relative probabilities for different damage scenarios. The difference between analytical and experimental vibration properties was used to estimate relative posterior properties. A nondimensional parameter was used as damage indicator. A structure was considered damaged if a value of the defined damage indicator was less than a predefined threshold. Wu and Li [2006] proposed a two-stage eigensensitivity-based finite element model updating procedure for structural parameter identification and damage detection. The procedure is based on combining both weighted least squares and Bayesian estimation methods to identify beam-column joints stiffness and Young's modulus of a studied structure. Then, the same procedure was applied after introducing damage to the structure to

detect damage. Yuen et al. [2006] presented a Bayesian system identification based probabilistic method for damage detection in a structural system considering noisy, incomplete inputs and response measurements. Data obtained from initial undamaged and damaged states of a studied system was used to compute the probability of damage of various levels in specified locations. An approximation was used to represent a conditional probability density expansion of updated probability functions of studied input parameters. Zhang et al. [2011] proposed a probabilistic method to identify damage of structures with uncertainties under unknown input. A damage index was obtained from the statistical parameters of physical parameters of the intact and damaged structure. Hegenderfer et al. [2012] utilized modal analysis and Bayesian inference model calibration techniques to detect connection damage in steel frames. A developed finite element model was calibrated against experimental data using natural frequencies. Ng et al. [2011] proposed a two-stage optimization strategy using a Bayesian statistical framework to present a model-based probabilistic damage characterization methodology for beams using guided waves. Chandrashekhar and Ganguli [2009] applied a probabilistic analysis to develop a robust fuzzy logic system with new fault isolation (sliding window) technique for damage detection. A Monte Carlo Simulation was used to calculate statistical properties of the variation in natural frequencies including material properties' uncertainty. Simoen et al. [2013] applied Bayesian calibration techniques to quantify uncertainty in case of progressive damage of a 7-story structure.

Other methods and damage indicators have been used in case of special problems. For example, Uchida et al. [1992] applied a positron annihilation lineshape analysis method to detect fatigue damage in different types of steel. Kranock [2000] presented damage detection filters, which were model-based observers, as an alternative to other global methods for structural health monitoring. Futakawa et al. [2004] conducted acoustic vibration measurement to investigate the correlation between erosion damage and acoustic vibration in an electric Magnetic Impact Testing Machine. Kögl et al. [2004] presented a transient finite element calculation based approach to detect cracks in concrete slabs using a Fast Fourier transform analysis. Lauwagie et al. [2002] compared the modal parameters of an undamaged beam to the vibration behavior of the beam subjected to controlled damaging. Scanning Laser-based equipment was used to measure the response of the beam. Meruane and Heylen [2010] implemented a real-coded parallel Genetic algorithm, which is a Genetic algorithm based on real number representation, to detect structural damage based on modal data. Boonlong [2014] proposed a cooperative co-evolutionary genetic algorithm for an optimization problem with a large number of weak coupling decision variables for damage detection. Shi et al. [2010] employed a mature computer vision technology to capture a static deformation profile of a structure. Profile analysis methods were applied to detect locations of damage. Kumar et al. [2012] presented an algorithm for damage detection in lightly reinforced concrete beams based on changes in the power spectral density of the measured acceleration. Bastani et al. [2012] applied an adaptive linear prediction model, which was developed using data from an undamaged structure, for damage detection.

Tables 2.4 and 2.5 present an overview about the inspection method for damage detection.

Table 2.4: Damage detection inspection methods part 1

Reference	Frequency	Mode shape	FRF	Frequency-time domain	Time domain	Space stat	Statistic	Probabilistic	Data- or Model-based
Ratcliffe [1997]		x							Model
Maeck and De Roeck [1999]		x							Data
Ahmadian et al. [2000]		x							Model
Khiem [2006]	x								Model
Perera and Ruiz [2008]	x	x					x		Model
Shih [2009]	x	x							Data
Perera et al. [2009]	x	x							Model
Wang [2010]		x					x		Data
Tomaszewska [2010]	x	x							Data
He and Zhu [2011]	x								Model
Fang and Perera [2011]	x								Model
Jimbo et al. [2012]	x	x			x				Model
Di [2004]	x	x							Model
Araújo dos Santos et al. [2005]			x						Data
Fang et al. [2005]			x						Data
Golubović-Bugarski and Blagojević [2010]			x						Data
Dackermann [2010]	x	x	x						Data
Reddy and Swarnamani [2012]		x	x				x		Data
Taha [2006]				x					Data
Zabel [2002]				x					Data
Zhu et al. [2011]				x					Data
Basseville et al. [2007]						x			Data
Inocente-junior and Mechbal [2010]						x			Data
Worden and Manson [2000]					x				Data
Fugate et al. [2001]					x				Data
Basseville et al. [2003]						x			Data

Table 2.5: Damage detection inspection methods part 2

Reference	Frequency	Mode shape	FRF	Frequency-time domain	Time domain	Space stat	Statistic	Probabilistic	Data- or Model-based
Yan et al. [2005]				x			x		Data
Mattson and Pandit [2006]				x			x		Data
Yan and Golinval [2006]						x	x		Data
Zhang [2007]				x			x		Data
Krishnan Nair and Kiremidjian [2007]				x			x		Data
Rao and Ratnama [2010]				x			x		Data
de Loutour and Omenzetter [2010]				x			x		Model
Haghighi [2010]				x			x		Data
Yao and Pakzad [2012]				x			x		Data
Sohn [1998]	x							x	Model
Wu and Li [2006]								x	Model
Yuen et al. [2006]								x	Model
Hegenderfer et al. [2012]	x							x	Model
Ng et al. [2011]								x	Model
Chandrashekar and Ganguli [2009]	x							x	Data
Simoen et al. [2013]		x						x	Model
Uchida et al. [1992]		positron annihilation lineshape analysis based method					x		Data
Kranock [2000]		Filters based method				x	x		Data
Futakawa et al. [2004]		Acoustic vibration based method							Data
Kögl et al. [2004]		Fast Fourier transform based method							Data
Lauwagie et al. [2002]		Scanning laser modal equipment based method							Data
Meruane and Heylen [2010]		Parallel Genetic algorithm based method	x						Model
Boonlong [2014]	x	Cooperative co-evolutionary genetic algorithm based method	x						Data
Shi et al. [2010]		Static deformation profile based method using camera							Data
Kumar et al. [2012]		Changes in the power spectral density of the measured acceleration							Data
Bastani et al. [2012]		Adaptive linear prediction model based method					x		Data

2.2 The reliability of an inspection method

2.2.1 Reliability

Generally, reliability refers to the probability that a system performs successfully without failure for a specified period. Reliability has been used in different engineering disciplines. For example, risk analysis, environmental protection, quality assessment, optimization of maintenance and operation, engineering design, verification of quality/reliability, etc. The principles of reliability and its applications were presented in Rausand and Høyland [2004].

The reliability and the quality of several inspection methods in case of civil engineering structures were inspected by Rytter [1993] considering nine critical issues:

1. usability for global inspection;
2. requiring cleaning;
3. sensibility to measurement noise;
4. ability to stand alone;
5. detection of internal defects;
6. detection of defects far away from the sensors;
7. detection of defects in areas with one surface accessible;
8. detection of defects in areas with two surfaces accessible;
9. estimation of the size and location of the defect.

Based on that evaluation, Rytter [1993] found that vibration monitoring is one of the promising methods that can be used to detect damage in civil engineering structures.

2.2.2 Design of experiments

Generally, in the case of civil engineering structures, geometry, boundary conditions, and physical phenomena are so complicated that it is sometimes beyond the present technical capabilities to formulate satisfactory analytical or numerical models and approaches. In this case, experiments are necessary to gain more information about studied system behavior, Coleman and Steele [2009]. Structural health monitoring (SHM) and nondestructive testing (NDT) have often been used to describe the process of nondestructively evaluating a structural condition. The difference between SHM and NDT is that SHM requires a global and on-line

implementation of various damage detection technologies, which require periodically spaced measurements while NDE is commonly applied offline and locally in regions of expected damage, Staszewski and Worden [2009]. To reach the objectives of a SHM or an NDT, it has to be designed to obtain useful information about the system under investigation. For this reason, many questions should be addressed when a test has to be designed. These questions are related to many factors that influence the designed test, for example, goals, accuracy, physical principles, type of tests, tested variables, measured outputs, type of instruments, measurement points, limitation of the test, reporting result, etc.

The reliability of an inspection method depends directly on a chosen design of experiment (DOE). DOE for vibration-based methods includes a wide range of problems that should be taken into account before conducting experiments. For example, type and location of sensors, technical issues related to cables and acquisition systems, time of the acquisition and frequency rate, preparing specimens, etc. Moreover, each inspection method can have some special properties which lead to a different or unique DOE.

Rytter [1993] introduced a step by step strategy to perform a vibration-based inspection. In this strategy, the designing and planning of the measuring program are based on the results from sensitivity analysis. The primary objective of the sensitivity analysis is to choose the damage indicators that can detect damage in the selected areas of a structure. It was mentioned that it is important to include all potential not damage depending variation of the structural properties during the sensitivity analysis.

Although DOE was not mentioned explicitly, many previous studies investigated the influence of test arrangements on damage detection. For example, Araújo dos Santos et al. [2005] studied the effect of the number of frequencies and mode shapes, frequency range, number of sensors and excitation location on damage detection using a vibration-based method. Park et al. [2010] proposed a method to achieve a tradeoff between data transmission rate in wireless sensors and damage detection capability based on wavelet coefficients. Shih [2009] provided an overview of the functionality of different types of sensors and the types of excitations that can be used for structural health monitoring. Yan et al. [2007] mentioned that selecting an optimal number and optimal positions of sensors to obtain full information related to structural damage to be detected is a very important factor. Kiremidjian et al. [1997] indicated that the conceptual design of a civil, structural damage monitoring system was based on a simple hierarchical scheme consisting of three distinct but interrelated levels: sensor, structure and central monitoring facility. Moreover, a robust, an efficient, and economic damage detection system critically depend on the information extracted from sensors. However, due to economic constraints, it is impossible to completely instrument civil structures for damage monitoring. Reddy and Swarnamani [2012] investigated a relationship between a developed damage index and a considered frequency range (bandwidth) to provide further information about the choice of optimum frequency range response analysis. Moreover, the influence of the excitation location

for damage detection was considered. Kögl et al. [2004] indicated that the detection of cracks depended upon the type and frequency of excited vibrations. Sohn [1998] indicated that load-dependent Ritz vectors were more sensitive to damage than corresponding modal vectors. As a result, careful selection of excitation can lead to better damage detection. Billmaier and Bucher [2013] applied a selective sensitivity approach to obtain a structural response which is sensitive to a certain group of parameters and insensitive to others. As a result, the ill-posed problem can be solved when a model updating procedure is applied to estimate the required parameters. Reaching this goal required using selective, sensitive excitations. It was indicated that the application of periodic excitation time series leads to reliable and stable results. Friswell et al. [1997] investigated the relationship between the best selection of subset parameters that should be updated and damage location identification. The study was based on an idea that the main difference between model updating and damage/error location was that in damage location only a limited number of parameters were likely to be in error. A finite element model was used to model several damage scenarios.

Since one of the objectives of designing experiments is to estimate the optimal location and the number of sensors, Yuen [2010] investigated this issue to enhance the quality of a model parameter estimation. It was mentioned that the amount of information depends on the sensor configuration. Although the main goal was to be more informative about the condition of a structure, it was not always good to search for the most optimal configuration because it can be computationally prohibitive and not robust. On the other hand, the suboptimal configuration can be more robust. Papadimitriou and Lombaert [2012] studied the influence of spatially correlated prediction errors on the optimal sensor locations for parameter estimation. The information entropy, which was built from the parameter uncertainty identified by applying a Bayesian identification framework, was used as a performance measure of a sensor configuration. A forward and backward sequential sensor placement was introduced to select a sensor configuration that minimizes the information entropy. It was concluded that an optimal sensor location design depends on the type of parameters considered for estimation. Also, the spatial correlation of the prediction error tended to shift a sensor away from the existing sensor location.

Stepinski et al. [2013] mentioned nine major steps required for designing a structural health monitoring system:

1. Choosing the type of damage that should be detected;
2. Choosing an output which is sensitive to a chosen damage;
3. Developing method algorithms;
4. Method simulation;
5. Laboratory validation;

6. Testing the method on a chosen structure;
7. Testing the system performance using the probability of detection;
8. Checking the implementation and the operation of the system;
9. The installation and operation phase.

Moreover, it was mentioned that a sensitivity analysis of a structure's response to damage accuracy is a basic tool which helps to design a monitoring system. Furthermore, an overview related to designing a structural health monitoring system was provided by Kiremidjian et al. [1997].

In case of local inspection methods for NDT, the U.S. Department of Defense published a handbook as inspection guidance for more reliable NDT in 1999. The handbook was updated in 2004 and 2009 MIL-HDBK-1823A [2009]. This handbook gives detailed guidance about experimental design of the most popular local inspection methods to obtain a reliable probability of detection curves, for example, Eddy current test system, Fluorescent penetrant inspection test system, etc. Generazio [2009] presented a design of experiment tool for validating probability of detection curves. The tool was based on the application of the binomial distribution to a set of discontinuities that have been grouped into size classes, where each class has a width.

2.2.3 Probability of detection

Nondestructive testing (NDT) has been used in different fields and for many purposes. Rummel and Matzkanin [1997] presented the application of NDT to general industrial process control, general exchange in commerce and to maintenance purposes among other fields. Recently, NDT has been applied in civil engineering research and applications. This arises from the need of evaluating the reliability of the structures and determining their continuing service beyond a designed lifetime. A review of the development of NDT reliability assessment between 1970 and 2000 can be found in Singh [2000].

Statistical approaches have been applied to assess the reliability of an NDT using performing tests several times on a large number of specimens. The specimens should be divided into several groups. Each group has a certain size of the damage. Finally, the probability of damage detection (POD) curves were computed and used to check the reliability of an NDT. The analysis of statistical data to obtain POD curves in both hit/miss and signal response methods were explained in detail by Berens and Hovey [1981] and Berens [1989]. Different examples related to applications and limitations of this approach in different fields were presented in Petrin et al. [1993] as well as by Rummel and Matzkanin [1997], Georgiou [2006], Müller et al. [2006] and Gandossi and Annis [2010]. Furthermore, many studies have been performed

to investigate the reliability of POD curves as an assessment tool. For example, the influence of different factors on POD curves which were estimated using a hit/miss method was discussed in Annis and Gandossi [2012].

Calculating reliable POD curves need a large number of specimens and experiments which can be costly and time-consuming. For most civil engineering applications such investigations are impossible due to the uniqueness of the systems. However, recently, the statistical methods have been supported by a new tool that makes their applications more practical, simpler and less expensive. This tool is called Model-Assisted method, Knopp et al. [2006], Thompson et al. [2009], Mandache et al. [2011], Stepinski et al. [2013] where numerical models have been developed to estimate POD curves.

Another method to compute POD curves was presented in Guo et al. [2011]. The developed method which is called truncated logistic regression method was based on using a model to combine different nondestructive evaluation (NDE) measurements into one optimal POD curve and to overcome the uncertainties introduced by naturally occurring flaws and to cancel out the influence of lacking knowledge of undetectable flaws.

Several probabilistic models have been proposed to fit the variation of measured data and estimate POD curves. For example, Lockheed, Probit, Log Probit, Log Odds, Arcsine, etc. It was found that Log Odds and Log Probit had better performance than other models for most applications, Stepinski et al. [2013].

To evaluate an inspection method for damage detection at least two of four different probabilities should be used. Generally, the probability of detection and the probability of false alarm have often been used to perform the evaluation. The probability of detection (POD) refers to the probability that an inspection system detects damage when it is present, the probability of false alarm (PFA) or probability of false positive (PFP) refers to the probability that an inspection system shows that there is damage when it is not, Stepinski et al. [2013]. The probability that an inspection system fails to detect damage when it is present (1-POD) and the probability that an inspection system shows that there is no damage where there is none (1-PFP) were rarely used.

2.3 Model quality

2.3.1 Models

A Model is a description of a specific physical phenomenon including geometrical, material, initial, and boundary data, Thacker et al. [2004]. Generally, models are imperfect abstractions of reality for specific purposes, and the usefulness of a model is based on its accuracy and reliability, Loucks et al. [2005]. Therefore, understanding the physical problem is the most

important for modeling, Yuen [2010]. As a result, a conceptual model can be developed based on this understanding. In the next step, the conceptual model should be transformed into an experimental model and/or a mathematical model. A mathematical model is represented by equations containing known and unknown parameters. Mathematical models can be classified into different categories. For example, linear and nonlinear, static and dynamic, black box and white box, etc. Models can also be classified as physical-based models. Physical-based models have been developed based on a physical behavior of a studied system, for example, laws of mechanics, continua models, etc. Non-Physical-based models have been developed to fit available data such as Semantic models, Meta-models, Probabilistic models, etc., Ciloglu [2006].

Mathematical models are the backbone of computational models. Computational models can be analytical models or approximated models based on a discretization method such as a Finite Element method. As a result, a model can be implemented and solved by available computational effort.

An experimental model can be developed based on the conceptual model to conduct experimental tests to gain more knowledge about a studied system. An experimental model can be a part of a studied structure or a scaled model at the laboratory.

2.3.2 Uncertainty

Thacker et al. [2004] defined uncertainty as a potential deficiency in any phase or activity of modeling or an experimentation process that is due to inherent variability or lack of knowledge. The process of characterizing uncertainty is called uncertainty quantification. Uncertainty quantification is essential for further investigations such as damage detection, Yuen [2010]. Coleman and Steele [2009] used the word uncertainty to describe the degree of goodness of measurement, experimental result or analytical (simulation) results. The degree of goodness describes how well the model results match the data.

In literature, uncertainty can be aleatory or epistemic. Aleatory uncertainty represents a random behavior of a phenomenon. Generally, aleatory uncertainty cannot be reduced. Epistemic uncertainty is due to the lack of complete knowledge about a phenomenon. Epistemic uncertainty can be reduced by doing more investigations. More information about this topic can be found in Thacker et al. [2004], Shih [2009], Reuter [2012], Most [2011].

Generally, many random phenomena cannot be predicted precisely, Loucks et al. [2005]. However, ignoring such random phenomena is ignoring reality. There are many ways to deal with uncertainty. For example, using a mean or median value or use critical values to represent the worst case. Another approach to represent uncertainty is using a probabilistic model which is employed to perform an uncertainty analysis to obtain a probability distribution of model

outputs.

There are many sources of uncertainty in case of damage detection. For example, Law et al. [2001] indicated that if the number of measured degrees of freedom is significantly smaller than the number of the degrees of freedom of the analytical model, then severe degradation of accuracy in model updating and damage detection is expected. Araújo dos Santos et al. [2005] demonstrated that for small damage, measurement errors due to noise and other uncertainties have the primary influence on the identification quality. However, in the case of massive damage, if measurement data was not sufficient, damage could not be detected. Yan et al. [2007] mentioned that in practice collectible sample data of structural damage was always insufficient and limited. Moreover, structural damage detection is a complex problem since there are still a lot of difficulties in the practical application of inspection methods because of the complexity of structural damage and the uncertainty of various influencing factors. Chandrashekhar and Ganguli [2009] investigated the influence of material properties' uncertainty on frequency as an evaluation damage parameter. Perera et al. [2009] indicated that modeling errors in a baseline model whose effects exceed a modal sensitivity to damage were critical and made an accurate estimation of damage impossible. Meruane and Heylen [2010] considered initial errors in a numerical model when a genetic algorithm is used for damage detection. False damage detection was avoided by using damage penalization.

Yuen [2010] mentioned that a lot of assumptions were considered when a model was developed. For example, a building with relatively uniform properties over the height can be simplified as a continuous beam with its structural properties distributed uniformly along the length, considering that only low order modes contribute to a model response, neglecting the shear effect in slender buildings, assuming that a dynamic behavior is well approximated by linear dynamic models, etc. Moreover, it was mentioned that not only damage is affecting the health of the structure but also different factors such as temperature and relative humidity. An example was given to demonstrate the influence of the temperature on the fundamental frequency of the 22-story structure which was monitored for six months. The monitoring shows that the variation of the fundamental frequency because of temperature can reach 13%. Also, the uncertainty of the measured data due to aliasing and leakage, short duration of measurement and insufficient data should be considered. Zhang et al. [2011] indicated that because of measurement uncertainty, deterministic simultaneous identification methods of structural parameters and inputs were limited in application. Yan et al. [2005] studied the influence of varying environmental and operational conditions on the performance of a structural health monitoring system to distinguish between changes due to these conditions and due to damage. Sohn [1998] indicated that complicated geometry and material properties made accurate modeling of civil engineering structures very difficult. Moreover, in the case of analytical models, if mode shape expansion or model reduction techniques were applied, damage could be detected far from its actual location. In case of experiments, using ambient vibration tests could cause lack of data since higher order

mode shapes could not be obtained.

2.3.3 Model quality assessment methods

Uncertainty-based model assessment methods were investigated by Most [2011]. The influence of model choice on a model output was considered. Two methods were proposed to evaluate the quality of a model without measurement data. A specific procedure was presented to choose a reference model. The objective was comparing several relevant models and selecting the optimal model. It was mentioned that a reference model could be the most complex one. Yuen [2010] indicated that more complicated models could fit data better than a less complicated one which has fewer adjustable/uncertain parameters. In this case, the most complex one is optimal. However, this model is an over-fitted model and may lead to poor results. Therefore, a simpler model is preferable. The complexity of a model can be investigated by the Ockham factor which is independent of the number of the degrees of freedom. The Ockham factor has been used to choose the best model including the complexity where not only the number of the parameters was tested but also the possibility to reduce parameter uncertainty. The Ockham factor is based on the idea that: 'it is vain to do with more what can be done with fewer', *William of Ockham*. However, less uncertainty does not indicate better fitting. Sometimes the Ockham factor was as a robustness measure. Moreover, it is important to investigate the sensitivity of a model around an optimal parameter. Loucks et al. [2005] mentioned that it is not a good idea to add complexity to a model if the increased complexity is based on processes whose parameters are difficult to measure.

Bombasaro [2011] investigated the quality of load models for a vortex shedding phenomenon which was employed to design structures against fatigue. The studied models were compared and evaluated based on experimental data taken from literature by applying a Bayesian model selection approach and a response surface analysis. Araújo dos Santos et al. [2005] studied damage detection using a vibration-based method considering complete and incomplete models. if measurement data were available for all degrees of freedom, the model was considered complete otherwise the model was considered incomplete. Law et al. [2001] proposed a damage detection-oriented modeling approach to improve the sensitivity of the results to small physical changes and to reduce the complexity of a model by decreasing the required number of the degrees of freedom. The approach was based on using super-elements to model large-scale structures and sub-elements to model individual structural components. The performance of the developed numerical model and updating method was quantified by the errors in mode shapes before and after updating. Wang [2010] presented a procedure to develop a reliable finite element model of a reinforced concrete beam considering damage. The influence of mesh density was investigated. A validation process was introduced. The validation was accomplished by applying three methods: performing a correlation analysis, comparing natural frequencies

and comparing mode shapes. He and Zhu [2011] mentioned that accurate modeling of a studied structure and a robust inverse algorithm are essential to detect damage by observing changes in natural frequencies. Sohn [1998] utilized a branch-and-bound search scheme to expedite the search for the most likely damage case without checking all the possible combinations of damage scenarios.

Coleman and Steele [2009] investigated the quality of data obtained from different types of models based on data uncertainty which was estimated by applying verification and validation principles. Verification has been used to indicate if the equations which represent a system (Real-world) were solved correctly. Validation has been used to indicate if a model was representing the Real-world accurately. Thacker et al. [2004] mentioned that verification and validation are processes that accumulate evidence of the model's correctness or accuracy for a specific scenario. In other words, they quantify the level of agreement between experiments and model prediction. However, they do not prove that a model is correct for all possible scenarios. An overview of several validation methods and their application in engineering can be found in Hills and Trucano [1999].

In Research Training Group 1462 in Weimar, several approaches have been developed to assess the performance of numerical models in engineering disciplines. For example, Keitel [2011] developed a method to evaluate the quality of concrete creep models with and without considering experimental data. A total uncertainty of a predicted creep, which includes uncertainties of measurements, the internal uncertainty of the creep phenomenon and uncertainty of the model prognosis, compliance has been used to assess the quality of a creep model. The total uncertainty was obtained by combining both parameters and model uncertainty. A Bayesian updating approach has been used to update the stochastic properties of creep model parameters if experimental data was available. Moreover, a Bayesian model selection was applied to evaluate rheological creep models with hierarchical complexity. Graph theory and sensitivity analysis were employed to assess the quality of global models which were developed by coupling creep models as partial models with other partial models such as shrinkage models, geometry, loads, material models, etc. Reuter [2012] presented an approach to assess the quality of complex engineering models in structural engineering. The approach was developed assuming that no calibration was accomplished before. Multi-criteria categories were applied. The model quality was represented by combining test results of system behavior, system functionality and system dependability using weighting factors which should be chosen based on the objective of the evaluation. Karaki [2011] proposed an extension concept of uncertainty and sensitivity analysis to assess the dynamic response of a coupled model in a bridge considering time-dependent vehicular loading. The influence of considered parameters and models on the dynamic response was investigated. The model quality was evaluated by a total uncertainty concept. Nikulla [2012] developed an adaptive process based on the application of error estimators to kinematical models to assess the necessity of a geometrical

non-linear computation. Nasser [2012] developed an approach based on energy measures to evaluate the quality of soil-structure interaction models. The evaluation approach was based on investigating the uncertainty and the complexity of the developed model. Fröbel [2012] proposed a method to evaluate the quality of coupling several elements using different software if a numerical model has to be established. Several classifications of coupling were presented. For example, coupling based on data flow direction (uni- and bi-directional coupling), based on synchronization (synchronous and asynchronous coupling), based on runtime behavior (online and offline coupling), etc. The quality evaluation was based on assessing the uncertainty caused by mapping errors.

2.4 Conclusion

In this chapter, a review of the most important topics related to damage and damage detection was presented. The review showed that a lot of work had been done in this field. However, since many challenges and problems were not solved, damage and damage detection remain nontrivial problems.

The literature review shows that many damage types can be observed in civil engineering structures. Many factors influence an occurrence of damage in structures, for example, type of a structure, loads, environment, etc. Moreover, each civil engineering structure is a unique structure. Therefore, observing identical damage properties in different civil engineering structures may be not possible. As a result, developing a sophisticated model to study specific damage in a structure can be a serious challenge especially before the construction phase. Therefore, many of the previous studies focused on modeling an effect of certain damage on a structure, for example, reducing stiffness.

Previous studies showed that global vibration-based methods, which are not sensitive to local damage, were preferred to detect damage in civil engineering structures. Many methods and damage indicators have been developed and applied. However, most of them were tested on specific numerical or experimental examples. Therefore, the reliability of these methods and indicators, if they were applied to different examples, is questionable. A strategy to select the best damage indicator based on the type of the problem under consideration is still missing. Also, no explicit general framework or approach has been developed to evaluate the performance of an inspection method for damage detection in civil engineering structures. In most cases, false alarms observed by modifying the material and geometrical properties of a studied structure to obtain a structural response similar to what damage produces were not investigated.

Many of the developed damage detection methods depend on analyzing a measured response without requiring a numerical model of a monitored structure. However, proving the reliability of such methods requires an existing structure and long-term monitoring data. Therefore, the

application of these methods on future structures which are still in the plan or construction phase is not possible. In such cases, methods based on numerical models can be applied. However, because of the uniqueness and the complexity of civil engineering structures and associated damage type, several numerical models can be developed to represent a specific problem. It is obvious that choosing a certain model can influence the final results. Therefore, a reasonable model selection procedure is essential. Generally, in most of the previous studies, if a numerical model was used to detect damage, the quality of the model or the argument behind a model choice against other models was not provided. Many methods and tools have been developed to assess model quality. Similar to damage detection methods, model quality assessment methods were applied to specific examples where specific features were measured such as uncertainty, robustness, sensitivity, etc. A framework to relate these features to damage detection process is still missing.

In this work, a model-based strategy has been developed as a probabilistic framework to assess and to improve the reliability of an inspection method for damage detection, especially in civil engineering structures, efficiently. Moreover, the strategy can be used to compare several inspection methods with different adjustments, for example, by comparing several damage indicators. The strategy is explained in detail in the following chapter.

Chapter 3

Strategy for Reliability Assessment

3.1 Overview

This chapter aims to introduce a model-based strategy to assess and improve the performance of an inspection method for damage detection. Since the proposed strategy is a combination of several methods, figure 3.1, the contribution of each method to the entire framework is explained in detail in the next sections.

Accomplishing the reliability assessment of an inspection method requires a precise definition of the damage properties in a specific structure. Next, an appropriate design of the experiment is arranged to distinguish between the variation of the outputs due to the uncertainty of the selected input parameters and due to damage. Evaluating the validity of the chosen design of the experiment is achieved by performing a sensitivity analysis. Based on the results of the performed sensitivity analysis, the critical parameters which influence the studied outputs significantly are selected. The uncertainty of the critical parameters is updated by a Bayesian inference approach. A Meta-Modeling approach is followed to reduce the computational effort. A damage indicator is developed based on the target damage size and the response of the studied structure considering obtained posterior density functions of the updated input parameters. The damage indicator is combined with a probability of detection method to estimate the probability of the detection curve. In the end, the reliability of an inspection method is assessed using the probability of detecting the predefined target damage size.

For illustrating the application of the strategy, an inspection method is tested to detect a specific type of damage in a single degree of freedom system (SDOF). The behavior of a SDOF system under harmonic excitation is well established analytically. As a result, it is possible to investigate each step of the strategy introduced in this chapter in detail independently from numerical problems. The following steps will be carried out to present the chosen example in this chapter:

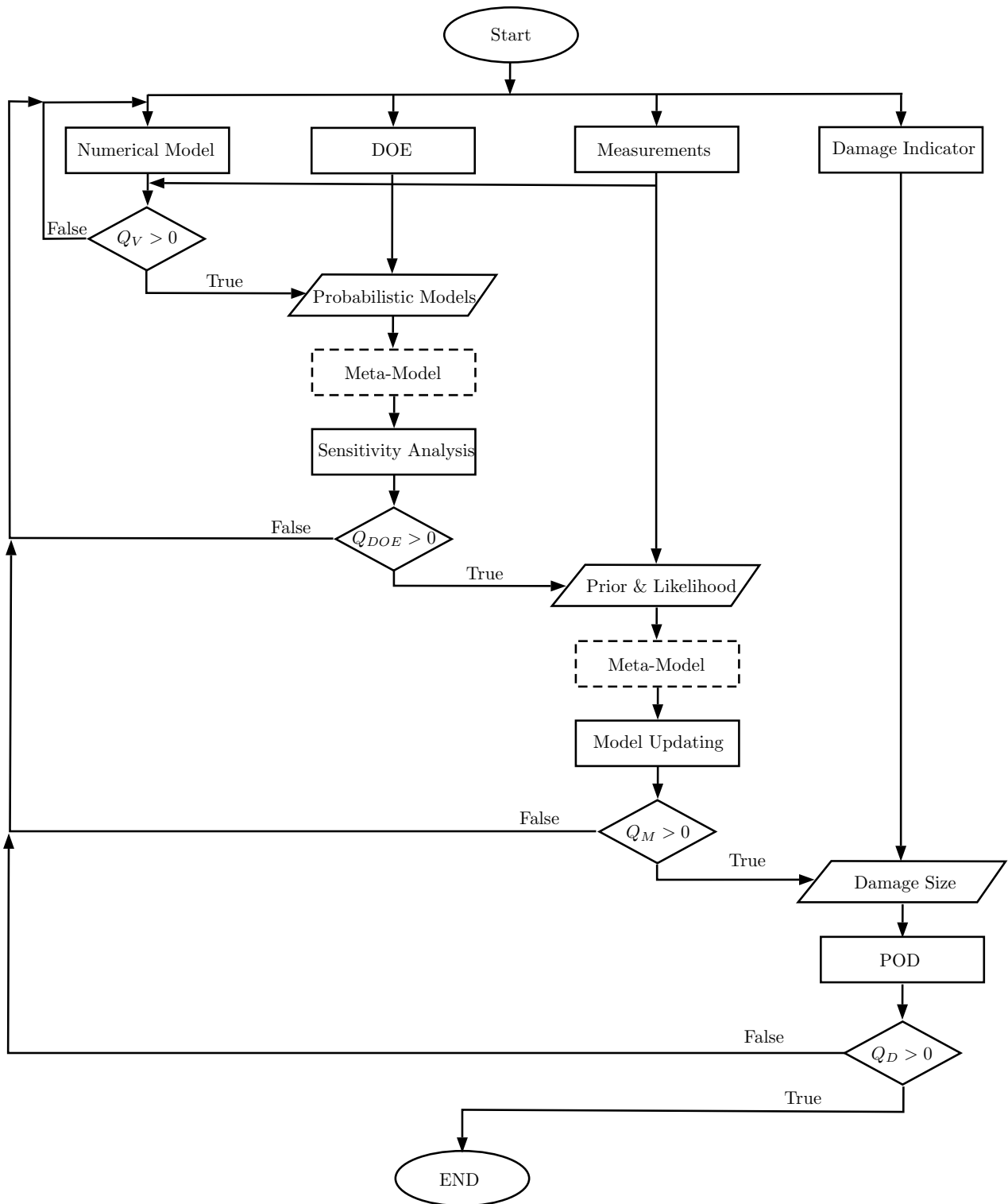


Figure 3.1: Developed strategy to investigate the relationship between the quality of the models and the reliability of an inspection method

1. Section 3.2: Problem definition in a SDOF system: defining damage type and the objectives.
2. Section 3.3: Design of Experiment to detect damage in the SDOF system: choosing excitation proprieties and assigning uncertainty to the input parameters (stiffness, mass, and damping).
3. Section 3.4: Investigating the validity of the chosen DOE by performing the sensitivity analysis and illustrating how the sensitivity analysis can be applied to obtain the optimal design of the experiment.
4. Section 3.5: Model updating using Bayesian inference: investigating the types of uncertainty that should be considered and updating the important input parameters.
5. Section 3.6: Calculating the probability of damage detection (POD) and the probability of false alarm (PFP) and evaluating the reliability of the inspection method.

3.2 Problem definition

Choosing a specific damage θ^g to be traced is necessary. Therefore, the problem definition includes selecting an undesired change (damage) in a certain structure or a part of it to be detected. This selection can be made after specifying limit states related to the stability or the serviceability of a studied structure. If the type, the severity and the location of damage are specified, a model can be chosen to quantify damage severity based on its type. It should be possible to include the damage model within the global model of the structure at the selected damage locations. An inspection method can be chosen to observe the changes in the structural response due to the selected damage model by performing experiments.

In civil engineering, it is usually difficult or even impossible to use physical models to perform real experiments to investigate the influence of a damage model on an actual structure. Therefore, a numerical model G_M is required to conduct this investigation by simulating the needed experiments. Several numerical models can be developed to describe a particular problem. However, some restrictions should be taken into account when a numerical model has to be chosen. Since the goal of the model is damage detection, it has to be possible to combine an appropriate numerical model of the selected damage with the numerical model of the structure. If a sophisticated model is required, a trade-off between the computational efforts and uncertainty may be considered.

For a proper use of a developed numerical model G_M to simulate a certain test for damage detection, an assessment procedure has to be applied to evaluate the performance of the chosen model. In this work, an index Q_V has been defined to quantify the quality of the chosen

numerical model G_M . Q_V is limited in a range $[0, 1]$, $\{Q_V \in \mathfrak{R} : 0 \leq Q_V \leq 1\}$. If a test is performed to measure a response \bar{d}_i considering damage size θ_i^g and \bar{d}_{i+1} considering damage size $\theta_{i+1}^g > \theta_i^g$ using an experimental model G_E , an appropriate model G_M can be chosen to calculate the response $d = G_M(\{\theta\}, \theta^g)$, which should be directly proportional to the measured response \bar{d} :

$$\forall \theta^g : \theta_i^g \leq \theta^g \leq \theta_{i+1}^g \Leftrightarrow d(\theta^g) \propto \bar{d}(\theta^g) \quad (3.1)$$

Q_V can be defined as the correlation between the structural response of both models G_M and G_E considering damage θ^g . If $\sigma_{d(\theta^g)}$ refers to the standard deviation of the structural response d computed using a numerical model G_M due to the variation of damage size θ^g and if $\sigma_{\bar{d}(\theta^g)}$ refers to the variation of the structural response \bar{d} measured using an experimental model G_E due to the variation of damage size θ^g , Q_V can be defined assuming a uniform distribution of θ^g in the interval as follows:

$$\forall \theta^g : \theta_i^g \leq \theta^g \leq \theta_{i+1}^g : Q_V = \begin{cases} \frac{E \left[(d(\theta^g) - \mu_{d(\theta^g)}) (\bar{d}(\theta^g) - \mu_{\bar{d}(\theta^g)}) \right]}{\sigma_{d(\theta^g)} \sigma_{\bar{d}(\theta^g)}} > 0 \\ 0 \end{cases} \quad (3.2)$$

If $Q_V = 1$, an agreement between the structural response obtained from the both models G_M and G_E due damage θ^g is achieved. $0 \leq Q_V < 1$ indicates that there is an error that can lead to wrong evaluation of the selected inspection method. The error could occur if some important phenomena were not included within the numerical model or/and if inappropriate experiments were performed. In this step, the error appears as a lack of correlation between the structural responses of the numerical and experimental models.

For N_d responses:

$$\forall \theta^g : \theta_i^g \leq \theta^g \leq \theta_{i+1}^g : Q_V = \begin{cases} \frac{1}{N_d} \sum_{j=1}^{N_d} \frac{E \left[(d_j(\theta^g) - \mu_{d_j(\theta^g)}) (\bar{d}_j(\theta^g) - \mu_{\bar{d}_j(\theta^g)}) \right]}{\sigma_{d_j(\theta^g)} \sigma_{\bar{d}_j(\theta^g)}} > 0 \\ 0 \end{cases} \quad (3.3)$$

If the experimental model G_E is not available, a reference model G_{MR} can be used to evaluate the model G_M . The reference model can be chosen based on experience or based on other features, for example, selecting the most complex model as a reference model.

Problem definition in a SDOF system

The performance of a vibration-based inspection method was assessed to detect the degradation of the stiffness k in a single degree of freedom system with stiffness (k) mass (m) damping $c = 2 \times m \times \omega_n \times \zeta$ system, figure 3.2, $\{\theta\} = \{\theta_1, \theta_2, \theta_3\} \equiv \{k, m, \zeta\}$, where ω_n is the angular frequency of the studied system. Since accelerometers have been commonly used in practice to measure the dynamic response of engineering structures, the acceleration time history $\ddot{x}(t)$ was selected as output. The inspection method is based on observing the influence of damage θ^g on the measured acceleration $\ddot{x}(t)$ of the system under a certain excitation $F(t)$. Since this influence can be at each time step t_i of the time history, the cumulative signal energy d of the acceleration time history for a specified time period $T = t_e - t_0$ was chosen as an objective function to monitor this variation, eq. (3.5), where t_0 is the time when the signal starts and t_e is the time when the signal ends. The initial conditions were chosen $x(0) = 0$ and $\dot{x}(0) = 0$ in next the steps if nothing else is mentioned.

$$d = \Delta t \sum_{i=1}^{T/\Delta t} \ddot{x}^2(i) \quad (3.4)$$

As Δt is constant, one can omit it in the context of the applications described here. The cumulative signal energy d becomes then:

$$d = \sum_{i=1}^{T/\Delta t} \ddot{x}^2(i) \quad (3.5)$$

In order to avoid the influence of the numerical error, which can result from applying numerical methods to solve the studied system, on the assessment of the inspection method, the analytical solution of the equation of motion for a SDOF system, eq. (3.6), under a chosen harmonic exciton $F(t)$ with an amplitude F_a and angular frequency ω was used for both G_M and G_E . Therefore, $Q_V = 1$.

$$m\ddot{x} + c\dot{x} + kx = F_a \sin(\omega t) \quad (3.6)$$

If $\theta^g = \Delta k : k = k_0 - \Delta k$, where k_0 is the stiffness of the undamaged system, refers to the

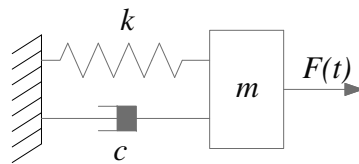


Figure 3.2: A stiffness-mass-damping system excited by a force $F(t)$

degradation of the stiffness $\theta_1 = k$, the considered problem is the reliability of the chosen inspection method to detect a specific target damage size θ^{g*} which is the allowed damage size.

Damage is considered unacceptable if:

Δk exceeds $15\% \times k_0$. The inspection method is considered reliable if the probability of detecting any damage size $\theta^g \geq 15\% \times k$ is at least 95% associated with a probability of false alarm that does not exceed 5%. As a result, the problem definition of the studied example can be written as follows:

$$\begin{aligned} H_o &: \forall \theta^g : \theta^g \geq 15\% \times k_0 \Rightarrow POD(\theta^g) \geq 95\%, PFP \leq 5\% \\ H_1 &: \text{The inspection method is not reliable} \end{aligned} \quad (3.7)$$

3.3 Design of Experiment

As mentioned in the previous section, the chosen inspection method aims to detect specified target damage θ^g by observing the change of the output d . Since the response varies due to the uncertainty of the input parameters $\{\theta\}$ as well, it can be difficult to detect the target damage size. As a result, it is necessary to collect information which explains the variation of the outputs due to the uncertainty in the input parameters $\{\theta\}$. In this work, the variation of the input parameters in time is not included since experiments have to be conducted in a short period (seconds and minutes). If a monitoring system has to be designed, the variation of the input parameters in time has to be included. An appropriate DOE means designing an experimental setup to detect a specified damage θ^g . For a vibration-based inspection method, DOE may involve choosing excitation properties (amplitude, frequency, etc.) and sensor locations.

To obtain an appropriate DOE, theoretical background and/or preliminary experiments can be used. The input parameters $\{\theta\}$ and their initial assigned values should be selected. The initial value of a selected input parameter is associated with uncertainty which is given by a probabilistic model. Several approaches can be used to select an appropriate probabilistic model. For example, a statistical test can be conducted to measure the rate of getting a particular value of an input parameter and fitting the resulting histogram by an appropriate distribution function. On the other hand, a subjective selection of a probabilistic model based on formal experience and/or knowledge is possible. In this case, a probabilistic model indicates how likely a chosen value of an input parameter represents the actual value of a parameter in a given model. A sampling method has to be selected to transfer this uncertainty to samples that can be used later to compute the response d and perform an uncertainty analysis.

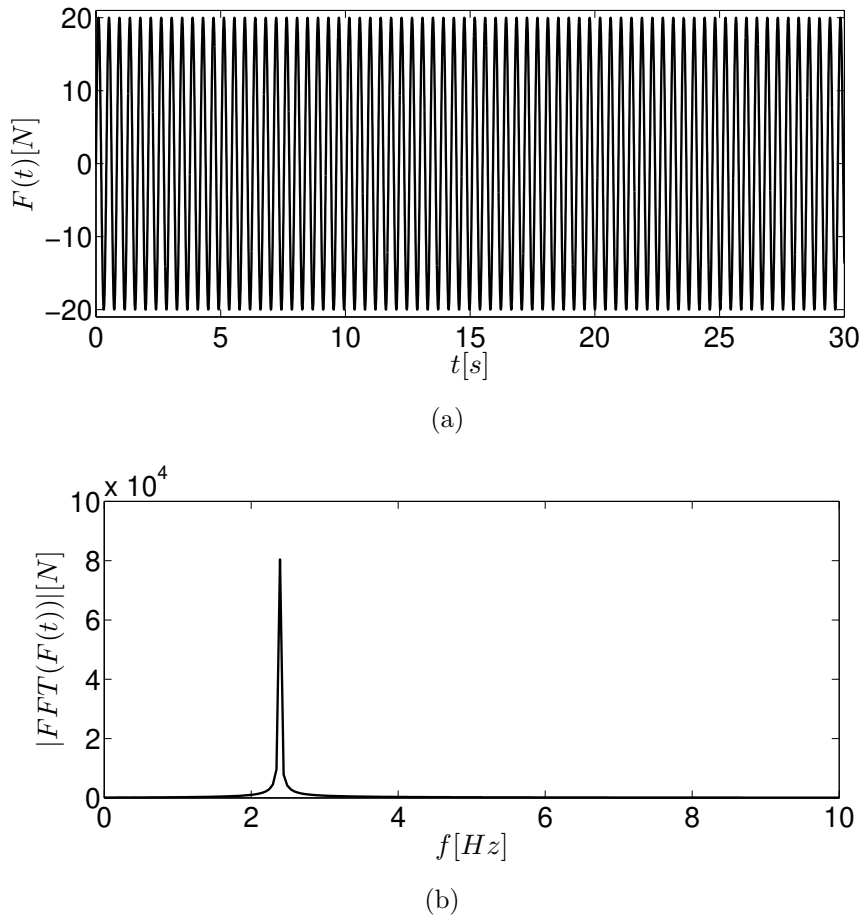


Figure 3.3: The chosen harmonic excitation $F(t)$ (a) and its $|FFT|$ (b)

Design of Experiment to detect damage in the SDOF system

In the SDOF example, damage is related to stiffness degradation $\theta^g = \Delta k$. Therefore, it is reasonable to choose an excitation $F(t)$ that generates an output d which is sensitive to stiffness $\theta_1 = k$. This means, a slight stiffness variation induces a significant modification of the output. Therefore, a harmonic excitation $F(t) = F_a \sin \omega t$ was chosen, figure 3.3, where ω was chosen to be smaller than the natural angular frequency ω_n of the system such that the frequency ratio $\eta = \omega / \omega_n < 1$. If $\eta = 0$, then the force is static and the response is influenced completely by the stiffness. In this case, no acceleration is measured and $d = 0$. Therefore, a trade off between η and F_a should provide a measurable response and a significant stiffness contribution. In addition, $T = t_e - t_0$ was chosen to obtain a steady state response where the stiffness dominates, figure 3.4.

In this example, the real values of the input system parameters are given in table 3.1. The true value of the natural angular frequency of the system $\omega_n^* = 50.5$ radians/second and the excitation properties were chosen $F_a = 20$ N, $\omega = 15$ radians/second. Accordingly, the frequency ratio ω / ω_n was $\eta \approx 0.3$. The amplitude of the Fast Fourier Transform (FFT),

eq (3.8), shows two peaks, figure 3.4 (c), the high peak is related to the excitation frequency and the small peak is related to the natural frequency of the system. This means that F_a value is large enough to obtain clearly the forced response of the studied system under the chosen excitation.

$$Y(k) = FFT(\ddot{x}) = \sum_{j=1}^n \ddot{x}(j)W_n^{(j-1)(k-1)} \quad (3.8)$$

where $Y(k)$ is the response transformed from the time domain into the frequency domain, $W_n = e^{(-2\pi i)/n}$, $i = \sqrt{-1}$ and $k, j = 1, 2, \dots, n$

The discrete FFT was applied to the discrete acceleration signal generated from eq (3.10) by calculating the $\frac{\partial^2 x}{\partial t^2}$ for each $t_i : 0 \leq t_i \leq 30$ s where $t_{i+1} = t_i + \Delta t$.

$$\frac{\partial^2 x}{\partial t^2} = \frac{\partial^2}{\partial t^2} [e^{-\zeta\omega_n t} (a_1 \sin \omega_d t + a_2 \cos \omega_d t) + a_3 \sin \omega t + a_4 \cos \omega t] \quad (3.9)$$

By performing the differentiation, eq (3.9) can be written as follows:

$$\begin{aligned} \frac{\partial^2 x}{\partial t^2} = & -e^{-\zeta\omega_n t} [(a_1\omega_d^2 - 2a_2\zeta\omega_d\omega_n - a_1\zeta^2\omega_n^2) \sin \omega_d t + (a_2\omega_d^2 + 2a_1\zeta\omega_d\omega_n - a_2\zeta^2\omega_n^2) \cos \omega_d t] \\ & - \omega^2 (a_3 \sin \omega t + a_4 \cos \omega t) \end{aligned} \quad (3.10)$$

a_1 and a_2 are constants related to the initial conditions at $t_0 = 0$ s. a_3 and a_4 are constants related to the particular solution of eq (3.9). a_1, a_2, a_3 and a_4 can be calculated as shown in Chopra [2012]. Considering the values given in table 3.1, $[a_1, a_2, a_3, a_4] = [5.95 \times 10^{-5}, -13 \times 10^{-4}, 43 \times 10^{-4}, -5.95 \times 10^{-5}]$. $\omega_d = \omega_n \sqrt{1 - \zeta^2}$ is the damped natural angular frequency. Uniform distribution density functions were assigned to the studied parameters $\{\theta\}$ as a subjective uncertainty, table 3.2. The coefficients of variation (COV), which is defined as the ratio of the standard deviation σ to the mean μ : $COV = \sigma/\mu$, were assigned based on the difficulty of measuring the assigned value of the input. Therefore, the COV of the damping ratio is larger than the COV of the mass and the stiffness since it is difficult to identify the damping ratio with a similar accuracy of the mass and the stiffness.

To explore the validity of the suggested design of experiment considering the assigned subjective

Table 3.1: True values assumed for the studied input parameters $\{\theta\}$

	$\theta_1^* = k^*$ [N/m]	$\theta_2^* = m^*$ [kg]	$\theta_3^* = \zeta^*$ [-]
$\{\theta^*\}$	5050	1.98	0.021

uncertainty, samples which are combinations of the input parameters between their maximum and minimum values given in table 3.2 with constant intervals $\Delta\theta = (\theta_{max} - \theta_{min})/100$ were generated and used to calculate the signal energy. The results in figures 3.6 show that the signal energy is sensitive to the variation of the stiffness and less sensitive to the mass and damping ratios variations.

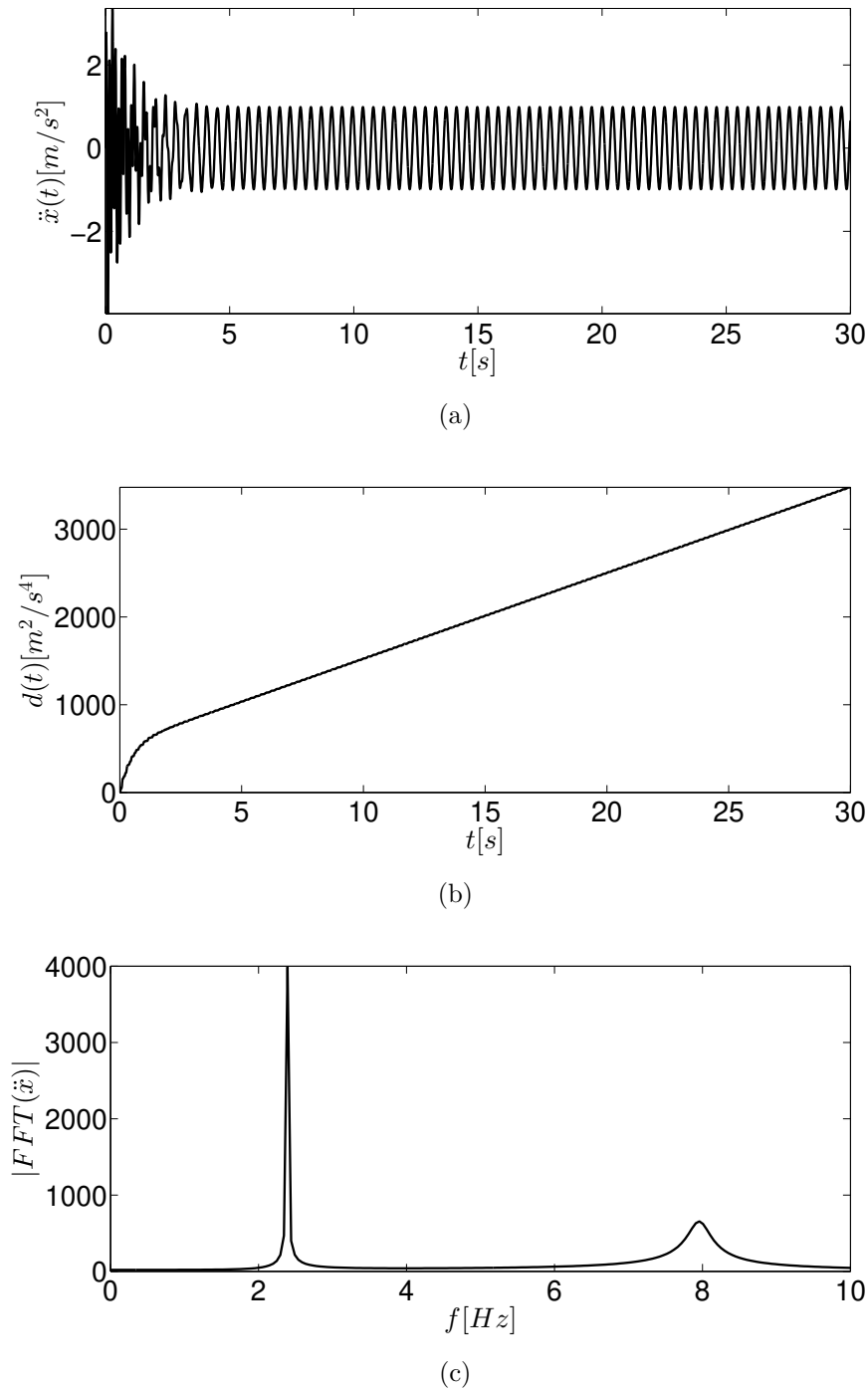


Figure 3.4: Structural response $\ddot{x}(t)$ (a), cumulative signal energy $d(t)$ (b), and FFT of the acceleration signal using the mean values, table 3.2, (c)

In many cases, the amplitude of the ambient excitation caused by surrounding noise can be considerable compared to the chosen excitation. To investigate the influence of the ambient excitation on the validity of the chosen design of experiment the input excitation was contaminated with white noise $\gamma_F \sim \mathcal{N}(0, \sigma_{\gamma_F}^2)$, eq (3.11), before calculating the signal energy, figure 3.5. Figures 3.7 show the variation of the response considering the ambient excitation. The response has been calculated using the Newmark $\beta = 1/4$ method (constant average acceleration) since the analytical solution is not applicable anymore. The results show that indicating the influence of the mass and the damping on the response is more difficult. Moreover, the increment in energy values can be observed. Figure 3.7 (b) show that despite the noise, the influence of stiffness variation on the response remains significant.

$$F(t) = F_a \times \sin \omega t + \gamma_F \quad (3.11)$$

Validating the chosen DOE using the process described above may be expensive especially for more complex examples. Therefore, the sensitivity analysis supported by Meta-models will be used in the next step to validate the suggested DOE.

Table 3.2: Mean values $\{\mu\}$, minimum and maximum values of the studied parameters $\{\theta\}$ and their coefficients of variation COV

	$\theta_1 = k$ [N/m]	$\theta_2 = m$ [kg]	$\theta_3 = \zeta$ [-]
μ	5000	2.00	0.020
Min	4480	1.87	0.0165
Max	5520	2.13	0.0235
COV	0.06	0.037	0.1

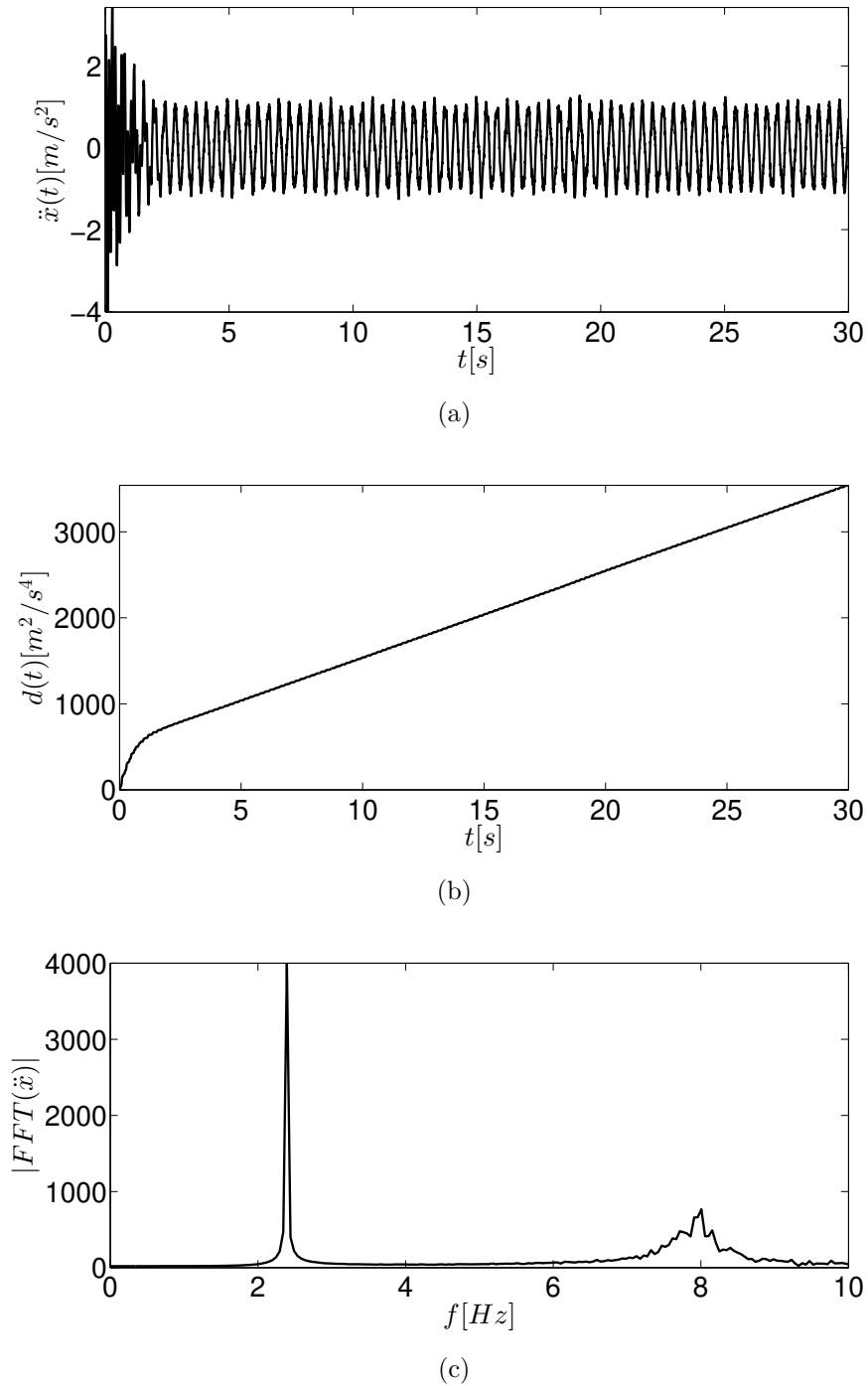


Figure 3.5: Structural response $\ddot{x}(t)$ (a) under the contaminated excitation, cumulative signal energy $d(t)$ (b), and FFT of the acceleration signal using the mean values, table 3.2, (c)

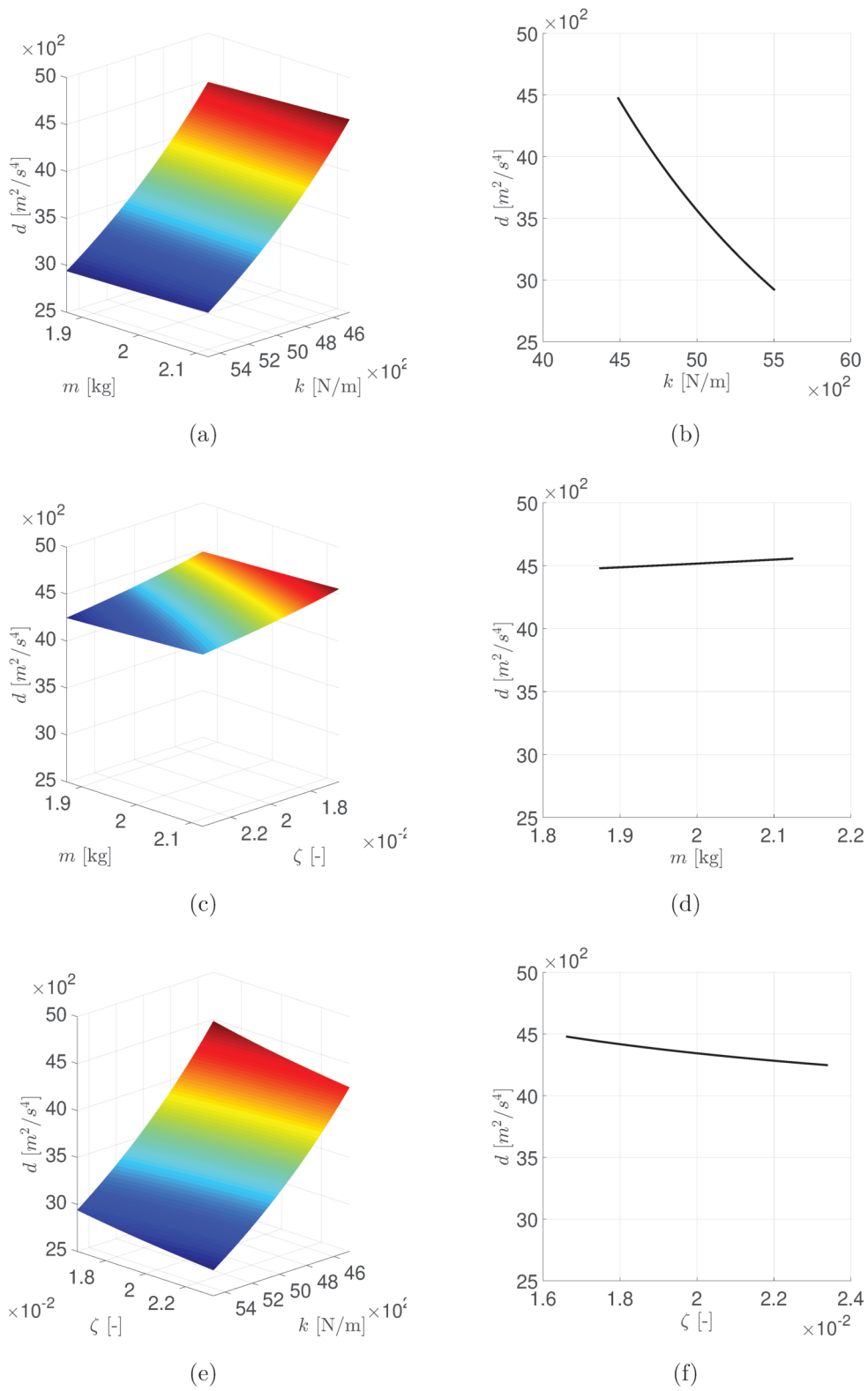


Figure 3.6: The relationship between the input parameters and the output parameter without considering the ambient vibration excitation

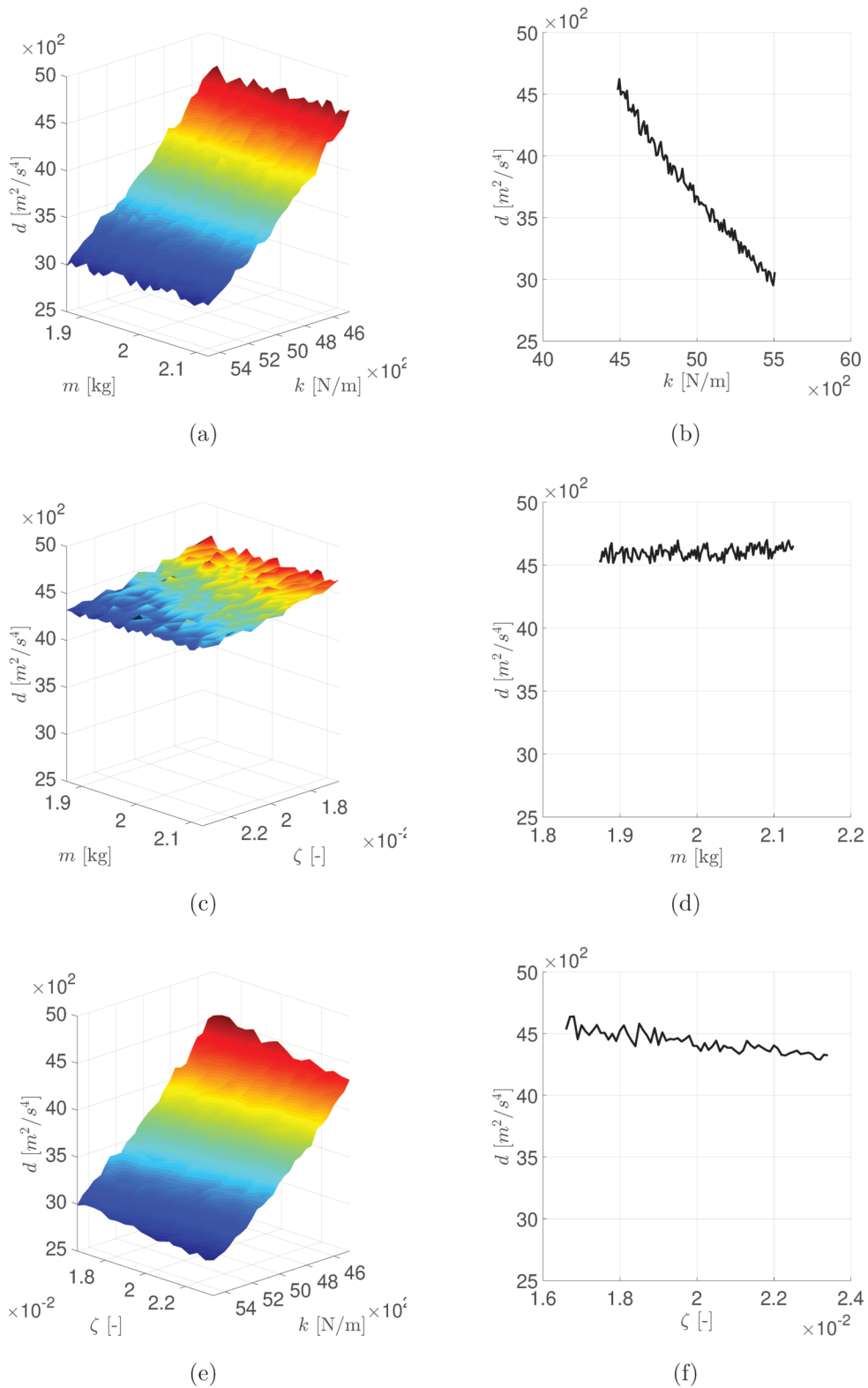


Figure 3.7: The relationship between the input parameters and the output parameter considering white noise ambient vibration excitation

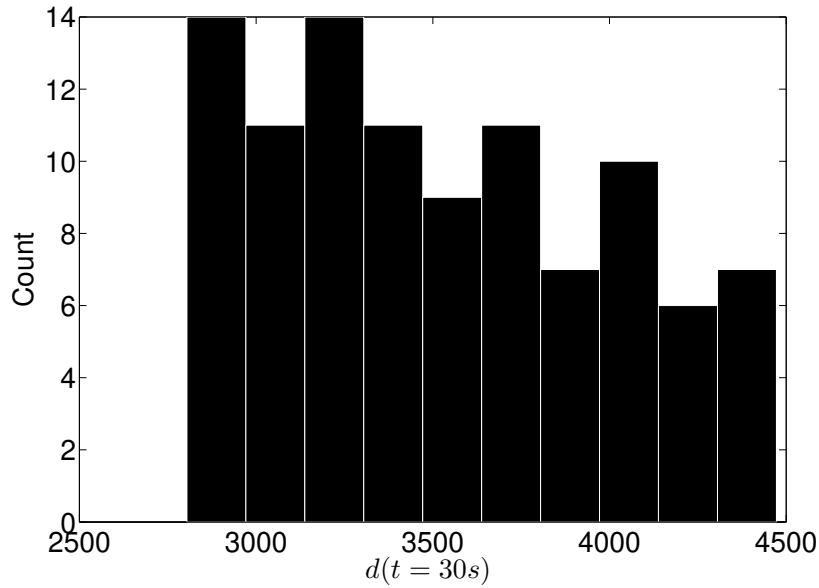


Figure 3.8: A histogram shows the cumulative signal energy $d(t_e)$ variation due to the inputs $\{\theta\}$ uncertainty using $N = 100$ samples

A Latin hypercube sampling method was used to generate $N = 100$ samples. The acceleration time histories $\ddot{x}(t)$ were computed using the analytical solution shown in eq (3.9) with time interval $\Delta t = 0.005$ s for each sample. The cumulative signal energy $d(t)$ was computed between $t_0 = 0$ and $t_e = 30$ s, figure 3.4. The variation of the cumulative signal energy $d(t = 30$ s) shown in figure 3.8 indicates that the structural response is significantly influenced by the inputs uncertainty. This may lead to a large number of false alarms and difficulties detecting damage.

3.4 Sensitivity analysis

Since the aim of a design of an experiment is to find the best arrangement to detect damage, sensitivity analysis evaluates the quality of the chosen design. The design was considered valid if the contribution of the desired parameters $\{\hat{\theta}\} \subseteq \{\theta\}$ is significant. The $\{\hat{\theta}\}$ are the parameters that lead to detect the chosen damage type. Moreover, the design is optimal if the influence of the undesired parameters is minimized. In complex models where a large number of input parameters is involved, sensitivity analysis is a powerful tool to quantify their contributions and the contribution of the interaction between these parameters.

Sensitivity analysis procedures explore and quantify the impact of possible errors in input data on predicted outputs and system performance indices, Loucks et al. [2005]. Different methods can be used to perform a sensitivity analysis. In this work, both the contribution of each input

parameter and the interaction between the parameters were tested. Therefore, the Total-effect sensitivity analysis described by Saltelli et al. [2007] was used. eq. (3.12).

$$sT_{i,j} = \frac{E(\text{Var}(d_i|\theta_j \sim \theta))}{\text{Var}(d_i)} \quad (3.12)$$

where d_i is the studied system output and $\text{Var}(d_i)$ is the variance of the output.

The term $E(\text{Var}(d_i|\theta_j \sim \theta))$ is the expected amount of variance that would remain unexplained (residual variance) if θ_j and only θ_j was left free to vary over its uncertainty range, assuming all other variables had been determined. High values of the Total-effect index $sT_{i,j}$ mean that the input θ_j influences the response d_i significantly.

The quality of a chosen DOE was quantified by an index Q_{DOE} . As mentioned before, an optimal DOE should provide large values of sT for the desired parameters $\{\hat{\theta}\}$ and small values of sT for undesired parameters. The developed index is limited in a range $[0, 1]$, $\{Q_{DOE} \in \mathfrak{R} : 0 \leq Q_{DOE} \leq 1\}$. If $Q_{DOE} = 1$, then the chosen DOE is optimal. If $0 < Q_{DOE} < 1$, then the chosen design is not optimal and a false alarm due to the uncertainty of the input parameters should be expected. If $Q_{DOE} = 0$, then the DOE is not able to provide any information about the desired parameters. If the value $sT_{d,\hat{\theta}}$ represents the influence of $N_{\hat{\theta}}$ desired parameters $\{\hat{\theta}\}$ on the response d and the value $sT_{d,\theta}$ represents the influence of the all N_{θ} parameters $\{\theta\}$ on the response d , the index Q_{DOE} can be calculated as follows:

$$Q_{DOE} = \frac{\sum_{i=1}^{N_{\hat{\theta}}} sT_{d,\hat{\theta}}}{\sum_{i=1}^{N_{\theta}} sT_{d,\theta}} \quad (3.13)$$

3.4.1 DOE based on numerical model quality and sensitivity analysis

For vibration-based inspection methods, the excitation properties and sensors locations should be chosen to increase the reliability of the inspection method for damage detection.

In case of harmonic excitation, the frequency of the chosen excitation can be selected based on the sensitivity analysis results, eq. (3.14). ω_{sT} represents the excitation frequency that leads to the highest $sT_{\hat{\theta}}$ value due to the influence of the studied damage θ^g on the structural response d .

$$\omega_{sT} : \arg \max_{\omega} sT_{\hat{\theta}} \quad (3.14)$$

Evaluating the performance of a chosen inspection method using a numerical model G_M can be accurate if the agreement between the computed and the measured structural response of

the studied structure is obtained. If \mathbf{X} refers to all possible locations where a sensor can be placed on the studied structure to measure the structural response, the sensor locations x for damage detection can be optimized based on Q_V and Q_{DOE} as follows:

$$x \subseteq \mathbf{X} : \arg \max_x [Q_V, Q_{DOE}] \quad (3.15)$$

After choosing ω_{sT} and x , the amplitude of the selected excitation can be chosen in a way that the structural response $d(x, \omega_{sT}, F_a)$ can be distinguished from the response of the structure due to noise or ambient vibration $d(x, \gamma_F)$, where γ_F can be a random noise excitation. The chosen F_a value improves $sT_{\hat{\theta}}$ value due to the influence of the studied damage θ^g on the structural response d .

$$F_a : \arg \max_{F_a} sT_{\hat{\theta}} \quad (3.16)$$

DOE to detect damage in the SDOF example

Eq. (3.14) was applied to the studied SDOF example to obtain the optimum excitation frequency ω_{sT} that maximizes the sensitivity of structural response to the stiffness. The sensitivity analysis was performed as explained in the next sections. The analysis proceeds as follows:

1. $\eta_{i+1} = \eta_i + \Delta\eta$ where $\eta_0 = 0.1$, $\omega_{i+1} = \eta_{i+1} \times \omega_n$ and $\Delta\eta = 0.1$ for this example. ω_n was calculated based on the mean values given in table 3.2.
2. Calculating the structural response d using the numerical model G_M for $N = 100$ samples. The variation of the input parameters is based on table 3.2.
3. Performing sensitivity analysis and calculate sT .
4. Repeat the process until $\eta = 5$.

The result shown in figure 3.9 indicates that for $\eta < 1$ the stiffness has a significant effect on the response. This effect reaches its peak if $\eta = 0.3$ where $\omega_{sT} \approx 0.3 \times 50 = 15$ rad/s. If $\eta > 1$ the influence of the stiffness decreases and it can be omitted for $\eta \gg 1$. Since a harmonic excitation is used to excite the structure the influence of the damping as the results indicate is unimportant. If $\eta = 1$, which represents the resonance phenomenon, a sudden peak appears, where all input parameters (stiffness, mass, and damping) are activated. For $\eta \ll 1$ longer time should be used to calculate the response d and sT otherwise the excitation behaves like a static force and no vibration was observed in the selected period $T = 30$ s. In reality, applying

low-frequency excitations associated with high amplitudes is difficult if not impossible. In this work, low excitations frequencies which cause responses, that are not measurable within the predefined observation period T , were not considered.

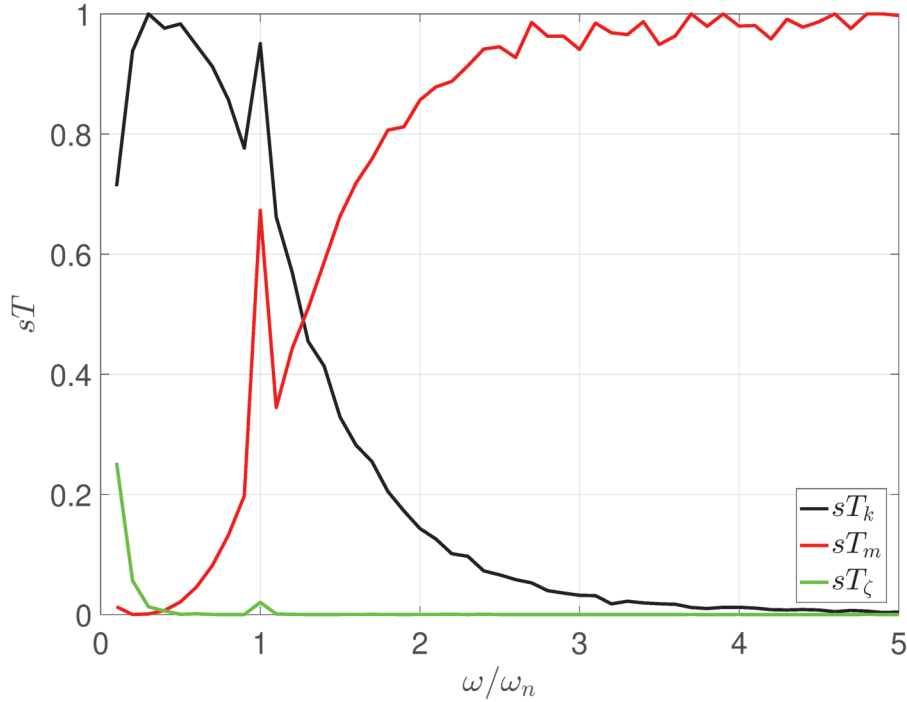


Figure 3.9: The relationship between the angular frequency of the excitation and the Total-effect index sT of the input parameters

Eq. (3.16) was applied to the studied SDOF example to choose the excitation amplitude F_a that amplifies the influence of the stiffness considering ω_{sT} . The sensitivity analysis was performed as explained in the next sections. The analysis proceeds as follows:

1. $F_{a,i+1} = F_{a,i} + \Delta F_a$ given that $F_{a,0} = 0$ [N] and $\Delta F_a = 0.25$ [N] for this example.
2. The input excitation was contaminated with white noise $\gamma_F \sim \mathcal{N}(0, 0.1^2)$, eq (3.11).
3. Calculating the structural response d using the numerical model G_M for $N = 100$ samples. The variation of the input parameters is based on table 3.2.
4. Performing sensitivity analysis and calculating sT .
5. Repeating the process until $F_a = 50$ [N].

The results, presented in figure 3.10, show that for small F_a values the transient response at frequency ω_d is dominant and all input parameters are activated. If F_a is large enough, the steady-state structural response is dominant, and only the stiffness influences the response.

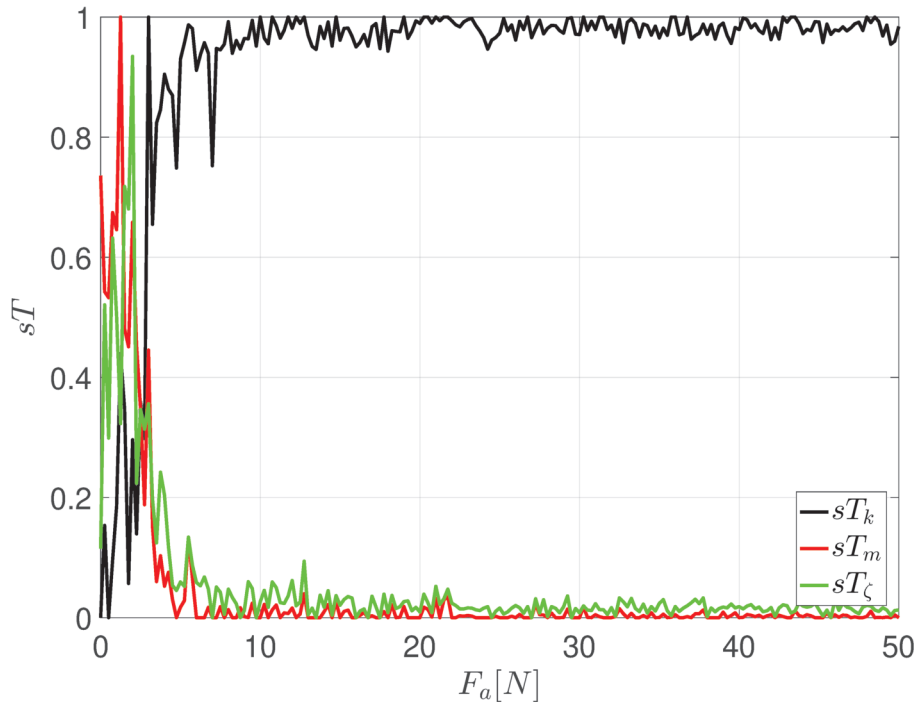


Figure 3.10: The relationship between the amplitude of the excitation and the Total-effect index sT of the input parameters

3.4.2 Meta-Modeling

A model must represent all important phenomena that influence the response of a studied structure. Since calculating a model multiple times may be computationally expensive an approach based on developing a Meta-model (response surface model) has been used to simplify a relationship between a structural response d and the physical properties of a studied structure $\{\theta\}$. The meta-modeling approach is a powerful tool to reduce computational efforts. A Meta-model can be used as an approximation of a complex model after computing a reasonable number of samples or support points using the complex model. In Fang and Perera [2011], Cundy [2003] and Deeb and Zabel [2014] are examples that present the application of a Meta-modeling approach to damage identification in structural engineering.

There are several methods to develop a Meta-model such as global or local polynomial regression, stochastic methods or artificial intelligence. The choice of the best method depends on the studied problem and the objective of the Meta-model. Procedures for developing a Meta-model can be found in Box and Wilson [1951], Box and Draper [1987], Forrester et al. [2008] and Myers et al. [2009]. More information about the principles of Meta-models and their application in structural engineering can be found in Bucher and Most [2008], Loucks et al. [2005].

3.4.3 Choosing the terms of a Meta-model

In order to obtain an optimal or suboptimal Meta-model, a strategy for selecting the terms of a polynomial regression-based Meta-model was developed and applied, figure 3.11. This selection will be validated in the next steps. If the chosen Meta-model is not valid, other types of regressions can be applied. After defining the input parameters $\{\theta\}$, the outputs $\{d\}$, the degree of the polynomial equation, and the maximum degree of the mixed terms ψ_θ , all possible terms $\{\Theta_i\} : i = 1 : n$ can be generated where n is the number of generated terms and Θ_i refers to a term from the group $\{\Theta_i\}$: $\Theta_i \in \{\Theta_i\}$. Based on Algebra principles, if a set has n_θ elements and the number of combinations n of the mixing term degree $r_\theta = 1 \cdots \psi_\theta$ is required, then:

$$n = \sum_{r_\theta=1}^{\psi_\theta} C(n_\theta, r_\theta) = \sum_{r_\theta=1}^{\psi_\theta} \frac{n_\theta!}{r_\theta!(n_\theta - r_\theta)!} \quad (3.17)$$

where $C(n_\theta, r_\theta)$ is the number of r_θ -combinations from a given set A of n_θ elements. The Meta-model will be developed as follows:

1. A single term sub-Meta-model i is developed using only the term Θ_i . The correlation $\rho_{\underline{d}, \underline{d}_i}^2$ between the predicted value \underline{d}_i computed using the developed sub-Meta-model and the output of the numerical model d is calculated as shown in eq. (3.18), where $cov(d, \underline{d}_i)$ refers to the covariance, σ_d is the standard deviation of the response d because of the variation of the input parameters and $\sigma_{\underline{d}}$ is the standard deviation of the response \underline{d} because of the variation of the input parameters and fitting error because of using Meta-models.

$$\rho_{\underline{d}, \underline{d}_i}^2 = \left[\frac{cov(d, \underline{d}_i)}{\sigma_d \times \sigma_{\underline{d}}} \right]^2 \quad (3.18)$$

2. Based on $\rho_{\underline{d}, \underline{d}_i}^2$, the terms $\{\Theta_i\}$ are sorted from largest $\rho_{\underline{d}, \underline{d}_i}^2$ to smallest $\rho_{\underline{d}, \underline{d}_i}^2$.
3. Starting from the first sorted term Θ_1 , which has the largest $\rho_{\underline{d}, \underline{d}_i}^2$, a set of combined terms $\{\Theta\}$ is created. At step $i = 1$ the initial set is $\{\Theta\} = \Theta_1$.
4. At step i a new term Θ_i is added to the set $\{\Theta\}$ before generating a multi term sub-Meta-model i and calculating the correlation $\rho_{\underline{d}, \underline{d}_i}^2$. If the added term Θ_i improves the correlation between the predicted value \underline{d}_i and d_i , the term Θ_i is considered otherwise it is ignored.
5. The final Meta-model contains only N_Θ terms that improve the correlation $\rho_{\underline{d}, \underline{d}_i}^2$, $N_\Theta \leq n$.

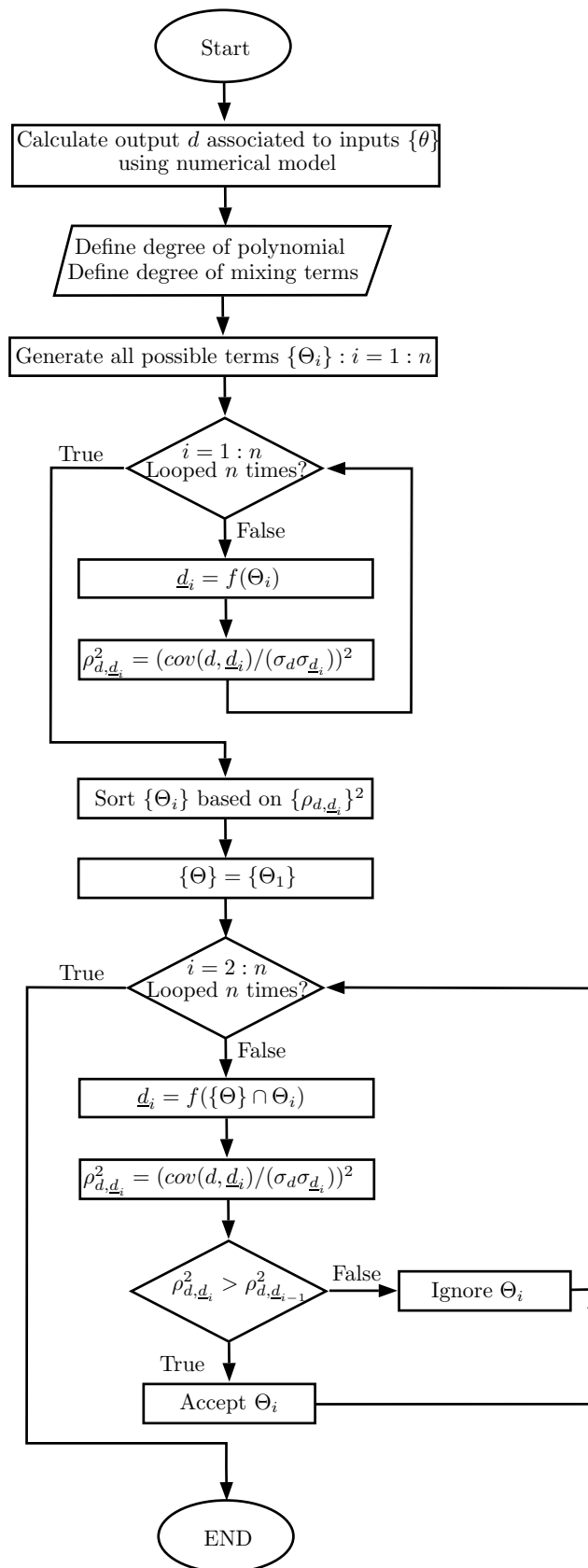


Figure 3.11: A Strategy to select the terms of a Meta-model

3.4.4 Meta-Model for Sensitivity analysis

Performing the sensitivity analysis may require running a model G_M for a large number of samples which can be expensive. Therefore, in this work, a Meta-modeling approach was applied to minimize the computational burdens.

A developed Meta-model should satisfy several statistical requirements. These requirements are:

1. the relationship between the input and the output variables is linear.
2. the residuals are random and normally distributed.
3. constant variance of the residuals with zero mean.

In literature, there are several criteria to check these requirements, for example, graphical analysis of the residuals and regression diagnostic using a quantitative analysis of the residuals. In this work, the linearity is checked by calculating the coefficient of determination R^2 , eq. (3.19), which measures the contribution of the independent variable(s) in the model, Rawlings et al. [1998].

$$R^2 = \frac{\sum_{i=1}^N (d_i - \underline{d}_i)^2}{\sum_{i=1}^N (d_i - \mu_d)^2} \quad (3.19)$$

To check the other assumptions, a graphical analysis of the residuals is used. Graphical methods are a kind of regression diagnostics techniques for detecting failures in the assumptions, unusual observations, and inadequacies in the model, statistics to flag observations that are dominating the regression, and detecting situations in which strong relationships among the independent variables are affecting the results, Rawlings et al. [1998]. The following tools were applied to check the assumptions:

1. The histogram of the residuals and the normal probability plot are used to check if the residuals are approximately normally distributed.
2. The lag plot, which is formed by plotting each residual value versus its successive residual value, is used to check the randomness of the residuals.
3. Plotting the residuals versus the predicted values is used to check if the variance is constant with zero mean.

In case that one or more of these assumptions are not satisfied, another scale of the outputs $\{d\}$ may be used to develop the required Meta-model, for example, $\log(d)$ or d^ι where $\iota \neq 0$.

In this work, a global polynomial regression is used to reformulate the studied problem. As a result, the relationship between a structural response and the highlighted parameters is obtained in eq. (3.20):

$$\{d\} = [\beta]\{1 \ \theta_i \ \theta_i\theta_j \ \theta_i\theta_j\theta_r \ \dots\}^T \quad (3.20)$$

where $1 \geq i, j, r, \dots \leq N_\theta$, N_θ is the number of the input parameters. $[\beta]_{N_d \times N_\Theta}$ is the estimated regression coefficients matrix, N_Θ is the number of terms of the Meta-model, N_d is the number of outputs. $\{d\}_{N_d \times 1}$ is the vector of outputs. Developing a Meta-model requires defining four sets of data. They are the inputs $\{\theta\}$, the outputs $\{d\}$, the degree (order) of the polynomial equation, and the degree of the mixed terms: $\{\theta_i\theta_j \ \theta_i\theta_j\theta_r \ \dots\}$. It is worth to mention that in Meta-models increasing the degree of the polynomial could reduce the fitting error but not necessarily the prediction error, Yuen [2010]. There are several methods to obtain the regression coefficients matrix $[\beta]_{N_d \times N_\Theta}$. In this work, a least square method was used. If N samples are used to generate data using a numerical model G_M , then

$$[\Theta]_{N \times N_\Theta} = \begin{bmatrix} 1 & \theta_{1,1} & \dots & \theta_{1,1}^2 & \theta_{1,1} \times \theta_{1,2} & \dots & \theta_{1,1}^3 & \theta_{1,1} \times \theta_{1,2} \times \theta_{1,3} & \dots \\ 1 & \theta_{2,1} & \dots & \theta_{2,1}^2 & \theta_{2,1} \times \theta_{2,2} & \dots & \theta_{2,1}^3 & \theta_{2,1} \times \theta_{2,2} \times \theta_{2,3} & \dots \\ \vdots & \vdots & \vdots & \vdots & \vdots & \vdots & \vdots & \vdots & \vdots \\ 1 & \theta_{i,1} & \dots & \theta_{i,1}^2 & \theta_{i,1} \times \theta_{i,2} & \dots & \theta_{i,1}^3 & \theta_{i,1} \times \theta_{i,2} \times \theta_{i,3} & \dots \\ \vdots & \vdots & \vdots & \vdots & \vdots & \vdots & \vdots & \vdots & \vdots \\ 1 & \theta_{N,1} & \dots & \theta_{N,1}^2 & \theta_{N,1} \times \theta_{N,2} & \dots & \theta_{N,1}^3 & \theta_{N,1} \times \theta_{N,2} \times \theta_{N,3} & \dots \end{bmatrix} \quad (3.21)$$

The regression coefficients are obtained as follows:

$$[\beta] = [([\Theta]^T[\Theta])^{-1}[\Theta]^T[d]]^T \quad (3.22)$$

The residual $[\delta]$ between both a numerical model and a Meta-model is given in eq. (3.23):

$$[\delta] = [d] - [d] \quad (3.23)$$

Meta-model for the response of the SDOF example

A Meta-model was developed to represent the relationship between the cumulative signal energy d and the input parameters $\{\theta\} = \{\theta_1, \theta_2, \theta_3\}^T \equiv \{k, m, \zeta\}^T$. The dataset which includes 100 samples calculated in the previous subsection was used. Trying a larger number of samples shows that if $N \geq 100$, only small changes, which do not influence the sensitivity analysis results, were observed. The degree of the polynomial equation was chosen as 2, and the degree of the mixed terms was chosen as 2. The developed strategy described in the previous sections was used to choose the best terms of the Meta-model, eq. (3.24).

$$\underline{d}^{-1/2} = \{\beta\}^T \{1 \ \theta_1^2 \theta_2^2 \ \theta_1^2 \theta_3^2 \ \theta_1^2 \theta_2 \ \theta_1^2 \theta_3 \ \theta_1^2 \ \theta_1 \theta_2^2 \ \theta_1 \theta_3^2 \ \theta_1 \theta_2 \ \theta_1 \theta_3 \ \theta_1 \ \theta_2 \theta_3^2 \ \theta_2^2 \ \theta_2 \ \theta_3\} \quad (3.24)$$

The statistical properties of the residuals are shown in figure 3.12. $\{\beta\}^T$ was estimated by applying eq. (3.22). For this example $N_d = 1$. The coefficient of the determination $R^2 = 100\%$ indicates that the model shows good fitting of the data. The histogram of the residuals, figure 3.12(a), shows approximately a normal distribution. This is confirmed by the normal probability plot, figure 3.12(b), where all data points are located close to a straight line given that Z - value as follows:

$$Z - value = \frac{\delta - \mu_\delta}{\sigma_\delta} \quad (3.25)$$

Plotting the residuals versus the predicted value, figure 3.12(c), shows a constant variance with zero mean since no outlier can be observed. The results were also confirmed by calculating the mean value of the residuals. The lag plot, figure 3.12(d), shows that the residuals are satisfying the randomness condition since the residuals plot does not show a specific shape that can be fitted by a model. As a result, the developed Meta-model was used to perform the sensitivity analysis. For this example:

$$\{\beta\}^T = \{-2.530 \times 10^{-02}, -2.202 \times 10^{-10}, -5.223 \times 10^{-08}, 8.963 \times 10^{-10}, 3.830 \times 10^{-09}, -9.872 \times 10^{-10}, 2.236 \times 10^{-06}, -1.801 \times 10^{-04}, -8.998 \times 10^{-06}, 9.450 \times 10^{-06}, 1.273 \times 10^{-05}, -3.776 \times 10^{-01}, -6.598 \times 10^{-03}, 2.427 \times 10^{-02}, 4.224 \times 10^{-02}\}^T.$$

Since the Meta-model developed in the last step was used instead of the numerical model G_M , the Total-effect index $sT_{i,j}$ can be written as:

$$sT_{i,j} = \frac{E(Var(d_i | \theta_j \sim \Theta_j))}{Var(d_i)} \quad (3.26)$$

The sensitivity analysis was performed using $N = 10000$ samples generated using a Latin hypercube sampling method. Comparing the computational time of both numerical and

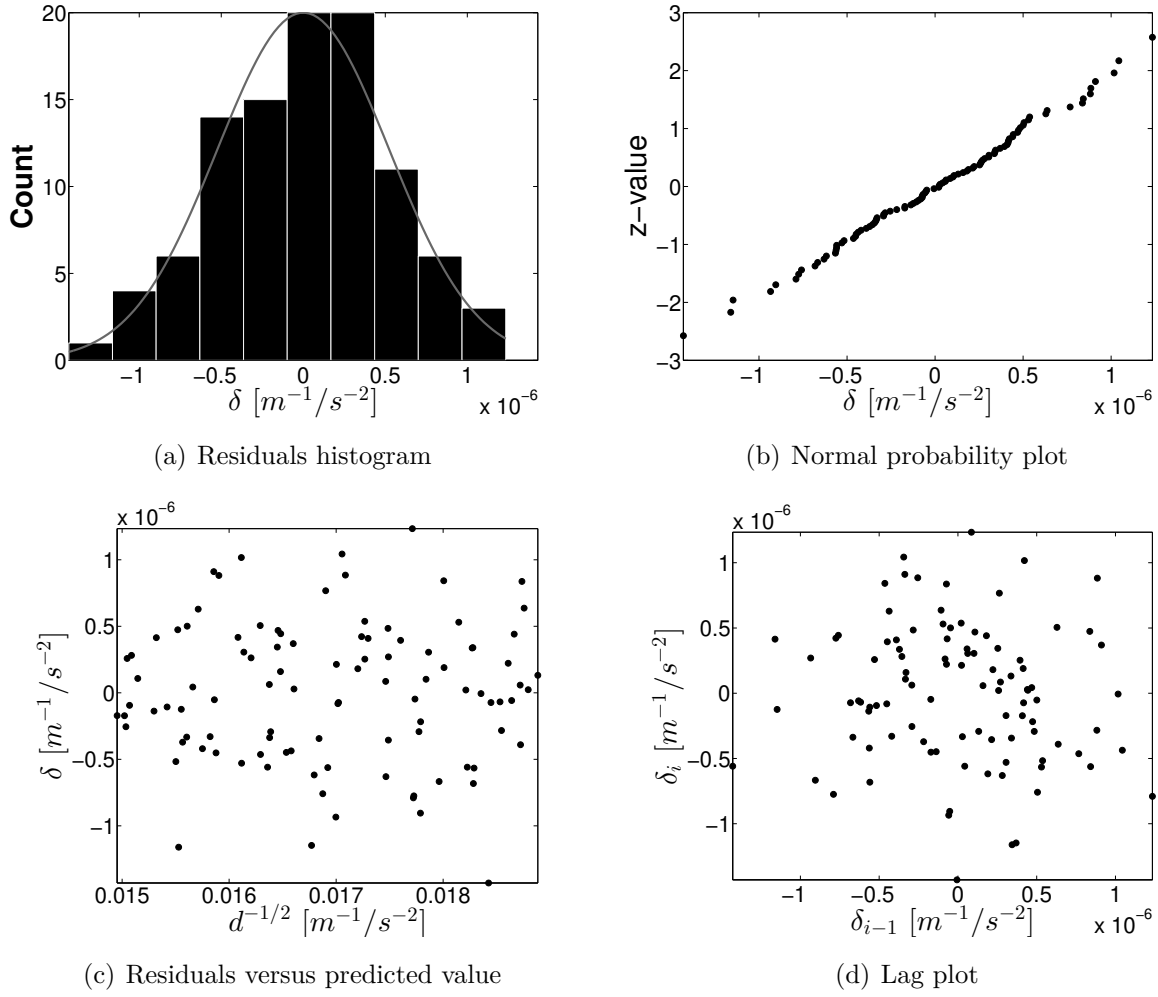


Figure 3.12: Statistical properties assessment of the residuals

regression models to obtain the sensitivity analysis results, the Meta-model was almost 180 times faster without including the time required to generate the Meta-model which took only a few seconds. As a result, using the Meta-model as an alternative of the numerical model G_M brings a significant improvement for the efficiency.

In figure 3.13, the sensitivity analysis results calculated using the numerical model G_M and the Meta-model \underline{d} are presented. The results show good agreement between the results of both models.

Since the result of the sensitivity analysis shows that the output \underline{d} is influenced mainly by the variation of the stiffness $\theta_1 = k$, the chosen DOE is appropriate to detect damage related to the degradation of the stiffness $\theta^g = \Delta k$. Moreover, the variation of the mass and damping ratio does not influence the output significantly.

In order to evaluate the quality of the chosen design, eq.(3.13) was applied. In this example, $\sum sT_{\hat{\theta}} = 0.96$ and $\sum sT_{\theta} = 0.9977$ As a result $Q_{DOE} = 0.95$. The ideal DOE in this example

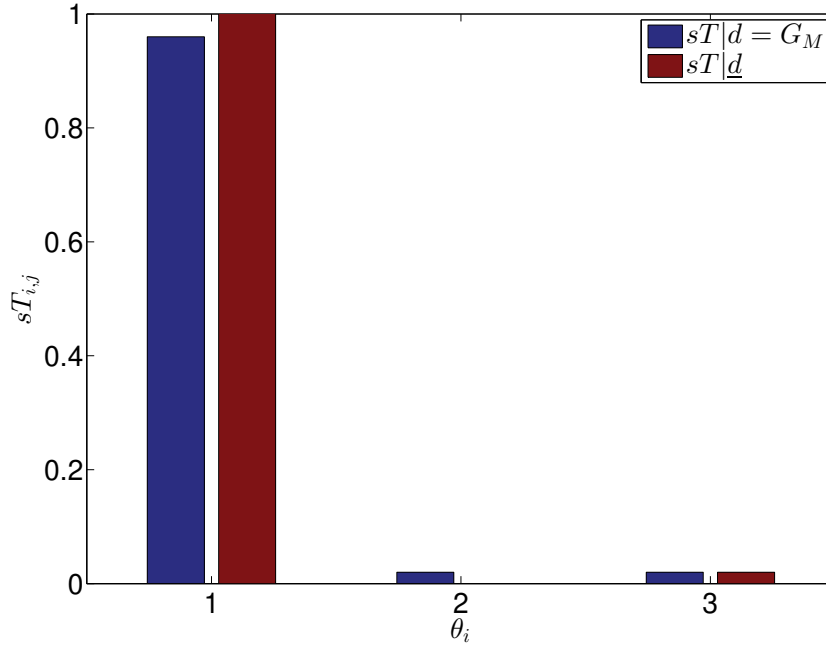


Figure 3.13: The Total-effect index sT calculated using the numerical model G_M and the Meta-model \underline{d} using 10000 samples. Good agreement is observed

will give $\sum sT_{\hat{\theta}} = 1$ and $\sum sT_{\theta} = 1$, as a result, $Q_{DOE} = 1$.

For illustrating the importance of the chosen excitation in case of damage detection, the sensitivity analysis procedure explained in this subsection was applied using a high-frequency harmonic excitation compared to the system's natural frequency, $\eta = 10$, and an impulse excitation separately. Figure 3.14 shows the result of the applied sensitivity analysis. The results show that a high-frequency harmonic excitation was sensitive to the variation of the mass and the impulse excitation was sensitive to both the mass and damping variation. These results were obtained if the described signal energy used as an objective function. As a result, both excitations are not valid to detect damage related to stiffness degradation. Moreover, using a harmonic excitation that has a frequency close to the system's natural frequency, $\eta \approx 1$, leads to a significant response where the stiffness, mass, and damping are activated.

The number of samples N required to obtain reliable sensitivity analysis results can be determined by increasing N until the convergence of sT values is reached.

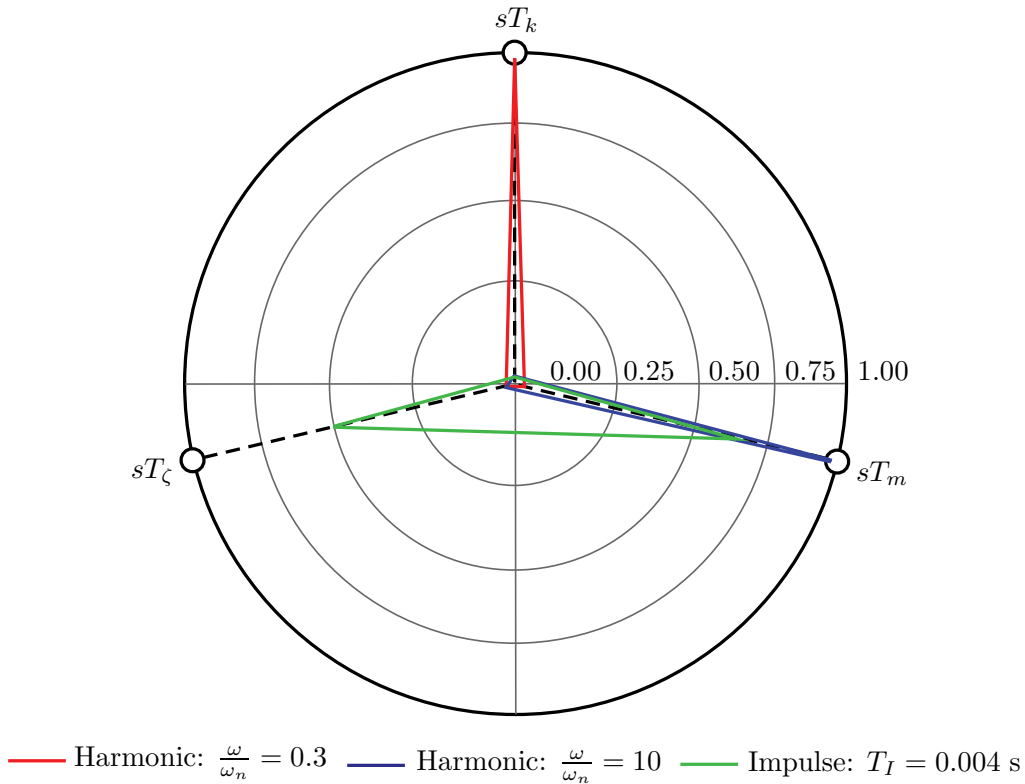


Figure 3.14: The Total-effect index sT using different excitation types

3.5 Model Updating

In this section, the contribution of measurements to the developed strategy is illustrated. If a number of experiments similar to those designed using a numerical model was conducted, it can be possible to reduce the uncertainty of the input parameter by updating the model. Model updating is important if the reliability of the inspection method has to be improved. However, this step requires an existing structure.

There are many methods that can be applied to perform model updating. Some of these methods are deterministic and others are probabilistic. Deterministic updating methods are based on finding a best combination of input values that maximize/minimize an objective function. Information from prior knowledge or measurement uncertainty can be considered by adding penalty, regularization terms and weighting factors. On the other hand, probabilistic model updating methods employ knowledge obtained from measurements, measurement uncertainty and/or the experience of the user in order to obtain a best combination of inputs values. Probabilistic model updating methods are useful if the updating of the statistical properties of the input parameters is required.

In this work a Bayesian updating approach was used. As a result, the statistical properties of the updated parameters were directly obtained. These properties are useful to compute the probability of damage detection in the next step. In order to apply the chosen Bayesian

inference approach the prior density functions and the likelihood function have to be chosen. After that, the posterior density functions can be calculated.

3.5.1 Bayesian inference

Bayesian Inference is a kind of a statistical inference which was derived depending on Bayes Theorem. The principle of this approach is based on the conditional probability. The objective of applying Bayesian Inference can be to identify the input parameters and/or choosing a suitable model class to represent the studied problem. The basic concepts of many Bayesian methods and their application in structural dynamics and civil engineering can be found in Yuen [2010] and Most [2011].

Given A and B are individual events with known probabilities $P(A)$ and $P(B)$. The conditional probability of B given A occurs is:

$$P(B|A) = \frac{P(A \cap B)}{P(A)} \quad (3.27)$$

The conditional probability of A given B occurs can be written as follows:

$$P(A|B) = \frac{P(A \cap B)}{P(B)} \quad (3.28)$$

The Bayesian Inference model is estimated replacing B by the measured outputs $\{\bar{d}\}$; A by the input parameters $\{\theta\}$, and the probability P by the probability density functions p . As a result, the posterior density functions $p(\{\theta\}|\{\bar{d}\})$ are proportional to the likelihood function $p(\{\bar{d}\}|\{\theta\})$ and prior density functions $p(\{\theta\})$ as follows:

$$p(\{\theta\}|\{\bar{d}\}) \propto p(\{\bar{d}\}|\{\theta\})p(\{\theta\}) \quad (3.29)$$

There are different techniques that can be used to apply a Bayesian Inference approach to a numerical method. However, one of the well-known challenges by applying Bayesian Inference is the computational efficiency. In order to overcome this problem several simulation techniques have been developed. For example, the traditional and the adaptive Markov Chain Monte-Carlo simulation have been mostly used. Another example is Kalman filter that can be used as Bayesian updating procedure for linear and slightly nonlinear systems. Many other solutions can be found in literature. However, these simulation techniques must be carefully implemented and applied in order to obtain robust solutions.

In this work, the computational efficiency problem was improved by using Meta-models. The advantage of adapting this solution is that calculating Meta-models is very fast compared to

numerical models. Therefore, the domain of the inputs can be investigated using a large number of samples generated from any prior distribution density function to obtain a robust solution. Moreover, modeling errors due to the simplification process can be considered as shown in the next subsections. In order to generate samples a sampling method is applied. The method is based on sampling from prior density functions of the inputs using a Latin Hypercube Sampling method.

3.5.2 Prior density function

Before considering measurements, preliminary knowledge related to the uncertainty of an input θ is given by a prior probability density function $p(\theta)$. Generally, structural drawings and the properties of the materials can be used to estimate prior information about a studied structure. Yuen [2010] suggested that it is better to choose the prior distribution and its boundaries based on experience than observing the measurements. In literature, there are many classifications of prior probability density functions. For example $p(\theta)$ can be improper or conjugate prior distribution functions. Improper prior distribution functions may lead to posterior distribution functions which have a different family of the prior distribution functions. On the other hand, conjugate prior distribution functions benefit from the knowledge provided by measurements to obtain the statistical properties of posterior distribution functions but keeping the same distribution type.

Prior probability density functions can be either informative or uninformative. For many engineering applications, prior information about studied parameters is in-between. This is because in most cases the physical laws limit their variations, but it is still hard to estimate their actual uncertainty distribution. Generally, a flat prior distribution does not influence the parametric identification in the range where the likelihood dominates. However, it influences a model class selection. More information can be found in Yuen [2010] and Gelma et al. [2004]

There are different methods to choose a prior probability density function. For example, maximum information entropy methods have been used to assigned prior probability density functions based on maximizing the Shannon-Jaynes information entropy which is given as follows, Gray [2009]:

$$S = - \int p(\theta) \log p(\theta) d\theta \quad (3.30)$$

where p is the probability mass function which has to sum to one. Gray [2009] mentioned that although natural logarithms are more convenient for mathematics, it was indicated that logarithms to the base two instead of natural logarithms should be used. This is because base two logarithms provide more intuitive descriptions than natural logarithms.

Another method to select a prior distribution was presented by Chen and Ibrahim [2000]. The method was based on the idea of raising the likelihood function of historical data to a particular power which was limited between 0 and 1. Such prior distribution, which was called the power prior distribution, was proposed to improve arbitrary regression models. These priors were found quite useful in a wide variety of applications, including carcinogenicity studies and clinical trials.

3.5.3 Likelihood function

A likelihood function represents the contribution of the measured data in establishing the posterior distribution, Yuen [2010]. This information describes the quality of a chosen model class which is parametrized by $\{\theta\}$ to explain observations $\{\bar{d}\}$. A likelihood function for data measurement \bar{d} is written as follows

$$L(\bar{d}|\{\theta\}) \equiv p(\bar{d}|\{\theta\}) \quad (3.31)$$

Moreover, if $\{\bar{d}\} = \{\bar{d}_1, \dots, \bar{d}_i, \dots, \bar{d}_n\}^T$ are independently identically distributed random variables with a density function $p(\bar{d}_i|\{\theta\})$, the likelihood function can be written as follows:

$$L(\{\bar{d}\}|\{\theta\}) \equiv \prod_{i=1}^n p(\bar{d}_i|\{\theta\}) \quad (3.32)$$

The density function $p(\bar{d}_i|\{\theta\})$ depends on the studied problem.

In this work, the likelihood function was obtained assuming that uncertainty was independent and normally distributed if no information about the statistical properties of measurements are provided. If $\{\bar{d}\} = \{\bar{d}_1, \dots, \bar{d}_i, \dots, \bar{d}_n\}^T$ are independently identically normally distributed random variables $\bar{d}_i \sim \mathcal{N}(\bar{d}_i, \sigma_{\bar{d}_i}^2)$, then:

$$L(\{\bar{d}\}|\{\theta\}) \propto \prod_{i=1}^n \exp[-\sigma_{\bar{d}_i}^{-2}(\bar{d}_i - d_i)^2] \quad (3.33)$$

where $[\sigma_\epsilon^2]$ is a diagonal matrix referring to the covariance of the total uncertainty $\{\epsilon\} = \{\epsilon_{\bar{d}}\} + \{\epsilon_{d\theta}\}$. Given that $\{d^*\}$ is a set of true response of a structure, then $\{\epsilon_{\bar{d}}\} = \{\bar{d}\} - \{d^*\}$ is the measurement uncertainty and $\{\epsilon_{d\theta}\} = \{d^*\} - \{d\}$ is the model uncertainty related to the input parameters uncertainty. As a result, we can describe the uncertainty between measurements $\{\bar{d}\}$ and the outputs of the numerical model G_M as $\{\epsilon\} = \{\bar{d}\} - \{d\}$. Moreover, if a Meta-model is used to approximate a numerical model, then the uncertainty due to this approximation is $\{d\} - \{\hat{d}\} = \{\delta\}$. Therefore, it is possible to write that $\{\epsilon\} = \{\epsilon_{\bar{d}}\} + \{\epsilon_{d\theta}\} + \{\delta\}$. As a result we can write:

$$[\sigma_\epsilon^2] = [\sigma_d^2] + [\sigma_\theta^2] + [\sigma_\delta^2] \quad (3.34)$$

Investigating $\sigma_{\bar{d}}$ for the SDOF example

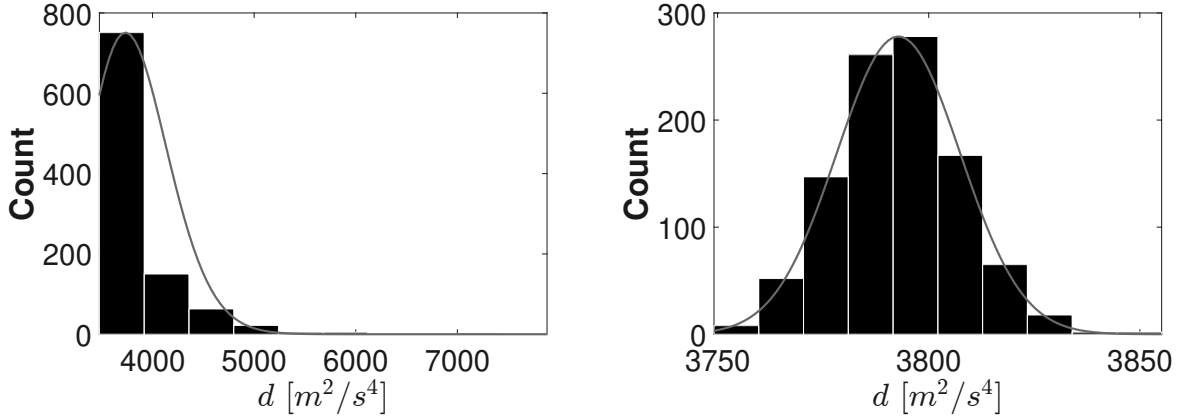
In case of SDOF example, calculating the cumulative energy of the recorded acceleration signal requires defining a start t_0 and an end time t_e of the signal. The initial conditions of the measured response in real tests are expected to differ from the initial conditions defined in the model. If acquiring data is started after the system reaches its steady-state response under periodic excitation, the energy calculated for the entire number of periods, the signal energy becomes independent of the initial condition. However, if the input excitation is contaminated with different types of noise, the influence of the variation of the initial conditions may influence the signal energy.

The standard deviation $\sigma_{\bar{d},1}$, which represents the variation of the response \bar{d} because of the variation of the initial conditions, can be estimated by running the numerical model given in eq. (3.10) assuming different initial conditions and observing the variation of the output d as follows:

1. The variation of the initial conditions was introduced in the model as initial displacements and velocities which are considered as normally distributed random variables. If the system is slightly vibrating with its natural frequency it is possible to assume that $\dot{x}_0 = \omega_n \times x_0$. In this case, the statistical properties of the initial conditions of the studied example can be given as follows: $x_0 \sim \mathcal{N}(0, 0.001^2)$ [m], $\dot{x}_0 \sim \mathcal{N}(0, 0.001^2 \times \omega_n^2)$ [m/s].
2. Running the model for N samples considering the mean values of the input parameters given in table 3.2 the value $\{\bar{d}_1, \bar{d}_2, \dots, \bar{d}_i, \dots, \bar{d}_N\}$ are obtained considering different initial conditions.
3. If \bar{d} is the mean value of $\bar{d}_i : i = 1, 2, \dots, N$, \bar{d} has a distribution close to the normal distribution $\bar{d} \sim \mathcal{N}(\bar{d}, \sigma_{\bar{d},1}^2)$, where $\sigma_{\bar{d},1} = \sigma_{\bar{d}_i,1} / \sqrt{N}$ figure 3.15 (b).
4. $\epsilon_{\bar{d},1} = d^* - \bar{d}$ is the variation of \bar{d} from d^* due to the initial conditions. $\epsilon_{\bar{d},1}$ was considered as a normally distributed random variable with zero mean and a constant standard deviation $\sigma_{\bar{d},1}$, Eq. (3.35).

$$\epsilon_{\bar{d},1} \sim \mathcal{N}(0, \sigma_{\bar{d},1}^2) \quad (3.35)$$

A contamination of the recorded signal by noise is expected. As a result, it is important to investigate the influence of this noise on the structural response. Ideally, if a harmonic



(a) A histogram shows the cumulative signal energy conditions, SDOF example, $N = 1000$ samples

(b) A histogram shows the mean value of the $\bar{d}(t)$ variation due to the variation of the initial conditions, SDOF example, $N = 1000$ tests and each test contains $N = 1000$ samples

Figure 3.15: Statistical properties of the cumulative signal energy $\bar{d}(t)$ considering the variation of the initial conditions.

excitation, which has a constant amplitude F_a and constant frequency ω , is used N times to excite a structure, the same response and a constant signal energy d^* are expected in each test. However, because of the noise signal γ_F , the total energy \bar{d}_t is obtained, figure 3.16, As a result, if N test using identical excitation are performed and $\{\bar{d}_t\} = \{\bar{d}_{t,1}, \bar{d}_{t,2}, \dots, \bar{d}_{t,i}, \dots, \bar{d}_{t,N}\}$ are observed, where $\bar{d}_{t,i}$ is associated with test i .

For the SDOF example the relationship between $\bar{d}_t - d^*$ and the noise γ_F was investigated as follows:

1. $F(t) = F_a \times \sin \omega t + \gamma_F$ given that $\gamma_F \sim \mathcal{N}(0, \sigma_{\gamma_F}^2)$ for this example. $\sigma_{\gamma_F, i+1} = \sigma_{\gamma_F, i} + \Delta \sigma_{\gamma_F}$ where $\sigma_{\gamma_F, 0} = 0$ and $\Delta \sigma_{\gamma_F} = 0.01$ [N]
2. Running the model for N samples considering the mean values of the input parameters given in table 3.2 the value $\{\bar{d}_{t,1,i}, \bar{d}_{t,2,i}, \dots, \bar{d}_{t,r,i}, \dots, \bar{d}_{t,N,i}\}$ where $r = 1, 2, \dots, N$ and $i : \sigma_{\gamma_F} = \sigma_{\gamma_F, i}$.
3. calculating the probability $P(\bar{d}_{t,i} - d^* > 0 | \sigma_{\gamma_F, i})$ as follows:

$$P(\bar{d}_{t,i} - d^* > 0 | \sigma_{\gamma_F, i}) = \frac{N_{\bar{d}_{t,i} > d^*}}{N} \quad (3.36)$$

4. N the size of the sample was increased until $P(\bar{d}_{t,i} - d^* > 0 | \sigma_{\gamma_F, i})$ converged. $N_{\bar{d}_{t,i} > d^*}$ refers to the number of the samples that give $\bar{d}_{t,i} > d^*$.

The results show that for small noise level $\bar{d}_{t,i} \approx d^*$ and for large noise level $\bar{d}_{t,i} > d^*$, figure 3.16 (a). Assuming that the noise level is large enough to obtain $P(\bar{d}_{t,i} > d^*) = 1$, figure 3.16 (b), the minimum value $\bar{d}_{t,min} \in \{\bar{d}_{t,i}\}$ is the closest value to d^* and the likelihood function for \bar{d} , can be written as follows:

$$L(\{\bar{d}\}|\{\theta\}) = \begin{cases} 0 & \text{if } \bar{d} > \bar{d}_{t,min} \\ p(\{\bar{d}\}|\{\theta\}) > 0 & \text{if } 0 < \bar{d} < \bar{d}_{t,min} \end{cases} \quad (3.37)$$

Assuming large noise level is reasonable since the structure was excited far from its natural frequency. As a result, the amplitude of the response is small compared to the amplitude of the response close to the natural frequency. The signal energy of the noisy measurements $\bar{d} = \bar{d}_{t,min} - d_\gamma$ are used to update the numerical model G_M where d_γ refers to the additional energy because of γ_F . $\epsilon_{d,2} = d^* - \bar{d} = d^* - \bar{d}_{t,min} + d_\gamma$ is the variation of \bar{d} from d^* due to γ_F , which has a standard deviation $\sigma_{\bar{d},2}^2 = \sigma_{\bar{d}_{t,min}}^2 + \sigma_\gamma^2$. In the end, it is possible to write $\sigma_d^2 = \sigma_{\bar{d},1}^2 + \sigma_{\bar{d},2}^2$. Assuming that $\epsilon_{d,2}$ is normally distributed and based on eq. (3.38) truncated normal distribution $f(d, \bar{d}, \sigma_{\bar{d},2}, 0, \bar{d}_{t,min})$, P. Robert [1995], can be used for the likelihood function.

$$f(d, \bar{d}, \sigma_{\bar{d},2}, 0, \bar{d}_{t,min}) = \frac{1}{\sigma_{\bar{d},2}} \times \frac{\phi\left(\frac{d-\bar{d}}{\sigma_{\bar{d},2}}\right)}{\Phi\left(\frac{\bar{d}_{t,min}-\bar{d}}{\sigma_{\bar{d},2}}\right) - \Phi\left(\frac{0-\bar{d}}{\sigma_{\bar{d},2}}\right)} \quad (3.38)$$

where

$$\phi\left(\frac{d-\bar{d}}{\sigma_{\bar{d},2}}\right) = \frac{e^{-0.5 \times \left(\frac{d-\bar{d}}{\sigma_{\bar{d},2}}\right)^2}}{\sqrt{2 \times \pi}} \quad (3.39)$$

$$\Phi\left(\frac{0-\bar{d}}{\sigma_{\bar{d},2}}\right) = \frac{1}{\sqrt{2 \times \pi}} \int_{-\infty}^0 e^{-0.5 \times \left(\frac{d-\bar{d}}{\sigma_{\bar{d},2}}\right)^2} \quad (3.40)$$

$$\Phi\left(\frac{\bar{d}_{t,min}-\bar{d}}{\sigma_{\bar{d},2}}\right) = \frac{1}{\sqrt{2 \times \pi}} \int_{-\infty}^{\bar{d}_{t,min}} e^{-0.5 \times \left(\frac{d-\bar{d}}{\sigma_{\bar{d},2}}\right)^2} \quad (3.41)$$

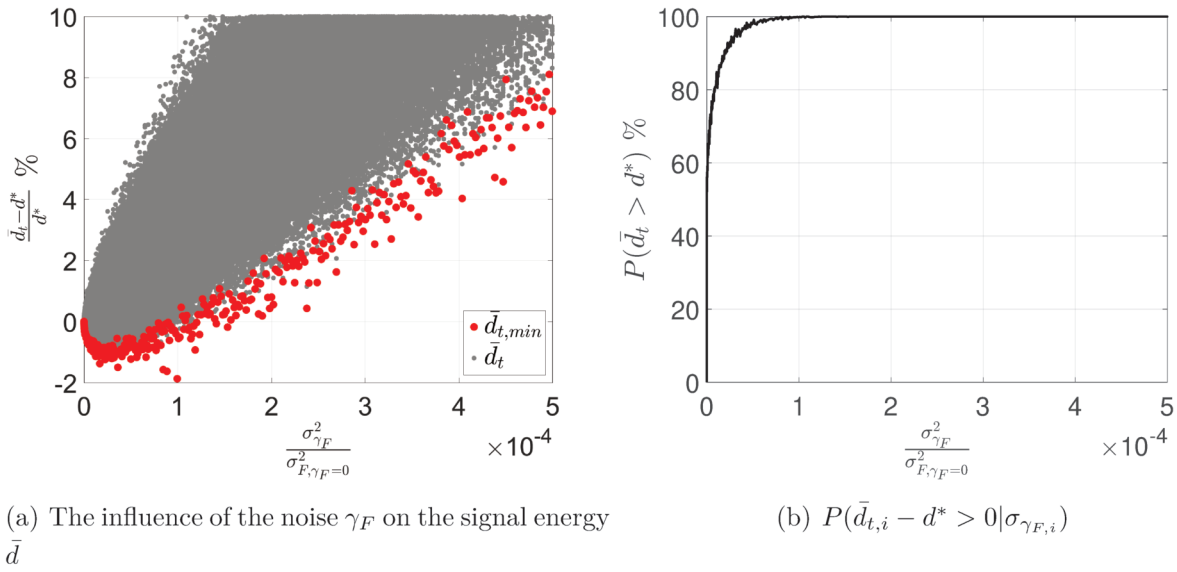


Figure 3.16: Investigating the influence of the noise level γ_F on $\bar{d}_t - d^*$.

3.5.4 Posterior density function

In this step, the result of the Total-effect index sensitivity analysis performed in section 3.4 can be used to reduce the computational effort by updating only important parameters $\{\hat{\theta}\} \subseteq \{\theta\}$. The important parameters are the parameters that influence the studied response significantly.

$$p(\{\theta\} | \{\bar{d}\}) = \frac{p(\{\bar{d}\} | \{\theta\})p(\{\theta\})}{\int p(\{\bar{d}\} | \{\theta\})p(\{\theta\})d\theta} \quad (3.42)$$

A Latin hypercube sampling method is applied to generate N samples from the prior probability density functions. $\int p(\{\bar{d}\} | \{\theta\})p(\{\theta\})d\theta$ is constant and works as a normalizing factor. It is important to mention that small posterior uncertainty does not mean a good fitting, Yuen [2010]. However, it indicates that measurements contain useful information that can lead to reducing the uncertainty the considered inputs.

Meta-Model for model updating

In order to reduce the computational efforts, a Meta-model is used for model updating. This is necessary if a large number of important parameters has to be updated using a complex model G_M . The same procedure explained to develop the Meta-model for sensitivity analysis can be applied. However, the Meta-model for model updating can be developed considering only the important parameters $\{\hat{\theta}\} \subseteq \{\theta\}$. The relationship between a structural response and the highlighted parameters is obtained as follows:

$$\{\hat{d}\} = [\hat{\beta}]\{1 \ \hat{\theta}_i \ \hat{\theta}_i\hat{\theta}_j \ \hat{\theta}_i\hat{\theta}_j\hat{\theta}_r \ \dots\} \quad (3.43)$$

The residual $[\hat{\delta}]$ between a numerical model and a Meta-model is given in eq. (3.44):

$$[\hat{\delta}] = [d] - [\hat{d}] \quad (3.44)$$

The regression coefficients are obtained as follows

$$[\hat{\beta}] = [(\hat{\Theta})^T[\hat{\Theta}]]^{-1}[\hat{\Theta}][d]^T \quad (3.45)$$

Meta-model for the SDOF example model updating

For the SDOF example, a Meta-model was used for model updating, figure 3.17. The Meta-model was developed considering only the important parameters $\{\hat{\theta}\} \subseteq \{\theta\}$.

Since the result of the sensitivity analysis indicated that the stiffness $\theta_1 = k$ is the dominant parameter, the Meta-model considers only the stiffness $\{\hat{\theta}\} = \{\theta_1\}$. The degree of the polynomial equation was chosen as 2. Since there is only one parameter, there are no mixed terms. The least-squares method was used to obtain the regression coefficients matrix $[\hat{\beta}]_{N_d \times N_{\hat{\Theta}}}$. The Meta-model, eq. (3.46), was obtained based on the same data set used for developing the Meta-model for sensitivity analysis. The same approach was followed to assess the statistical properties of the residuals.

Figure 3.18 shows the statistical properties of the residuals. The results show that by considering only the stiffness, the coefficient of determination reduced to $R^2 = 98.8\%$. Moreover, both the histogram of the residuals, figure 3.18(a), and the normal probability plot, figure 3.18(b), show that excluding the unimportant parameters influenced the residual distribution. However, the lag plot, figure 3.18(c), shows that the residuals are still satisfying the randomness condition since the residuals plot does not show a specific shape that can be fitted by a model. Plotting the residuals versus the predicted value, figure 3.18(d), shows a constant zero mean variation since no outlier can be observed. The results were also confirmed by calculating the mean value of the residuals. The developed Meta-model was used to update the stiffness. For this example:

$$\{\hat{\beta}\}^T = \{4.67 \times 10^{-04}, 5.90 \times 10^{-11}, 3.00 \times 10^{-06}\}^T.$$

$$\{\hat{d}\} = \{\hat{\beta}\}^T \{1 \ \theta_1^2 \ \theta_1\} \quad (3.46)$$

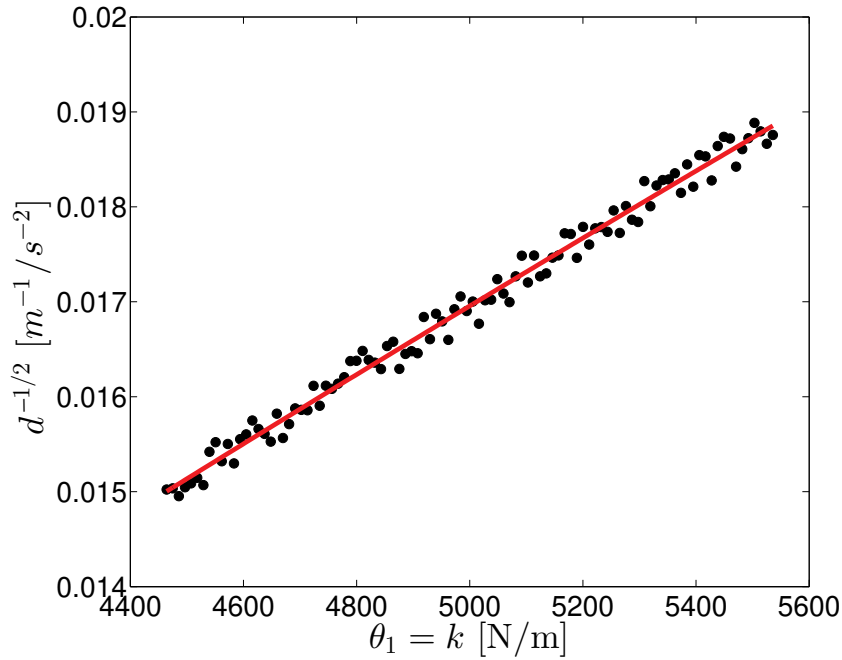


Figure 3.17: Developed Meta-model for model updating

Model updating results

In this example, the true values of the studied input parameters $\{\theta^*\}$ given in table 3.1 are used to simulate the test to obtain \bar{d} by solving the analytical model. It was assumed that COV of \bar{d} is 5% which includes the uncertainty of the structural response due to initial boundary conditions and white noise. This value is obtained if $\frac{\sigma_{\gamma_F}^2}{\sigma_{F, \gamma_F=0}^2} \approx 7 \times 10^{-4}$. As a result, the measurement was given as $\bar{d} \sim \mathcal{N}(3376, 168^2)$. By applying the Bayesian inference approach explained in section 3.5, the uncertainty of the important parameters $p(\hat{\theta}) \equiv p(k)$ was updated to $p(\hat{\theta}|\bar{d}) \equiv p(k|\bar{d})$ using the Meta-model in eq. (3.46). The results were compared with the updated uncertainty using the model in eq. (3.24) and the numerical model in eq. (3.9). The posterior was calculated by generating $N = 100$ samples. Using more samples does not have a significant influence on the results. It took about 0.11 seconds to calculate the posterior density function of the stiffness using the Meta-model in eq. (3.46) and about 0.34 seconds to update the uncertainty of all the parameters using the model in eq. (3.24). Updating the uncertainty of the parameters using the numerical model G_M required about 1600 seconds.

The results shown in figures 3.19, 3.20 and 3.21 indicate good agreement of the posterior density functions updated by different models. The importance of the model updating step can be quantified in the next subsection where the probability of damage detection is computed.

In order to evaluate the quality of a set of measurements for model updating, an index Q_M has been used. The developed index is limited in range $[0, 1] = \{Q_M \in \mathbb{R} : 0 \leq Q_M \leq 1\}$. Based on

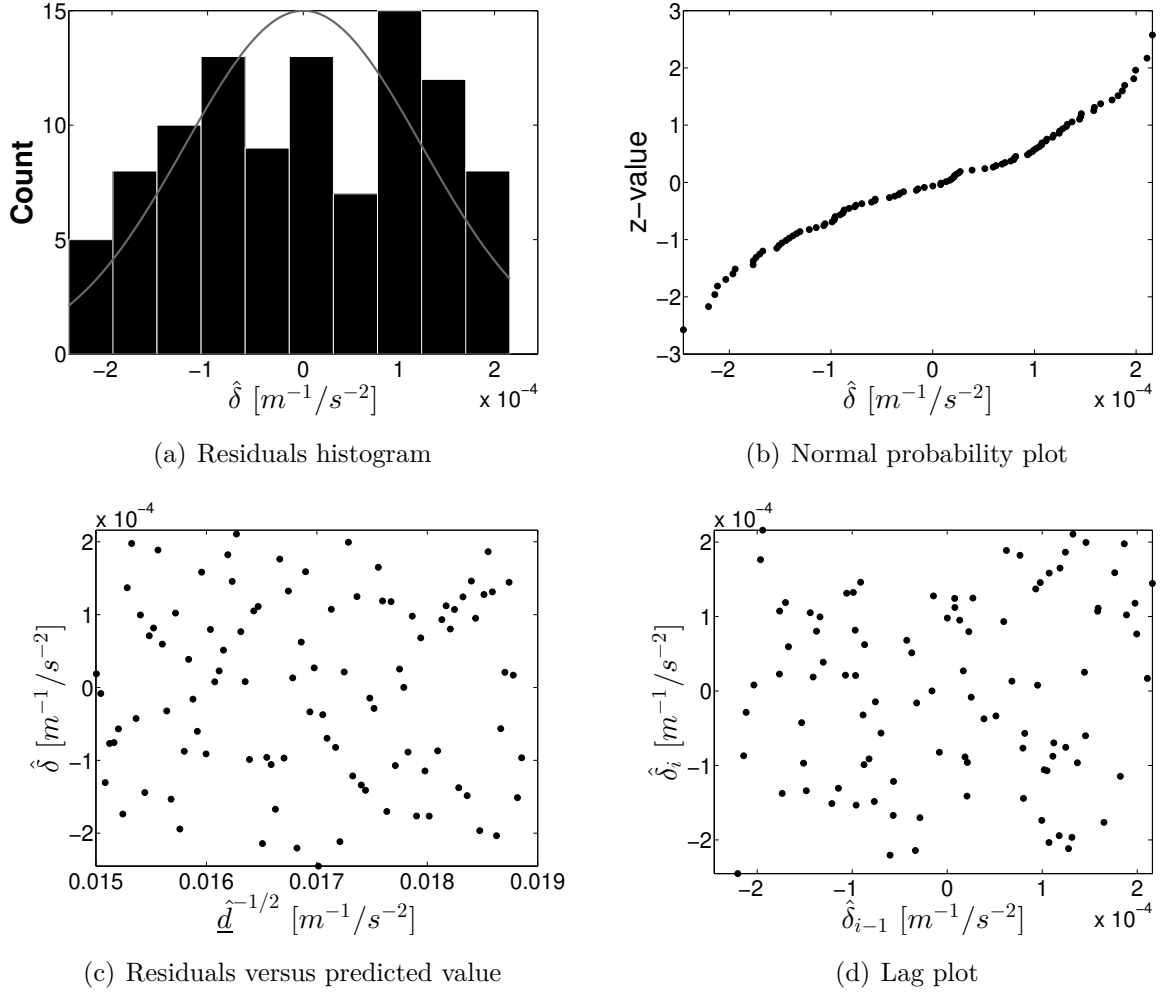


Figure 3.18: Statistical properties assessment of the residuals

the standard deviations of the $N_{\hat{\theta}}$ important parameters before updating $\sigma_{\hat{\theta}}$ and after updating $\sigma_{\hat{\theta}|\bar{d}}$ the index Q_M can be written

$$Q_M = 1 - \frac{1}{N_{\hat{\theta}}} \sum_{j=1}^{N_{\hat{\theta}}} \frac{\sigma_{\hat{\theta}_j|\bar{d}}}{\sigma_{\hat{\theta}_j}} \quad (3.47)$$

Eq.(3.47) means that if measurements do not provide any new information to a model, then $\sigma_{\hat{\theta}} = \sigma_{\hat{\theta}|\bar{d}}$ and $Q_M = 0$. If measurements lead to $\sigma_{\hat{\theta}} \gg \sigma_{\hat{\theta}|\bar{d}}$, then measurements contain valuable information about the studied problem and $Q_M \approx 1$. Obtaining $0 < Q_M < 1$ means, there is possibility to reduce the uncertainty by improving the quality of the measurements.

Eq.(3.47) was applied to evaluate the quality of the measurements based on the information they provide. Given that $\mu_k = \sum_{i=1}^N k_i p_i(k|\bar{d})$ is the mean value of the stiffness k after updating, the standard deviation of the stiffness before updating $\sigma_{\hat{\theta}}$ and after updating $\sigma_{\hat{\theta}|\bar{d}}$ were computed

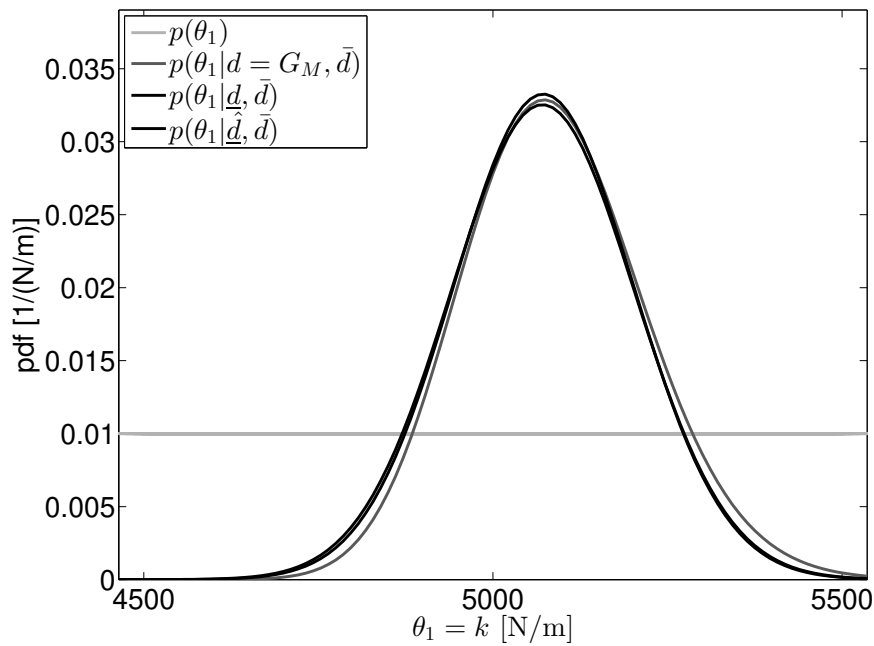


Figure 3.19: Prior and posterior density functions of the uncertainty of the stiffness k obtained using the numerical model G_M , the Meta-model for sensitivity analysis \underline{d} and the Meta-model for model updating $\hat{\underline{d}}$

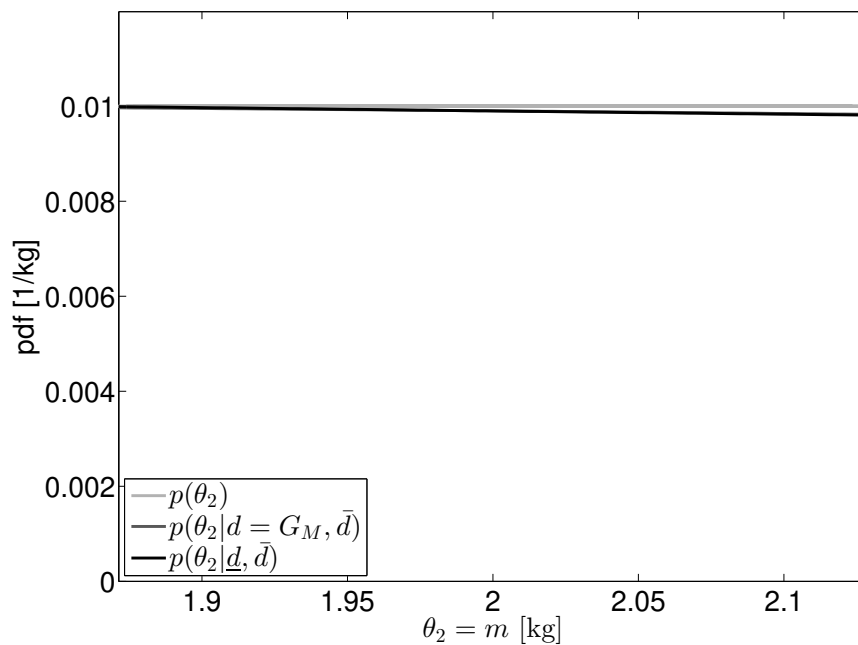


Figure 3.20: Prior and posterior density functions of the uncertainty of the mass m obtained using the numerical model G_M and the Meta-model for sensitivity analysis \underline{d}

as follows:

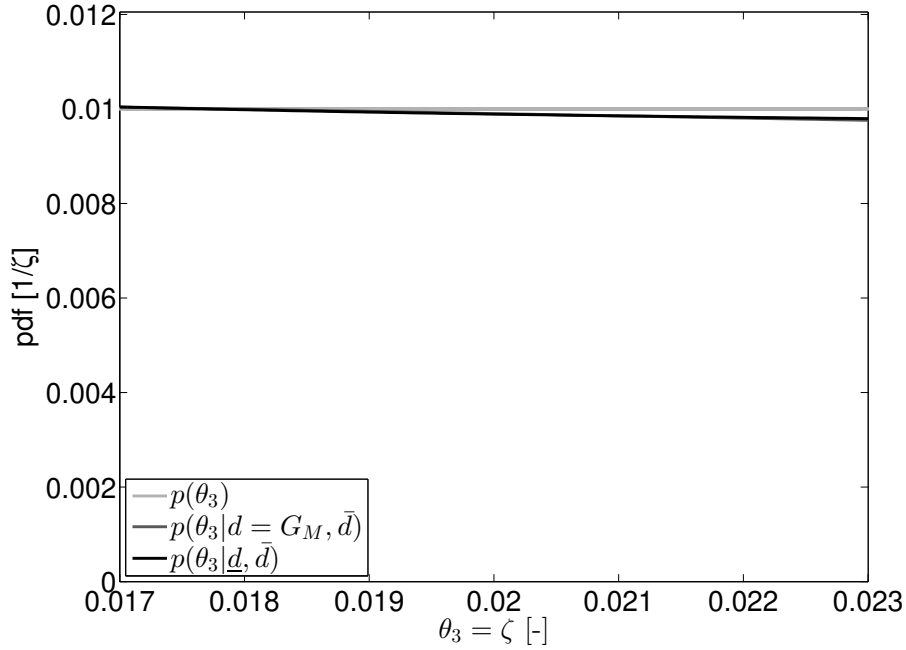


Figure 3.21: Prior and posterior density functions of the uncertainty of damping ratio ζ obtained using the numerical model G_M and the Meta-model for sensitivity analysis \underline{d}

$$\sigma_{k|\bar{d}} = \sum_{i=1}^N [(k_i - \mu_k)^2 p_i(k)]^{0.5} = 1250 \quad (3.48)$$

$$\sigma_{k|\bar{d}} = \sum_{i=1}^N [(k_i - \mu_k)^2 p_i(k|\bar{d})]^{0.5} = 130.4 \quad (3.49)$$

As a result, the quality of the measurements Q_M can be obtained as follows:

$$Q_M = 1 - \frac{\sigma_{k|\bar{d}}}{\sigma_k} = 1 - \frac{130.4}{1250} = 0.90 \quad (3.50)$$

3.6 The reliability of an inspection method

The evaluation of an inspection method was accomplished by the probability of detection POD curve. The POD curve can be obtained using different approaches. For example, an approach was suggested in MIL-HDBK-1823A [2009] which is useful to avoid a large number of simulated/real experiments if the relationship between the size of the damage and a structural response can be represented using a simple linear equation. In this work, an approach was developed and applied to more general cases. The developed method can be used if more

than one structural response or damage indicator is used to detect damage. In this case, the relationship between damage size and a damage indicator may take any shape. However, the developed method requires a sufficient number of simulated/real experiments.

3.6.1 Damage indicator

In this work, the difference between a damage model θ^g and a damage indicator model $f(\theta^g)$ is that a damage indicator model is based on the studied structural response which is chosen to detect damage, for example, modal parameters obtained from applying a system identification method or a structural response in time domain. The damage indicator is affected by the variation of other input parameters and the variation of the experimental data. A damage model represents the physical influence of studied damage on a structure or a part of it, for example, reducing stiffness. If ϵ_t refers to the total uncertainty from different resources and based on eq. (1.4) it is possible to define a damage indicator model f as follows:

$$f : \theta^g \rightarrow d(\theta^g, \epsilon_t) \quad (3.51)$$

A damage indicator based on the cumulative energy of a structural response of a studied system was used. The structural response d_i due to damage target size θ_i^g was obtained by generating samples from the posterior density functions of the important parameters $p(\{\hat{\theta}\}|\{\bar{d}\})$ and the initial prior density functions of the unimportant parameters $p(\{\theta\} \setminus \{\hat{\theta}\})$, eq. (3.52), given that $\theta_i^g \in [\theta_{min}^g, \theta_{max}^g]$. The measurement uncertainty $\epsilon_{\bar{d}}$ should be considered as well.

$$d(\theta_i^g) = f(G_M(\{\hat{\theta}\}, \{\theta\} \setminus \{\hat{\theta}\}, \theta_i^g) + \epsilon_{\bar{d}}) \quad (3.52)$$

where $\{\theta\} \setminus \{\hat{\theta}\}$ refers to the parameters in $\{\theta\}$ but not in $\{\hat{\theta}\}$. A damage indicator should be sensitive to damage only. If this is not the case, a high probability of false alarm is expected. It is important to mention that the variation of input parameters in time is not included in this work since the structure is investigated in a particular point of time of its life. If a monitoring system has to be developed, the variation of input parameters in time should be included.

3.6.2 Probability of damage detection

In civil engineering structures, many sensor types and sensor locations have been used to monitor a response of a structure. Therefore, combining and abstracting the whole system results in a damage indicator can be a nontrivial problem. This is because of normalization requirements and the necessity of converting some response types to fit other types before combining them, for example, converting velocity to acceleration. As a result, several types of

uncertainty should be considered. For example, one type of uncertainty could be the uncertainty when measuring each quantity separately — for example, acceleration measurement uncertainty, velocity measurement uncertainty, etc. A different kind of uncertainty can be observed when computing further quantities from a certain measurement such as calculating acceleration from velocity. In this case, uncertainty propagation has to be taken into account.

In this work, a method to calculate the probability of detection POD was developed based on reliability principles. If a studied structure has a response d_i considering damage size θ_i^g and d_{i+1} considering damage size θ_{i+1}^g and if $\theta_{i+1}^g \geq \theta_i^g \Leftrightarrow d_{i+1} \geq d_i$, the probability of damage detection can be computed as follows:

$$POD(\theta^g) = P(d(\theta^g) > d_c | \theta^g) \quad (3.53)$$

where d_c is the threshold related to a response d . d_c should be chosen by studying the influence of the variation of other input parameters on the response d . It is possible to rewrite eq. (3.53) as follows:

$$POD(\theta^g) = 1 - P(d(\theta^g) < d_c | \theta^g) \quad (3.54)$$

Similarly, the probability of the false alarm PFA or the false positive PFP can be computed as follows

$$PFA \equiv PFP = P(d(\theta^g) > d_c | \theta^g = 0) \quad (3.55)$$

It is possible to rewrite eq. (3.55) as follows

$$PFA \equiv PFP = 1 - P(d(\theta^g) < d_c | \theta^g = 0) \quad (3.56)$$

If $N_d = n$ outputs $\{d\} = \{d_{i,1}, d_{i,2}, \dots, d_{i,n}\}$ were observed given damage size θ_i^g and $\{d\} = \{d_{i+1,1}, d_{i+1,2}, \dots, d_{i+1,n}\}$ were observed given damage size θ_{i+1}^g and if $\theta_{i+1}^g \geq \theta_i^g \Leftrightarrow d_{i+1,1} \geq d_{i,1} \cap d_{i+1,2} \geq d_{i,2} \cap \dots \cap d_{i+1,n} \geq d_{i,n}$ $POD(\theta^g)$ and PFA can be computed based on the equations mentioned above as follows:

$$POD(\theta^g) = 1 - P(d_1 < d_{c1} \cap d_2 < d_{c2} \cap \dots \cap d_n < d_{cn} | \theta^g) \quad (3.57)$$

$$PFP = 1 - P(d_1 < d_{c1} \cap d_2 < d_{c2} \cap \dots \cap d_n < d_{cn} | \theta^g = 0) \quad (3.58)$$

where $\{d_c\} = \{d_{c1}, d_{c2}, \dots, d_{cn}\}$ are the thresholds related to the response $\{d\} = \{d_1, d_2, \dots, d_n\}$. If a model updating approach was applied using a model G_M , then information obtained from measurements $\{\bar{d}\}$ can be introduced in the $POD(\theta^g)$ by considering the posterior density functions $p(\{\theta\}|\{\bar{d}\})$ as follows:

$$POD(\theta^g) = 1 - P(d_1 < d_{c1} \cap d_2 < d_{c2} \cap \dots \cap d_n < d_{cn} | \theta^g, \bar{d}) \quad (3.59)$$

In civil engineering, identifying the location of damage can be the most difficult problem. For this reason, it is important to include the influence of damage location on the reliability of global inspection methods. If damage θ^g is located at element el^g , then the $POD(\theta^g)$ including damage location can be written as

$$POD(\theta^g) = 1 - P(d_1 < d_{c1} \cap d_2 < d_{c2} \cap \dots \cap d_n < d_{cn} | \theta^g, \bar{d}, el_{min}^g \leq el^g \leq el_{max}^g) \quad (3.60)$$

where el_{min}^g and el_{max}^g refer to the accepted limits of damage location. In this case, PFA includes that damage was detected but at the wrong location, $el^g < el_{min}^g$ or $x^g > el_{max}^g$. In this case, the chosen damage indicator should be able to provide information about the location of damage.

Another critical issue is multi-location damage detection. In this case, damage exists in several locations at a structure. The reliability of a chosen inspection method can be defined based on its ability to detect damage at all or most locations. If different types of damage were introduced, then the reliability of the chosen inspection can be investigated for each damage separately.

In order to evaluate the quality of a chosen inspection method for detecting a certain damage size θ^{g*} , an index Q_D has been developed based on the probability of detection of a certain damage size and the probability of false alarm. The developed index is limited in range $[0, 1]$, $\{Q_D \in \mathfrak{R} : 0 \leq Q_D \leq 1\}$. In this work, Q_D is computed as follows:

$$Q_D = POD(\theta^{g*})(1 - PFP) \quad (3.61)$$

where $POD(\theta^{g*})$ is the probability of detection of a certain damage size θ^{g*} and PFP is the probability of false positive or probability of false alarm PFA. If $POD(\theta^{g*}) = 1$ and $PFP = 0$, then it is possible to detect damage θ^{g*} without any misleading because of the false alarm. As a result, $Q_D = 1$ which is the ideal case. If $0 \leq Q_D < 1$, it is possible that the studied damage size can be missed and/or a false alarm has to be expected.

Obtaining a reliable POD curve requires a sufficient number of samples N . It is possible to estimate N based on the PFP, $N = f(PFP)$. If d_{ci} introduced in eq. (3.58) is chosen in way that $P(d_1 < d_{c1}) = P(d_2 < d_{c2}) = \dots P(d_i < d_{ci}) = \dots P(d_n < d_{cn})$ and if d_i and d_j are

independent, where $\theta^g = 0$ and $i \neq j$, it is possible to write:

$$PFP = 1 - (P(d_1 < d_{c1} | \theta^g = 0))^n \quad (3.62)$$

In this work the relationship between N and PFP was assumed for a single output d , $n = 1$, $N = 1/PFP$. For example, if $PFP = 0.01$ is required, it should be $N \geq 100$. For $n \geq 1$, N can be calculated as follows:

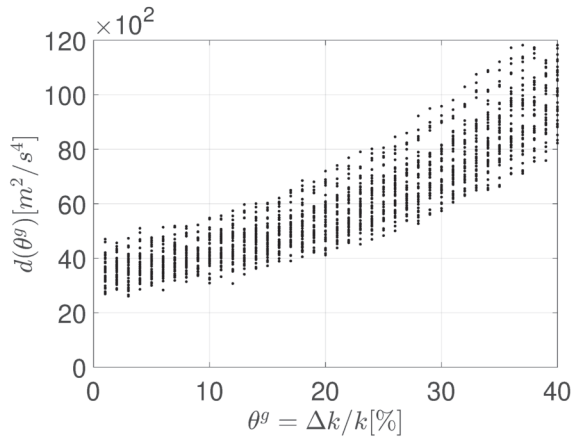
$$N = f(P(d_1 < d_{c1} | \theta^g = 0)) \geq \frac{1}{1 - (1 - PFP)^{1/n}} \quad (3.63)$$

Eq. (3.63) indicates that by reducing the PFP, N should be increased. For example, if $PFP=0.05$ and $n=5$, $P(d_1 < d_{c1} | \theta^g = 0) = 0.9898$. $N = 1/(1 - 0.9898) \geq 98$. N should be increased until convergence of the POD curves is obtained.

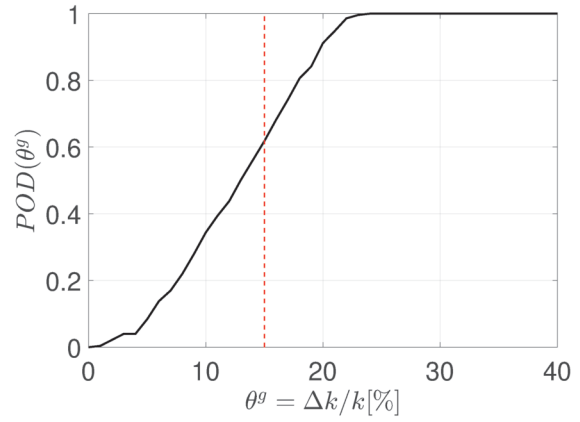
POD in the SDOF example

The method was applied to the SDOF example. The $\theta_i^g \in [0, 40\%] \times k$ was used to calculate the response $d_i(\theta_i^g)$ as in eq. (3.52) with an interval $\Delta\theta^g = 1\%$. As a result, 41 damage size steps were investigated. The threshold was chosen $PFA \equiv PFP = POD(\theta^g | \theta^g = 0) \leq 0.01$. It means that if there was no damage, only 1% of the indicator values d exceeded d_c and leads to false alarm. As a result, eq. (3.55) can be used to select the threshold value that satisfies the PFP condition. Based on eq. (3.54) and the chosen threshold value, the POD curve can be computed. From eq. (3.63), $N = 100$. To ensure a constant POD, at each damage size step $N = 500$ samples were generated and solved using the numerical model G_M . The total number of problems solved was $500 \times 41 = 20500$ times. The results show that model updating improved the reliability of the chosen inspection method. Without model updating, the inspection method is not reliable based on the problem definition in eq. (3.7)

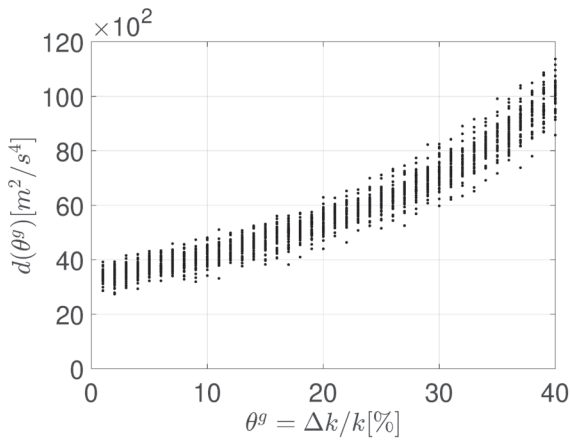
In order to evaluate the inspection method for detecting 15% stiffness degradation with and without model updating based on the index Q_D developed in this work, eq. (3.61) was applied, table 3.3.



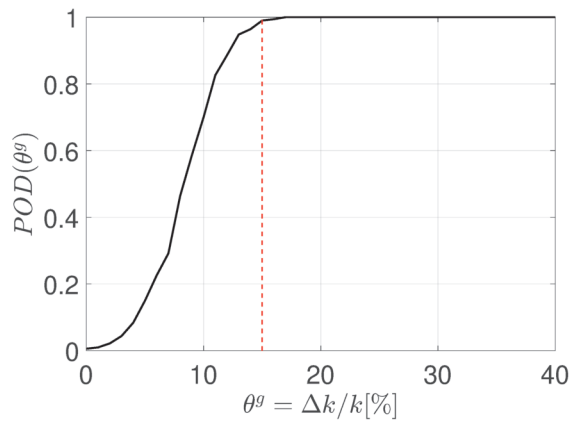
(a) Damage-structural response relationship without model updating



(b) $POD(\theta^g)$ without model updating



(c) Damage-structural response relationship with model updating



(d) $POD(\theta^g)$ with model updating

Figure 3.22: Results of developed POD method

Table 3.3: Evaluation the inspection method for detecting 15% stiffness degradation with and without model updating using Q_D

	$p(\theta)$	$p(\theta \bar{d})$
POD	0.61	0.98
PFP	0.01	0.01
Q_D	0.60	0.97

3.7 Model quality and inspection method reliability

The relationship between the assessment procedure of the partial models presented in this chapter and the reliability of an inspection method for damage detection is concluded in table 3.4.

Table 3.4: Partial models assessment procedures and the reliability of an inspection method

Level	Assessment question	Assessment Procedure	Partial model	Coupling	Index	Possible improvement
1	Is the agreement between the response of the numerical model G_M and the experimental model G_E or the reference model G_{MR} achieved?	$d(\theta^g) \propto \bar{d}(\theta^g)$	Numerical model	—	Q_V	Improve the numerical model and / or damage model
2	Does a chosen DOE provide information about a desired parameter related to a chosen damage type?	Sensitivity analysis	Numerical model+DOE	Probabilistic models	Q_{DOE}	Applying different independent tests (for example, using several types of excitations, modifying sensors' location)
3	Do experiments reduce the uncertainty of the desired parameter related to a chosen damage type by means of model updating?	Model updating	Numerical model + DOE + experiments	Prior, likelihood density functions	Q_M	Repeating experiments, reducing noise, using high quality sensors
4	Is the chosen inspection method reliable for detecting a certain damage type and size?	POD, PFA	Numerical model + DOE + experiments + damage indicator	POD method	Q_D	Improving Q_V , Q_{DOE} , Q_M , choosing another inspection method

Chapter 4

Numerical Study: Three degrees of freedom frame like structure

4.1 Introduction

The main objective of this example is to investigate the performance of a vibration-based method for damage detection in three degrees of freedom system. The reliability of the inspection method for detecting multi-locations damage scenarios is studied. Several types of excitations were applied to compute the structural response at the considered degrees of freedom. The POD method developed in this work is used to obtain the POD curves. In this example, the reliability of the inspection method considers the influence of the location of damage.

4.2 Problem definition

A three degrees of freedom (DOF) frame $\{x\} = \{x_1, x_2, x_3\}$, figure 4.1, is used to illustrate the influence of the considered uncertainty types on the reliability of a chosen inspection method. In this example a stiffness-damping-lumped mass model, G_M , was developed considering the stiffness $\{\theta_1, \theta_2, \theta_3\} = \{k_1, k_2, k_3\}$, the masses $\{\theta_4, \theta_5, \theta_6\} = \{m_1, m_2, m_3\}$ and the damping ratios $\{\theta_7, \theta_8, \theta_9\} = \{\zeta_1, \zeta_2, \zeta_3\}$. The mass matrix $[M]$ is considered diagonal which means $M_{i,j} = 0$ if $i \neq j$ and $M_{i,j} = m_i$ if $i = j$. In this example it was assumed that the system is linear and only modal damping was considered. The equations of motion, eq.(4.1), can be written using the matrices in eq.(4.2), eq.(4.3) and eq.(4.4).

$$[M]\{\ddot{x}\} + [C]\{\dot{x}\} + [K]\{x\} = \{F_t\} \quad (4.1)$$

$$[K] = 2 \times \begin{bmatrix} k_1 & -k_1 & 0 \\ -k_1 & k_1 + k_2 & -k_2 \\ 0 & -k_2 & k_2 + k_3 \end{bmatrix} \quad (4.2)$$

$$[M] = \begin{bmatrix} m_1 & 0 & 0 \\ 0 & m_2 & 0 \\ 0 & 0 & m_3 \end{bmatrix} \quad (4.3)$$

The damping matrix is assumed as a linear combination of the mass and stiffness matrices. The damping matrix can be written in this case as follows:

$$[C] = \alpha \times [M] + \beta \times [K] \quad (4.4)$$

where:

$$\alpha = \frac{2(\zeta_2 \omega_{n,1}^2 \omega_{n,2} - \zeta_1 \omega_{n,2}^2 \omega_{n,1})}{\omega_{n,1}^2 - \omega_{n,2}^2} \quad (4.5)$$

$$\beta = \frac{2(\zeta_1 \omega_{n,1} - \zeta_2 \omega_{n,2})}{\omega_{n,1}^2 - \omega_{n,2}^2} \quad (4.6)$$

Finding α and β requires assuming the damping ratio for two modes. The remaining damping ratio ζ_3 for the third mode can be calculated as follows

$$\zeta_3 = \frac{\alpha}{2\omega_{n,3}} + \frac{\beta\omega_{n,3}}{2} \quad (4.7)$$

where $\omega_{n,r}$ and ζ_r refer to the natural frequency and the damping ratio associated with the mode r . The response of the structure $\ddot{x}(t)$ under an excitation $F(t)$ has been obtained using the Newmark $\beta = 1/4$ method (constant average acceleration).

The inspection method is based on observing the influence of damage θ^g on the measured acceleration $\ddot{x}(t)$ of the system under a certain excitation $F(t)$. The cumulative signal energy d of the acceleration time histories for a specified time period $T = t_e - t_0$ was chosen as an objective function, eq. (3.5).

Giving that $k_{i,0}$ refers to the initial (undamaged) stiffness value, $i \in \{1, 2, 3\}$, four damage cases were studied:

1. $\theta^g = \Delta k_1 = k_{1,0} - k_1$ refers to the degradation of the stiffness of the top story $\theta_1 = k_1$.

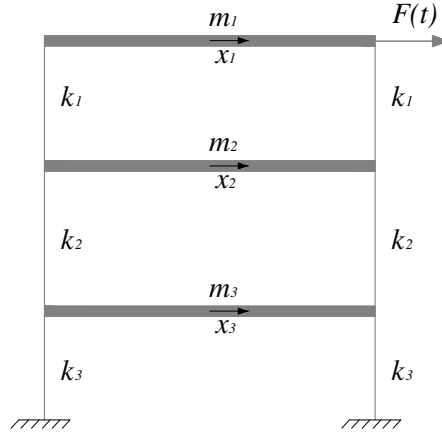


Figure 4.1: Three degrees of freedom frame structure excited by a force $F(t)$ at x_1

2. $\theta^g = \Delta k_2 = k_{2,0} - k_2$ refers to the degradation of the stiffness of the middle story $\theta_2 = k_2$.
3. $\theta^g = \Delta k_3 = k_{3,0} - k_3$ refers to the degradation of the stiffness of the ground story $\theta_3 = k_3$.
4. $\theta^g = \Delta k_1 + \Delta k_2 + \Delta k_3$ refers to the degradation of the stiffness of all storys together.

The main objective of the chosen inspection method is to detect $5\% \times k_{i,0}$ stiffness degradation with $POD \geq 95\%$ and $PFP \leq 15\%$ considering the location of damage $el^g = el^{g*}$, where el^{g*} refers to the true location of damage.

$$\begin{aligned}
 H_o : \forall \theta^g \geq 5\% \times k_{i,0} \Rightarrow POD(\theta^g) \geq 95\%, PFP \leq 15\% \text{ and } el^g = el^{g*} \\
 H_1 : \text{The inspection method is not reliable}
 \end{aligned} \tag{4.8}$$

Since the developed numerical model G_M was used as G_E to simulate the experiments and obtain \bar{d} , the condition defined in eq. (3.1) was satisfied and $Q_v = 1$.

4.3 Design of Experiments

Based on the results of the SDOF system example, a harmonic excitation $F(t) = F_a \sin \omega t$ that generates an output d which is sensitive to stiffness was chosen. Since the studied structure contains three stiffness values $\{k_1, k_2, k_3\}$, three harmonic excitations were used. Generally, civil engineering structures have a low fundamental frequency. In real tests, it can be difficult to generate a dynamic harmonic excitation with low frequency and sufficient force amplitude to obtain measurable response using accelerometers. Therefore, harmonic excitations with frequencies larger than the fundamental natural frequencies of the structure have to be used. In this case, it is expected that the chosen excitations may be sensitive to the mass variation

Table 4.1: Applied excitations used to simulate the tests

Test No.	Type	F_a [N]	frequency [Hz] / impulse duration T_I [s]	location
1	F_1 Harmonic	160	40	x_1
2	F_2 Harmonic	200	50	x_2
3	F_3 Harmonic	250	60	x_3
4	F_4 Harmonic	100	20	x_1
5	F_5 Harmonic	125	25	x_2
6	F_6 Harmonic	140	30	x_3
7	F_7 Impulse	3000	0.025	x_1
8	F_8 Impulse	2000	0.022	x_2
9	F_9 Impulse	1500	0.02	x_3

as well. Another set of three harmonic excitations in a higher frequency range compared to the frequencies of the first excitation group was chosen to obtain sufficient information about the influence of the mass on the response d . Since the dynamic response can have a transient state before reaching the required steady state, the influence of damping could be unavoidable during the transient state. Therefore, impulse excitations were used to obtain more information about modal damping ratios.

Three excitations were applied at the top x_1 , three at x_2 and three at x_3 . In case of the harmonic excitations, lower force amplitudes and frequencies were applied at the top to avoid continuous large response amplitude, which may be destructive. As a result, The force amplitudes and the frequencies of the harmonic excitation applied at x_3 are higher than at the top and in the middle. Only impulse amplitudes were chosen independently of the position of the force of the structure. table 4.1.

The true values of the input parameters $\{\theta^*\}$ were chosen as in table 4.2. As a result, the true natural frequencies f_n^* of the studied frame are $\{f_{n1}^*, f_{n2}^*, f_{n3}^*\} = \{5.27, 11.36, 16.82\}$ Hz. Therefore, the time step was chosen as $\Delta t = 0.002$ s to ensure a robust numerical solution for eq.(4.1). The damping ratios for the first two modes were assumed as follows: $\zeta_1 = 1.7\%$ and $\zeta_2 = 3.1\%$. By applying the equations (4.5), (4.6), $\alpha = 1.9149$ and $\beta = 8.0879 \times 10^{-4}$. The damping ratio of the third mode $\zeta_3 = 5.18\%$ was calculated following the eq.(4.7).

Table 4.2: True values of the studied input parameters. ζ_3 was calculated following the eq.(4.7)

$\theta_1^* = k_1$	$\theta_2^* = k_2$	$\theta_3^* = k_3$	$\theta_4^* = m_1$	$\theta_5^* = m_2$	$\theta_6^* = m_3$	$\theta_7^* = \zeta_1$	$\theta_8^* = \zeta_2$	$\theta_9^* = \zeta_3$
[kN/m]	[kN/m]	[kN/m]	[kg]	[kg]	[kg]	%	%	%
$\{\theta^*\}$ 1616	3168	4704	507.5	757.5	1000	1.7	3.1	5.18

$$p(\theta) = \begin{cases} \frac{1}{\theta_{max} - \theta_{min}} & \text{if } \theta_{min} \leq \theta \leq \theta_{max} \\ 0 & \text{otherwise} \end{cases} \quad (4.9)$$

The acquisition time was chosen as 10 s to obtain a steady state response and to gain sufficient information related to the influence of damping on the structural response. The prior probability density function $p(\theta)$ of a parameter θ was considered as a bounded uniform distribution in a range $\theta_{min} \leq \theta \leq \theta_{max}$, Eq. (4.9), table 4.3. If more accurate information is required, more experiments and investigations can be done to improve the prior knowledge of these parameters $\{\theta\}$. A Latin hypercube sampling method was used to generate $N = 500$ samples from the prior probability density functions. The number of samples N was chosen to obtain sufficient information about the variation of the structural response d due to $\{\theta\}$ which helps to develop Meta-models that satisfy the statistical conditions. The structural response $\ddot{x}(t)$ at each degree of freedom and for each excitation was computed for each sample. The cumulative signal energy values d of the acceleration time histories $\ddot{x}(t)$ were calculated for each degree of freedom. The initial conditions were chosen as $x(0) = \dot{x}(0) = 0$.

4.4 Sensitivity analysis results

Similar to the SDOF system example, the method described in section 3.4 was applied. Meta-models $\{d\}$ were developed to represent the relationship between the cumulative signal energy $\{d\}$ and the input parameters $\{\theta\}$. The data set which includes the $N = 500$ samples, calculated in the previous subsection, was used. The statistical properties of the residuals were examined to ensure that they satisfy the requirements described in section 3.4.4. The Total-effect index sT values, table 4.4, were calculated using $\{d\}$ for all excitations and input parameters $\{\theta\}$. In order to evaluate the quality of the chosen design of experiment, eq. (3.13) was applied. The results in table 4.4 show that the quality of a design of experiment is based on the objective

Table 4.3: The statistical properties of the stiffness, masses and damping ratios of the studied structure. ζ_3 was calculated following the eq.(4.7)

	$\theta_1 = k_1$ [kN/m]	$\theta_2 = k_2$ [kN/m]	$\theta_3 = k_3$ [kN/m]	$\theta_4 = m_1$ [kg]	$\theta_5 = m_2$ [kg]	$\theta_6 = m_3$ [kg]	$\theta_7 = \zeta_1$ %	$\theta_8 = \zeta_2$ %
μ	1600	3200	4800	500	750	1000	2.00	3.00
Min	1530.9	3060.2	4592.6	489.2	733.8	978.4	1.57	2.35
Max	1669.1	3338.3	5007.4	510.8	766.2	1021.6	2.43	3.65
COV	0.025	0.025	0.025	0.0125	0.0125	0.0125	0.125	0.125

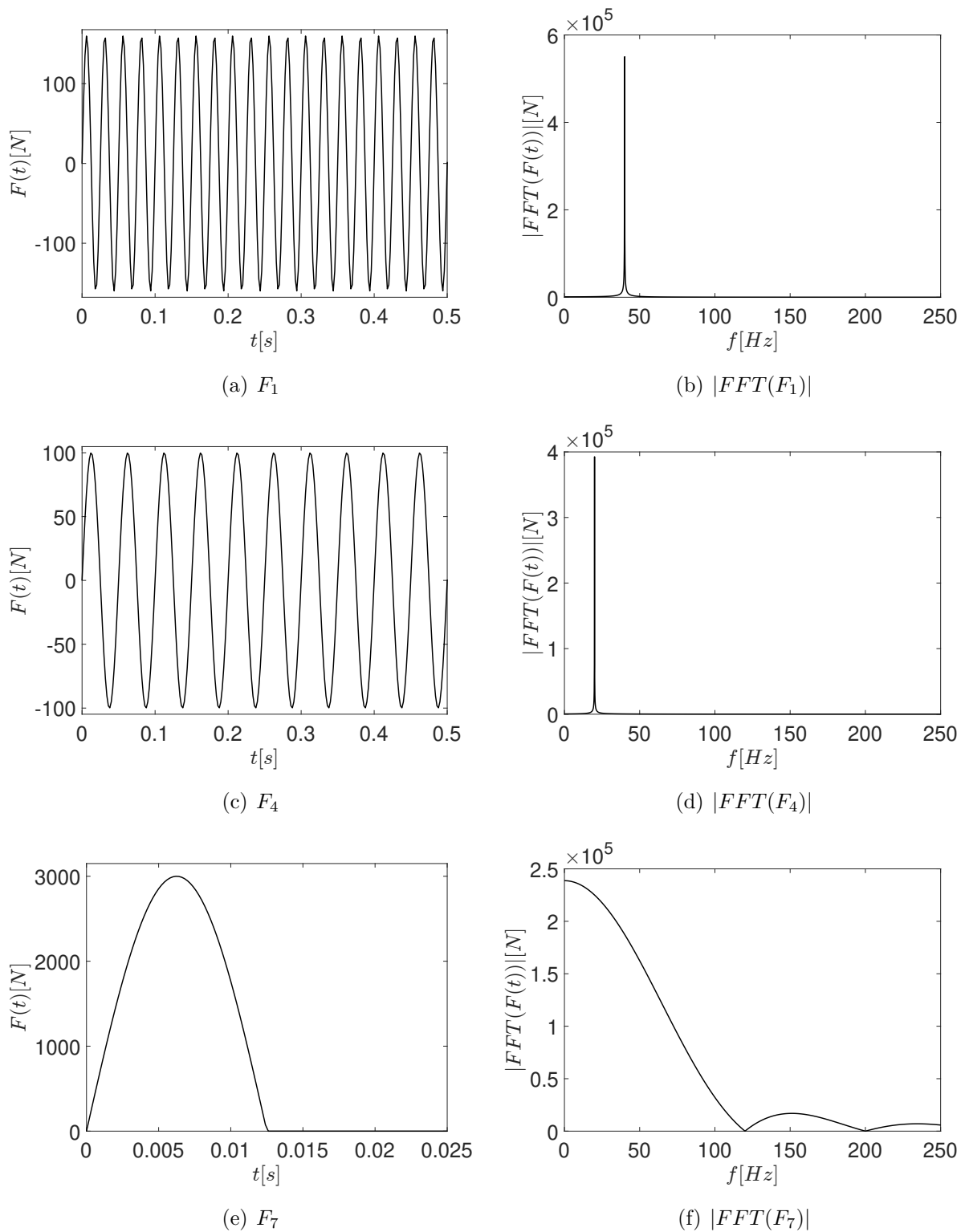


Figure 4.2: Time series and Fourier transforms of the excitation forces applied at x_1 and used to simulate the modal tests

of this experiment. If $\theta^g = \Delta k_1$, then only information about k_1 is required. In this case, an optimal design should give $sT = 1$ for the desired parameter k_1 and $sT = 0$ for all other

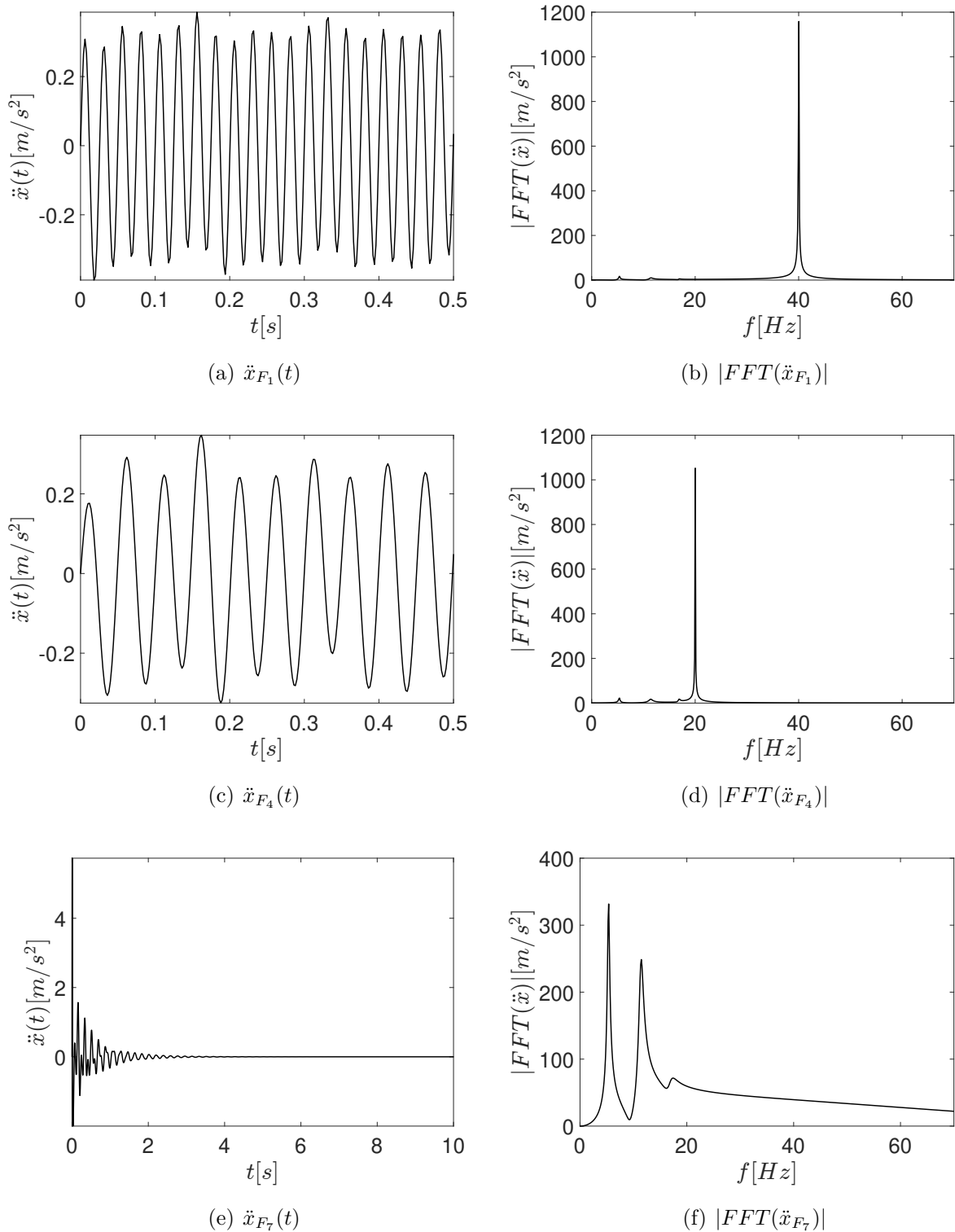


Figure 4.3: Time series and Fourier transforms of the structural response of the studied structure at x_1

parameters. However, in this example, test No.2, d_{x_1} gives $sT = 0.68$ for k_1 and the influence of m_1 and m_2 is observed by $sT = 0.17$ for m_1 and $sT = 0.12$ for m_2 . Therefore, $Q_{DOE} \approx 0.68$.

Test No.1, d_{x2} gives $sT = 0.66$ for k_1 . Similarly the design of experiment obtained in case of $\theta^g = \Delta k_2$ and $\theta^g = \Delta k_3$ can be evaluated, table 4.5. If $\theta^g = \Delta k_1 + \Delta k_2 + \Delta k_3$, then information about k_1, k_2 and k_3 is required.

In conclusion, an optimal design would be that $\sum sT$ for the desired parameter is 1 and $\sum sT$ for the undesired parameter is 0. In this case $Q_{DOE,optimal} = 1.00$. However, in most cases, undesired parameters could influence the structural response of the studied system. As a result, low probability of damage detection and/or high rate of false alarm has to be expected. Solving this problem may require conducting more experiments to gain more information about the important parameters. In this example, table 4.4 shows that tests 1, 2, 3, 4, 5 and 6 provide also information about m_1, m_2, m_3 since large sT values were obtained. Similarly, tests 7, 8 and 9 provide information about $\zeta_1, \zeta_2, \zeta_3$.

In table 4.4 the input parameters that have $sT \geq 0.05$ were marked in red. Choosing this threshold, $sT \geq 0.05$, is to eliminate nonsensitive parameters but not k_3 from the Meta-models. This means, the input parameters that have $sT > 0.05$ were used to develop the Meta-models for model updating $\{\hat{d}\}$ in the next step.

$$\forall \hat{\theta} : sT_{\hat{\theta}} \geq 0.05 \quad (4.10)$$

Table 4.4: Total-effect index sT values calculated for all excitations, input parameters $\{\theta\}$ and computed response $\{\underline{d}\}$

Force	DOF	k_1	k_2	k_3	m_1	m_2	m_3	ζ_1	ζ_2
$F_1 = 160 \sin(40t)$	x_1	0.02	0.00	0.00	1.01	0.00	0.00	0.00	0.00
	x_2	0.66	0.01	0.00	0.14	0.18	0.00	0.01	0.01
	x_3	0.03	0.00	0.00	0.02	0.01	0.01	0.03	0.93
$F_2 = 200 \sin(50t)$	x_1	0.68	0.01	0.01	0.17	0.12	0.00	0.00	0.02
	x_2	0.00	0.01	0.00	0.00	1.01	0.00	0.00	0.00
	x_3	-0.01	0.7	0.01	0.00	0.18	0.12	-0.01	0.00
$F_3 = 250 \sin(60t)$	x_1	0.02	-0.02	-0.01	-0.02	-0.03	-0.02	0.01	0.91
	x_2	0.09	0.64	0.09	0.12	0.17	0.18	0.09	0.12
	x_3	0.00	0.00	0.01	0.00	0.00	1.04	0.00	0.01
$F_4 = 100 \sin(20t)$	x_1	0.28	0.01	-0.01	0.68	0.00	-0.01	-0.01	-0.01
	x_2	0.49	0.25	0.00	0.08	0.2	0.00	0.00	0.00
	x_3	0.21	0.53	0.03	0.03	0.03	0.1	-0.01	0.00
$F_5 = 125 \sin(25t)$	x_1	0.65	0.03	0.01	0.15	0.17	0.01	0.01	0.01
	x_2	0.05	0.18	-0.01	0.00	0.75	-0.01	0.00	-0.01
	x_3	-0.01	0.7	0.01	-0.01	0.14	0.15	-0.01	-0.01
$F_6 = 140 \sin(30t)$	x_1	0.03	0.00	0.00	0.04	0.04	0.04	0.01	0.61
	x_2	0.00	0.7	0.02	0.00	0.18	0.18	0.01	0.00
	x_3	0.00	0.00	0.00	0.00	0.00	0.87	0.00	0.00
$F_7 = \begin{cases} 3000 \sin(125.66t) & \text{if } t \leq 0.025 \text{ [s]} \\ 0 & \text{if } t > 0.025 \text{ [s]} \end{cases}$	x_1	-0.02	-0.02	-0.02	0.12	-0.01	-0.02	0.09	0.90
	x_2	0.02	0.02	0.02	0.00	0.03	0.02	0.09	0.91
	x_3	0.05	0.00	0.00	0.00	0.00	0.04	0.09	0.91
$F_8 = \begin{cases} 2000 \sin(142.8t) & \text{if } t \leq 0.022 \text{ [s]} \\ 0 & \text{if } t > 0.022 \text{ [s]} \end{cases}$	x_1	0.00	-0.04	-0.04	0.02	-0.01	-0.04	0.10	0.92
	x_2	0.01	0.00	0.02	-0.01	0.12	0.01	0.10	0.93
	x_3	0.01	0.01	0.01	0.01	0.02	0.02	0.10	0.94
$F_9 = \begin{cases} 1500 \sin(157.08t) & \text{if } t \leq 0.020 \text{ [s]} \\ 0 & \text{if } t > 0.020 \text{ [s]} \end{cases}$	x_1	-0.05	-0.05	-0.05	0.03	-0.02	-0.01	0.12	0.91
	x_2	0.01	0.02	0.01	0.01	0.02	0.02	0.10	0.88
	x_3	0.04	0.02	0.02	0.01	0.04	0.07	0.14	0.85

Table 4.5: The quality of the DOE considering the excitation type and the sensor position

Force	DOF	$Q_{DOE}(\Delta k_1)$	$Q_{DOE}(\Delta k_2)$	$Q_{DOE}(\Delta k_3)$	$Q_{DOE}(\Delta k_1 + \Delta k_2 + \Delta k_3)$
$F_1 = 160 \sin(40t)$	x_1	0.02	0.00	0.00	0.02
	x_2	0.65	0.01	0.00	0.66
	x_3	0.03	0.00	0.00	0.03
$F_2 = 200 \sin(50t)$	x_1	0.67	0.01	0.01	0.69
	x_2	0.00	0.01	0.00	0.02
	x_3	0.00	0.71	0.01	0.71
$F_3 = 250 \sin(60t)$	x_1	0.02	0.00	0.00	0.00
	x_2	0.06	0.43	0.06	0.55
	x_3	0.00	0.00	0.01	0.01
$F_4 = 100 \sin(20t)$	x_1	0.30	0.01	0.00	0.30
	x_2	0.48	0.25	0.00	0.73
	x_3	0.23	0.58	0.03	0.84
$F_5 = 125 \sin(25t)$	x_1	0.63	0.03	0.01	0.66
	x_2	0.05	0.19	0.00	0.23
	x_3	0.00	0.73	0.01	0.73
$F_6 = 140 \sin(30t)$	x_1	0.04	0.00	0.00	0.04
	x_2	0.00	0.64	0.02	0.66
	x_3	0.00	0.00	0.00	0.00
$F_7 = \begin{cases} 3000 \sin(125.66t) & \text{if } t \leq 0.025 \text{ [s]} \\ 0 & \text{if } t > 0.025 \text{ [s]} \end{cases}$	x_1	0.00	0.00	0.00	0.00
	x_2	0.02	0.02	0.02	0.05
	x_3	0.05	0.00	0.00	0.05
$F_8 = \begin{cases} 2000 \sin(142.8t) & \text{if } t \leq 0.022 \text{ [s]} \\ 0 & \text{if } t > 0.022 \text{ [s]} \end{cases}$	x_1	0.00	0.00	0.00	0.00
	x_2	0.01	0.00	0.02	0.03
	x_3	0.01	0.01	0.01	0.03
$F_9 = \begin{cases} 1500 \sin(157.08t) & \text{if } t \leq 0.020 \text{ [s]} \\ 0 & \text{if } t > 0.020 \text{ [s]} \end{cases}$	x_1	0.00	0.00	0.00	0.00
	x_2	0.01	0.02	0.01	0.04
	x_3	0.03	0.02	0.02	0.07

4.5 Model updating results

Meta-models $\{\hat{d}\}$ were developed for model updating to reduce the computational effort. As mentioned before, the input parameters that have $sT \geq 0.05$ were considered and used to select the important parameters $\{\hat{\theta}\} \subseteq \{\theta\}$. Applying the Bayesian updating approach explained before in section 3.5, the posterior density functions $p(\{\theta\}|\{\bar{d}\})$ of the updated parameters were computed, figure 4.4, table 4.6. To include the uncertainty due to the assumed initial condition and noise because of ambient vibration $\epsilon_{\bar{d}} \sim \mathcal{N}(0, (0.02\bar{d})^2)$ was considered when $p(\{\theta\}|\{\bar{d}\})$ was computed. Larger $\epsilon_{\bar{d}}$ may lead to lose information about k_3 . More accurate value could be chosen for $\epsilon_{\bar{d}}$ if the ambient vibration excitation was investigated.

In order to evaluate the quality of the measurements for model updating, the index Q_M given in eq.(3.47) was computed, table 4.7.

4.6 Reliability of the inspection method

4.6.1 Damage indicator

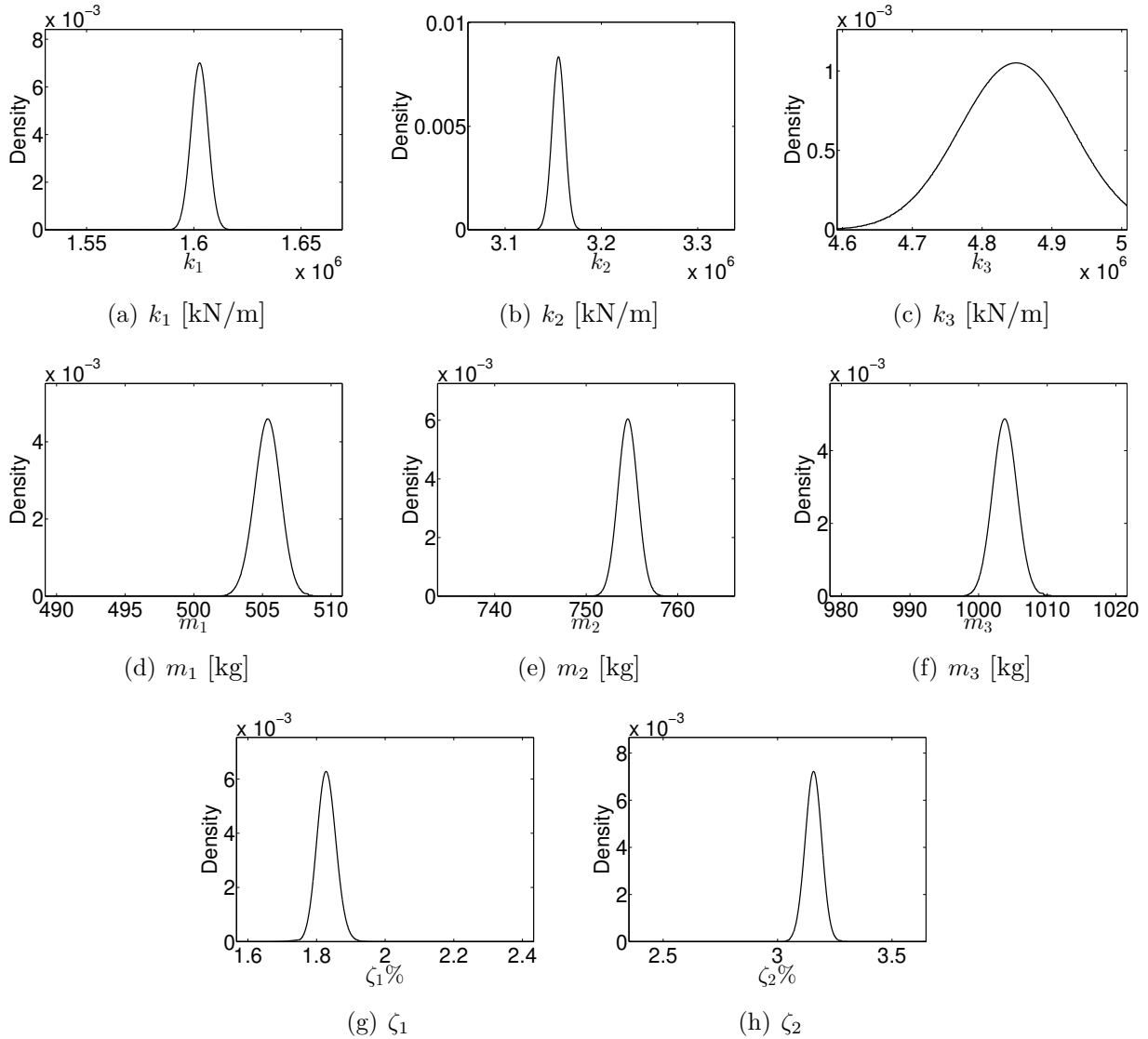
The method developed in section 3.6.2 was applied. $\theta_i^g \in [0, 20\%] \times k_0$ was used to calculate the response $d(\theta^g)$ as in eq. (3.52) with an interval $\Delta\theta^g = 1\% \times k_0$. In this example, it was assumed that $PFP = POD(\theta^g|\theta^g = 0, d) \leq 0.01$ for each response d . It means that if there was no damage, only 1% of the indicator values exceeds d_c and leads to a false alarm. As a result, eq. (3.55) can be used to select the threshold value for each response that satisfies the PFP condition. Based on eq. (3.59) and the chosen threshold values, the POD curves could be computed. Based on eq. (3.63) if the number of the outputs is $n = 27$ (9 tests \times 3 degrees of freedom), then the minimum number of samples is $N = 167$ and $PFP \leq 0.16$. To obtain constant POD curves, $N = 500$ samples were generated and solved for each $\theta^g + \Delta\theta^g$ using the numerical model G_M for each applied excitation. The total number of samples is $500 \times 21 \times 9 = 94500$ times. It is very important to mention that sometimes the relationship

Table 4.6: The statistical properties of the posterior density functions of the input parameters. ζ_3 was calculated following the eq.(4.7)

	$\theta_1 = k_1$	$\theta_2 = k_2$	$\theta_3 = k_3$	$\theta_4 = m_1$	$\theta_5 = m_2$	$\theta_6 = m_3$	$\theta_7 = \zeta_1$	$\theta_8 = \zeta_2$
	[kN/m]	[kN/m]	[kN/m]	[kg]	[kg]	[kg]	[%]	[%]
μ	1602.7	3155.4	4844	505.4	754.6	1003.8	1.83	3.16
$\sigma_{\hat{\theta} \bar{d}}$	3.9	6.9	74.96	0.93	1.1	1.7	0.028	0.038
COV	0.0024	0.0022	0.015	0.0018	0.0013	0.001	0.015	0.012

Table 4.7: The quality of the measurements based on damage scenario

$\hat{\theta}_i$	k_1	k_2	k_3	$k_1 + k_2 + k_3$
$\sigma_{\hat{\theta}_i}$	39.920	79.840	119.760	
$\sigma_{\hat{\theta}_i \bar{d}}$	3.9	6.9	74.96	
Q_M	90%	91%	37%	88%

**Figure 4.4:** Posterior density functions $p(\{\theta\}|\{\bar{d}\})$ of the input parameters computed using Bayesian updating method. ζ_3 was calculated following the eq.(4.7)

between damage size and a structural response can be an inverse relationship, on other words, the damage size increment causes a structural response decrement. As a result, eqs. (3.55) and (3.59) and should be modified as follows:

$$PFP = 1 - P(d(\theta^g) > d_c | \theta^g = 0) \quad (4.11)$$

$$POD(\theta^g) = 1 - P(d_1 > d_{c1} \cap d_2 > d_{c2} \cap \dots \cap d_n > d_{cn} | \theta^g, p(\{\theta\} | \{\bar{d}\})) \quad (4.12)$$

4.6.2 Damage location

An inspection method is reliable if damage is detected and located correctly. As a result, false alarm includes detecting damage at a wrong location. The relationship between damage size and a structural response was used as a damage pattern $DP(\theta^g)$. The defined damage patterns help to classify the type of damage and/or define its location. For example, in case of the first $\theta^g = \Delta k_1$ and the fourth $\theta^g = \Delta k_1 + \Delta k_2 + \Delta k_3$ damage scenarios, if the damage indicator, which is the cumulative signal energy $d(\theta^g)$, was computed from $\ddot{x}(t)$ obtained at the top of the studied frame x_1 under an excitation $F_4(t)$ for both undamaged and damaged states, then a decrement damage indicator value was observed if damage size increases. However, in case of the second $\theta^g = \Delta k_2$ and third $\theta^g = \Delta k_3$ damage scenarios, no relationship between damage and the damage indicator was observed, figure 4.5. This observation can be used to develop a concept of damage patterns which can be unique for each studied damage scenario. In this work, a damage pattern was defined as 1 if a proportional relationship between damage size and damage indicator was observed and -1 if an inverse relationship between damage size and damage indicator was observed. If the damage indicator is not sensitive to damage then the damage pattern value was 0, eq. (4.13). In order to obtain a reliable inspection method considering damage location, the defined damage patterns should be unique for each studied damage scenario. The damage patterns $DP(\theta^g)$ for the studied damage scenarios are listed in tables 4.8, 4.9, 4.10 and 4.11. The results show that each damage causes a unique damage pattern which indicates a reliable inspection method if damage location is considered. For test No. 7, 8 and 9 $DP(\theta^g) = 0$.

$$DP(\theta^g) = \begin{cases} 1 & \text{if } \Delta d_i / \Delta \theta^g > 0 \\ -1 & \text{if } \Delta d_i / \Delta \theta^g < 0 \\ 0 & \text{if } \Delta d_i / \Delta \theta^g = 0 \end{cases} \quad (4.13)$$

Table 4.8: Damage patterns $DP(\theta^g)$ for the first damage scenario $\theta^g = \Delta k_1$

	F_1	F_2	F_3	F_4	F_5	F_6
d_{x1}	0	-1	-1	-1	-1	-1
d_{x2}	-1	0	0	-1	-1	0
d_{x3}	-1	0	0	-1	-1	0

Table 4.9: Damage patterns $DP(\theta^g)$ for the second damage scenario $\theta^g = \Delta k_2$

	F_1	F_2	F_3	F_4	F_5	F_6
d_{x1}	0	0	0	0	-1	-1
d_{x2}	0	0	-1	-1	-1	-1
d_{x3}	0	-1	0	-1	-1	-1

Table 4.10: Damage patterns $DP(\theta^g)$ for the third damage scenario $\theta^g = \Delta k_3$

	F_1	F_2	F_3	F_4	F_5	F_6
d_{x1}	0	0	1	0	0	0
d_{x2}	0	0	0	-1	0	-1
d_{x3}	0	-1	0	-1	-1	-1

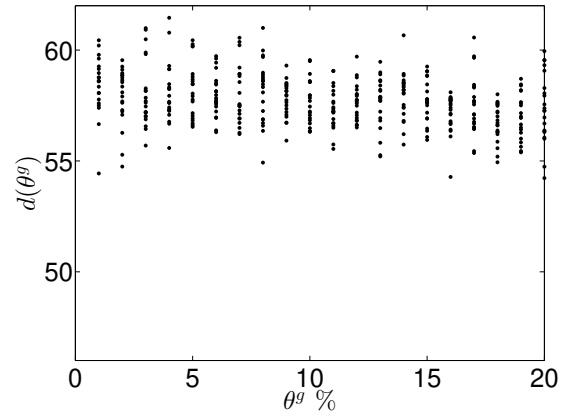
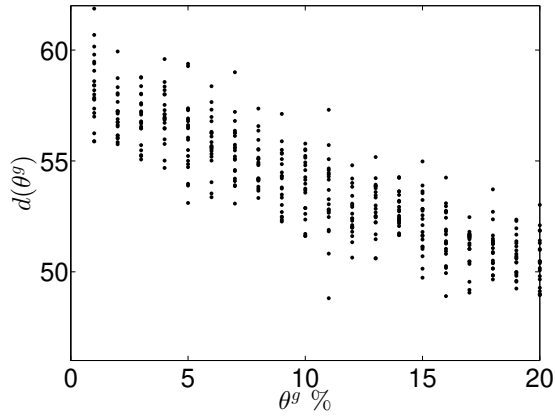
Table 4.11: Damage patterns $DP(\theta^g)$ for the fourth damage scenario $\theta^g = \Delta k_1 + \Delta k_2 + \Delta k_3$

	F_1	F_2	F_3	F_4	F_5	F_6
d_{x1}	0	-1	-1	-1	-1	-1
d_{x2}	-1	0	-1	-1	-1	-1
d_{x3}	-1	-1	0	-1	-1	-1

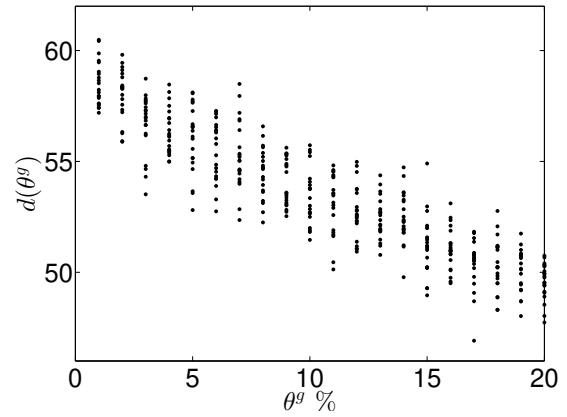
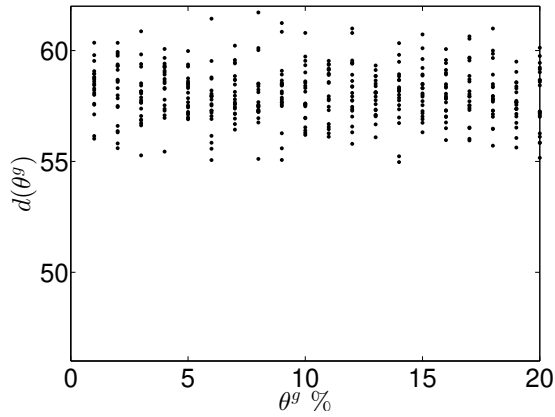
4.6.3 Probability of detection curves

The POD curves were computed based on eq. (3.59) and the threshold value $d_{c,i}$ which was selected to satisfy the false alarm condition $PFP_i = POD(\theta^g | \theta^g = 0) \leq 0.01$ for each output d_i . The results show that the reliability of the chosen inspection method depends on the location of the studied damage. A stiffness degradation of 5% at the top and middle storys were detectable with a $POD = 100\%$ and $PFP = 6\%$. However, the probability of detecting similar damage in the lower story is $POD = 42\%$ and $PFP = 7.5\%$. Moreover, damage at multiple locations will be detected faster than damage in one location, figure 4.6.

The quality of the inspection method was evaluated by calculating Q_D for each studied damage scenario by applying eq. (3.61), table 4.12. Based on the problem definition presented in



(a) $\bar{d}_1(\theta^g = \Delta k_1)$ under excitation F_4 , $DP(\theta^g) = -1$ (b) $\bar{d}_1(\theta^g = \Delta k_2)$ under excitation F_4 , $DP(\theta^g) = 0$



(c) $\bar{d}_1(\theta^g = \Delta k_3)$ under excitation F_4 , $DP(\theta^g) = 0$ (d) $\bar{d}_1(\theta^g = \Delta k_1 + \Delta k_2 + \Delta k_3)$ under excitation F_4 , $DP(\theta^g) = -1$

Figure 4.5: Damage pattern $DP(\theta^g)$ for different damage cases

eq. (4.8), the inspection is not reliable to detect the degradation of the stiffness k_3 at the ground story of the structure. As a solution, better design of experiments can be developed by choosing different excitation properties to gain more information about k_3 .

Table 4.12: Reliability of the inspection method for detecting 5% stiffness degradation for different damage scenarios based on Q_D including model updating

θ^g	$Q_D(\theta^g = \Delta k_1)$	$Q_D(\theta^g = \Delta k_2)$	$Q_D(\theta^g = \Delta k_3)$	$Q_D(\theta^g = \Delta k_1 + \Delta k_2 + \Delta k_3)$
5 % $k_{i,0}$	0.94	0.94	0.39	0.94

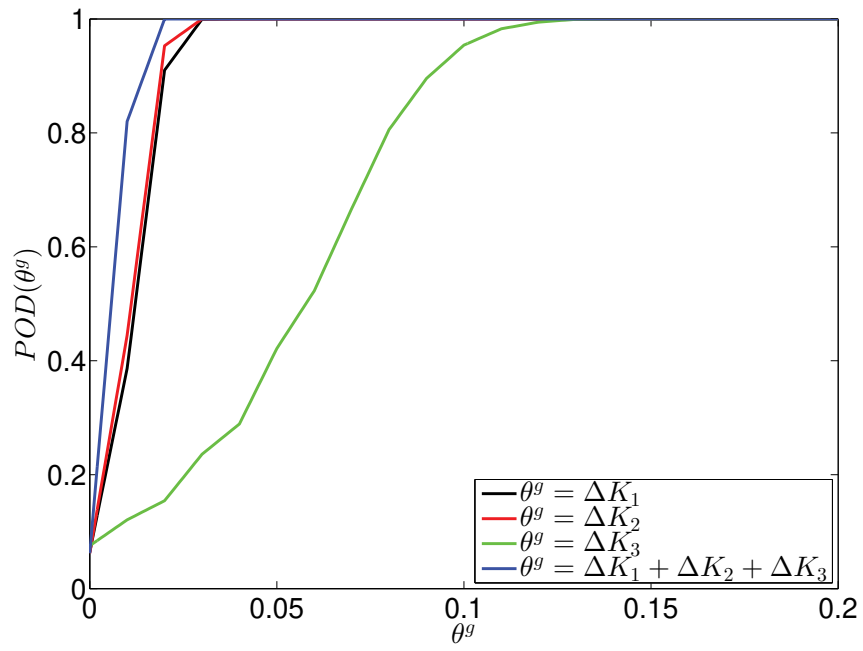


Figure 4.6: Probability of detection for different damage scenarios including model updating

Chapter 5

Experimental Study

5.1 Steel frame structure

5.1.1 Introduction

The performance of a vibration-based inspection method for damage detection is tested by applying the strategy developed in this work. The experimental models of the studied structure and damage are presented. The modal parameters obtained from initial experiments are used to design the experiments for damage detection.

A numerical model has been developed to perform a statistical study. The reliability of the inspection method is evaluated by taking into account the influence of damping, the number of the sensors, the location and the frequency of the excitation.

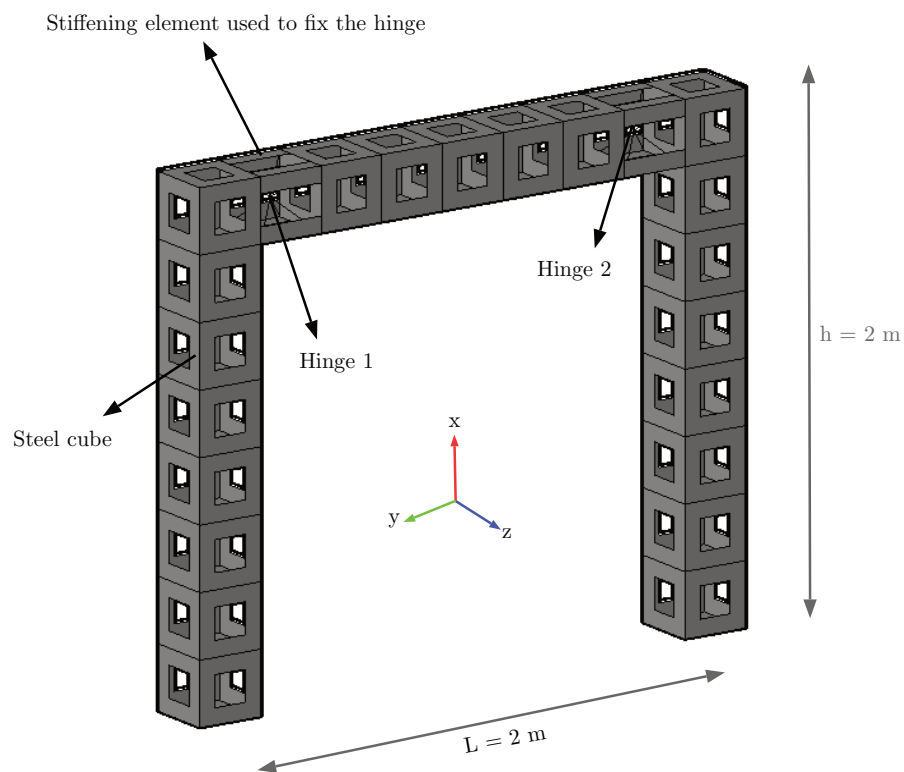
5.1.2 Problem definition and experimental test setup

The studied structure is a single-span-one-story steel frame structure. The length of the beam is 2 m measured between the centers of the columns. The height of the frame is 2 m measured between the base level and the top of the beam. The frame was constructed from hollow steel cubes connected to each other using bolts. These cubes can be arranged and connected to create different types of structures, for example, multi-story structures, tower, etc. Moreover, it is possible to replace any element, for example, by a 3D hinge which can be considered as a damage model, figure 5.1. However, using these cubes brings complexity to the numerical model because of the nonuniform cross-sections and the connection conditions between the cubes.

The frame contains 23 steel cubes. The interface connections were realized using 8 bolts. Cubes number 1 and 23 according to figure 5.2 were fixed to steel plates using 8 bolts for each, and the plates were fixed to the ground. Cubes number 9 and 15 which connect the beam to the columns



(a) Studied structure constructed from steel cubes



(b) A sketch describes the geometry and the elements of the studied structure

Figure 5.1: Studied single-span one-story steel frame structure and its elements

were replaced by hinges. It was possible to increase the stiffness of a hinge by adding up to 4 steel stiffening elements. As a result, the hinge is blocked if the 4 stiffening elements were fixed. Removing the stiffening elements increases the flexibility of the beam-column connection.

Five -3-axial-accelerometers were used to conduct a dynamic modal test. The accelerometers have been deployed following 3 setups, figure 5.2. As a result, the structural response at 11 points of the frame was measured. The setups were combined using reference sensors. The first reference sensor was placed on one of the columns, at cube 6, close to the top. The second was placed on the top of the beam at cube 14, table 5.1. The test setups were designed in a way that a trade-off was obtained between the number of sensors, the number of measurement points and the number of setups. Based on the orientation of the sensors, the coordinate system of the frame was defined as follows: x: vertical, y: longitudinal (in-plane) and z: lateral (out of plane).

Five damage cases were studied, table 5.2. In this example, the damage was created by releasing the hinge at one or/and both sides of the beam by removing the stiffening elements diagonally, figure 5.3.

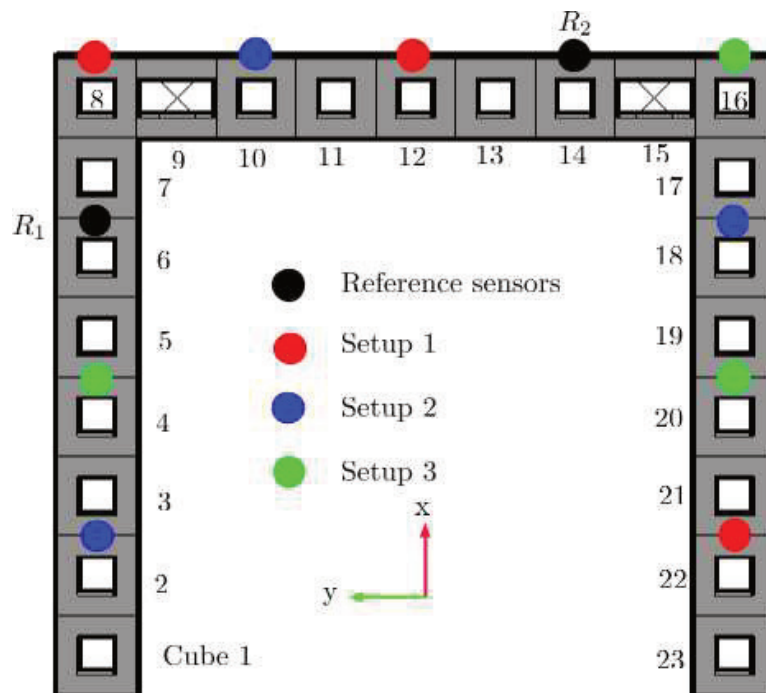


Figure 5.2: Sensors locations in each test setup

Table 5.1: Sensors locations for each test setup

Sensor No	Setup No		
	1	2	3
1	cube 6 (Refe.)	cube 6 (Refe.)	cube 6 (Refe.)
2	cube 14 (Refe.)	cube 14 (Refe.)	cube 14 (Refe.)
3	cube 8	cube 2	cube 4
4	cube 12	cube 10	cube 16
5	cube 22	cube 18	cube 20

Table 5.2: Studied damage cases

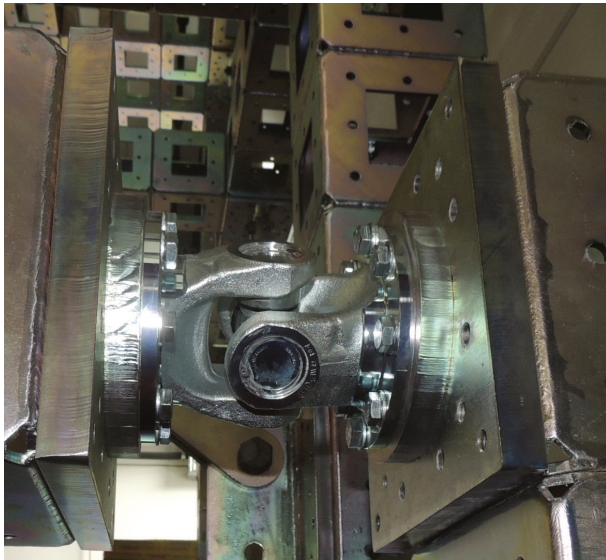
Damage case	Description
1	Both hinges are fixed
2	Hinge at cube number 9 is half released, Hinge at cube 15 is fixed
3	Hinge at cube number 9 is completely released, Hinge at cube 15 is fixed
4	Hinge at cube number 9 is completely released, Hinge at cube 15 half released
5	Both hinges are completely released

The chosen inspection method was applied to obtain a damage size θ^g that can be detected with a probability of detection $POD = P_1 \in [0, 1]$ and a probability of false alarm $PFP = P_2 \in [0, 1]$ after reaching damage case i ($\theta^g > \theta_i^g$) and before reaching damage case $i + 1$ ($\theta^g < \theta_{i+1}^g$), where $i = 1, 2, 3, 4$. The problem definition can be written as follows:

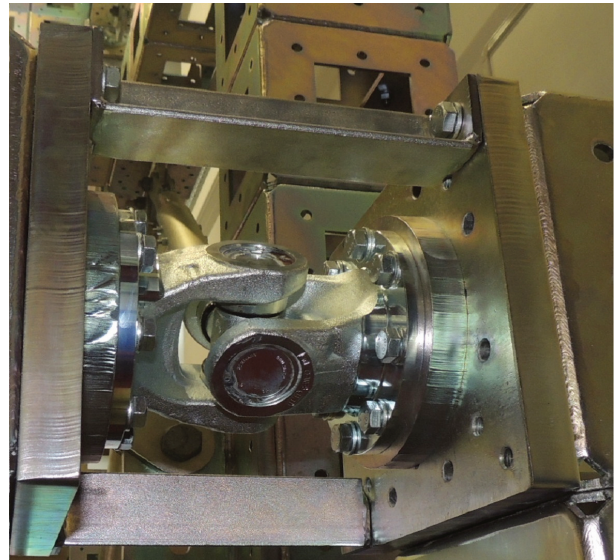
$$\begin{aligned}
 H_o : \forall \theta^g : \theta^g \in [\theta_i^g, \theta_{i+1}^g] &\Rightarrow POD(\theta^g) \geq P_1, PFP \leq P_2 \\
 H_1 : &\text{The inspection method is not reliable}
 \end{aligned} \tag{5.1}$$

In this example, the reliability of the inspection method was tested to detect damage θ^g given that $\theta_1^g < \theta^g < \theta_2^g$:

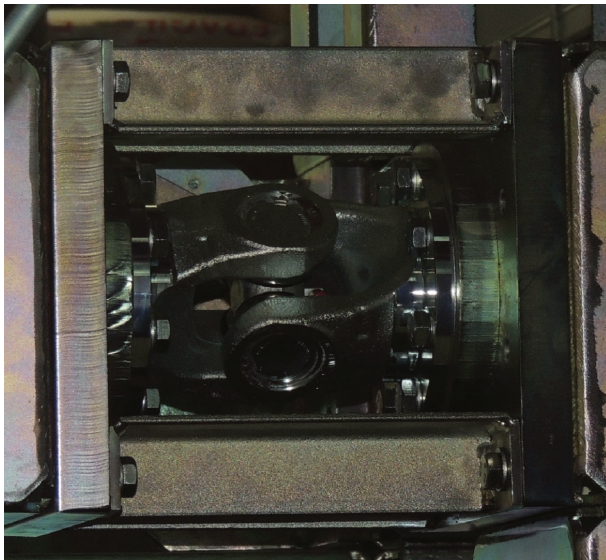
$$\begin{aligned}
 H_o : \forall \theta^g : \theta^g \in [\theta_1^g, \theta_2^g] &\Rightarrow POD(\theta^g) \geq 95\%, PFP \leq 5\% \\
 H_1 : &\text{The inspection method is not reliable}
 \end{aligned} \tag{5.2}$$



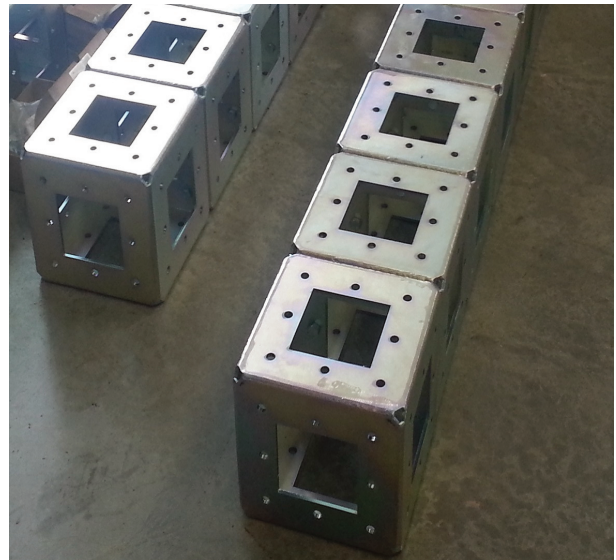
(a) Completely released hinge



(b) Half released hinge by removing 2 stiffening elements diagonally



(c) Completely fixed hinge by 4 stiffening elements



(d) Steel cubes connected together to construct the structure

Figure 5.3: Hinge and cube elements used to construct the frame and introducing damage in the physical model

5.1.3 Modal parameters

A modal test was conducted using impulse excitations applied at cube number 6 in the y -direction (in-plane), cube number 14 in the z -direction, and cube number 14 in the vertical direction. Six tests were performed: 2 in each direction. The impulse excitation is similar to what figure 5.4 shows. The goal was to obtain the modal parameters (natural frequencies $\{f_{n,E}\}$, mode shapes $\{\phi_E\}$ and damping ratios $\{\zeta_E\}$) of the frame and their statistical properties. Figure 5.5 shows an output acceleration signal recorded at cube 14 (reference No. 2) in case of applying the impulse at cube number 6 in the y -direction. The stochastic subspace identification method (data-driven) was applied following a procedure similar to the procedure described in appendix C to analyze the acceleration signals recorded at the 11 points shown in figure 5.2 to extract the modal parameters of the frame.

In the MACEC toolbox, Reynders et al. [2014], 13 nodes were defined by assigning the (x, y, z) coordinates to each node measured from the bottom left node which is given $(0, 0, 0)$ coordinates. Eleven nodes [1 – 11] define the positions of the sensors which were placed on the structure. The rest two nodes [0, 12] represent the positions where the structure was fixed to the base. Each node has a degree of freedom in each direction X , Y , and Z . A master-slave relationship should be defined to visualize nodes 0 and 12 later when plotting the mode shapes since those nodes were not measured. The node 1, which is the neighbor node of the node 0, was chosen as a master node for node 0 which is the slave node. The DOFs (X, Y, Z) of the node 0 were defined as a function of the DOFs (X, Y, Z) of the master node 1 as follows: $X_0 = 0 \times X_1$, $Y_0 = 0 \times Y_1$, $Z_0 = 0 \times Z_1$. The same relationship was defined between node 11 as a master node and node 12 as a slave node.

Showing the connections between the nodes when visualizing the mode shapes were defined by assigning beam elements between each two neighbor nodes. The measurement files for each setup which are saved in text-like format were selected and loaded to MACEC. Each file contains the acceleration signals measured in X , Y , and Z directions for each node in each setup. Since each setup contains the measurements of 5 sensors, 5.1, the number of signals is $3 \times 5 = 15$. Each signal contains several impulse responses. The duration of each signal is at least 2 minutes.

The signal should be transformed into MCSIGNAL type (to be recognized by MACEC) before processing it. In the processing step, each channel (signal) can be visualized and checked if the values in the frequency domain are reasonable. The frequency rate was reduced from 4096 Hz to 512 Hz for each channel before saving the new signal for further processing.

Next, each signal (channel) should be coupled to the associated node which was defined before. In this step, the node, the channel and the direction should be selected. For system identification, the Reference-based data-driven stochastic subspace identification (SSI-cov/ref) was applied after applying the previous step to each setup. The node number 3 and node

number 7 were chosen as references. The maximum system order was chosen 200.

After the analysis was finished, the mode should be chosen by selecting a point for each model from the stabilization diagram. When selecting the points, it is crucial to take into account that the imaginary part of the values of the mode shape is close to zero, the damping ratio is reasonable (for example, the damping ratio should not be 100 %). Moreover, the modal phase collinearity (MPC) value, which is a dimensionless measure to quantify the spatial consistency of the identification results, should be close to 1 in case of real modes. The frequencies, the damping ratios, and the mode shapes can be saved into text files for further processing. The described procedure above was applied to all six tests and each damage case. The mean values and the standard deviations of the frequencies and damping ratios are calculated from the six conducted tests. The extracted mode shapes are similar for the different tests.

Figures 5.6 and 5.7 show the first 12 mode shapes extracted from the excitations applied at cube number 6 in the y-direction (in-plane) for each studied damage case. For damage case 4 and 5, the order of the 1st and the 2nd mode shapes is switched, table 5.5. Mode shapes 3 to 6 show no significant changes due to the studied damage. Quantifying the variation in mode shapes 7 to 12 due to damage requires a larger number of sensors. The natural frequencies are shown in table 5.3. The results indicate significant changes in the natural frequencies, especially for modes 3, 6 and 12, because of releasing the stiffeners. Table 5.4 presents the extracted damping ratios. For some modes, especially for mode 3, the damping ratio increases if the stiffening elements are removed. More information about extracting the statistical properties of the modal properties in table 5.3 and table 5.4 can be found in Reynders [2012].

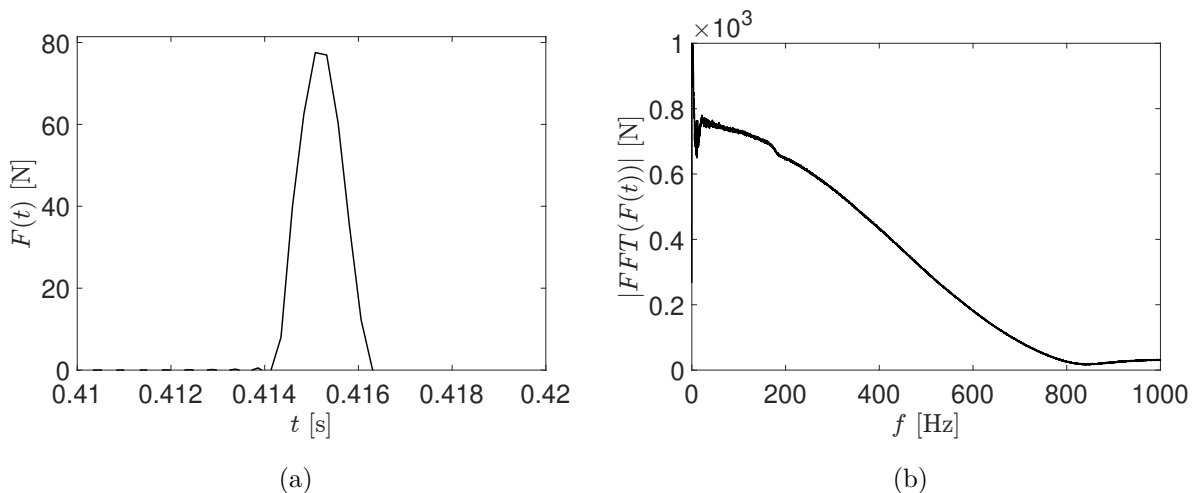


Figure 5.4: The impulse excitation $F(t)$ (a) applied at cube number 6 and its $|FFT|$ (b)

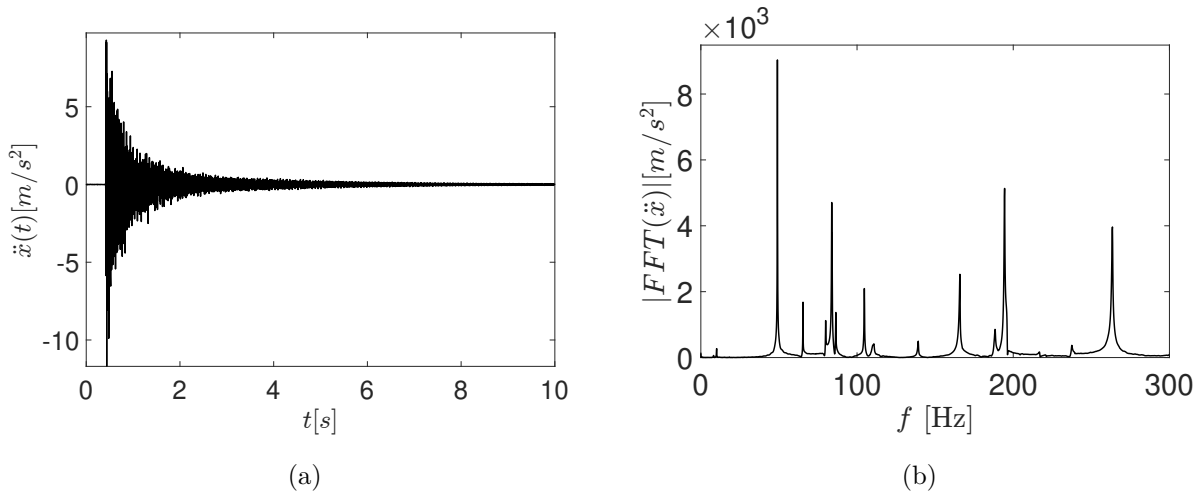


Figure 5.5: The response of structure recorded at cube 14 (reference No. 2) (a) and its |FFT| (b)

Table 5.3: Natural frequencies $f_{n,E}$ [Hz] of the frame for the studied damage cases

	Case 1		Case 2		Case 3		Case 4		Case 5	
	μ	σ	μ	σ	μ	σ	μ	σ	μ	σ
f_1	8.16	0.005	8.17	0.019	8.17	0.005	7.47	0.029	6.41	0.030
f_2	10.10	0.008	9.44	0.024	8.88	0.018	8.35	0.006	8.42	0.015
f_3	18.18	0.010	17.02	0.067	15.45	0.025	14.40	0.088	11.53	0.063
f_4	49.03	0.074	49.30	0.093	48.66	0.013	47.20	0.116	44.71	0.012
f_5	65.33	0.029	64.96	0.014	62.71	0.036	59.51	0.093	58.24	0.010
f_6	79.73	0.054	77.33	0.218	72.44	0.027	64.78	0.074	60.29	0.067
f_7	83.93	0.030	83.25	0.023	82.01	0.037	78.98	0.093	75.05	0.044
f_8	86.30	0.025	85.40	0.044	84.62	0.040	82.52	0.038	79.14	0.030
f_9	104.71	0.074	102.87	0.012	100.34	0.025	99.31	0.139	97.81	0.059
f_{10}	110.51	0.042	108.13	0.068	105.48	0.020	100.69	0.193	100.29	0.157
f_{11}	139.14	0.177	135.67	0.095	126.58	0.166	122.33	0.375	119.87	0.063
f_{12}	165.74	0.134	145.56	0.122	136.67	0.074	128.23	0.275	123.58	0.070

5.1.4 Results under harmonic excitations

Forced vibration test

A shaker was connected to the structure using magnets to produce harmonic excitations which can be sensitive to the studied damage similar to the numerical study introduced in the previous chapter. Since the natural frequencies presented in the previous section show that mode 3, 6

Table 5.4: Damping ratios ζ_E [%] of the frame for the studied damage cases

	Case 1		Case 2		Case 3		Case 4		Case 5	
	μ	σ	μ	σ	μ	σ	μ	σ	μ	σ
ζ_1	0.20	0.060	0.18	0.330	0.19	0.710	0.73	0.920	0.84	1.300
ζ_2	0.20	0.005	0.23	0.200	0.28	0.165	0.25	0.249	0.21	0.271
ζ_3	0.22	0.130	0.27	0.063	0.53	0.122	0.81	0.080	1.90	0.630
ζ_4	0.11	0.009	0.10	0.031	0.15	0.020	0.18	0.262	0.16	0.006
ζ_5	0.07	0.010	0.09	0.007	0.17	0.015	0.17	0.022	0.17	0.007
ζ_6	0.13	0.021	0.21	0.230	0.19	0.020	0.35	0.032	0.36	0.027
ζ_7	0.13	0.120	0.33	0.011	0.28	0.017	0.25	0.296	0.29	0.013
ζ_8	0.13	0.014	0.11	0.080	0.14	0.034	0.36	0.296	0.60	0.029
ζ_9	0.11	0.033	0.12	0.009	0.16	0.019	0.18	0.008	0.54	0.132
ζ_{10}	0.45	0.020	0.57	0.017	0.54	0.008	0.83	0.082	0.26	0.051
ζ_{11}	0.16	0.035	0.33	0.127	0.32	0.132	0.25	0.036	0.15	0.043
ζ_{12}	0.16	0.057	0.73	0.037	0.20	0.025	0.36	0.096	0.30	0.241

Table 5.5: The description of the mode shapes

	Case 1	Case 2	Case 3	Case 4	Case 5
$\phi_{E,1}$	out of plan (z)	out of plan (z)	out of plan (z)	in plan (y)	in plan (y)
$\phi_{E,2}$	in plan (y)	in plan (y)	in plan (y)	out of plan (z)	out of plan (z)
$\phi_{E,3}$	out of plan (z)	out of plan (z)	out of plan (z)	out of plan (z)	out of plan (z)
$\phi_{E,4}$	in plan (x)	in plan (x)	in plan (x)	in plan (x)	in plan (x)
$\phi_{E,5}$	out of plan (z)	out of plan (z)	out of plan (z)	out of plan (z)	mix (y,z)
$\phi_{E,6}$	in plan (y)	in plan (y)	in plan (y)	in plan (x)	mix (x,y)
$\phi_{E,7}$	in plan (y)	mix (y,z)	out of plan (z)	out of plan (z)	mix (y,z)
$\phi_{E,8}$	out of plan (z)	in plan (x)	in plan (x)	in plan (y)	in plan (x)
$\phi_{E,9}$	mix (x,z)	out of plan (z)	out of plan (z)	mix (x,z)	mix (x,z)
$\phi_{E,10}$	mix (x,z)	mix (x,z)	mix (x,y)	in plan (x)	mix (x,z)
$\phi_{E,11}$	in plan (x)	mix (x,z)	mix (x,z)	mix (x,z)	mix (x,z)
$\phi_{E,12}$	mix (y,z)	mix (x,z)	out of plan (z)	mix (y,z)	mix (x,z)

and 12 are significantly influenced by the studied damage model, harmonic excitations with frequencies of $\{f_F\} = \{20, 30, 60, 170\}^T$ Hz were used separately to excite the structure. The frequencies of the excitations were also chosen considering the lowest frequency that the shaker

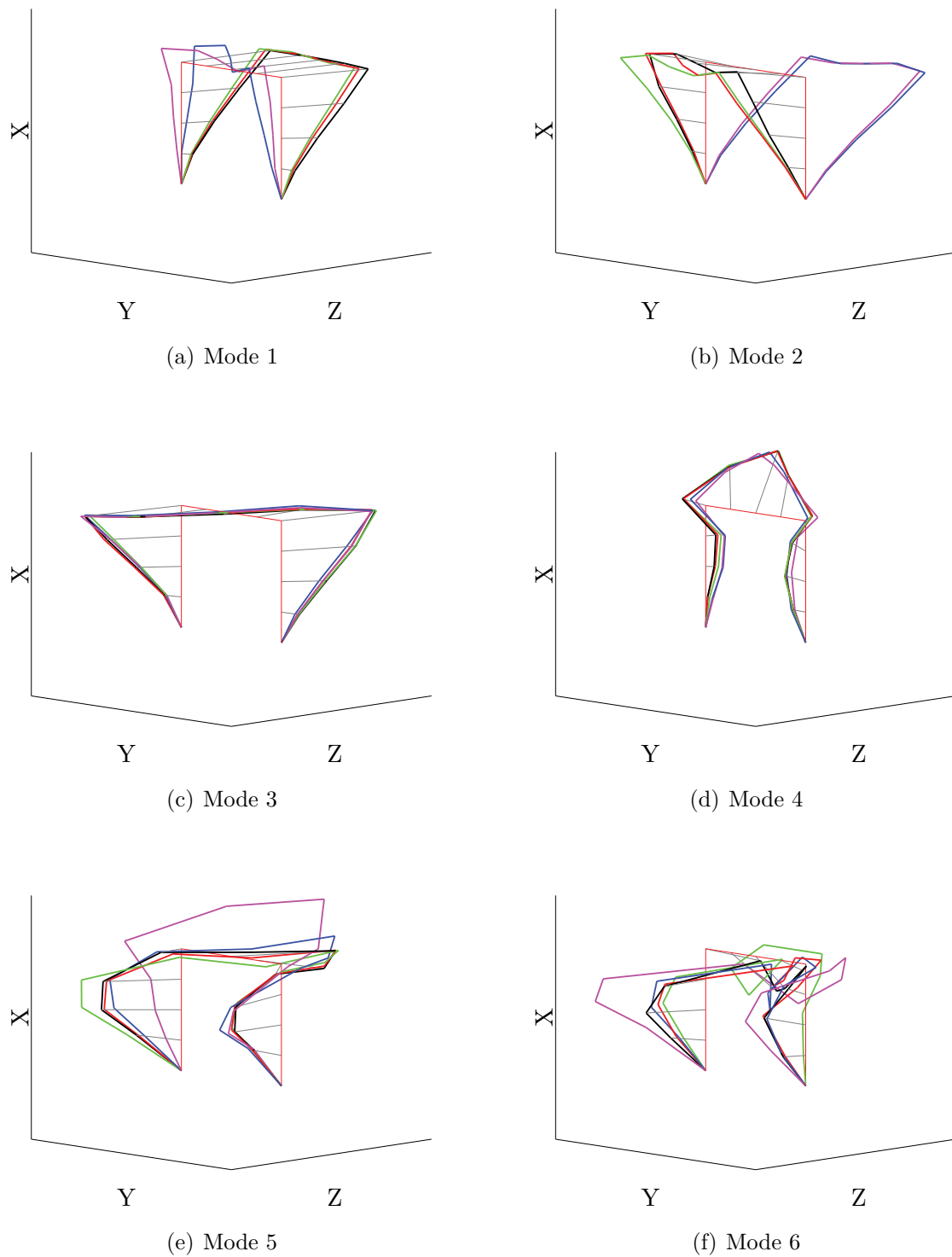


Figure 5.6: Mode shapes $[\phi_E]$ from 1 to 6: case 1 (black), case 2 (red), case 3 (green), case 4 (blue), case 5 (pink)

can produce, which is, in this case, $f_{F,1} = 20$ Hz, with a sufficient force amplitude. It was intended to keep the frequencies $\{f_F\}$ as low as possible to obtain a structural response which

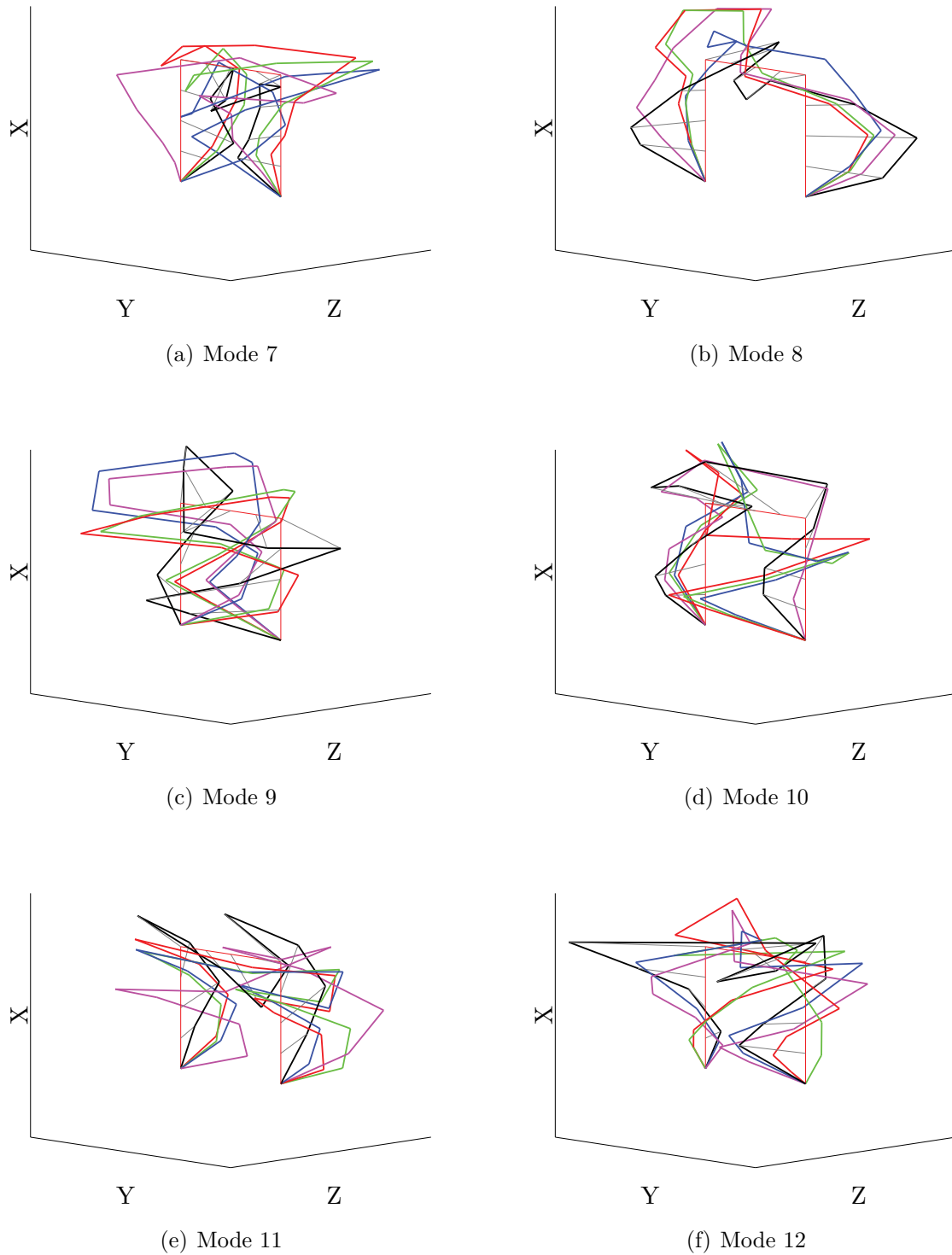


Figure 5.7: Mode shapes $[\phi_E]$ from 7 to 12: case 1 (black), case 2 (red), case 3 (green), case 4 (blue), case 5 (pink)

is essentially sensitive to the stiffness of the structure. Moreover, the frequencies $\{f_F\}$ were chosen avoiding the resonance frequencies of the frame. Exciting the structure close to its

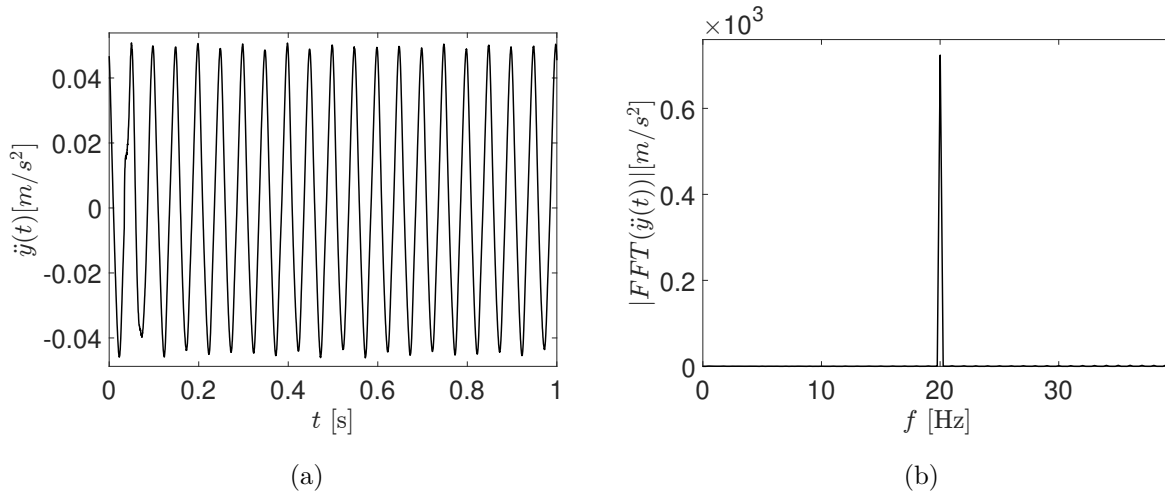


Figure 5.8: The acceleration output signal recorded using an accelerometer placed at the shaker (a) and its $|FFT|$ (b)

resonance frequencies produces a structural response which is sensitive to the variation of all physical parameter (mass, stiffness, damping). As a result, a large false alarm can be observed. The tests were performed as follows:

1. The shaker was placed at cube number 6 close to the first reference sensor and oriented to produce a harmonic excitation in longitudinal direction y (in-plane). After that, four independent modal tests were performed.
2. The shaker was moved to the cube number 14 close to the second reference sensor and oriented to produce a harmonic excitation in the vertical direction x (in-plane). Then, four independent modal tests were performed.
3. The described test procedure was applied for each setup and repeated for each studied damage case.

An accelerometer was placed on the shaker to measure its output signal. Figure 5.8 shows the acceleration output signal recorded using an accelerometer placed at the shaker when an excitation with the frequency of $f_F = 20$ Hz was applied.

The test procedure was arranged as follows:

1. An excitation signal $F = F_a \sin \omega t$ was produced in a desktop computer and transferred to an amplifier
2. The amplitude of the signal was amplified to a certain level before it was transferred to the shaker. The amplification level was chosen such that no large forces were produced, but it was possible to recognize the signal by most of the sensors, figure 5.10. The chosen force amplitude was constant for all damage cases.

Table 5.6: Arrangement of channels used to record the response and the corresponded cubes number where the sensors were placed

Channel Nr.	Channel label	Channel Nr.	Channel label	Channel Nr.	Channel label	Cube Nr.
1	x_1	12	y_1	23	z_1	2
2	x_2	13	y_2	24	z_2	4
3	x_3	14	y_3	25	z_3	6
4	x_4	15	y_4	26	z_4	8
5	x_5	16	y_5	27	z_5	10
6	x_6	17	y_6	28	z_6	12
7	x_7	18	y_7	29	z_7	14
8	x_8	19	y_8	30	z_8	16
9	x_9	20	y_9	31	z_9	18
10	x_{10}	21	y_{10}	32	z_{10}	20
11	x_{11}	22	y_{11}	33	z_{11}	22

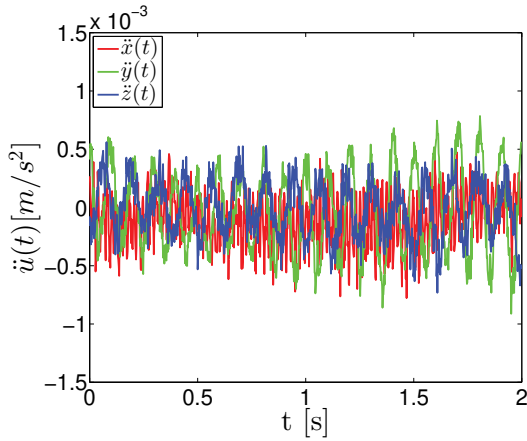
3. After the response of the structure reached its steady state under the given excitation; the acquisition system was started to save the response recorded by 5 sensors \times 3 channels = 15 channels and one channel to record the output of the shaker.

The sampling frequency is $\Delta f = 4096$ Hz and the acquisition time is $T = 60$ second. It is important to mention that the environmental conditions at the laboratory were constant for all test phases. Therefore, the influence of the environmental conditions on the test could be neglected. The channels of the sensors were arranged as shown in table 5.6.

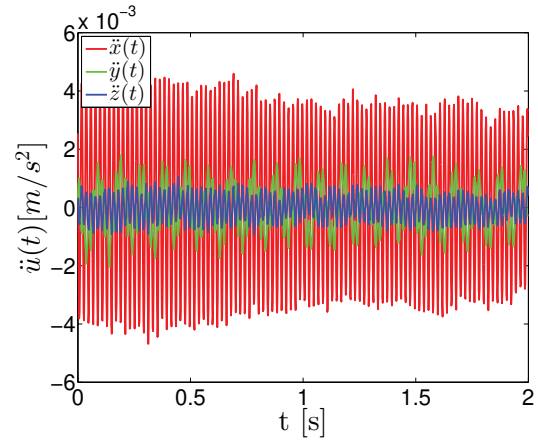
Damage indicator

Similar to the numerical study introduced in the previous chapter, the cumulative signal energy d of the structural response $[\ddot{u}] = [\ddot{x}, \ddot{y}, \ddot{z}]$ was used as a damage indicator. A certain procedure has been followed to obtain the cumulative signal energy $\bar{d}_{t,min}$ from measurements. The reason of choosing $\bar{d}_{t,min}$ is explained in chapter 3, section 3.5.3. The following steps are applied to obtain $\bar{d}_{t,min}$:

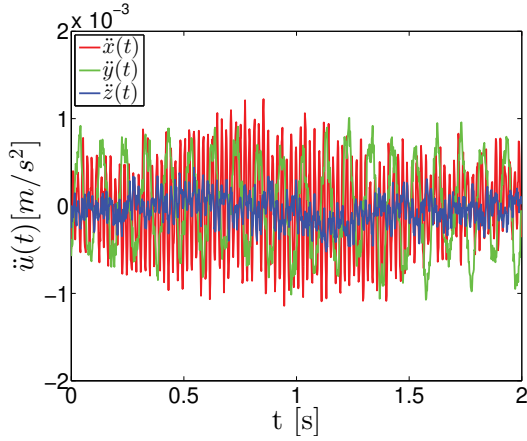
1. The frequency rate was reduced from 4096 Hz to 512 Hz.
2. The first and the last 5 s of the signal were ignored to avoid any possible influence from starting and ending the recording process. As a result, 50 s were used to compute the signal energy.
3. A time window which has a length of $t = 5$ s ($512 \times 5 = 2560$ time points) was moved between $j = 1$ to $j = 45 \times 512$, eq. (5.3), where j refers to the number of the time window.



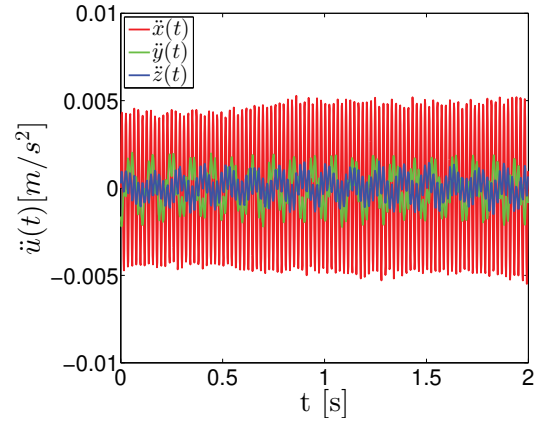
(a) The structural response recorded at cube 12 under harmonic excitations: $f_F = 20$ Hz applied in y direction



(b) The structural response recorded at cube 12 under harmonic excitations: $f_F = 20$ Hz applied in x direction



(c) The structural response recorded at cube 12 under harmonic excitations: $f_F = 30$ Hz applied in y direction



(d) The structural response recorded at cube 12 under harmonic excitations: $f_F = 30$ Hz applied in x direction

Figure 5.9: Examples of the recorded structural response under harmonic excitations

The size of the time window, which depends on the frequency of the excitation, must be fixed for all damage cases. In this example, each window contains 100 cycles if $f_{F,1} = 20$ Hz is applied and 850 cycles in case of $f_{F,1} = 170$ Hz. The size of the time window can be extended if necessary to obtain more information about the structural response of the studied system. However, the size of the time window has to be extended for all damage cases equally.

$$d_{t,j} = \Delta t \sum_{l=t_s/\Delta t}^{t_e/\Delta t} \ddot{u}^2(l) \quad (5.3)$$

4. The cumulative signal energies of each channel under each excitation were calculated for

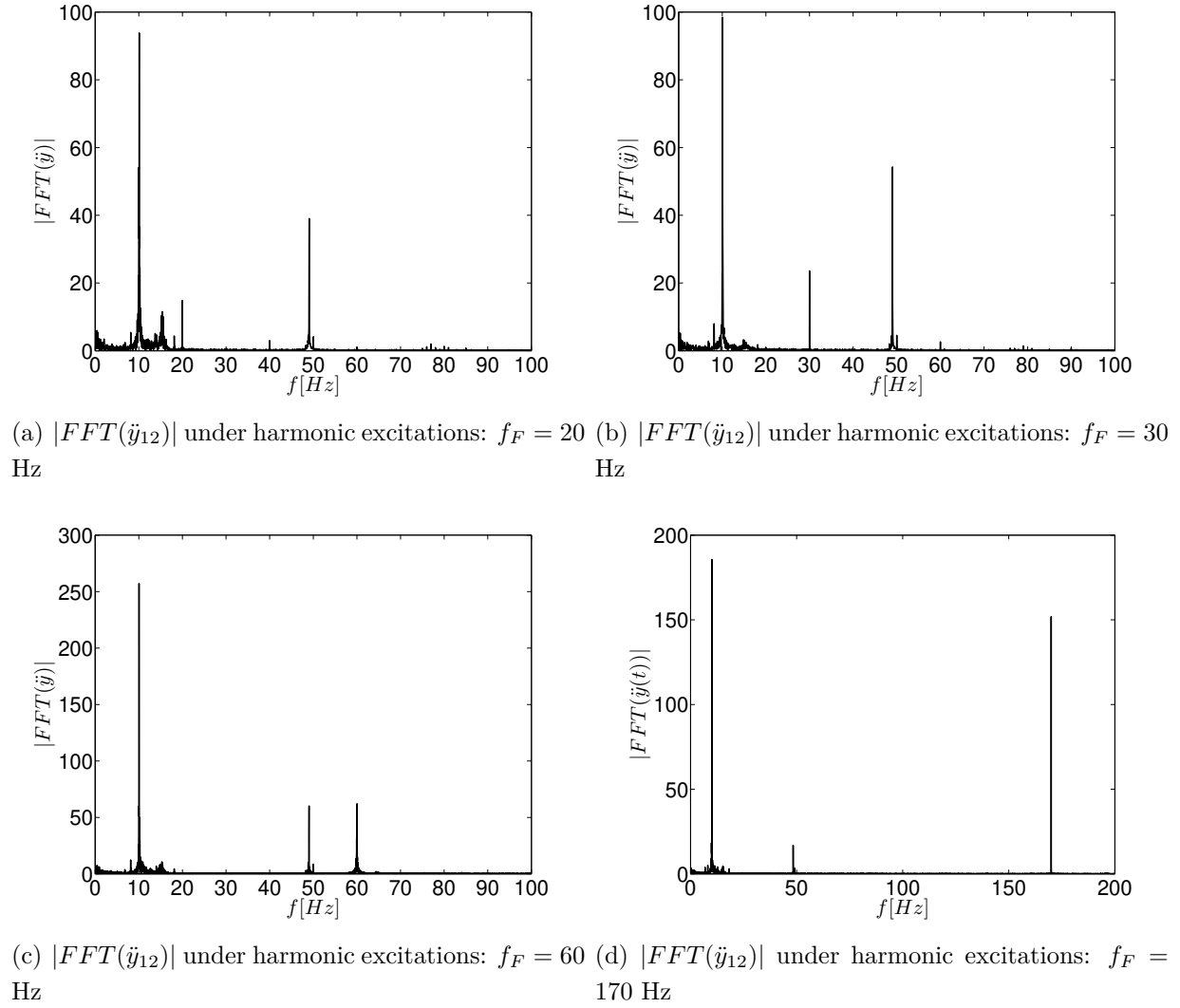


Figure 5.10: Fourier transform of the response \ddot{y} at cube 12 (middle of the beam) under the applied lateral harmonic excitations

each window j . The signal energy of the shaker output d_F was computed following the same procedure as well, eq. (5.4).

$$d_{F,j} = \Delta t \sum_{l=t_s/\Delta t}^{t_e/\Delta t} \ddot{u}_F^2(l) \quad (5.4)$$

5. The signal energy values of the outputs were normalized with respect to the signal energy of the shaker output. Since Δt was constant, Δt was omitted when the signal energy was calculated - similar to eq. (3.5). At the end, the normalized minimum value $\bar{d}_{t,min}/d_F = \min(\bar{d}_{t,1}/d_{F,1}, \bar{d}_{t,2}/d_{F,2}, \dots, \bar{d}_{t,j}/d_{F,j})$ was chosen.
6. The procedure was applied for all studied damage cases. Figure 5.11 and 5.12 show the

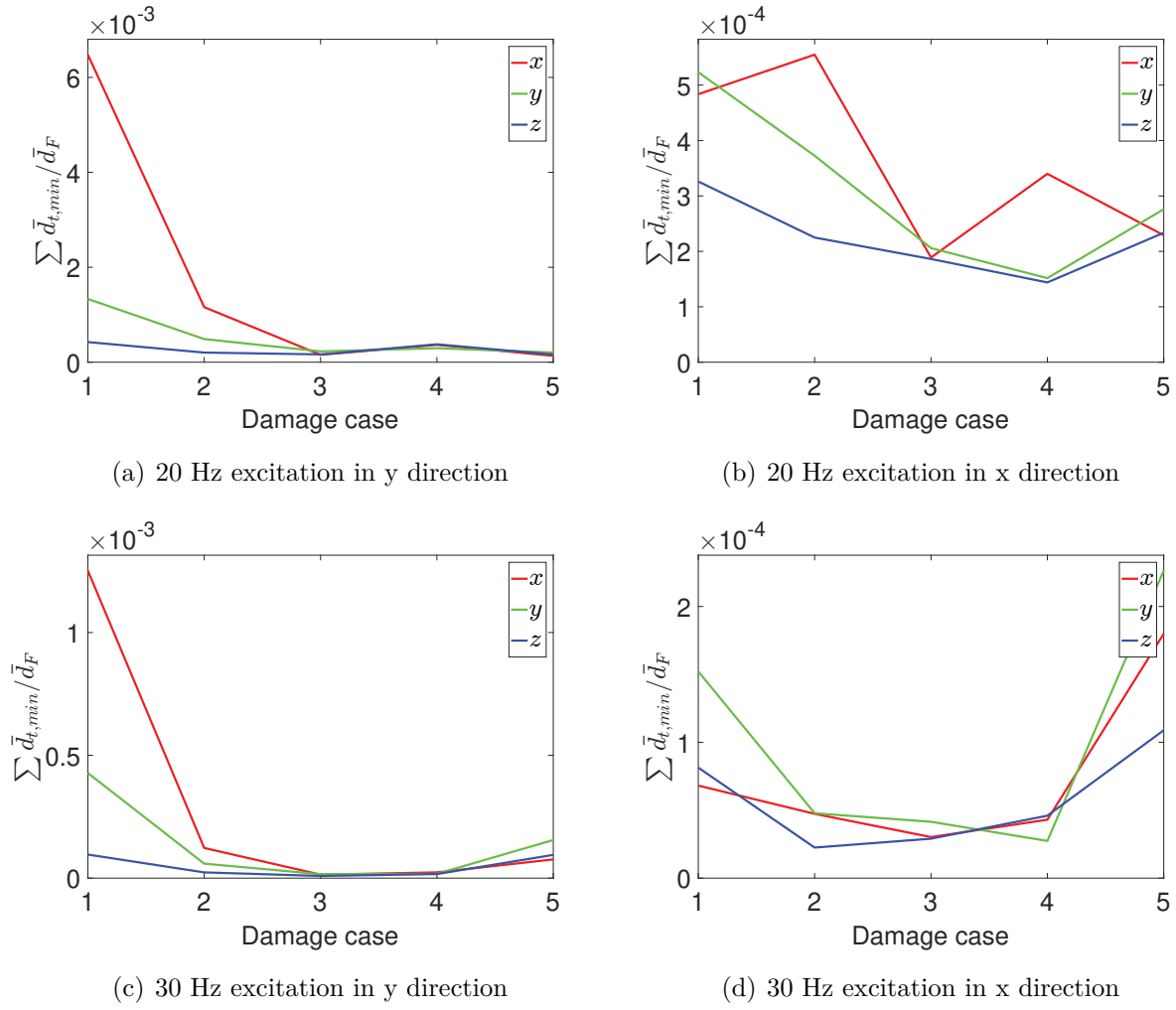


Figure 5.11: $\sum \bar{d}_{t,min,si} / \bar{d}_{F,si}$ computed based on initial conditions and eq. (5.4) for all the $si = 1 \dots 11$ sensors

variation of $\sum \bar{d}_{t,min} / \bar{d}_F$ considering different damage cases, excitation frequencies and excitation location.

The results show that increasing damage θ^g from θ_1^g to θ_3^g reduces the signal energy significantly if a harmonic excitation with $f_F = 20$ Hz or $f_F = 30$ Hz is applied in y or x directions. Applying excitation in x direction with $f_F = 170$ Hz helps to detect damage $\theta_1^g < \theta^g < \theta_2^g$.

Increasing damage θ^g from θ_3^g to θ_5^g increases the signal energy significantly if a harmonic excitation with $f_F = 60$ Hz or $f_F = 170$ Hz is applied in y or x directions.

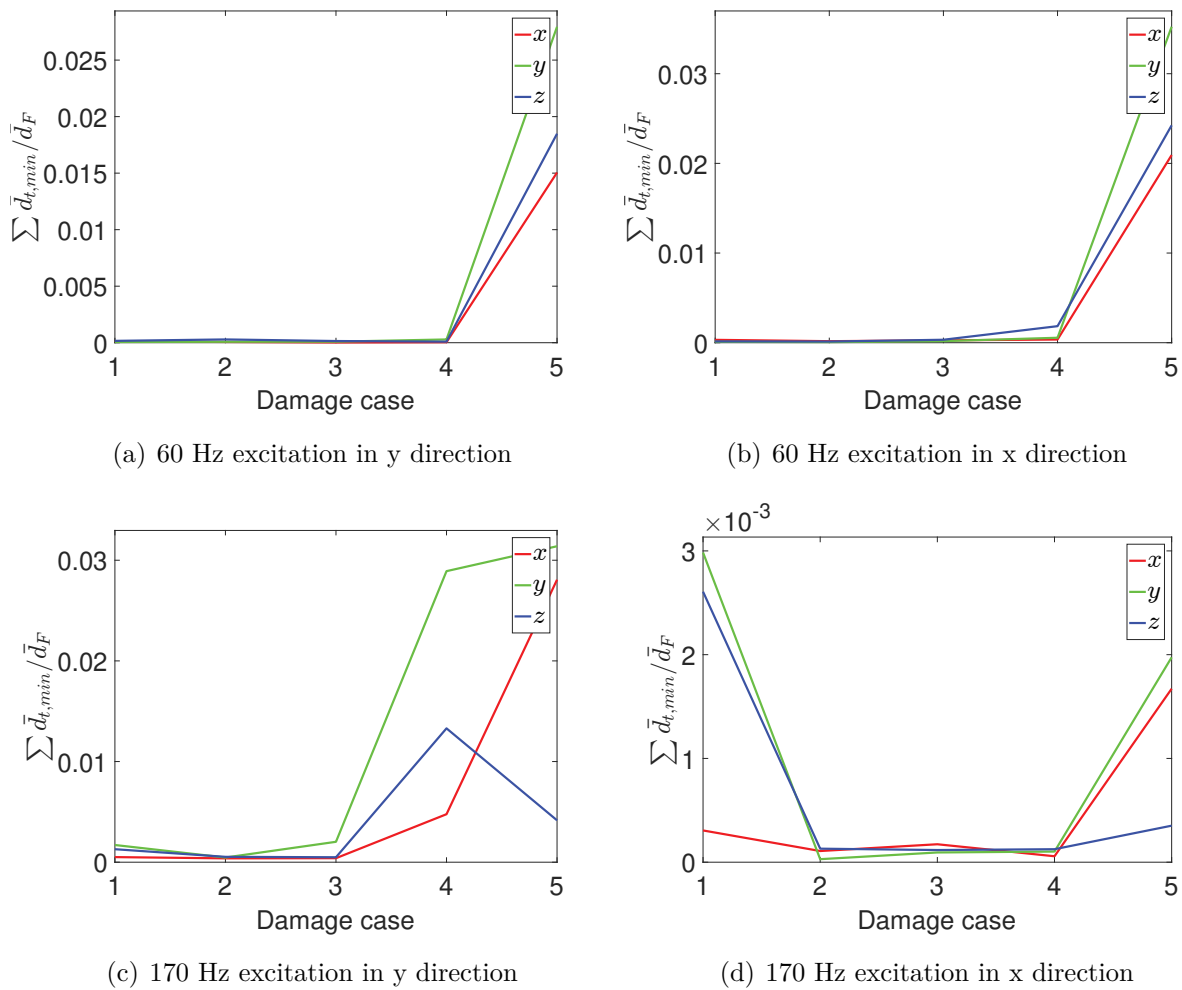


Figure 5.12: $\sum \bar{d}_{t,min,si} / \bar{d}_{F,si}$ computed based on eq. (5.3) and eq. (5.4) for all the $si = 1 \dots 11$ sensors

5.1.5 Numerical study

Numerical model

A numerical model was developed using shell elements to evaluate the performance of the chosen inspection method for damage detection. The bolted connections between every two cubes were modeled by constraining the (x, y, z) translational degree of freedom of 8 nodes from the first cube with their opposites from the second cube, figure 5.13 (a). The support conditions were modeled by constraining the translational degrees of freedom of 8 nodes located at the lower face of the cube at the column base.

The hinge was modeled using two opposite truncated pyramids from the same element type of the cubes. The base of the first pyramid was connected to a plate attached to the cube at the left side and the base of the second pyramid was connected to a plate attached to the cube at the

right side. The translational degrees of freedom of the nodes at the small bases of the pyramids were constrained, figure 5.13 (b). The thicknesses of the plate and the truncated pyramid shell elements were adjusted to obtain the mass of the hinge measured in the laboratory. Using a truncated pyramid to model the hinge can maintain the stiffness of the hinge due to friction caused by the relative motion of the hinge elements. The stiffening elements were modeled using the same element type and material properties of the cubes. The thickness of the cross-section is 6 mm and the length of the angle leg is 65 mm, figure 5.13 (c).

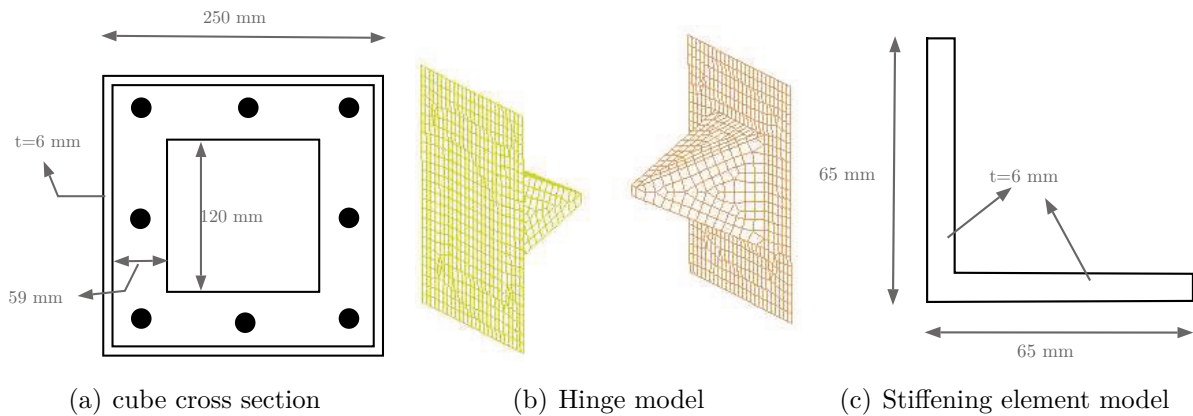


Figure 5.13: Models of the elements that form the global shell element model of the steel frame



Figure 5.14: Numerical model of the studied frame using shell elements

The model was meshed to smaller shell elements with maximum size 10×10 mm. A linear elastic material was used with Young's modulus $E = 2.070 \times 10^5$ MPa, density $\rho = 7.830 \times 10^{-9}$ t/mm³

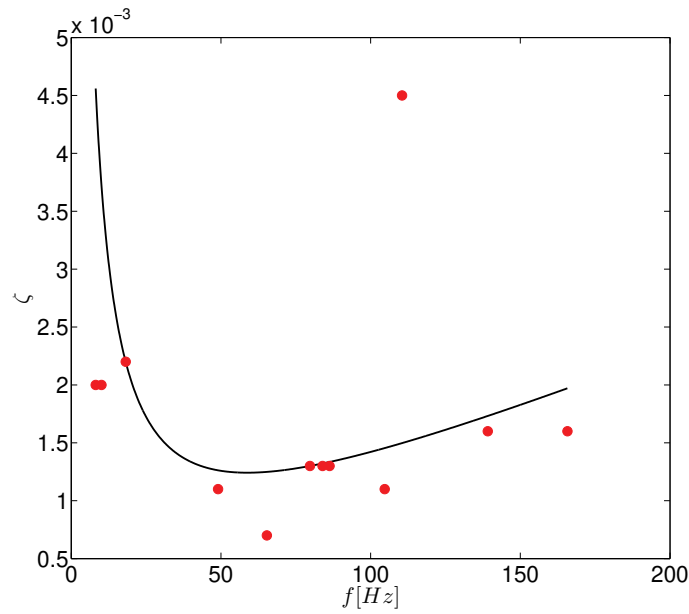


Figure 5.15: Rayleigh damping model included in the numerical model of the frame. Red points represents the damping ratios of undamaged structure obtained from measurements $\{\zeta_E\}$ and black line represents Rayleigh damping model, eq.(5.5)

and Poisson's ratio $\nu = 0.3$. Later the mass of the shaker (3.1036 kg) was added to a node where the shaker was placed on the frame before performing a transient analysis. Rayleigh damping model, which expresses damping as a linear combination of mass $[M]$ and stiffness $[K]$ matrices, eq. (5.5), with $\alpha = 0.459$ and $\beta = 3.364 \times 10^{-6}$ was introduced in the model based on the modal damping ratios obtained from the modal tests using the mean values from damage case 1, figure 5.15.

$$[C] = \alpha[M] + \beta[K] \quad (5.5)$$

It is important to mention some issues which were taken into account while developing the model:

- Improving the model by introducing a *Surface to Surface* connection between the cubes, hinges and stiffening elements increases the nonlinear behavior in the structural response of the frame. *Surface to Surface* contact algorithm establishes contact when the surface of one body penetrates the surface of another. It is used for bodies that have large contact areas and the contact surfaces are known. More technical information is explained in LSTC [2012]. In this case, the response of the structure depends on the distance between the surfaces of the connected elements, the excitation properties, and damage case. Moreover, if two surfaces hit each other, additional vibration noise was observed. The amplitude of the noise depends on the excitation and the initial distance between

the surfaces. It is possible to introduce numerical damping to reduce the influence of this noise on the output signal. However, long computational time is required which can be a challenge while performing a statistical study.

While conducting the modal test in the laboratory, the shaker did not produce large forces amplitude. In this example, it was assumed that the nonlinear behavior in the structural response of the frame was limited. Therefore, an investigation was done to find out the most sensitive locations where if *Surface to Surface* model is used, significant changes in frequencies and mode shapes are observed. The results indicate that the connection between the surfaces of the cubes in the middle of the columns is important. Therefore, *Surface to Surface* model was replaced by introducing more constraints between the cubes in those areas. It was noticed that the third, sixth and twelfth modes, which are significantly influenced by damage, are not influenced by considering the *Surface to Surface* model.

- The response of the structure is sensitive to the model of the hinge. Different models of the hinge were tested until reasonable frequencies and mode shapes were obtained, table 5.7, figure 5.16. It was noticed that the hinge model could change the influence of damage on some mode shapes or frequencies. It is recommended to improve the model of the hinge if better results are required. However, a trade-off between the model complexity and the computational time should be considered if a statistical study is performed.
- It was noticed from the experimental test that releasing hinges increased the impact between the cubes. As a result, large energy dissipation and significant damping influence were observed. In this study, the reliability of the inspection method was evaluated considering the damping as apart from damage, θ^g , as shown in eq. (5.6), where k_s refers to the stiffness of the stiffening elements, m_s is the mass of the stiffening elements and ζ_{θ^g} is the damping ratio because of removing the stiffening elements.

$$\theta^g = f(k_s, m_s, \zeta_{\theta^g}) \quad (5.6)$$

The frequencies and the mode shapes, calculated using the developed numerical model, are presented in table 5.7 and figure 5.16. It was mentioned before that, the order of the first and the second mode shapes are switched if the fourth and the fifth damage cases were introduced in the experimental model in the laboratory. In this numerical study, this phenomenon was observed only if the fifth damage case was modeled.

To check the similarity between the mode shapes of the studied structure obtained from tests $[\phi_{E,ri}]$ and the numerical model $[\phi_{S,rj}]$ the Modal Assurance Criterion (MAC) was calculated as follows:

Table 5.7: Natural frequencies of the numerical model $f_{n,S}$ [Hz] of the frame for studied damage cases and relative error between $f_{n,E}$ and $f_{n,S}$

	Case 1		Case 2		Case 3		Case 4		Case 5	
	$f_{n,S}$	$\frac{ f_{n,E} - f_{n,S} }{f_{n,E}}$	$f_{n,S}$	$\frac{ f_{n,E} - f_{n,S} }{f_{n,E}}$	$f_{n,S}$	$\frac{ f_{n,E} - f_{n,S} }{f_{n,E}}$	$f_{n,S}$	$\frac{ f_{n,E} - f_{n,S} }{f_{n,E}}$	$f_{n,S}$	$\frac{ f_{n,E} - f_{n,S} }{f_{n,E}}$
$f_{n,1}$	8.97	10%	9.08	11%	9.18	12%	9.29	24%	9.13	42%
$f_{n,2}$	10.70	6%	10.24	8%	9.99	13%	9.51	14%	9.41	12%
$f_{n,3}$	18.31	1%	17.66	4%	16.54	7%	15.37	7%	14.27	24%
$f_{n,4}$	50.86	4%	50.96	3%	51.10	5%	51.22	9%	51.28	15%
$f_{n,5}$	63.85	2%	63.65	2%	63.50	1%	63.37	6%	63.30	9%
$f_{n,6}$	81.73	3%	76.60	1%	73.84	2%	72.66	12%	70.73	17%
$f_{n,7}$	85.03	1%	81.97	2%	80.36	2%	78.89	0%	78.97	5%
$f_{n,8}$	85.84	1%	86.09	1%	86.36	2%	82.37	0%	79.23	0%
$f_{n,9}$	99.33	5%	99.41	3%	99.39	1%	99.26	0%	99.34	2%
$f_{n,10}$	104.27	6%	104.74	3%	105.23	0%	105.73	5%	106.23	6%
$f_{n,11}$	134.61	3%	131.89	3%	131.90	4%	128.86	5%	128.85	7%
$f_{n,12}$	157.94	5%	148.37	2%	132.41	3%	132.31	3%	129.28	5%

$$MAC(\phi_{E,ri}, \phi_{S,rj}) = \frac{([\phi_{E,ri}]^T [\phi_{S,rj}])^2}{([\phi_{E,ri}]^T [\phi_{E,ri}])([\phi_{S,rj}]^T [\phi_{S,rj}])} \quad (5.7)$$

where $ri = 1 \cdots 12$ and $rj = 1 \cdots 12$ refers to the mode order. The results are presented in figure 5.17 and table 5.8. The results show that the first 5 mode shapes are highly related. Mode shapes 7 to 12 show low MAC values. Improving the results may require using more sensors to obtain more information about the high order modes.

The structural response of the studied example was computed under harmonic excitation similar to what was recorded from the shaker. Figures 5.18 and 5.19 show examples of the computed acceleration in one of the nodes of cube 12. The structural response was calculated for each damage case under the same excitation. Therefore, it is possible to compare the signal energy d with and without normalizing it to the signal energy of the input excitation d_F , figures 5.20 and 5.21. The same procedure explained in Sec. 5.1.4 was applied to calculate the signal energy of the structural response computed using the developed numerical model.

To compare the similarity between the simulated \ddot{u}_S and measured \ddot{u}_E responses of the studied example, the correlation coefficient introduced in eq. (3.18) was calculated for each sensor and damage cases as follows:

1. A time window which has the same duration of the simulated signal T_s was moved along the measured response between $j = 1$ to $j = (T - T_s) * 512$, where 512 represents the rate of measurement points per second, $[1/s]$.

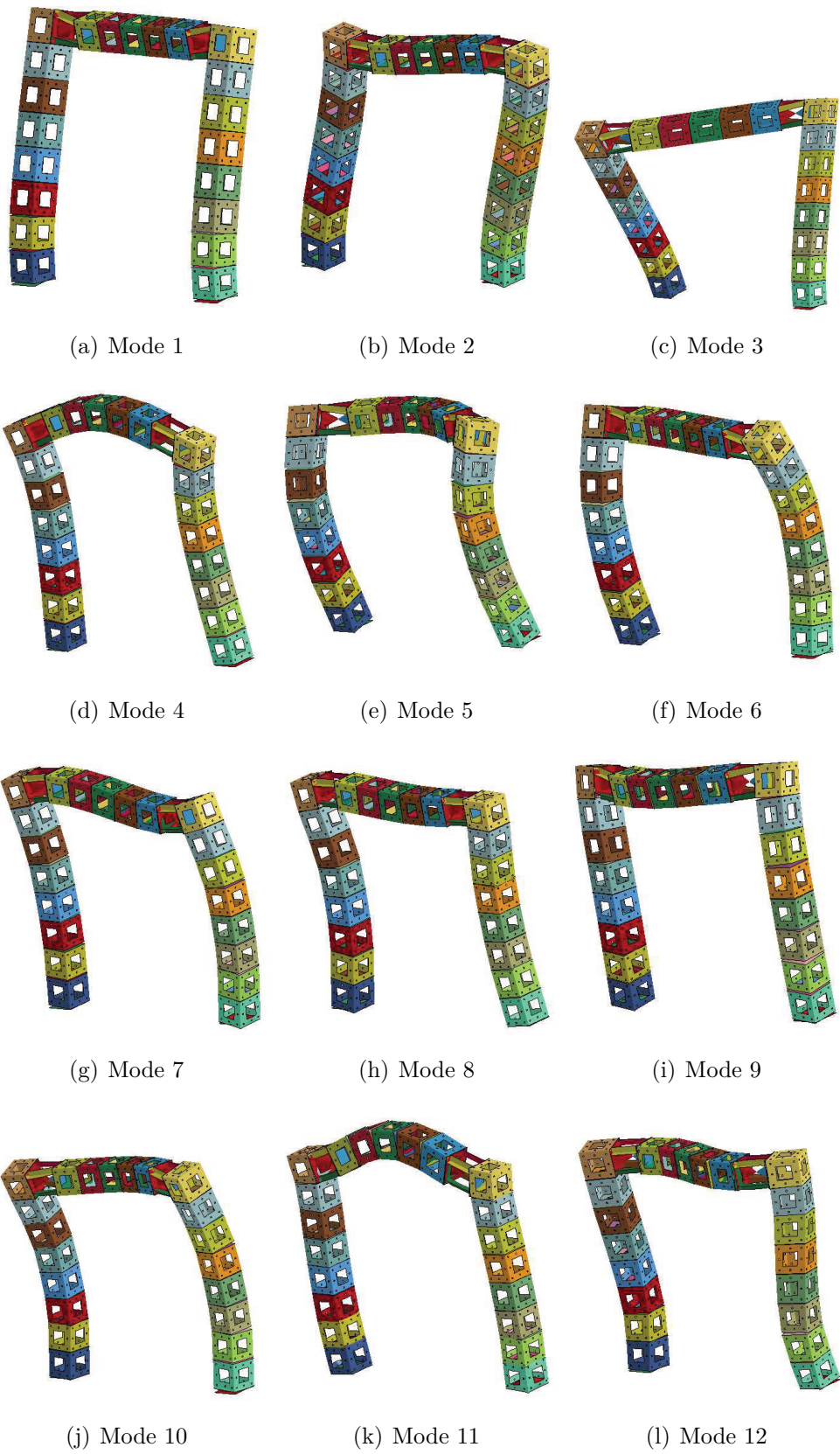


Figure 5.16: Mode shapes from 1 to 12: case 1

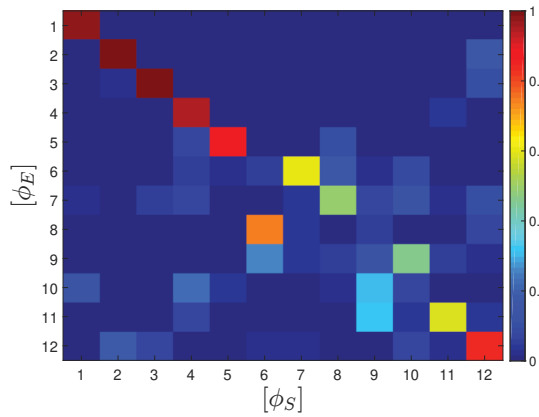
Table 5.8: Modal Assurance Criterion values (MAC) $MAC(\phi_{E,ri}, \phi_{S,rj})$

	Case 1	Case 2	Case 3	Case 4	Case 5
$MAC(\phi_{E,1}, \phi_{S,1})$	0.98	0.95	0.90	0.36	0.97
$MAC(\phi_{E,2}, \phi_{S,2})$	0.98	0.90	0.89	0.35	0.96
$MAC(\phi_{E,3}, \phi_{S,3})$	0.99	0.94	0.98	0.88	0.99
$MAC(\phi_{E,4}, \phi_{S,4})$	0.95	0.95	0.95	0.94	0.87
$MAC(\phi_{E,5}, \phi_{S,5})$	0.89	0.88	0.79	0.84	0.54
$MAC(\phi_{E,6}, \phi_{S,6})$	0.19	0.33	0.36	0.55	0.42
$MAC(\phi_{E,7}, \phi_{S,7})$	0.11	0.36	0.39	0.13	0.40
$MAC(\phi_{E,8}, \phi_{S,8})$	0.01	0.29	0.39	0.36	0.62
$MAC(\phi_{E,9}, \phi_{S,9})$	0.12	0.10	0.12	0.13	0.11
$MAC(\phi_{E,10}, \phi_{S,10})$	0.07	0.46	0.61	0.68	0.24
$MAC(\phi_{E,11}, \phi_{S,11})$	0.58	0.00	0.01	0.00	0.01
$MAC(\phi_{E,12}, \phi_{S,12})$	0.83	0.16	0.91	0.61	0.24

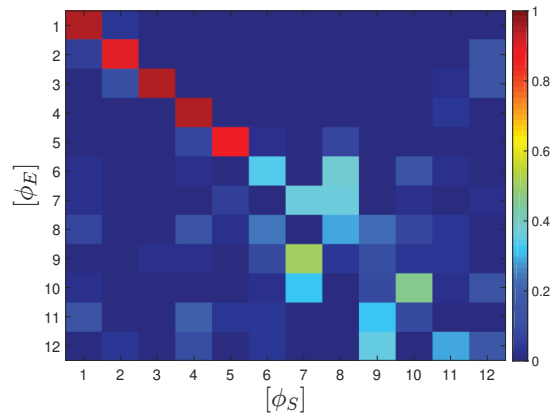
2. For each window the correlation was calculated $\rho(\ddot{u}_{E,j}, \ddot{u}_S)$
3. The maximum correlation coefficient was taken: $\rho(\ddot{u}_E, \ddot{u}_S) = \max(\rho(\ddot{u}_{E,j}, \ddot{u}_S))$ where $j = 1, 2, 3, \dots, (T - T_s) * 512$

The results are presented in figures 5.22 to 5.25. The results show that by increasing the frequency of the excitation, the correlation between \ddot{u}_E and \ddot{u}_S becomes higher which indicates larger agreement between the measured and computed responses more than if the low frequency of the excitation was used. In figure 5.26 the comparison between \ddot{u}_E and \ddot{u}_S was presented by comparing both measured and simulated responses that show the largest correlation. Since the amplitude of the input force was not measured during performing the tests, the amplitude of the responses were normalized to 1 as follows: $\frac{\ddot{u}(t)}{\max(\ddot{u}_{t=0}, \dots, \ddot{u}_{t=T})}$. The results show that for $f_F = 20$ and $f_F = 30$ [Hz] excitations the measured forced response of the structure was poorly observed compared to the computed forced response which explains the small correlation coefficient values. This indicates that larger force amplitude should be used for the tests. For $f_F = 60$ and $f_F = 170$ [Hz] the measured and computed forced responses were obtained, and they are highly correlated.

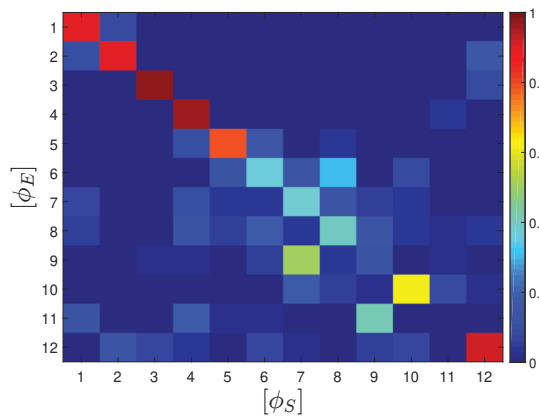
For measuring the agreement between the developed numerical model and the experimental model taking into account the studied damage model and the applied excitations, eq (3.3) was applied to calculate Q_V . The results are presented in table 5.9. The positive values of Q_V which was marked in red indicate an agreement between the response of the physical model and the numerical model considering the studied damage model. If $Q_V \approx 1$, it means that the $d \propto \bar{d}$.



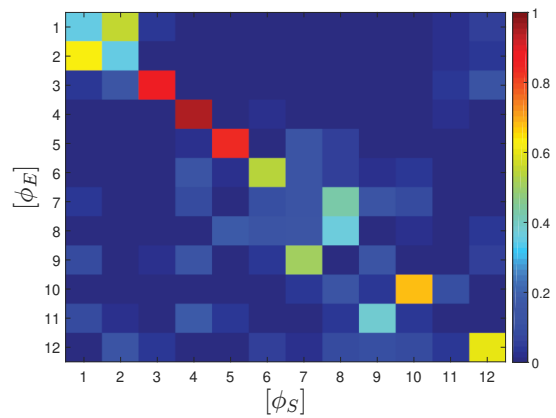
(a) Case 1



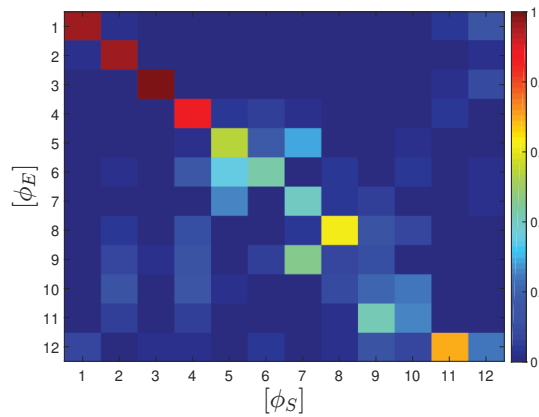
(b) Case 2



(c) Case 3



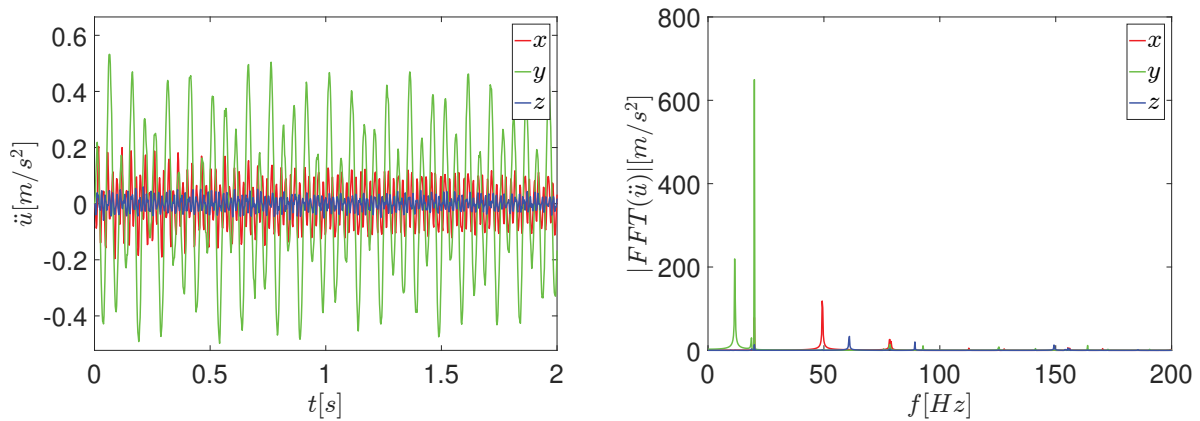
(d) Case 4



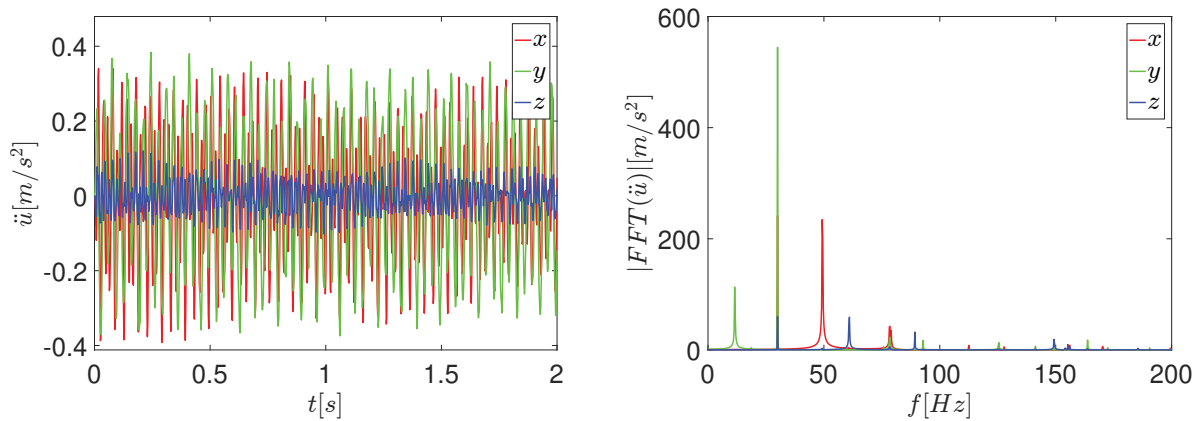
(e) Case 5

Figure 5.17: Modal Assurance Criterion values (MAC) $MAC(\phi_{E,ri}, \phi_{S,rj})$. $ri = 1 \dots 12$ and $rj = 1 \dots 12$ refers to the mode order

If $Q_V \approx 0$, it means that there is a modeling error and/or the noise in the experimental results is large: $d_\gamma \gg d^*$. In this case, inaccurate inspection method assessment should be expected.



(a) The response of the structure computed in cube 12 due to 20 Hz harmonic excitation applied in y direction
 (b) The |FFT| of the response of the structure computed in cube 12 due to 20 Hz harmonic excitation applied in y direction



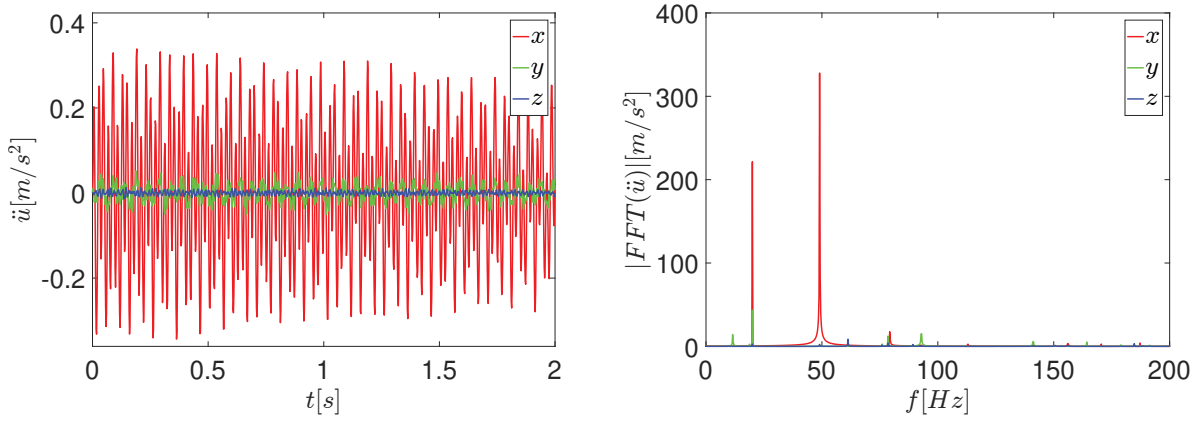
(c) The response of the structure computed in cube 12 due to 30 Hz harmonic excitation applied in y direction
 (d) The |FFT| of the response of the structure computed in cube 12 due to 30 Hz harmonic excitation applied in y direction

Figure 5.18: The structural response and its |FFT| under the harmonic excitations applied in y direction

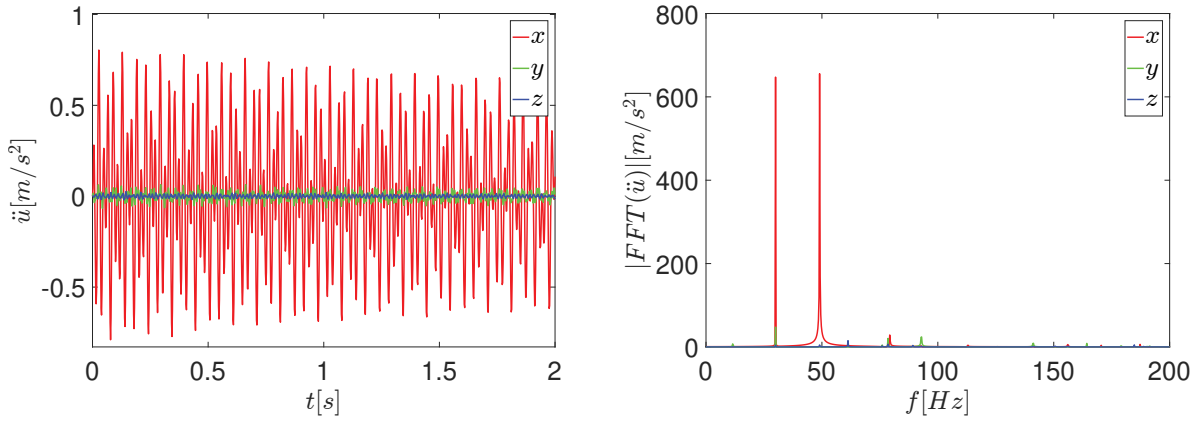
The results in table 5.9 show that the quality of the numerical model depends on the excitation properties and sensor location, $Q_V = f(F, \ddot{u}(x, y, z))$. High Q_V values, which indicate better agreement between both studied models, are obtained if an excitation with $f_F = 60$ Hz is applied.

Damage model

The assumed damping ratio increment depends on many factors. Some of these factors could be: the relative motion between the surfaces of the cubes A_c , the relative motion between the elements of the hinge, A_h , the relative motion between the surfaces of the hinge plates and the



(a) The response of the structure computed in cube 12 due to 20 Hz harmonic excitation applied in x direction
 (b) The |FFT| of the response of the structure computed in cube 12 due to 20 Hz harmonic excitation applied in x direction



(c) The response of the structure computed in cube 12 due to 30 Hz harmonic excitation applied in x direction
 (d) The |FFT| of the response of the structure computed in cube 12 due to 30 Hz harmonic excitation applied in x direction

Figure 5.19: The structural response and its |FFT| under the harmonic excitations applied in x direction

stiffening elements A_s , the stiffness of the stiffening elements k_s , the pre-stress force in each bolt F_b , the type of the excitation F and its amplitude F_a , the frequency of the excitation ω and the level of the ambient vibration \ddot{u}_a , eq. (5.8).

$$\zeta_{\theta^g} = f(A_c, A_h, A_s, k_s, F_b, F, F_a, \omega, \ddot{u}_a) \quad (5.8)$$

Including all the mentioned factors in the developed numerical model to investigate the damping due to damage requires effort and unobtainable time. Therefore, empirical damping models have been developed based on the experimental results. The developed damping models consider

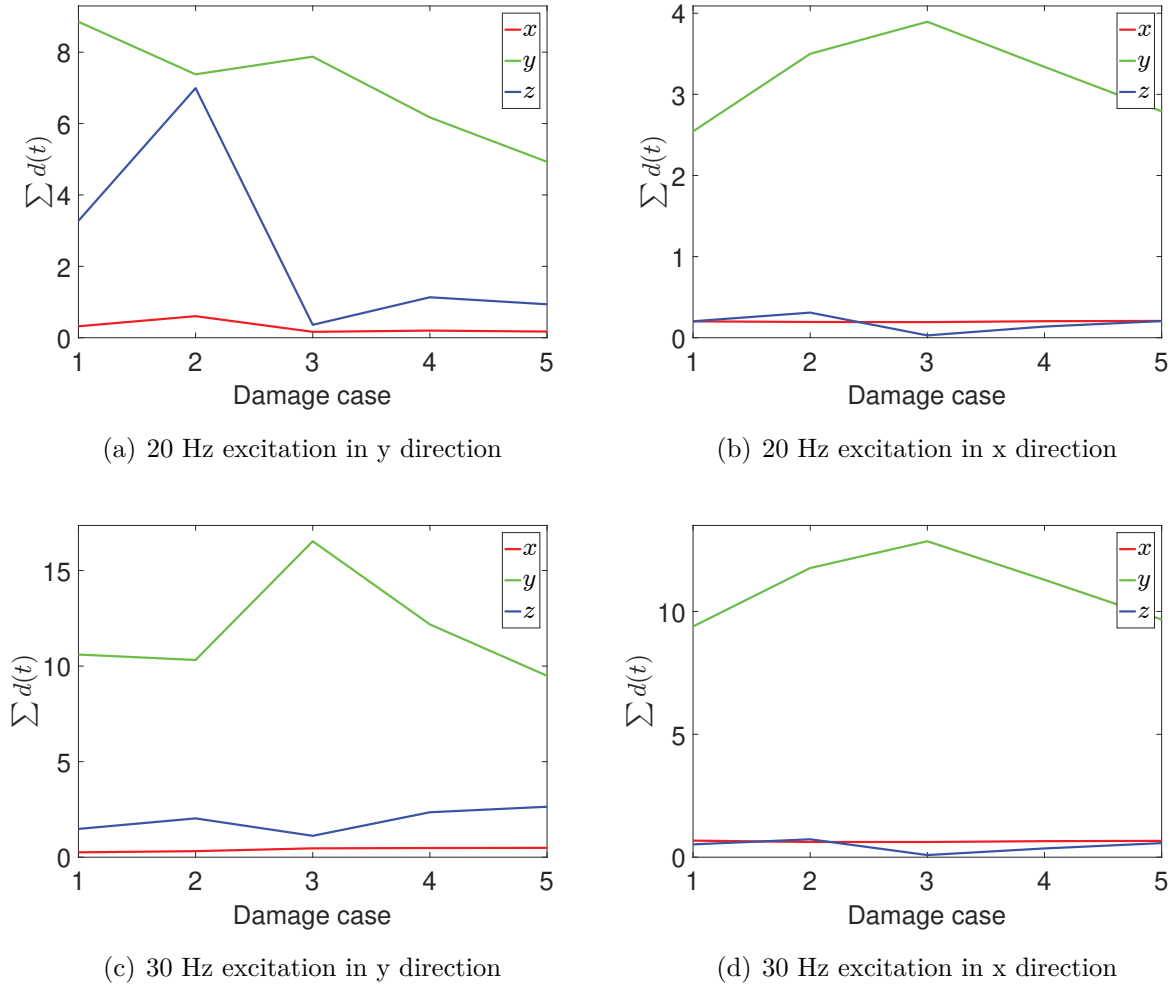


Figure 5.20: $\sum d_{t,si}$ computed based on eq. (5.3) for all sensors $si = 1, 2, \dots, 11$

the effect of damage size on damping. The empirical damping models were used to modify the signal energy d obtained from the response of the numerical model, considering the studied damage model. After applying those empirical models, the value of d matches the value of \bar{d} which obtained from the response of the physical model considering equivalent damage size. The value $C_{\zeta,i,j}$, eq. (5.9), refers to the ratio of \bar{d} to d for each sensor position $j = 1, 2, \dots, 11$ if damage case i was observed. $C_{\zeta,i,j}$ was used to consider the effect of damage $\theta_i^g \leq \theta^g \leq \theta_{i+1}^g$ on the damping ζ_{θ^g} . The change in damping because of damage can be observed in the dynamic response of the structure at each sensor position j .

In this example, four different interpolation models were used to obtain the value $C_{\zeta,i,j}$ for $\theta_1^g \leq \theta_i^g \leq \theta_2^g$, figure 5.27. The first model assumes that there was no influence on damping due to damage increment (figure 5.27, bold black), eq. (5.10). The second model assumes that damping was changing linearly if damage increases from case 1 to case 2 (figure 5.27, blue), eq. (5.11), eq. (5.12). The third and the fourth models represent nonlinear changes in damping due to damage (Parabolic models), eq. (5.13), eq. (5.14). The third model indicates that

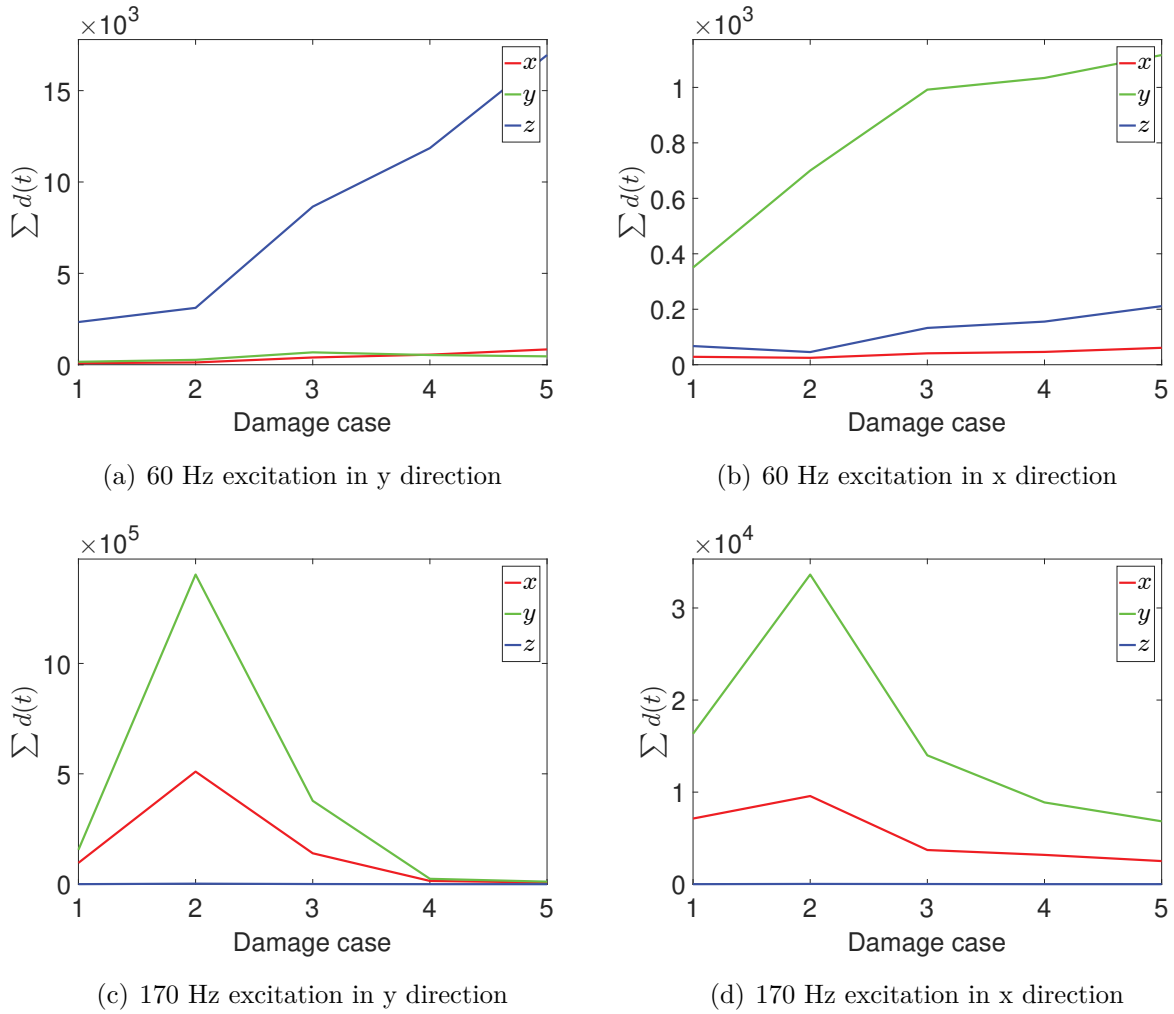


Figure 5.21: $\sum d_{t,si}$ computed based on eq. (5.3) for all sensors $si = 1, 2, \dots, 11$

damping change faster than what other models indicate if damage increase (figure 5.27, green), eq. (5.15). The fast change of damping was introduced by giving large weighting factor for $C_{\zeta,2,j}$, in this example the weighting factor is 5, which means that damping $C_{\zeta,\Delta,j}$, corresponded to damage size $\theta_{1,2}^g : \theta_1^g \leq \theta_{1,2}^g \leq \theta_2^g$, converges fast to the value $C_{\zeta,2,j}$. Damping change happens slowly by applying the fourth model (figure 5.27, red), eq. (5.16). The slow change of damping was introduced by giving large weighting factor for $C_{\zeta,1,j}$, in this example the weighting factor is 5, which indicates that damping $C_{\zeta,\Delta,j}$, corresponded to damage size $\theta_{1,2}^g : \theta_1^g \leq \theta_{1,2}^g \leq \theta_2^g$, converges slow to the value $C_{\zeta,2,j}$.

$d_{mi,j}(\theta^g)$ is the computed structural response of the frame using the developed numerical model at sensor position j considering damping model $mi : mi \in [1, 2, 3, 4]$ and damage θ^g . Damage θ^g was simulated by reducing the stiffness k_s and the mass m_s of the stiffening elements by reducing their thickness h_s of the stiffening elements corresponded to the elements that were removed from the physical model for each damage case. if $h_s \approx 0$, the stiffening elements were omitted from the numerical model.

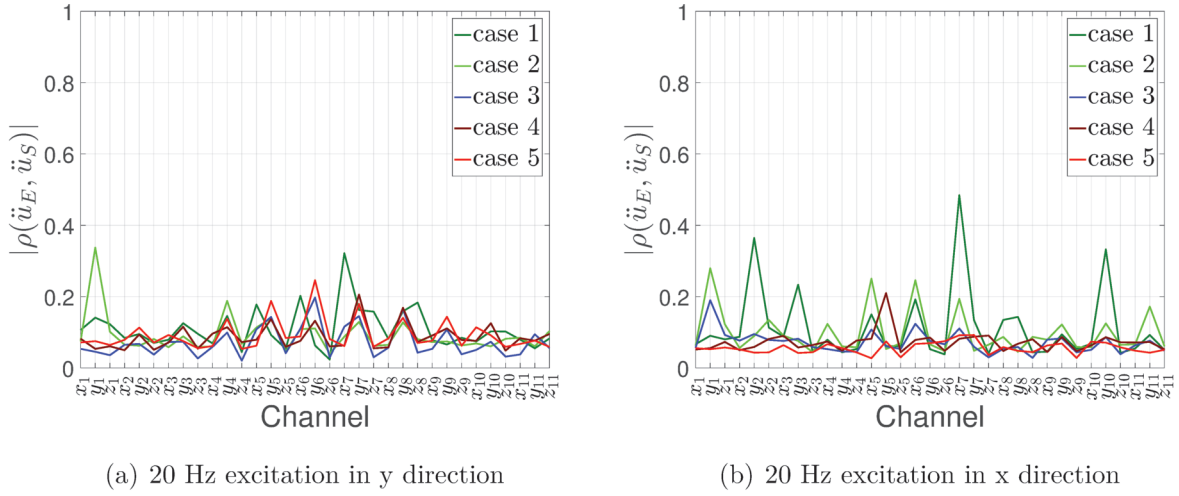


Figure 5.22: Correlation coefficient between the time histories of the computed and measured structural response for all studied damage cases under 20 Hz excitation

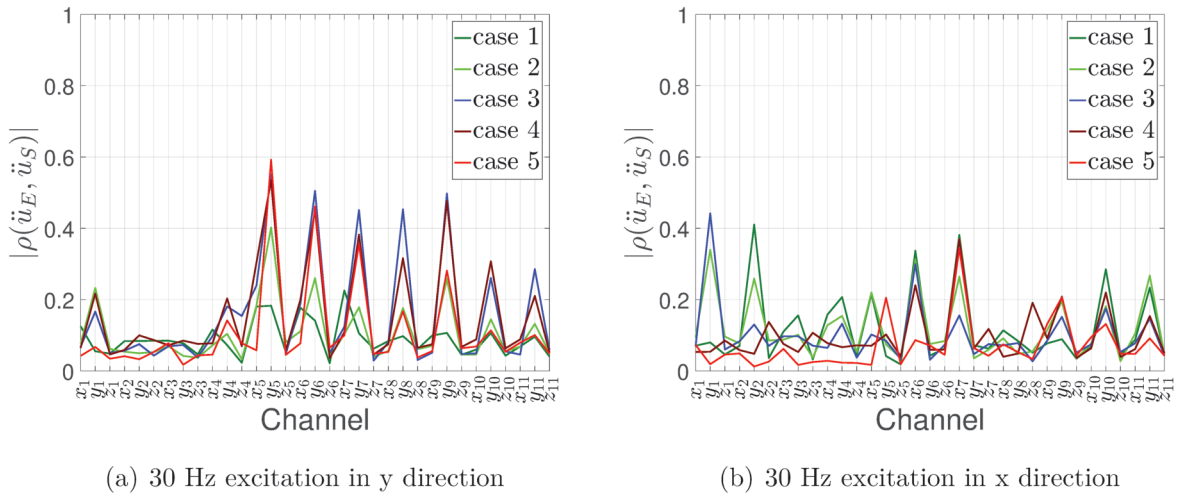
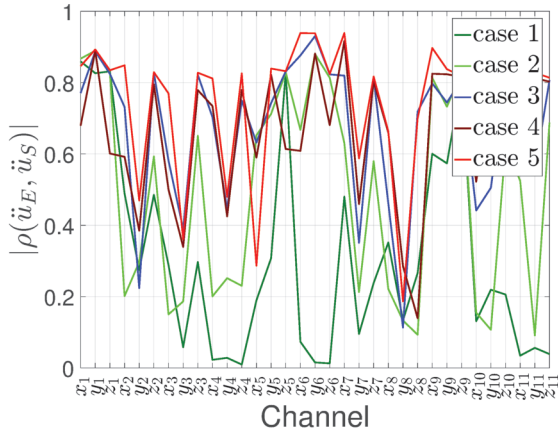


Figure 5.23: Correlation coefficient between the time histories of the computed and measured structural response for all studied damage cases under 30 Hz excitation

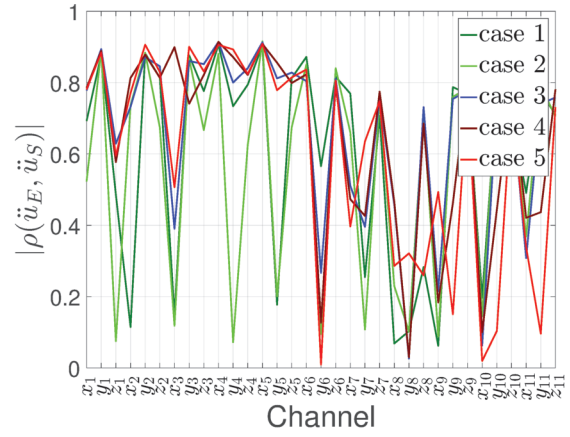
The influence of the damage size on damping was included as shown from eq. (5.10) to eq. (5.16). a_1 , a_2 , a_3 are constants that are calculated each time based on the experimental response at sensor j considering damage case 1: $\theta_1^g = 6$ mm and damage case 2: $\theta_2^g = 0$ mm, $\bar{d}_{1,j}$ and $\bar{d}_{2,j}$. For all cases $\theta_{1,2}^g = 3$ mm.

$$C_{\zeta,i,j} = f(\bar{d}_{i,j}, d_{i,j}) = \frac{\bar{d}_{i,j}}{d_{i,j}} \quad (5.9)$$

$$\forall \theta^g : \theta_1^g \leq \theta^g \leq \theta_2^g : d_{1,j}(\theta^g | \zeta_{\theta^g}) = C_{\zeta,1,j} \times d_j(\theta^g) \quad (5.10)$$

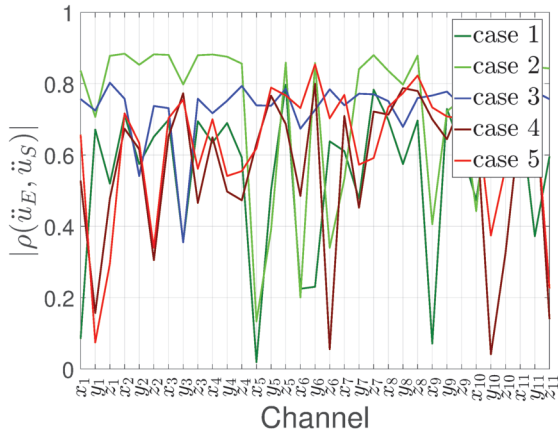


(a) 60 Hz excitation in y direction

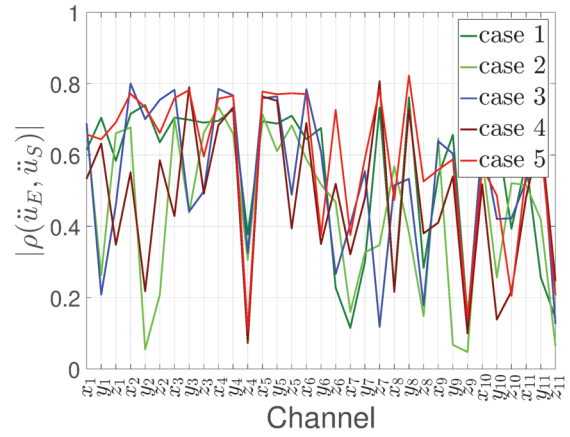


(b) 60 Hz excitation in x direction

Figure 5.24: Correlation coefficient between the time histories of the computed and measured structural response for all studied damage cases under 30 Hz excitation



(a) 170 Hz excitation in y direction

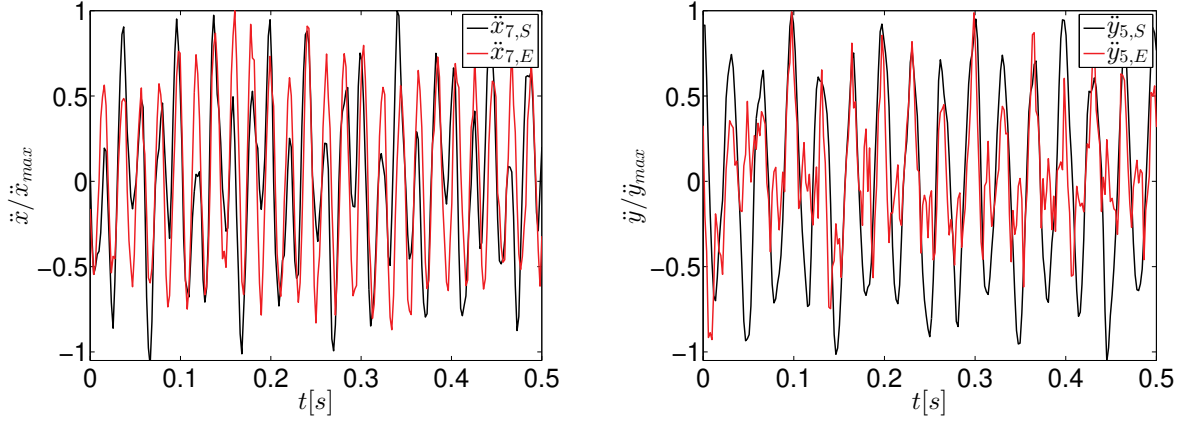


(b) 170 Hz excitation in x direction

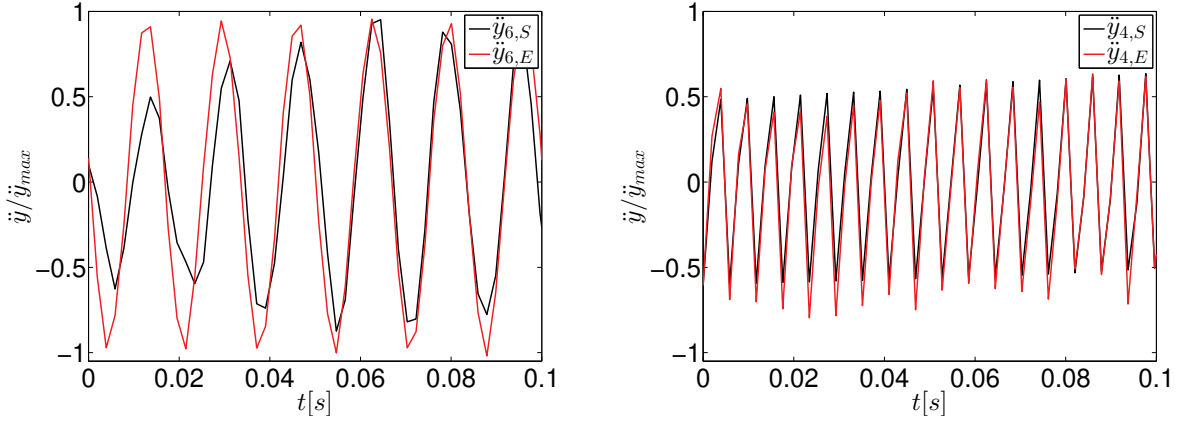
Figure 5.25: Correlation coefficient between the time histories of the computed and measured structural response for all studied damage cases under 30 Hz excitation

$$\forall \theta^g : \theta_1^g \leq \theta^g \leq \theta_2^g : d_{2,j}(\theta^g | \zeta_{\theta^g}) = \begin{bmatrix} a_1 & a_2 \end{bmatrix} \begin{bmatrix} \theta^g \\ 1 \end{bmatrix} \times d_j(\theta^g) \quad (5.11)$$

$$\begin{bmatrix} a_1 & a_2 \end{bmatrix} = \begin{bmatrix} C_{\zeta,1,j} & C_{\zeta,2,j} \end{bmatrix} \times \begin{bmatrix} \theta_1^g & \theta_2^g \\ 1 & 1 \end{bmatrix}^{-1} \quad (5.12)$$



(a) Structural response $\ddot{x}_{7,E}$ and $\ddot{x}_{7,S}$ under 20 Hz excitation applied in x direction, $\rho(\ddot{x}_{7,E}, \ddot{x}_{7,S}) > 0.4$ (b) Structural response $\ddot{y}_{5,E}$ and $\ddot{y}_{5,S}$ under 30 Hz excitation applied in y direction, $\rho(\ddot{y}_{5,E}, \ddot{y}_{5,S}) > 0.6$



(c) Structural response $\ddot{y}_{6,E}$ and $\ddot{y}_{6,S}$ under 60 Hz excitation applied in y direction, $\rho(\ddot{y}_{6,E}, \ddot{y}_{6,S}) > 0.9$ (d) Structural response $\ddot{y}_{4,E}$ and $\ddot{y}_{4,S}$ under 170 Hz excitation applied in y direction, $\rho(\ddot{y}_{4,E}, \ddot{y}_{4,S}) > 0.85$

Figure 5.26: Comparison between the simulated and measured structural response under different excitations after normalizing the amplitude to 1

$$\forall \theta^g : \theta_1^g \leq \theta^g \leq \theta_2^g : d_{3,j}(\theta^g | \zeta_{\theta^g}) = \begin{bmatrix} a_1 & a_2 & a_3 \end{bmatrix} \begin{bmatrix} \theta^{g^2} \\ \theta^g \\ 1 \end{bmatrix} \times d_j(\theta^g) \quad (5.13)$$

$$\begin{bmatrix} a_1 & a_2 & a_3 \end{bmatrix} = \begin{bmatrix} C_{\zeta,1,j} & C_{\zeta,2,j} & C_{\zeta,\Delta,j} \end{bmatrix} \times \begin{bmatrix} \theta_1^{g^2} & \theta_2^{g^2} & \theta_{1,2}^{g^2} \\ \theta_1^g & \theta_2^g & \theta_{1,2}^g \\ 1 & 1 & 1 \end{bmatrix}^{-1} \quad (5.14)$$

$$C_{\zeta,\Delta,j} = \frac{C_{\zeta,1,j} + 5 \times C_{\zeta,2,j}}{6} \quad (5.15)$$

Table 5.9: Quality of the numerical model compared to the physical model for different DOE given that d is the signal energy. Red values indicate an agreement between the response of the physical model and the numerical model considering the studied damage model

Sensor number and measured direction	$Q_V(d, \bar{d})$							
	20 Hz y	20 Hz x	30 Hz y	30 Hz x	60 Hz y	60 Hz x	170 Hz y	170 Hz x
x_1	0.00	0.15	0.00	0.70	0.76	0.80	0.00	0.00
x_2	0.11	0.09	0.00	0.89	0.77	0.84	0.00	0.00
x_3	0.36	0.00	0.00	0.60	0.65	0.92	0.00	0.00
x_4	0.00	0.76	0.00	0.18	0.71	0.82	0.00	0.00
x_5	0.00	0.00	0.00	0.00	0.46	0.84	0.00	0.27
x_6	0.00	0.25	0.00	0.00	0.30	0.47	0.00	0.61
x_7	0.00	0.00	0.00	0.00	0.44	0.00	0.00	0.00
x_8	0.00	0.00	0.81	0.00	0.64	0.48	0.00	0.00
x_9	0.32	0.84	0.00	0.57	0.66	0.55	0.00	0.00
x_{10}	0.43	0.00	0.00	0.16	0.76	0.38	0.00	0.00
x_{11}	0.04	0.18	0.00	0.16	0.78	0.67	0.00	0.00
y_1	0.62	0.00	0.00	0.00	0.11	0.49	0.00	0.00
y_2	0.00	0.06	0.00	0.00	0.11	0.50	0.00	0.00
y_3	0.17	0.00	0.00	0.00	0.59	0.46	0.00	0.00
y_4	0.00	0.00	0.00	0.00	0.76	0.75	0.00	0.00
y_5	0.94	0.00	0.79	0.00	0.89	0.09	0.00	0.25
y_6	0.77	0.00	0.96	0.00	0.74	0.56	0.00	0.00
y_7	0.17	0.00	0.00	0.30	0.83	0.17	0.00	0.00
y_8	0.03	0.00	0.00	0.10	0.72	0.95	0.95	0.13
y_9	0.76	0.00	0.93	0.00	0.86	0.85	0.00	0.00
y_{10}	0.52	0.00	0.03	0.40	0.88	0.91	0.00	0.00
y_{11}	0.80	0.84	0.00	0.87	0.89	0.91	0.00	0.00
z_1	0.01	0.32	0.02	0.00	0.72	0.77	0.00	0.00
z_2	0.00	0.21	0.59	0.33	0.77	0.74	0.00	0.00
z_3	0.02	0.35	0.48	0.02	0.77	0.72	0.00	0.19
z_4	0.24	0.56	0.00	0.37	0.77	0.86	0.00	0.00
z_5	0.00	0.00	0.00	0.19	0.74	0.71	0.00	0.00
z_6	0.00	0.00	0.21	0.00	0.77	0.75	0.00	0.58
z_7	0.00	0.00	0.46	0.18	0.76	0.71	0.00	0.00
z_8	0.00	0.00	0.20	0.20	0.68	0.67	0.00	0.00
z_9	0.00	0.22	0.00	0.00	0.72	0.86	0.00	0.37
z_{10}	0.00	0.47	0.00	0.00	0.78	0.88	0.00	0.00
z_{11}	0.20	0.08	0.65	0.00	0.76	0.90	0.00	0.00
Q_V	0.20	0.16	0.19	0.19	0.68	0.67	0.03	0.07

$$C_{\zeta,\Delta,j} = \frac{5 \times C_{\zeta,1,j} + C_{\zeta,2,j}}{6} \quad (5.16)$$

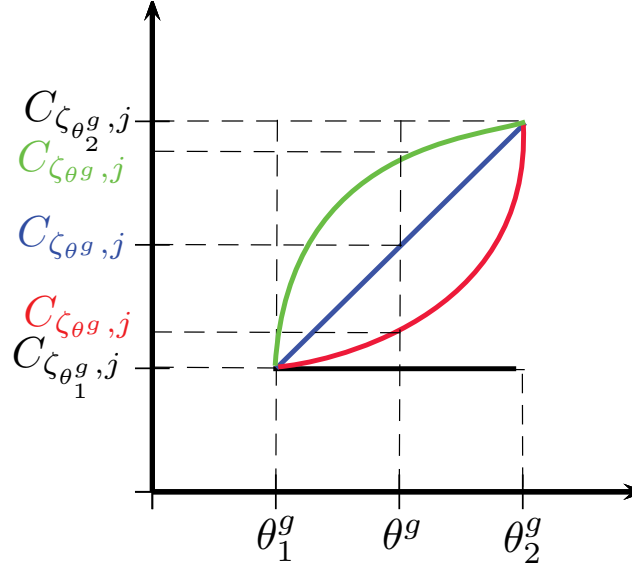


Figure 5.27: Empirical damping models illustrate the influence of damage on the damping of the structural response of the studied frame

5.1.6 Design of Experiments

The cumulative signal energy d of the acceleration time histories $[\ddot{u}(t)] = [\ddot{x}(t), \ddot{y}(t), \ddot{z}(t)]$ were used as an output structural response to detect damage. It was possible to measure the mass of the cubes and the hinges of the studied frame. Therefore, the variation of the structural response due to masses' uncertainty was omitted.

In this example, the uncertainty in the elastic modulus of the cubes E_c , hinges E_h and thickness of the stiffening elements h_s were considered, table 5.10. The studied uncertainty was introduced in the numerical model by assigning probabilistic models to the chosen parameters based on the uniform distribution.

The minimum energy of noise signal d_γ due to ambient vibration was assumed to be $0.3 \times d_{t,min}$ since the tests results show that the forced response is small compared to the response of the structure under ambient vibration γ_F especially for low frequency excitations (20 and 30 Hz), figure 5.10 . As a result, $\bar{d} = d_{t,min} - d_\gamma$. Uncertainty ϵ due to instrumentation, initial conditions and sensor quality was considered as a normally distributed uncertainty with zero mean and standard deviation $\sigma_\epsilon = 0.1\bar{d}$, eq. (5.17). In this case, σ_ϵ was assumed. However, larger value can be chosen if more factors may influence the response.

$$\epsilon \sim \mathcal{N}(0, \sigma_\epsilon^2) \quad (5.17)$$

Table 5.10: Mean values $\{\mu\}$, minimum and maximum values of the studied parameters $\{\theta\}$ and their coefficients of variation COV

	E_c MPa	E_h MPa	h_s mm
μ	1.790×10^5	1.770×10^5	6
Max	2.2504×10^5	2.2253×10^5	8.6
Min	1.3296×10^5	1.3147×10^5	3.40
COV	0.15	0.15	0.25

Table 5.11: Chosen design of experiments models to detect the studied damage θ^g

Model	f_F Hz	Setups	direction of F
DOE_1	20	1	y
DOE_2	20	1 \cap 2 \cap 3	y
DOE_3	30	1 \cap 2 \cap 3	y
DOE_4	20	1 \cap 2 \cap 3	x
DOE_5	30	1 \cap 2 \cap 3	x
DOE_6	170	1 \cap 2 \cap 3	x

The reliability of the inspection method was evaluated assuming that the design of experimental models in table 5.11, were chosen separately based on the experimental results.

A Latin hypercube sampling method was used to generate $N = 100$ samples to investigate the variation of the response d due to the input parameters $\{\theta\}$. The size of the sample was chosen as a trade off between the computational time and quality of the Meta-models that were developed in the next step to solve more samples. The structural response $[\ddot{u}(t)] = [\ddot{x}(t), \ddot{y}(t), \ddot{z}(t)]$ for damage case 1 ($\theta^g = 0$) under each excitation shown in table 5.11 was computed for each sample. The cumulative signal energy values $\{d\}$ of the acceleration time histories $\ddot{u}(t)$ were computed based on eq. (5.3). For all samples, the initial conditions $u(0) = \dot{u}(0) = 0$ and a constant excitation amplitude were applied.

5.1.7 Sensitivity analysis

The sensitivity analysis method described in section 3.4 was used to obtain information about the contribution of $\{\theta\}$ to the outputs $\{d\}$. Meta-models $\{\underline{d}\}$ were developed to perform the sensitivity analysis. The data sets which include 100 samples calculated in the previous subsection were used. The statistical properties of the residuals were examined to ensure that they satisfy the requirements described in section 3.4.4. The Total-effect index sT values were calculated using $[d]$ for all chosen design of experiments models given in table 5.11. Figure 5.28

shows the results of the applied sensitivity analysis. The Total-effect index sT values show that the studied structural response is not sensitive to the elastic modulus of the hinge, E_h which means false alarm due to E_h is not expected. Moreover, the results indicate that the response is sensitive to E_c . The variation of the thickness h_s influences the structural response recorded in the z -direction (channels 21 to 33). Based on eq.(5.18), the quality of the DOE models can be obtained, table 5.12. The results show that the variation of E_c can produce a false alarm. Therefore, including the damage patterns is important to avoid false alarm.

$$Q_{DOE} = \frac{sT(h_s)}{sT(E_c, E_h, h_s)} \quad (5.18)$$

5.1.8 Model updating

Meta-models $\{\hat{d}\} = f(\{\hat{\theta}\})$ were developed for model updating. In this example, all of the inputs were considered to be important $\{\hat{\theta}\} \equiv \{\theta\}$. The statistical properties of the prior density functions of the input parameters are given in table 5.10. Applying the Bayesian updating approach explained before in section 3.5, the posterior density functions $p(\{\theta\}|\{\bar{d}\})$ of the parameters were computed for each DOE model, figures 5.29 – 5.34. The statistical properties of the posterior density functions of the input parameters for each DOE model are presented in tables 5.13.

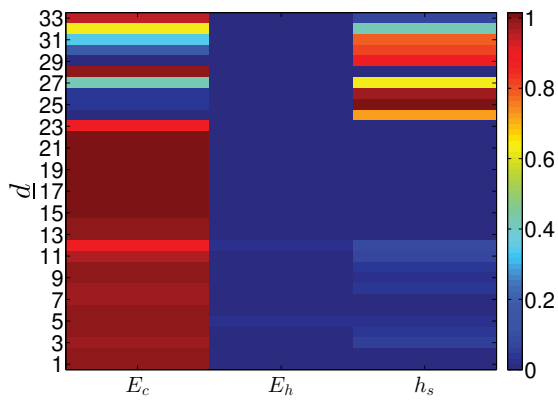
To evaluate the quality of the measurements for each design of experiment model given in table 5.11, the index Q_M given in eq. (3.47) was computed, table 5.14. The results show that although the low design of experiments quality values $Q_{DOE} < 30\%$ were obtained, it was possible to obtain $Q_M > 70\%$. This can be explained by the small number of the considered parameters $N_\theta = 3$.

5.1.9 Assessment of the inspection method

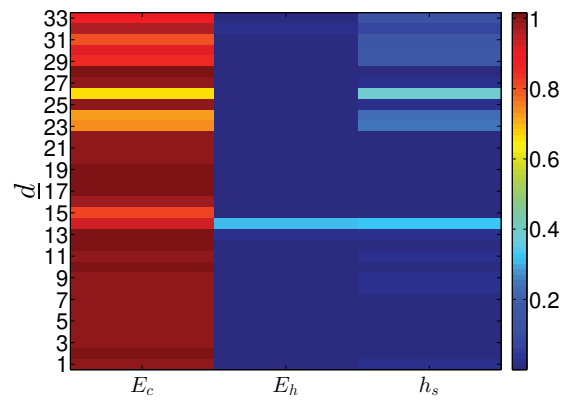
The developed method in section 3.6.2 was applied. The damage size $\theta_i^g \in [0-40\%] \times 6$ mm was used to calculate the response $d_i(\theta_i^g)$ with an interval $\Delta\theta^g = 0.015\% \times 6$ mm. The increment of the damage size from θ_1^g to θ_2^g included the possible influence of damping due to damage

Table 5.12: The quality of the chosen design of experiments models to detect the studied damage θ^g

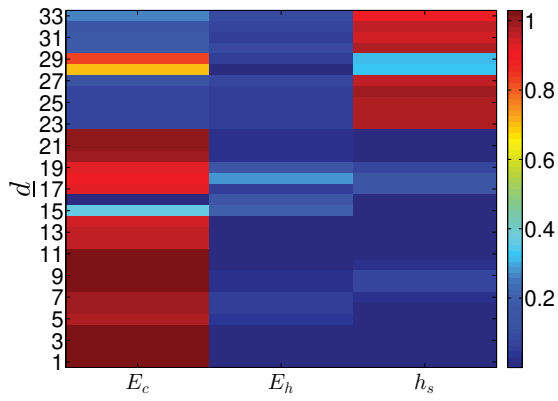
	DOE_1	DOE_2	DOE_3	DOE_4	DOE_5	DOE_6
Q_{DOE}	22 %	23 %	7 %	28 %	25 %	8 %



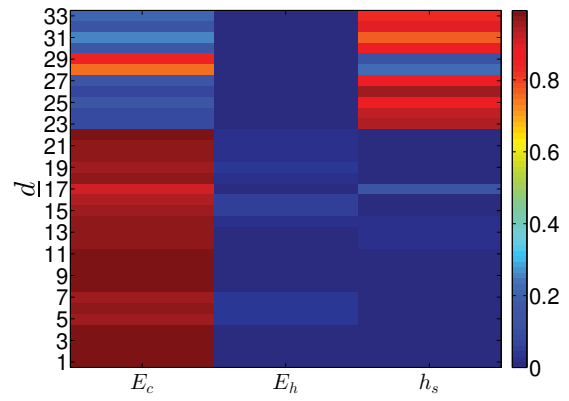
(a) 20 Hz excitation in y direction (DOE_1 and DOE_2)



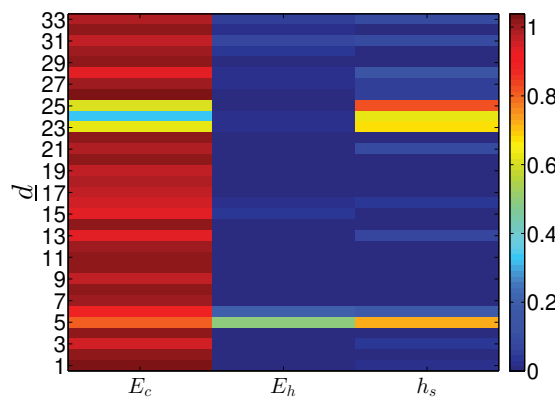
(b) 30 Hz excitation in y direction (DOE_3)



(c) 20 Hz excitation in x direction (DOE_4)



(d) 30 Hz excitation in x direction (DOE_5)



(e) 170 Hz excitation in x direction (DOE_6)

Figure 5.28: Total-effect index $sT_{i,j}$ calculated for all chosen design of experiments models given in table 5.11. Channel numbers from 1 to 11 are in x direction, 12 to 22 are in y direction and 23 to 33 are in z direction, table 5.6.

Table 5.13: The statistical properties of the posterior density functions of the input parameters

	DOE_1			DOE_2		
	E_c MPa	E_h MPa	h_s mm	E_c MPa	E_h MPa	h_s mm
μ	177991.6	173334	6.8	178676.3	154054.6	6.5
σ	1125.2	13205.4	0.24	803.4	10429	0.15
	DOE_3			DOE_4		
	E_c MPa	E_h MPa	h_s mm	E_c MPa	E_h MPa	h_s mm
μ	180987.8	176324	6	180122.8	193526.7	5.8
σ	737	9930.5	0.24	824.3	5318.2	0.047
	DOE_5			DOE_6		
	E_c MPa	E_h MPa	h_s mm	E_c MPa	E_h MPa	h_s mm
μ	179778.31	180408.5	5.72	179817.71	179123.7	5.98
σ	594.7	4015.4	0.049	384.1	4048.93	0.10

Table 5.14: The quality of the chosen measurements to detect the studied damage θ^g

	DOE_1	DOE_2	DOE_3	DOE_4	DOE_5	DOE_6
Q_M	76 %	82 %	81 %	91 %	93 %	92 %

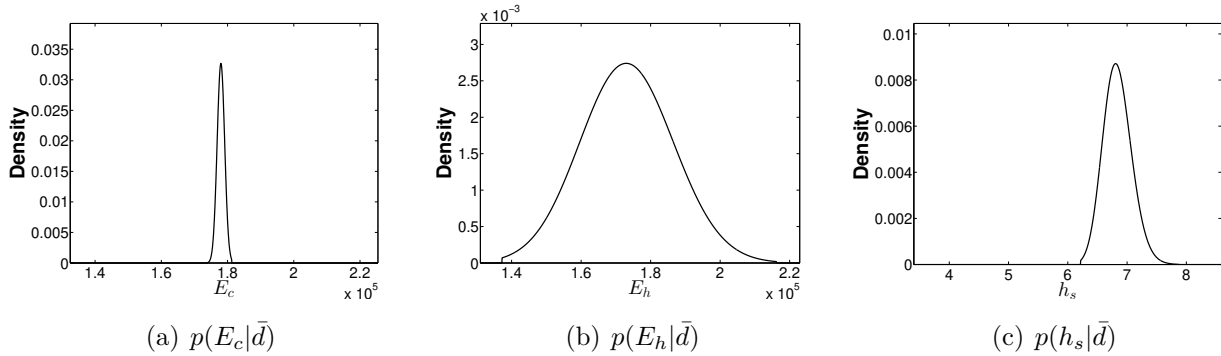


Figure 5.29: Posterior density functions of the updated input parameters using $\{\bar{d}|DOE_1\}$

presented in eq. (5.9), eq. (5.10), eq. (5.11) and eq. (5.13). In other words, damage was introduced in the model G_M by reducing h_s as follows:

$$\forall \theta_{\Delta hi}^g, \theta_{\Delta hi+1}^g : \theta_{\Delta hi+1}^g = \theta_{\Delta hi}^g + \Delta \theta^g \Rightarrow h_{s,\Delta hi+1} = h_{s,\Delta hi} - 0.015 \times 6 [\text{mm}] + \epsilon_{h_s|\bar{d}} \quad (5.19)$$

where $h_{s,\Delta hi}$ refers to the thickness of the stiffening element after reducing it by $hi \times \Delta \theta^g$, $hi = 1, 2, \dots$. $\epsilon_{h_s|\bar{d}} \sim \mathcal{N}(0, \sigma_{\epsilon_{h_s|\bar{d}}}^2)$ refers to the remained uncertainty represented by the standard

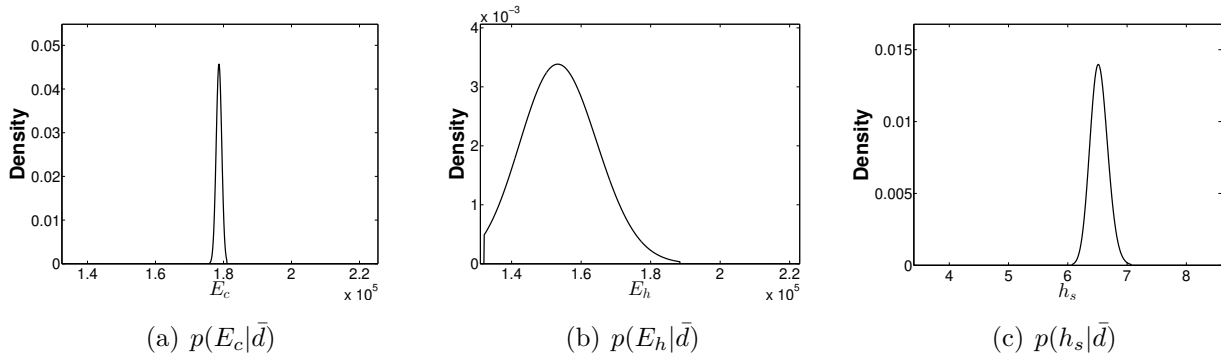


Figure 5.30: Posterior density functions of the updated input parameters using $\{\bar{d}|DOE_2\}$

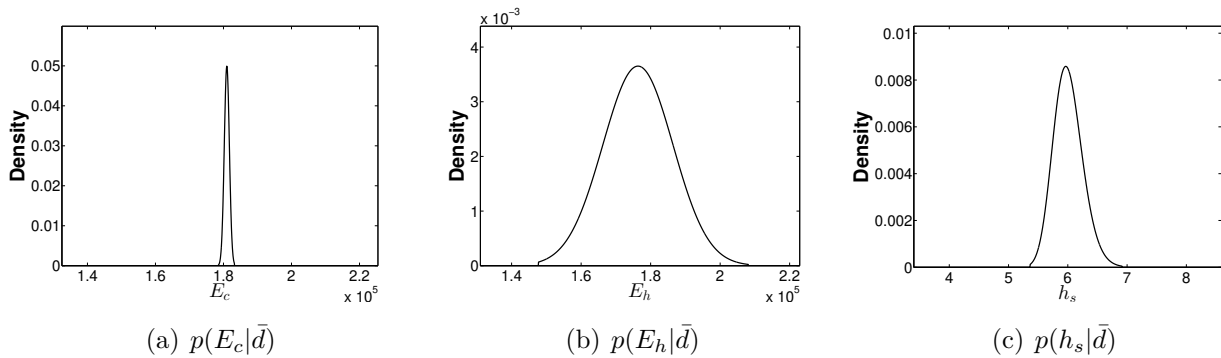


Figure 5.31: Posterior density functions of the updated input parameters using $\{\bar{d}|DOE_3\}$

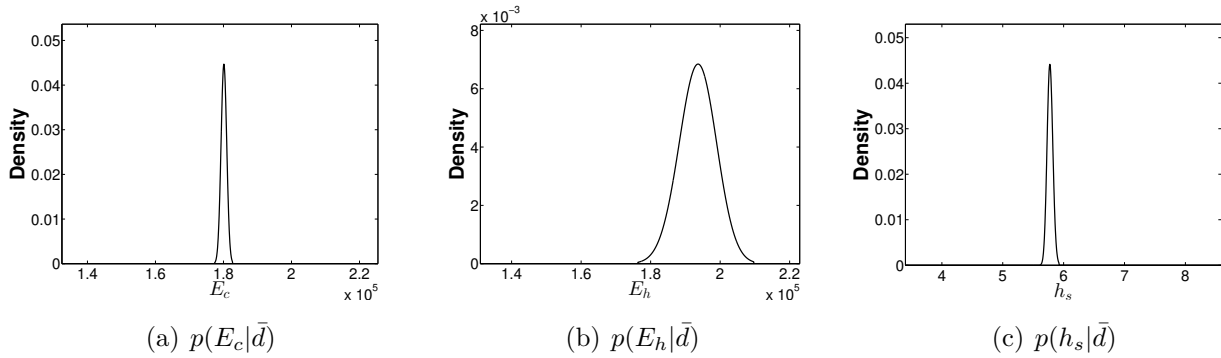


Figure 5.32: Posterior density functions of the updated input parameters using $\{\bar{d}|DOE_4\}$

deviation of the value of the h_s after model updating, table 5.13. The model updating results shown in figures 5.29 (c) – 5.34 (c) show that the posterior density functions $p(h_s|\bar{d})$ have a distribution shape close to the normal distribution. $\sigma_{\epsilon_{h_s|\bar{d}}}$ values for each DOE model are given in table 5.13. The computed response $d(\theta_{\Delta hi}^g)$ was modified as shown in eq. (5.9) – (5.13) to include the damping effect.

Based on eq. (3.63), if PFP=0.05 and for n=33 output (channels), $N = 643$. The number of samples for each damage step $\Delta\theta^g$ was increased until the value of $POD(\theta_i^g)$ converged. The

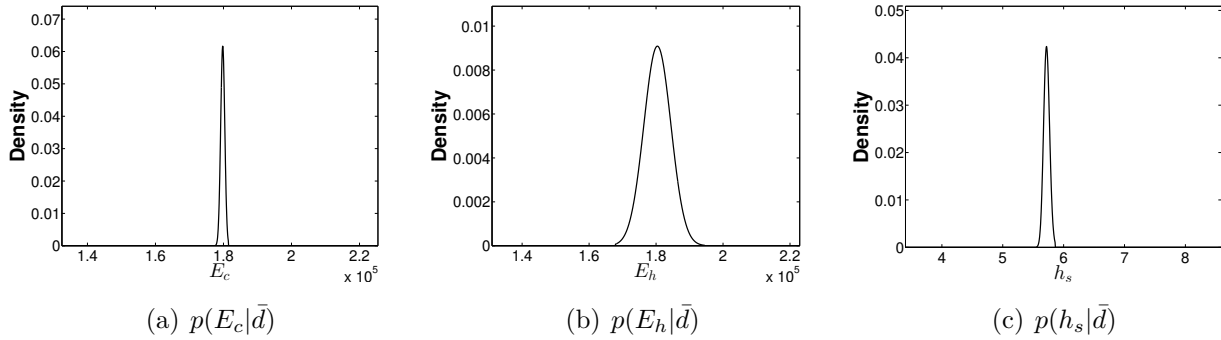


Figure 5.33: Posterior density functions of the updated input parameters using $\{\bar{d}|DOE_5\}$

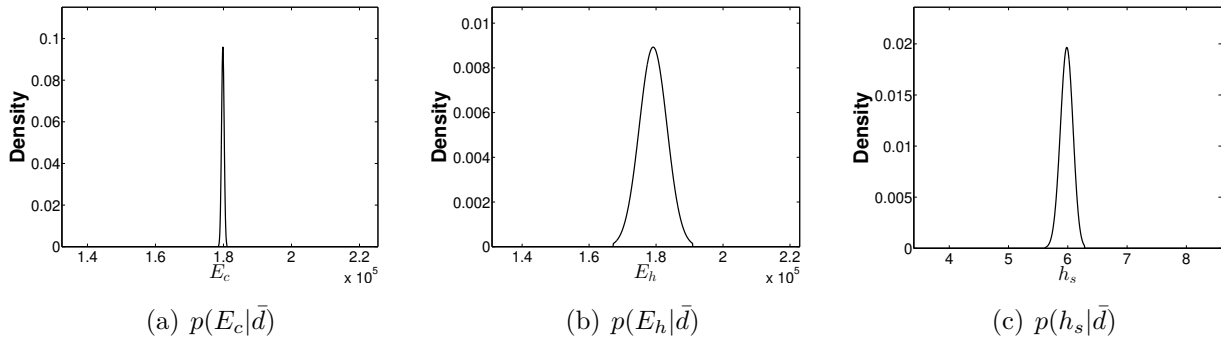
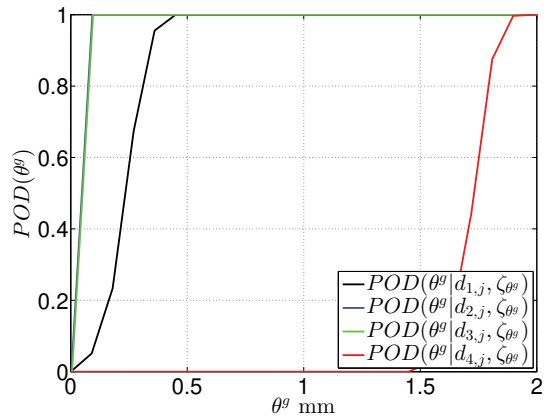


Figure 5.34: Posterior density functions of the updated input parameters using $\{\bar{d}|DOE_6\}$

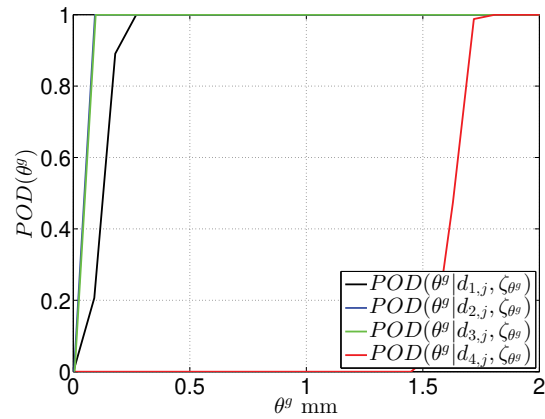
investigation shows that $N = 1000$ samples for each damage step are sufficient to obtain the convergence of the POD curves.

Damage patterns introduced in section 4.6.2 were considered when the POD was calculated. The threshold $d_{c,j}$ values were chosen $PFP_i = POD(\theta^g|\theta^g = 0, d_j) \leq 0.05$ for each response d_j in each direction x, y and $z, j = 1, 2, \dots, 11$ is the number of the sensor. It means that if there was no damage, only 5% of the indicator values $d_j(\theta^g)$ exceeds $d_{c,j}$ and produce false alarm. As a result, eq. (3.55) can be used to select the threshold value for each response that satisfy the PFP condition. Based on eq. (3.59) and the chosen threshold values, the POD curves can be computed for each DOE model, figure 5.35.

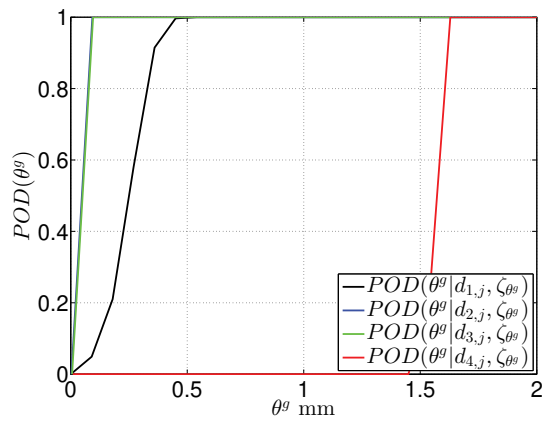
Table 5.15 shows the damage sizes θ^g that satisfy the condition given in eq. (5.2). The results show that the chosen inspection method is reliable for detecting the studied damage. However, the influence of the damping model due to damage on the minimum damage size that can not be missed ($POD(\theta_{\Delta hi+1}^g \geq \theta_{\Delta hi}^g) = 100\%, POD(\theta_{\Delta hi-1}^g < \theta_{\Delta hi}^g) < 100\%$) should be considered. If increasing damage causes that damping changes rapidly as shown in eq. (5.15), damage can be detected early as figure 5.35 (green line) shows. If increasing damage causes that damping changes slowly as shown in eq. (5.16), damage can be detected late as figure 5.35 (red line) shows.



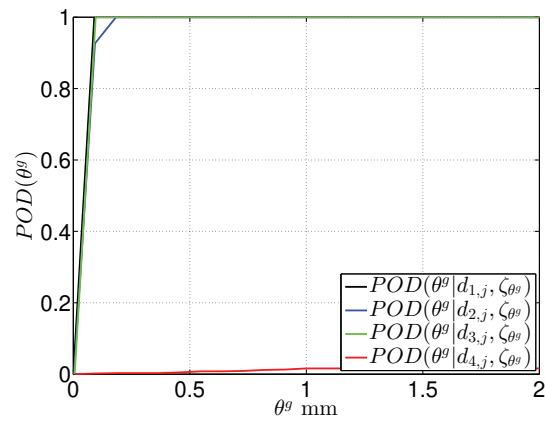
(a) $POD(\theta^g)$ curves using DOE_1



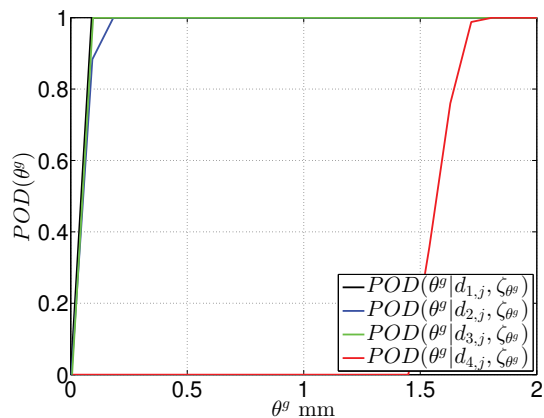
(b) $POD(\theta^g)$ curves using DOE_2



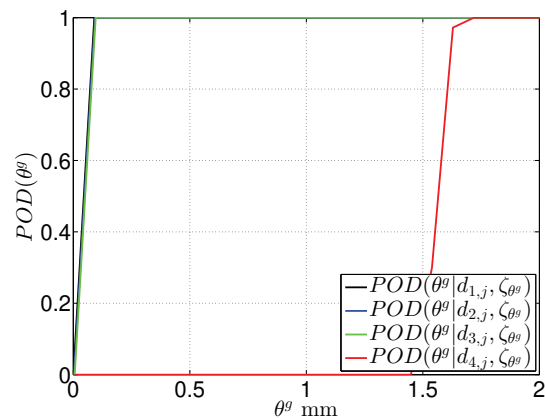
(c) $POD(\theta^g)$ curves using DOE_3



(d) $POD(\theta^g)$ curves using DOE_4



(e) $POD(\theta^g)$ curves using DOE_5



(f) $POD(\theta^g)$ curves using DOE_6

Figure 5.35: Probability of damage detection of the studied damage type using different designs of experiment and different damping models. The sensors of each DOE are defined in the tables 5.1 and 5.11.

5.1.10 Conclusion

In this example, the performance of a vibration-based inspection method to detect damage in a single-span-one-story steel frame structure was tested. Different design of experiments were considered. The following results can be pointed out:

- The reliability of the inspection method depends on the chosen design of experiments including the excitation properties, the number of the sensors and the location of the sensors.
- If an agreement is obtained between the structural response calculated using the developed numerical model and the structural response measured using the physical model before considering damage, it is not necessary that this agreement would remain after considering damage. Therefore, the quality of the numerical model should be evaluated after considering damage to ensure an accurate evaluation of the chosen inspection method.
- The reliability of the inspection method depends on the developed damage model.
- Increasing the complexity of the model by considering important phenomena to obtain better results can be prevented if the appropriate design of the experiment, which brings a structural response that is not sensitive to those complex phenomena, is used.

5.2 Cantilever

5.2.1 Introduction

The performance of a vibration-based inspection method for damage detection is evaluated considering two different numerical models. The studied example is a cantilever with an extension that includes two rubber bands and two suspended weights. The influence of the cable on the studied structural response of the cantilever is investigated.

The experimental models of the studied structure and damage, the test setups and the modal parameters obtained from experiments are presented. The numerical models are used to perform a statistical study and to evaluate the performance of the chosen inspection method through the probability of damage detection curves.

5.2.2 Problem definition and test setup

In this example the studied structure is a cantilever, figure 5.36. The cantilever is 3 m high measured from the top of its concrete foundation. The cross-section of the cantilever is a hollow circle which has 110 mm outer diameter and 3.2 mm wall thickness, figure 5.37. Since this type of systems is usually used as water pipes, the outer diameter of the last 66 mm of the upper part of the pipe is 15 mm wider for a possible connection to other pipes. A 90 liter mortar bucket filled with concrete was used as a foundation for the structure. The foundation has a truncated cone shape with a 35 cm height and 60 cm diameter at the top. The foundation was constructed to provide a fixed support condition for the cantilever. The cantilever was made of Polyvinyl chloride (PVC). The material properties are provided by the manufacturer. The density is $\rho = 1.39$ to 1.40 g/cm³, the Modulus of elasticity is $E \geq 3000$ N/mm² and the Poisson ratio $\nu = 0.4$.

The dynamic response of the studied structure was measured using five -3 axial- accelerometers. The sampling frequency was chosen as $\Delta f = 4096$ Hz. The accelerometers were fixed to the pipe using steel rings and magnets, figure 5.36. They were placed at 1, 1.5, 2, 2.5 and 2.96 m measuring from the top of the foundation. The system was excited using impulse forces which were applied at 2.04 m measured from the top of the foundation. The impulse was created by using a simple single degree of freedom system which contains a wooden mass fixed to the end of a thin aluminum beam, figure 5.38. The wooden mass was shifted each time within a certain distance and then released to hit the pipe where the force sensor was placed to measure the input excitation. Such excitation system provided relatively controlled input force amplitudes and frequency range, figure 5.40.

Since the cantilever is light, a large force amplitude can lead to large displacements causing geometrically nonlinear behavior. The mass of the sensors especially at the top of the cantilever

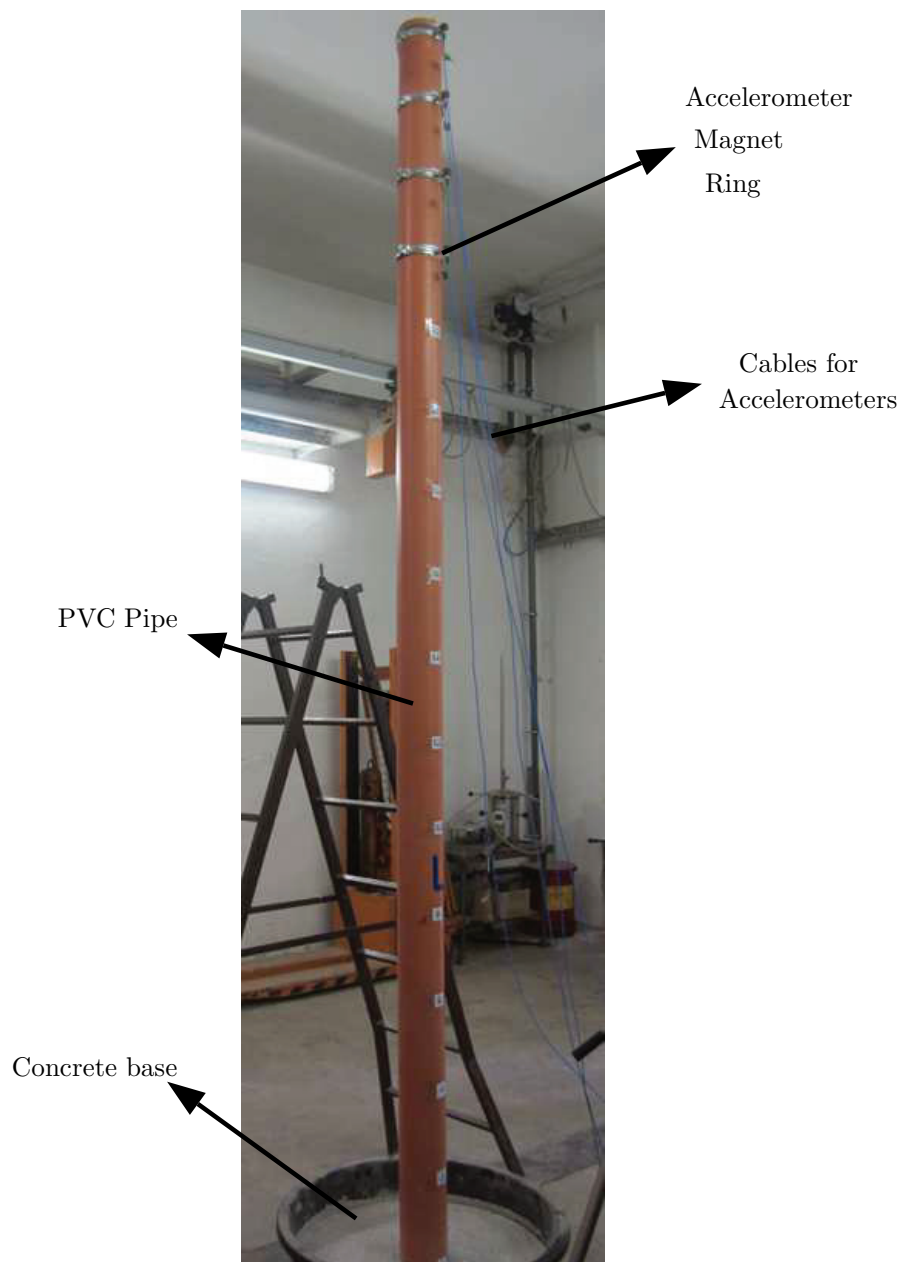


Figure 5.36: Studied PVC cantilever

can influence the response of the structure. In each modal test, the structure was excited using at least 10 impulses. After applying an impulse, sufficient time was kept to let the structural response to decay to the static state before applying the next impulse. As a result, the interaction between the cantilever and the excitation system was prevented. Since the surrounding environment conditions (temperature, humidity, etc.) of the laboratory were constant during the test, their influence was omitted.

To investigate the influence of changing the support conditions on the structure, an extension was developed and added to the original cantilever. Two rubber bands were fixed to the steel ring which was used to place the sensor at the top. The rubber bands were passed through

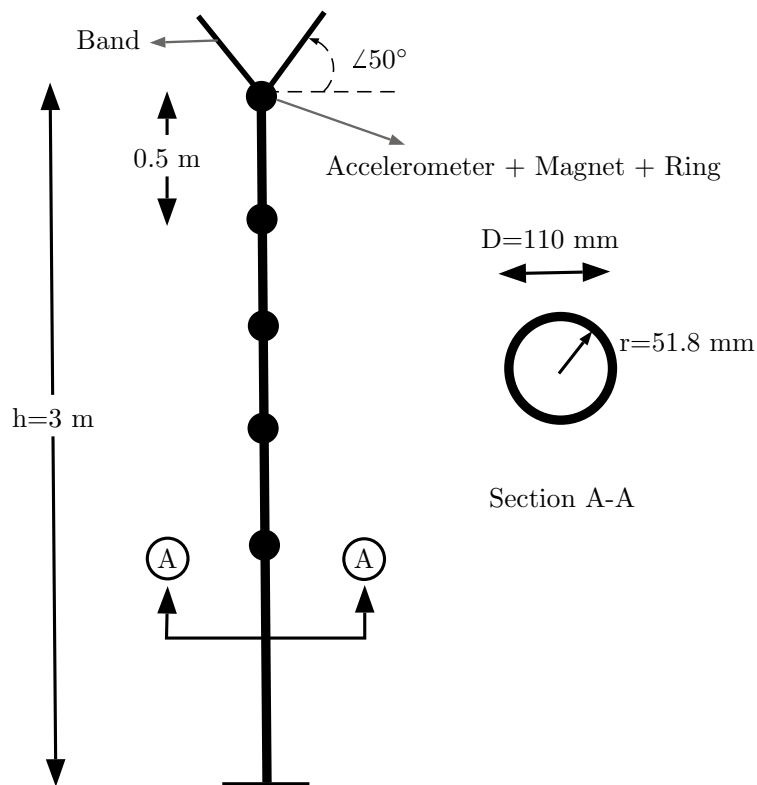


Figure 5.37: Test setup of the studied PVC cantilever of the dynamic modal test

guide rollers fixed to the ceiling. Two weights were suspended at the second ends of the bands to generate pretension forces, figure 5.39. The distance between each weight to the cantilever was adjusted to keep the total system symmetric as much as possible, figure 5.38. Each of the adjustable weights has a maximum mass of 1.5 kg. The no damage case was considered if both weights were at their maximum which provide tension forces at the end of the cantilever. Damage was developed by reducing the masses on both sides equally. Four damage cases were studied:

- Case 1: both masses 1.5 kg $\iff \theta_1^g = 0 \text{ kg}$ (no damage)
- Case 2: both masses 1.0 kg $\iff \theta_2^g = 0.5 \text{ kg}$
- Case 3: both masses 0.5 kg $\iff \theta_3^g = 1 \text{ kg}$
- Case 4: cables released $\iff \theta_4^g = 1.5 \text{ kg}$ (maximum damage)

At first, the test was performed without adding any weight to both ends of the bands. In the second step, 0.5 kg was added to both ends of the bands, and then the test was performed again. After that, the weight was increased to 1 kg and at the end to 1.5 kg. According to the orientation of the accelerometers, the coordinate system was defined as follows: x: vertical, y: horizontal perpendicular to the impulse excitation axis and z: horizontal in the same direction of the excitation force.

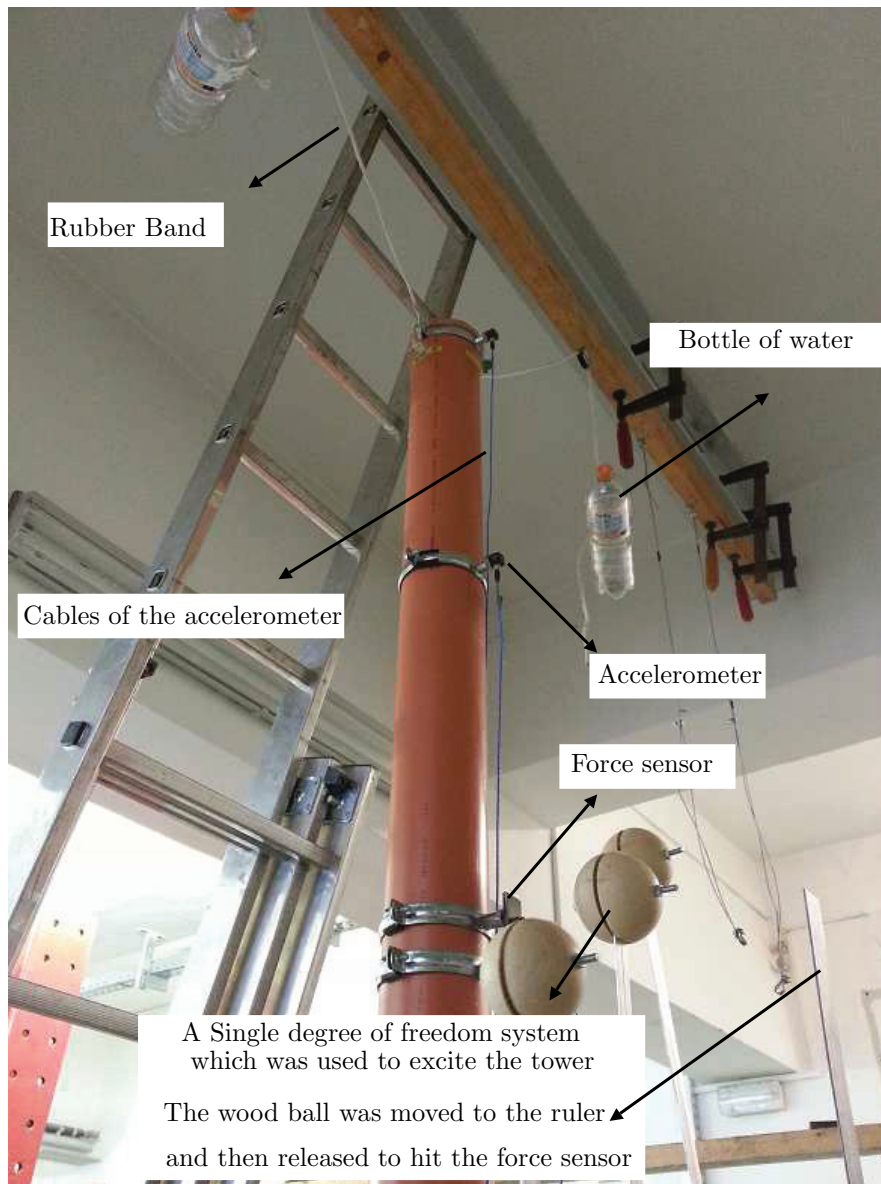


Figure 5.38: Introducing damage model in the studied PVC structure

The main goal was to obtain the minimum damage size that can not be missed:

$$\begin{aligned}
 H_o : \forall \theta^g : \theta^g \in [\theta_1^g, \theta_4^g] \Rightarrow POD(\theta^g + \Delta\theta^g) = 1, POD(\theta^g - \Delta\theta^g) < 1, PFP \leq 0.01 \\
 H_1 : \text{The inspection method is not reliable}
 \end{aligned} \tag{5.20}$$

5.2.3 Test results

A modal test was conducted using impulse excitations which have similar properties due to the excitation procedure introduced in the previous section, figure 5.38. The goal was to obtain the variation of the dynamic response of the cantilever due to the introduced damage. Figure 5.42

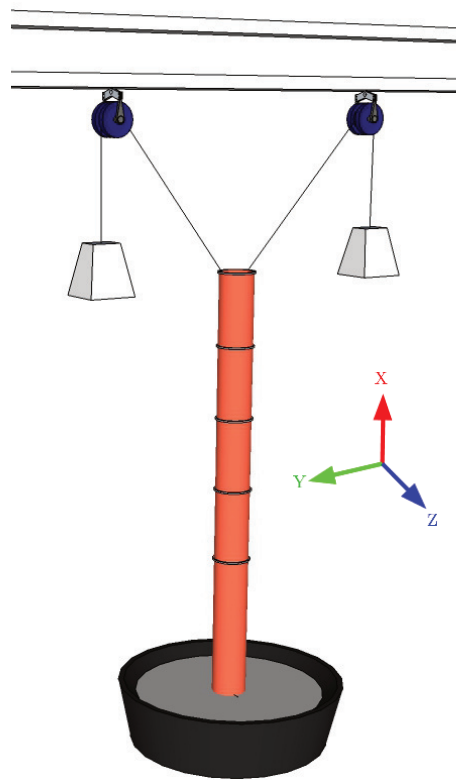


Figure 5.39: A sketch of damage modeling in the physical model

shows an example of the structural response at the top of the cantilever for case 1 under an impulse excitation presented in figure 5.41. Table 5.17 shows that the influence of the chosen damage on the extracted natural frequencies $\{f_{n,E}\}$ and damping ratios $\{\zeta_E\}$ is not significant.

Figures 5.44, 5.45 and 5.46 present the first 6 mode shapes extracted from measurements and scaled to unit modal displacement for all damage cases under the applied excitations. The mode shapes were obtained by applying the SSI method following the similar procedure explained in appendix C. The results show that the studied damage type influences the first two mode shapes significantly compared to the higher order modes. It was observed that when the weights at both sides reduced from the first damage case to the third damage case, the inclination of the first mode shape to z-axis decreases and similarly the inclination of the second mode shape to y-axis decreases. When the weights were completely removed (fourth damage case), the inclinations of the first two mode shapes to the axis y and z were between the second and the third damage cases. The MAC values between damage case 1 and other damage cases, figure 5.47, do not present changes due to damage. It is important to mention that the band reached its maximum elongation for damage case 1, 2 and 3.

There are many reasons that can lead to the observed results related to the first two mode shapes:

- Table 5.17 shows that the frequencies of modes 1 and 2 which have similar shapes are

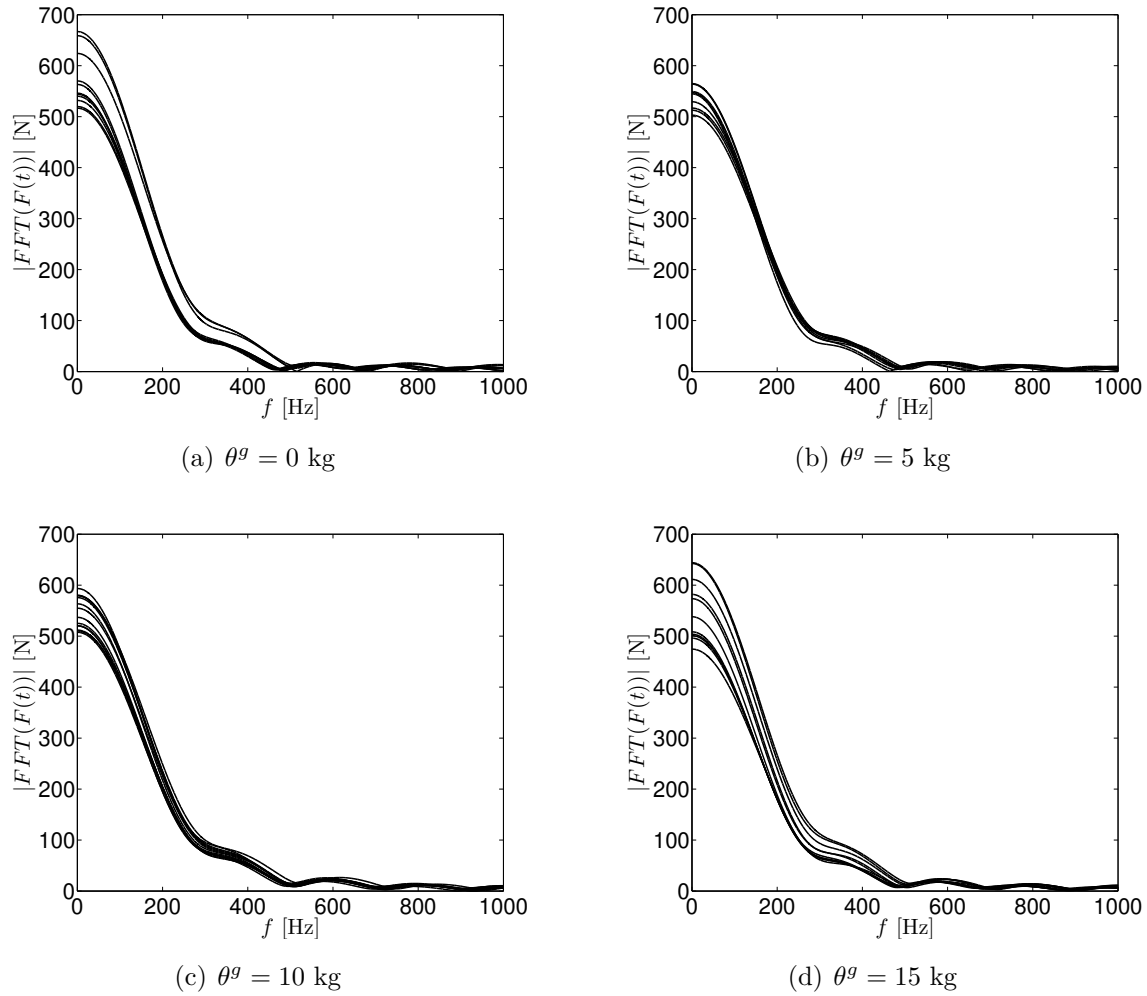
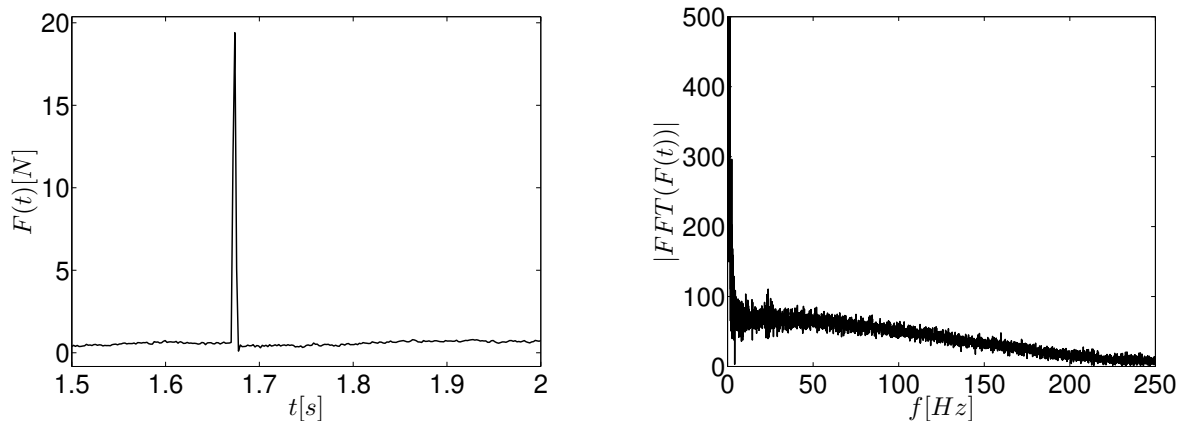


Figure 5.40: $|FFT|$ of input excitations in all studied damage cases

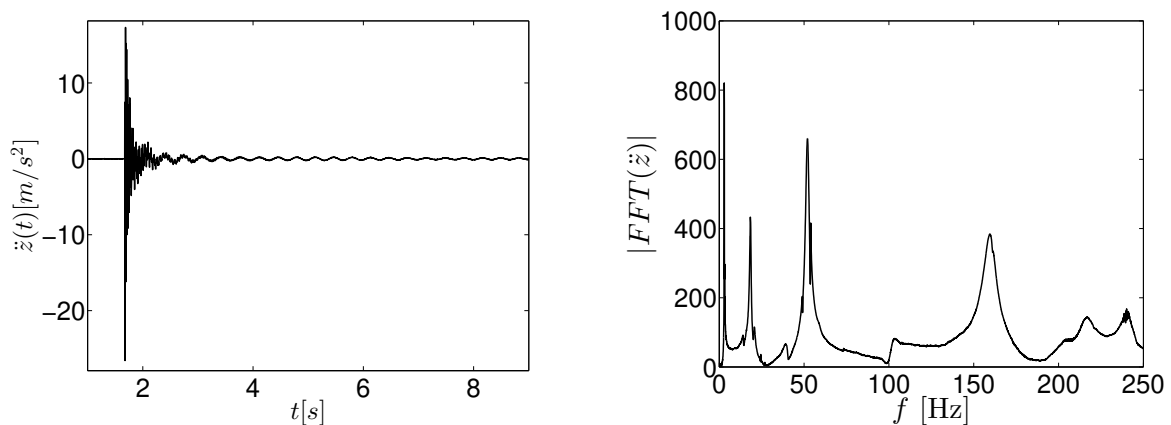
Table 5.17: Natural frequencies and damping ratios extracted from measurements for the studied damage cases

		1	2	3	4	5	6
Case 1	f Hz	2,97	3.23	18.41	20.64	51.57	52.07
	$\zeta\%$	1.34	2.57	2.43	2.07	1.54	1.67
Case 2	f Hz	2.93	3.18	18.23	20.72	51.5	52.10
	$\zeta\%$	1.45	2.71	2.10	2.83	1.79	1.98
Case 3	f Hz	2.90	3.40	18.42	20.81	51.38	52.09
	$\zeta\%$	1.50	3.77	2.36	2.47	1.75	2.16
Case 4	f Hz	2.83	3.11	18.44	20.72	51.50	52.15
	$\zeta\%$	1.40	3.99	2.44	2.21	1.79	2.08



(a) An example of the time history of a used excitation force
 (b) $|FFT|$ shows the frequency range of a used excitation force

Figure 5.41: Time histories and $|FFT|$ of an input excitation



(a) Time history of the acceleration measured at the top of the cantilever
 (b) $|FFT|$ shows the response of the structure in frequency domain

Figure 5.42: Structural response at the top of the cantilever under the excitation in figure 5.41, case 1

different. This difference indicates that the studied cantilever is asymmetric even if both weights are not added. Therefore, it is possible that if the weights were added, the structure could be shifted in the y -direction to one side more than the other side. Since the excitation system was not readjusted to consider this shifting, the excitation force may not be entirely applied in z -direction but also in the y -direction, figure 5.43.

- Another effect is the different friction factors of both rollers. This difference can lead to different forces in both bands. As a result, the asymmetry of the system increases by increasing the weights at both sides.

- The uncertainty in the angles between the bands' axes and the cantilever vertical axis (x-direction) can lead to an asymmetrical system. The asymmetry of the system increases by increasing the weights at both sides.

The signal energy \bar{d}_t of the recorded acceleration signals was calculated for each applied impulse and for each damage case in y and z direction based on eq. (3.5). In the next step, \bar{d}_t was normalized to the signal energy of the impulse force d_F which was calculated following the same procedure for calculating \bar{d}_t , figure 5.48 and 5.49. The results show that although the excitation force was applied in z direction, the values of the signal energy in y direction $\bar{d}_t(y)$ in many cases are more than 70% of the signal energy values in z direction $\bar{d}_t(z)$, $\bar{d}_t(y) \geq 0.7\bar{d}_t(z)$. The asymmetry of the system explained before can be the reason of obtaining these results.

In order to compare the values of signal energy for all damage cases, two methods were applied. The first is comparing the mean values, eq. (5.21), figure 5.50 and the second is to select similar impulse excitations, figure 5.51, for all damage cases and then to compare the signal energies caused by those excitations, figure 5.52.

If $i = 1, 2, 3, 4$ is the studied damage case and $j = 1, 2, \dots, n$ is the number of the applied excitations and n is the total number of excitations applied in damage case i , the mean value of the normalized signal energy $\bar{d}_{t,i}$ for damage case i can be calculated as follows:

$$\forall i, j : \bar{d}_{t,i} = \frac{\sum_{j=1}^n \bar{d}_{t,i,j}}{n} \quad (5.21)$$

Both methods show similar results for damage cases 1, 2 and 3. The difference was observed for damage case 4, figure 5.50. Moreover, the second method, where the impulses are similar, shows that the variation between the energy values due to the studied damage cases is more significant than the variation of the mean values of the energy due to the same studied damage cases. Since decreasing the weights increases the energy of the recorded signals, these bands and weight combination system may behave as dampers as well.

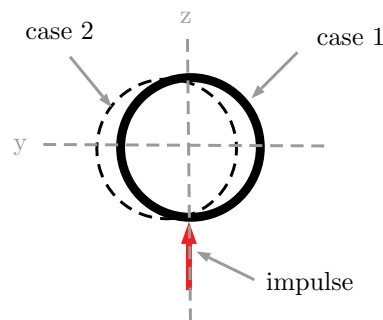
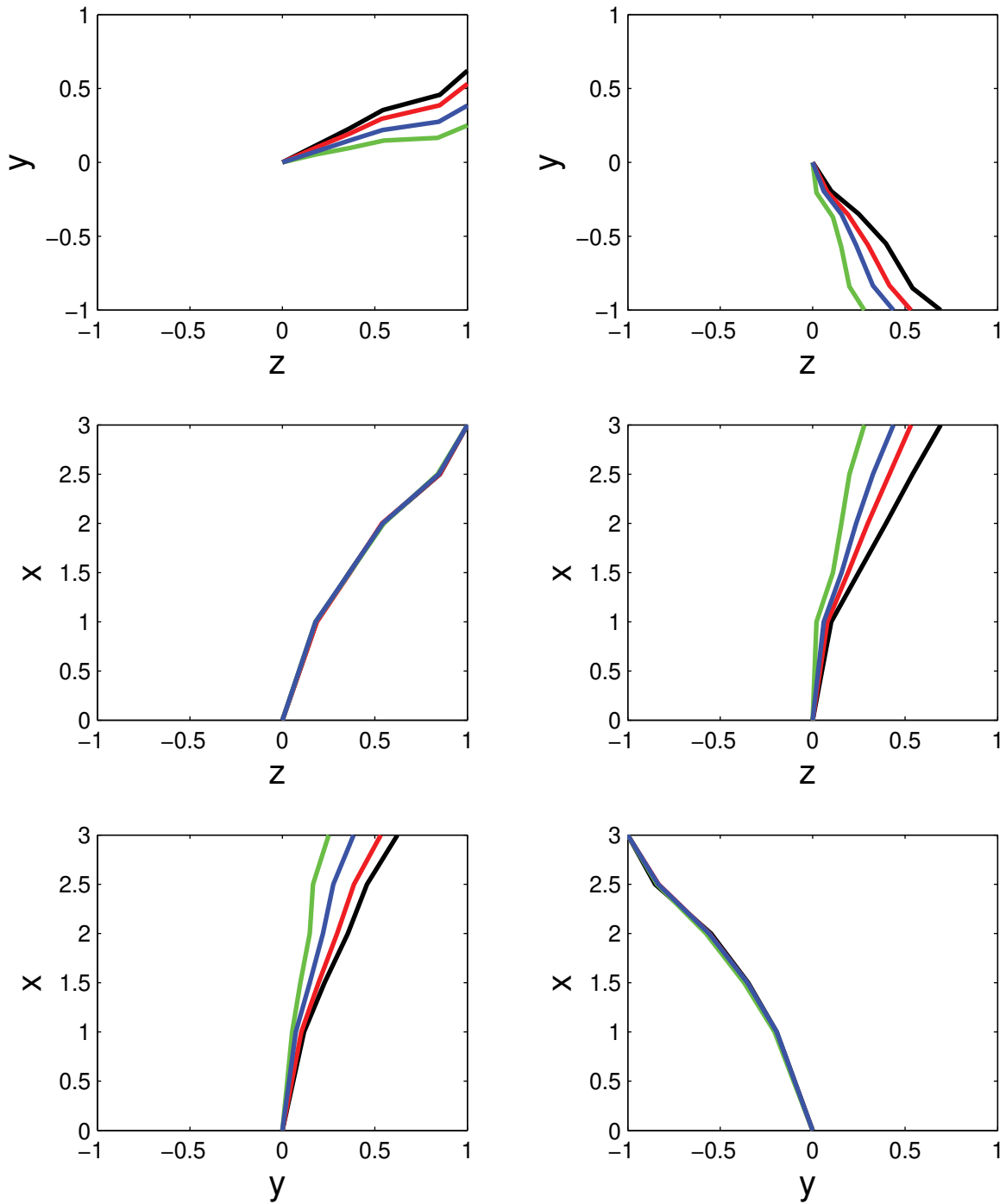


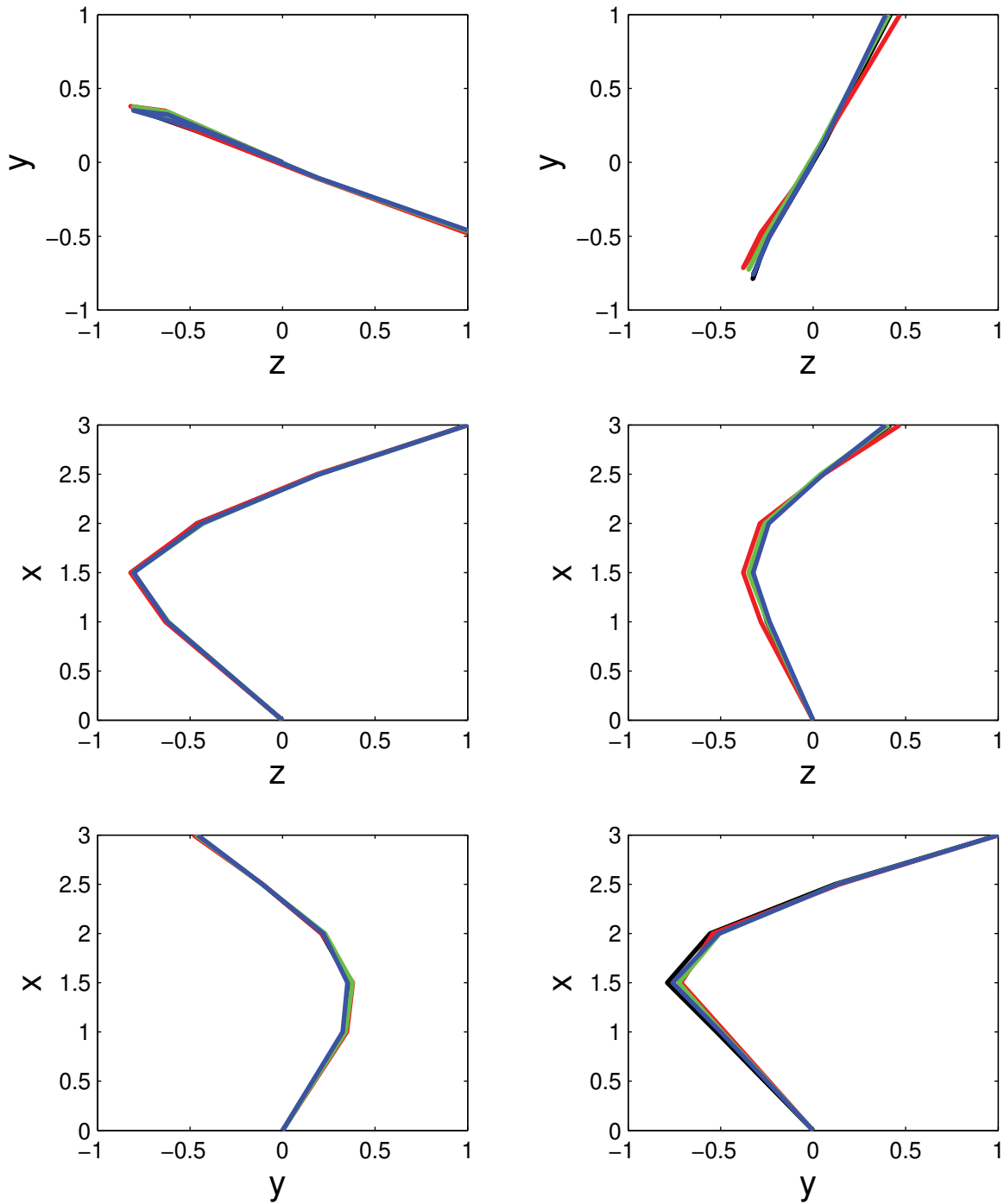
Figure 5.43: The structure is shifted in y direction due to the added weights and the asymmetry



(a) mode shape 1

(b) mode shape 2

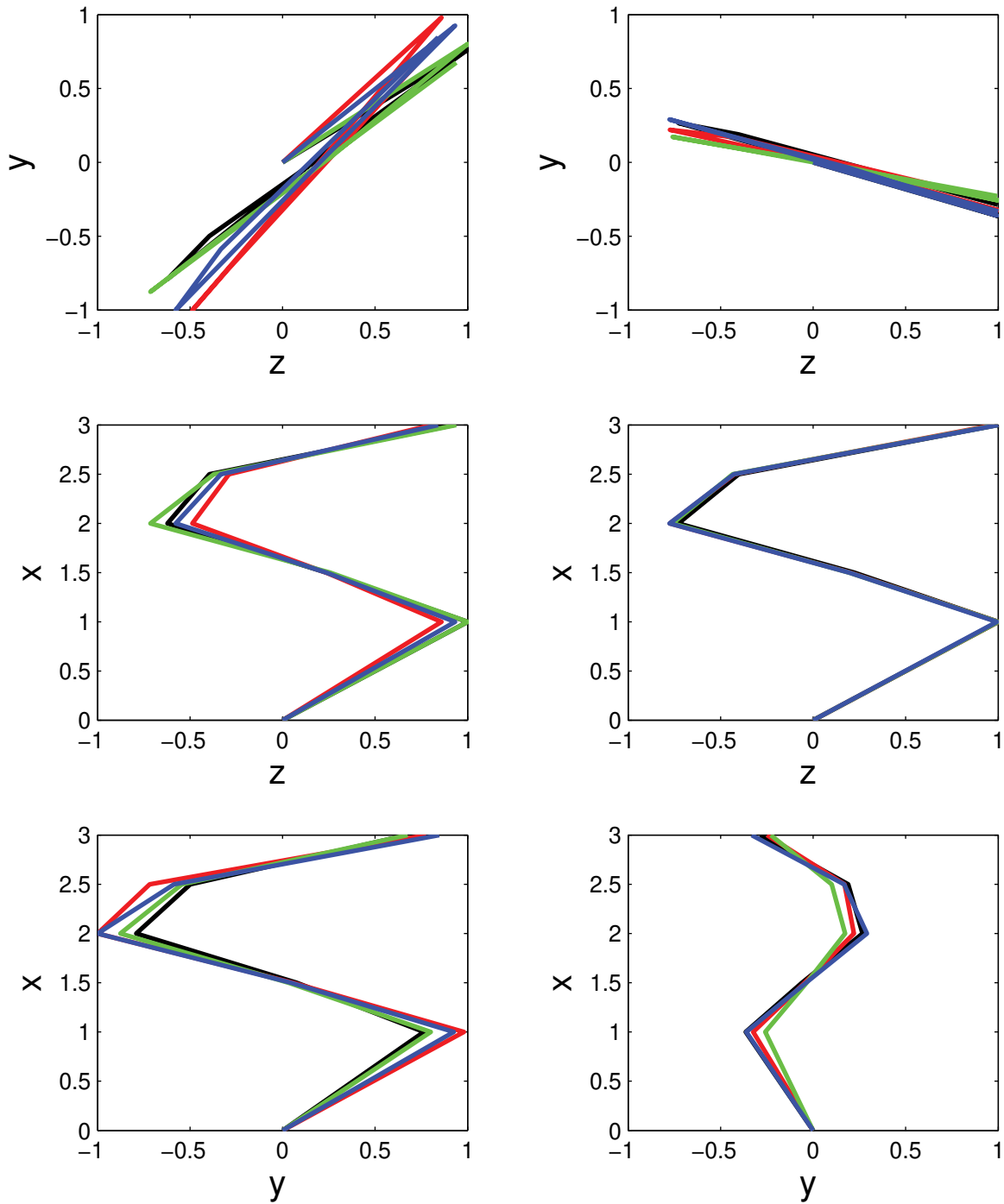
Figure 5.44: Mode shapes 1 and 2 scaled to unit modal displacement extracted from experimental data, θ_1^g :black, θ_2^g :red, θ_3^g :green, θ_4^g :blue



(a) mode shape 3

(b) mode shape 4

Figure 5.45: Mode shapes 3 and 4 scaled to unit modal displacement extracted from experimental data, θ_1^g :black, θ_2^g :red, θ_3^g :green, θ_4^g :blue



(a) mode shape 5

(b) mode shape 6

Figure 5.46: Mode shapes 5 and 6 scaled to unit modal displacement extracted from experimental data, θ_1^g :black, θ_2^g :red, θ_3^g :green, θ_4^g :blue

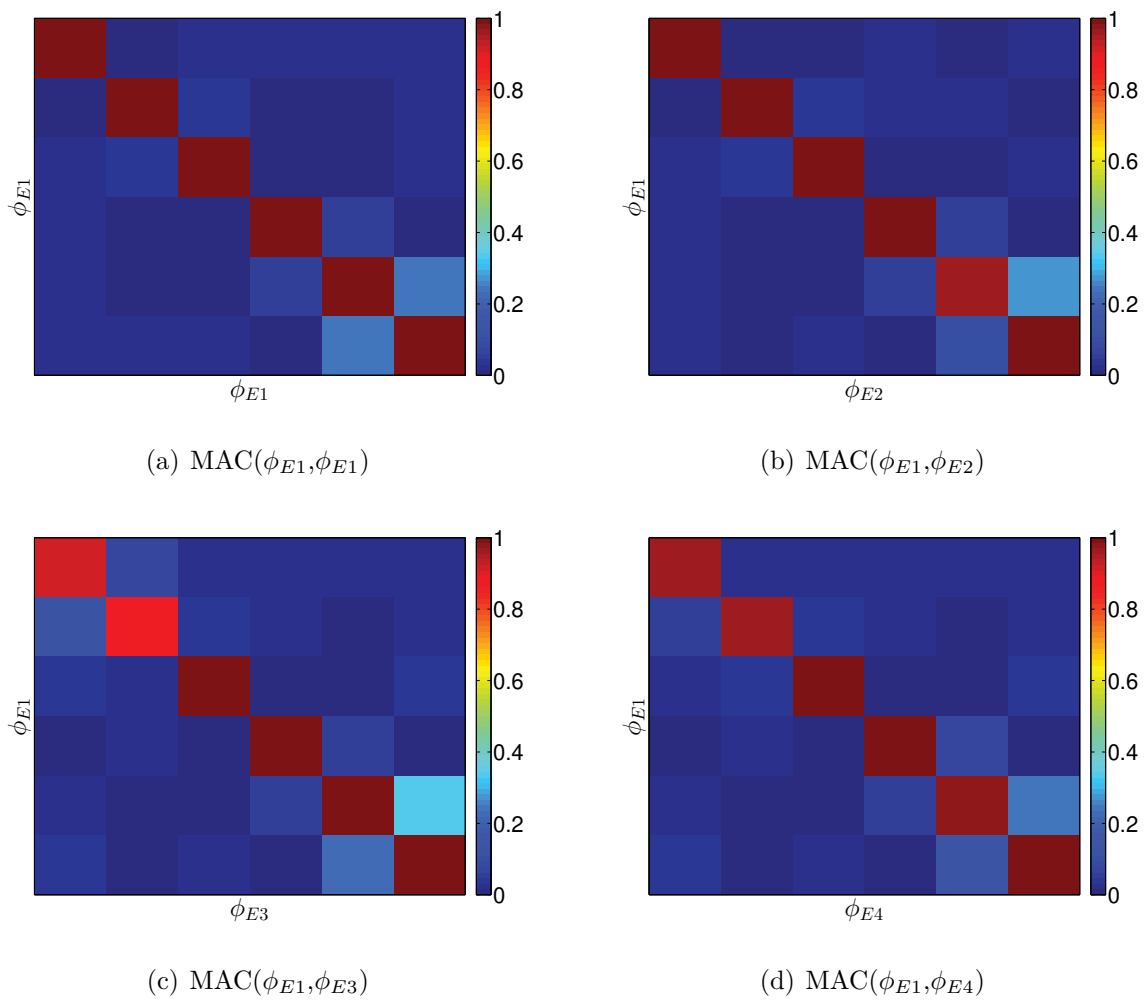


Figure 5.47: MAC value computed between damage case 1 and other damage cases

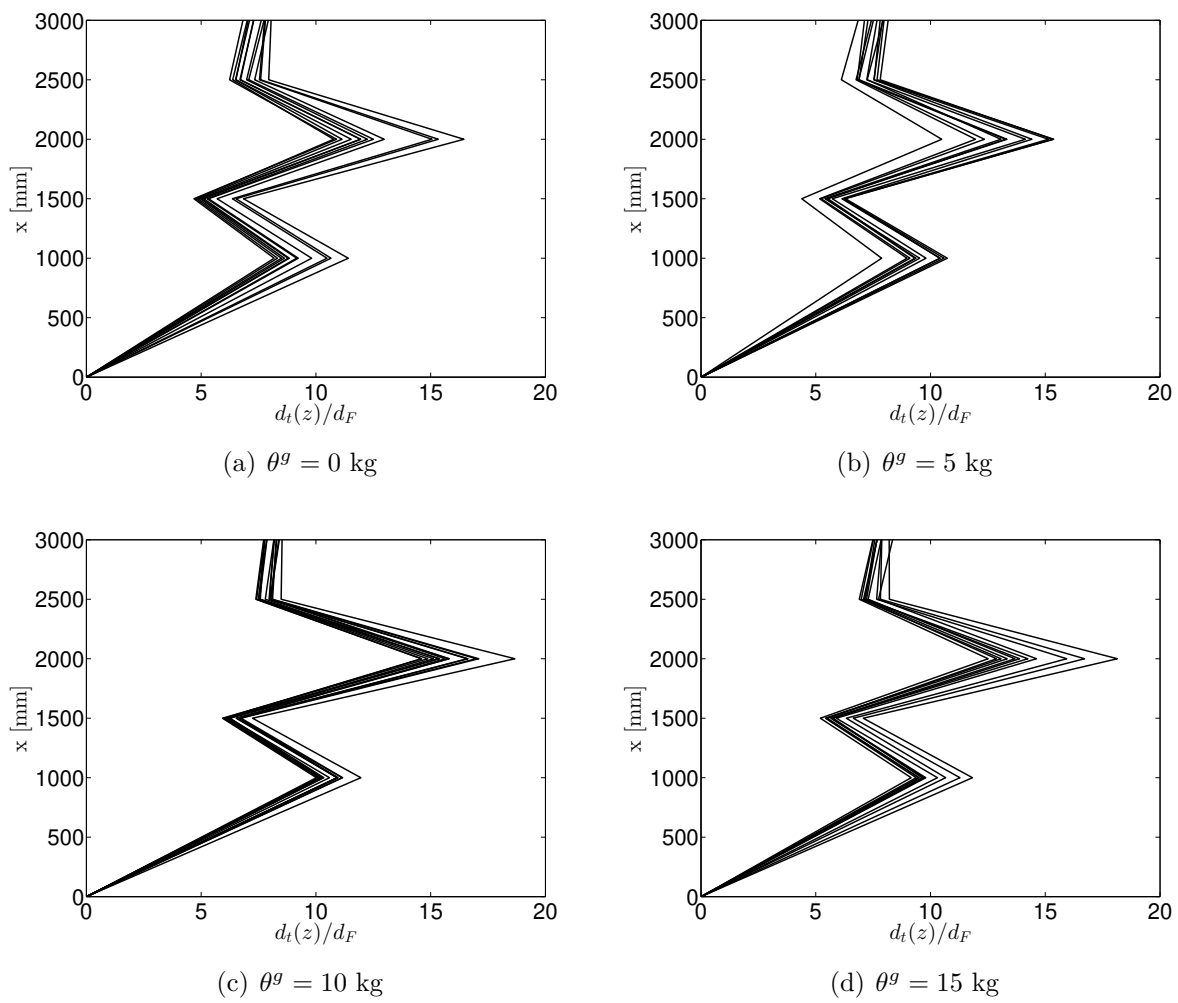


Figure 5.48: The statistical results of $\bar{d}_t(y)$ normalized to d_F for all studied damage cases

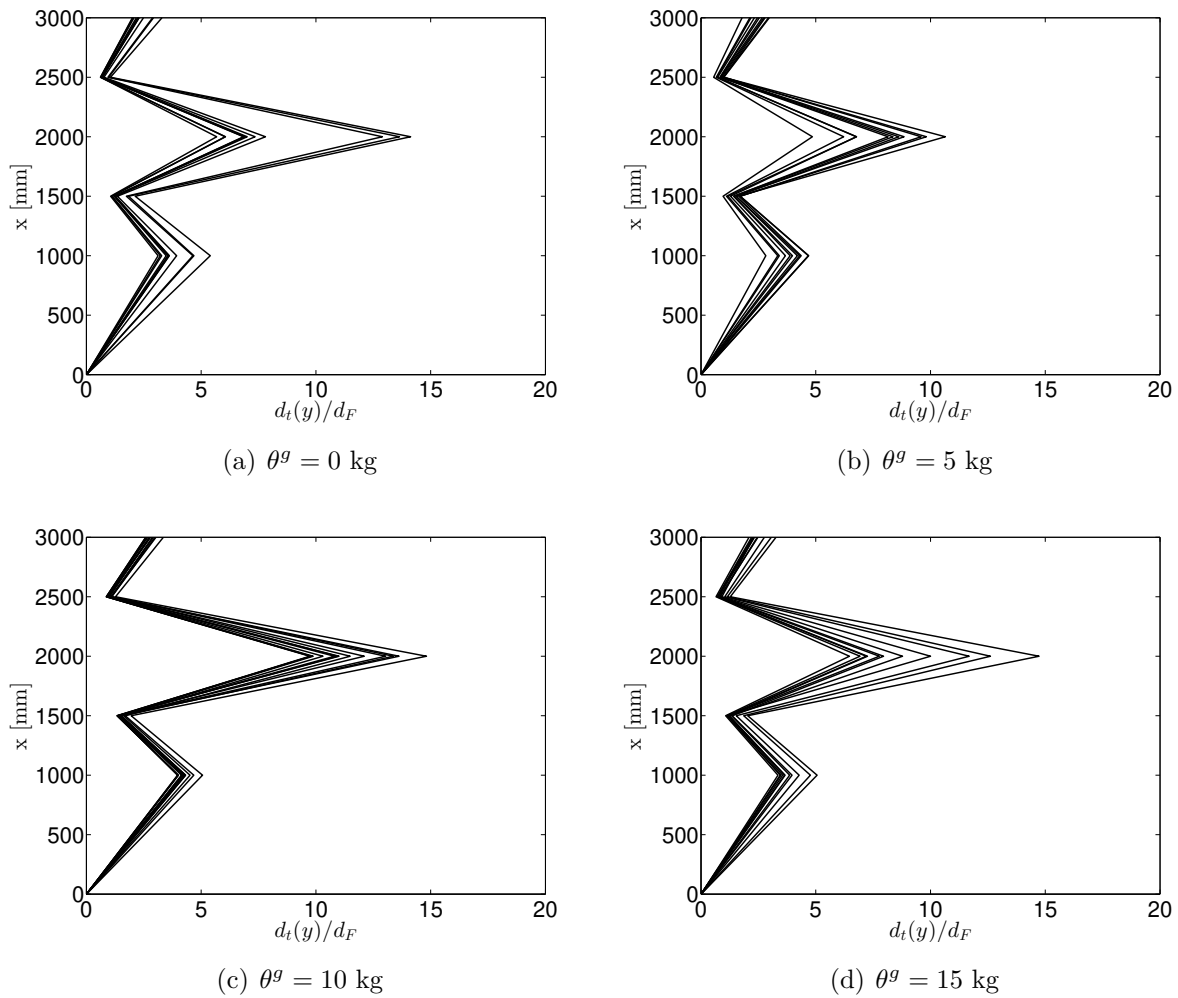


Figure 5.49: The statistical results of $\bar{d}_t(z)$ normalized to d_F for all studied damage cases

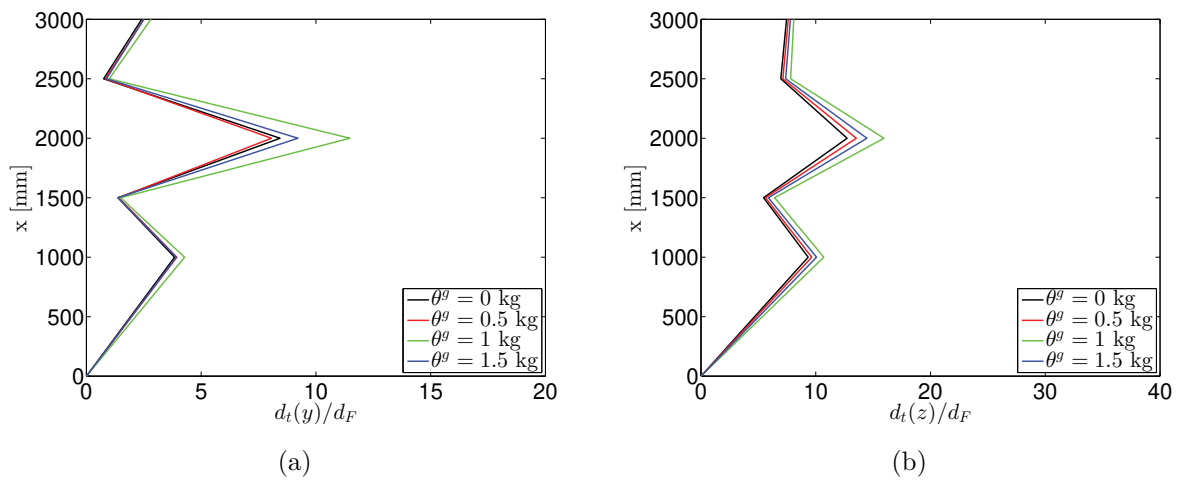
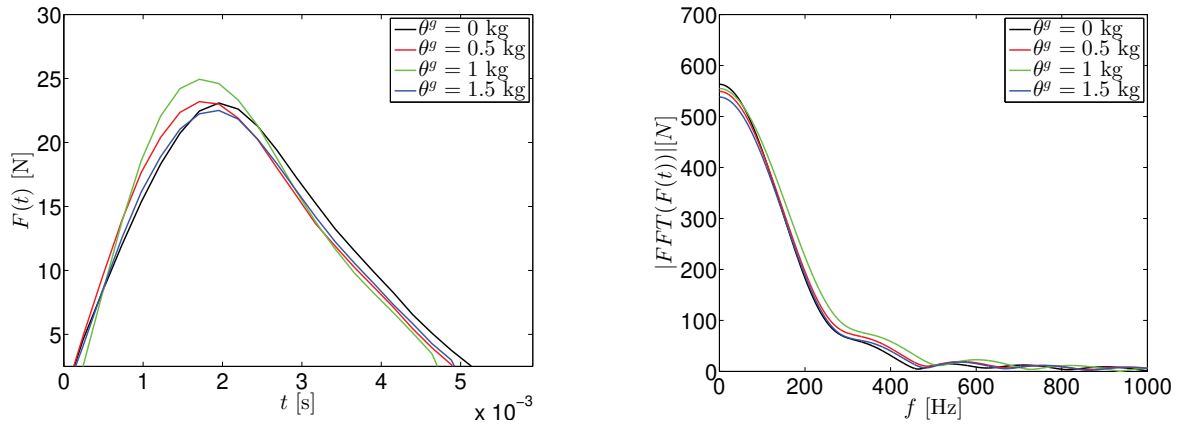


Figure 5.50: The mean value of \bar{d}_t/d_F



(a) Impulse excitations used to compare the response of the models in case of different damage cases (b) FFT shows the frequency range of the considered impulse excitations

Figure 5.51: Chosen excitations and their $|FFT|$ from conducted experiments in order to calculate the response of the studied models for each damage case

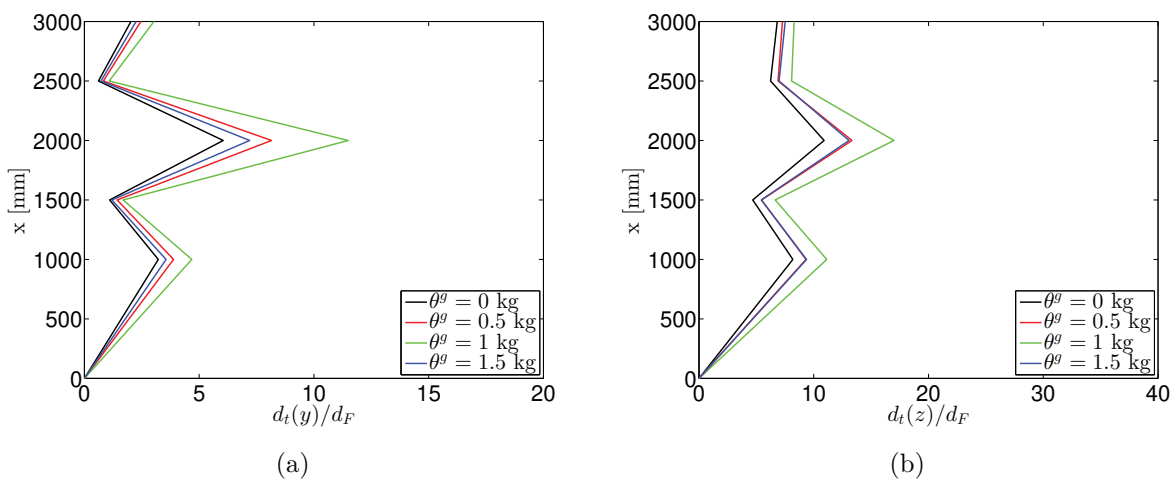


Figure 5.52: \bar{d}_t/d_F under similar impulses

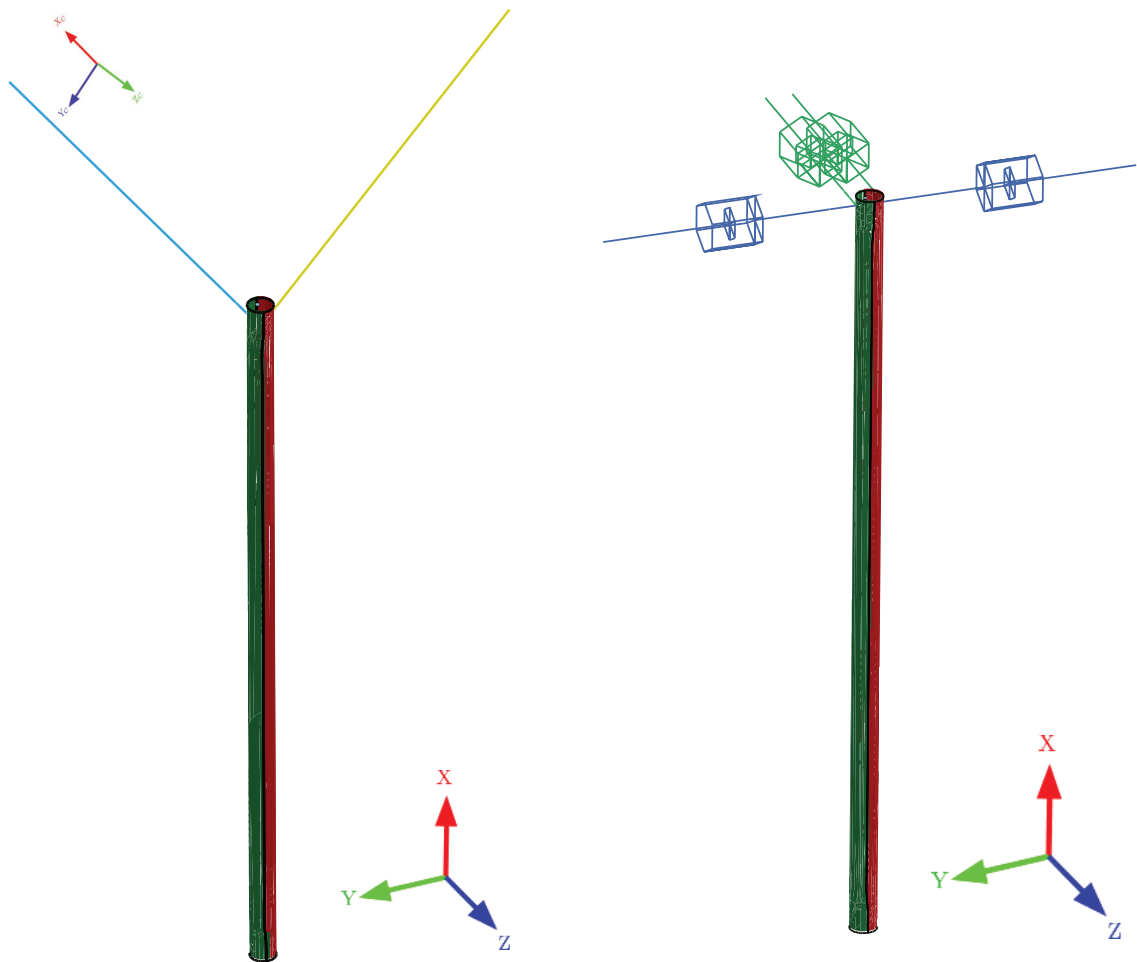
5.2.4 Numerical model

Two finite element models were developed to investigate the influence of the cables on the studied structure, figure 5.53. A shell element type was used to model the cantilever. The shell elements were meshed to smaller elements with a maximum size of 30 mm. A Mass point element type was used to consider the influence of the masses of the sensors. The mass of the sensor including the fixation ring was obtained by measuring its weight, $M_s = 210$ g. The masses of the sensors were placed at $\{x\} = \{1, 1.5, 2, 2.5, 2.96\}$ m measuring from the foundation $x = 0$ m. All six degrees of freedom of the nodes located at plan $x = 0$ m were fixed to represent the clamped support condition. The linear isotropic material was assigned to the cantilever. The natural frequencies of the studied system presented in table 5.17 indicate that the cantilever is asymmetric. To include the structure imperfection, the model was divided using a XZ plane where $y = 0$ into two equal parts. Different elastic modulus values were assigned to each part. The elastic modulus $E_{P,1}$ was assigned to the elements which are located at the first half: $y > 0 \rightarrow E_{P,1} = 3000$ N/mm² and $E_{P,2}$ was assigned to the elements which are located at the second half $y \leq 0 \rightarrow E_{P,2} = 4000$ N/mm². The Poisson's ratio ν_P and the density ρ_P are considered as follows: $\{\nu_P, \rho_P\} = \{0.4, 1.39 \text{ t/m}^3\}$.

In the first numerical model $G_{M,1}$, figure 5.53 (a), a cable element type was used to model the rubber cables. The cable element allows only to carry an axial tension force. The angle between the horizontal and the local axis of the cable is 50° , figure 5.37. A cable material type, which includes only the material properties in axial direction of the cable, was assigned to the cable elements. As it was mentioned in the previous section, the band reached its maximum elongation for damage cases 1, 2 and 3. This means that the stiffness of the band depends on the added weights which cause axial forces F_w in the cables. The relationship between the force and the stiffness after reaching the third damage case $F_w = 5$ N (both masses are 0.5 kg) is unknown. If the probability of damage detection doesn't reach 100% before damage case 3 is reached, then assessing the reliability of the inspection method for damage levels less than $F_w = 5$ N depends on how the rubber band behaves when the axial force decreases from 5 N to 0 N. For a precise evaluation, additional experiments help to discover more information about the behavior of the rubber band in this case. In this work, a simple linear model was chosen to represent the behavior of the rubber band in case of $F_w < 5$ N. Choosing other models is also possible, and this influences the probability of detection if large-size damage is late detected. In this case, the inspection method is not reliable by default. The difference $\Delta L = L_0 - L_1$ between the initial length of the cable $L_0 \approx 200$ mm before applying the load and the length of the cable L_1 after applying the load $F_w = 5$ N was measured. The test shows that $L_1 \approx 400$ mm. In order to calculate the elastic modulus of the bands, their stiffness K_c was estimated assuming the follows:

$$K_c = \begin{cases} \frac{F_w}{\Delta L} & \text{if } F_w < 5 \text{ N} \\ \frac{F_w}{200} = 0.005F_w & \text{if } 5 \leq F_w \leq 15 \text{ N} \end{cases} \quad (5.22)$$

In order to estimate E_C it was assumed that if $F_w \geq 5 \text{ N} \rightarrow A_C = \pi r_c^2 = \pi 0.32^2 = 0.32 \text{ mm}^2$, where A_C is the area of the cross-section of the cable and r_c is the radius of the cross-section which was assumed to be a circle. As a result, E_C is calculated as follows:



(a) Numerical model of the studied cantilever $G_{M,1}$ including cables
 (b) Numerical model of the studied cantilever $G_{M,2}$ without cables

Figure 5.53: Numerical models considered for evaluating the performance of the studied inspection method

$$E_C = \frac{K_c L_0}{A_C} = \frac{0.005 \times F_w \times 200}{0.32} \approx [15.6-46.8] \text{N/mm}^2 \quad (5.23)$$

The uncertainty in E_C due to the initial length L_0 , the area of the cables cross-section, ΔA_C , before and after applying the load and the hardening region of the rubber was considered in the statistical investigation in the next steps. The density ρ_C was considered as 1.1 t/m^3 . Local coordinate systems were defined to provide suitable boundary conditions for the cables. The x_c axis of the local coordinate system is associated with the local central axis of the cable. The translational degrees of freedom in both y_c and z_c directions of the top node of the cables were fixed in the local coordinate systems. The cable forces $F_w = V_w \times \rho_w \times g$ produced by the water volume V_w in each bottle were applied at the top node of the cables in x_c direction of the local coordinate systems. The axial cable forces F_w were directed to produce tension forces in the cables. The density of the water is considered as $\rho_w = 1 \text{ t/m}^3$ and the gravitational acceleration is $g = 9.81 \text{ m/s}^2$. In this case the damage model θ^g is a function of K_c and F_w : $\theta^g = f(K_c, F_w)$, where $0 \leq F_w \leq 15 \text{ N}$. Damage was increased by reducing K_c and F_w .

In the second numerical model $G_{M,2}$, figure 5.53 (b), the cables were replaced by 2 viscous dampers in each direction. The dampers were attached to the cantilever at the same nodes where the cables were attached to the cantilever in the first model. In this case the damage model θ^g is a function of F_w , the damping force in y direction $F_{\zeta,w,y}$ and the damping force in z direction $F_{\zeta,w,z}$: $\theta^g = f(F_w, F_{\zeta,w,y}, F_{\zeta,w,z})$. F_w was decoupled to two components: $F_{w,x} = F_w \sin 50^\circ$ and $F_{w,y} = F_w \cos 50^\circ$, see figure 5.37. F_w components were applied at the same nodes where the cables were attached to the cantilever in the first model. Damage was increased by reducing F_w , $F_{\zeta,w,y}$ and $F_{\zeta,w,z}$.

In order to include the influence of the force F_w on the dynamic response of the structure, an initial transient analysis was performed after applying F_w . In order to avoid the vibration of the structure during the performed analysis, large damping value was assigned to the model by increasing α in the Rayleigh damping model as shown in figure 5.54. In the next step, the time history of the impulse excitation F_z for damage case 1 (no damage: $\theta_1^g = 0 \text{ kg}$), which was recorded during the laboratory modal test and shown in figure 5.51, was applied after removing the noisy part. The noise was removed from the excitation time history by choosing a threshold F_c where $F(t) = 0$ if $F(t) < F_c$. In this example $F_c = 0.1 \times F_{Z,max}$. At each time step $\Delta t = 1/4096 \text{ s}$, the associated force $F_z(t)$ was applied at the node located at $x = 2.05 \text{ m}$ in z direction: $(x, y, z) = (2.05, 0, -r)$. Rayleigh damping model, eq. (5.5), with $\alpha = 0.45$ and $\beta = 9.78e - 05$ was introduced in both models, figure 5.55, based on the modal damping ratios obtained from the modal tests case 1. The acceleration time histories were calculated for the nodes where sensors were placed at the structure in the laboratory, figure 5.56 and 5.57.

The asymmetry explained in the previous section was considered, besides considering two elastic modulus values, by applying a horizontal impulse force F_y in the y-direction at the node located

at $(x, y, z) = (2.05, r, 0)$ in both models. The additional impulse force F_y has the same time history shape of the original impulse F_z but its amplitude was scaled with respect to the amplitude of F_z . Moreover, in order to include the possible effect of different friction factors of the roller, different axial forces were applied to the cables: for $y > 0 \Rightarrow F_w = F_{w,1}$, for $y < 0 \Rightarrow F_w = F_{w,2}$. Similarly for the model $G_{M,2}$, different values was assigned to the damping forces $F_{\zeta,w,z}$ and $F_{\zeta,w,y}$.

The modal parameters were estimated from the calculated response by applying the SSI method following the similar procedure presented in appendix C. The estimated frequencies and damping ratios are shown in tables 5.18 and 5.19. The results show that the asymmetry model introduced using different elastic modulus values, different cable forces and adding F_y helps to separate the frequencies of the close modes similar to what was measured in the laboratory. However, the mode shapes in figures 5.58 – 5.63 show smaller inclinations to y and z axes compared to the experimental results. The damping forces due to the cables can be calculated as follows:

$$F_{\zeta,w} = -C_d \dot{u} \quad (5.24)$$

where C_d is the damping constant and \dot{u} refers to the velocity in y and z directions. The initial values of $C_{d,z}$ and $C_{d,y}$ can be estimated roughly assuming that the critical damping constant C_c of the cantilever was not affected by the cables. The critical damping of the structure can be calculated as follows:

$$C_c = 2M_p \omega_E \quad (5.25)$$

where M_p refers to the kinetically equivalent mass which can be obtained as the modal mass normalizing the mode shape ϕ_r such that the modal displacement at the considered degree

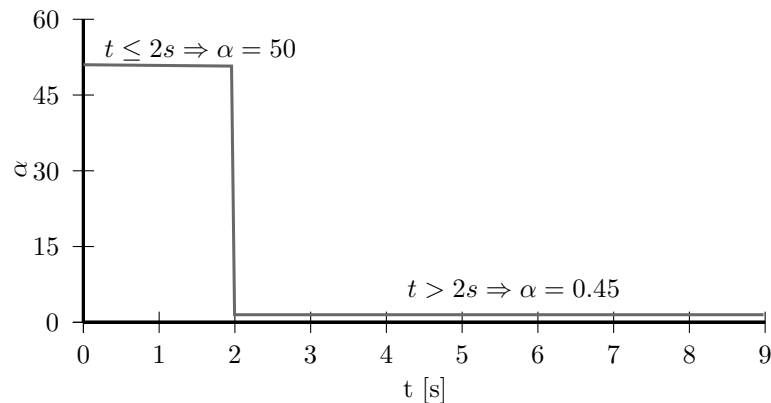


Figure 5.54: The contribution of the mass of the structure in the Rayleigh damping model during performing transient analysis

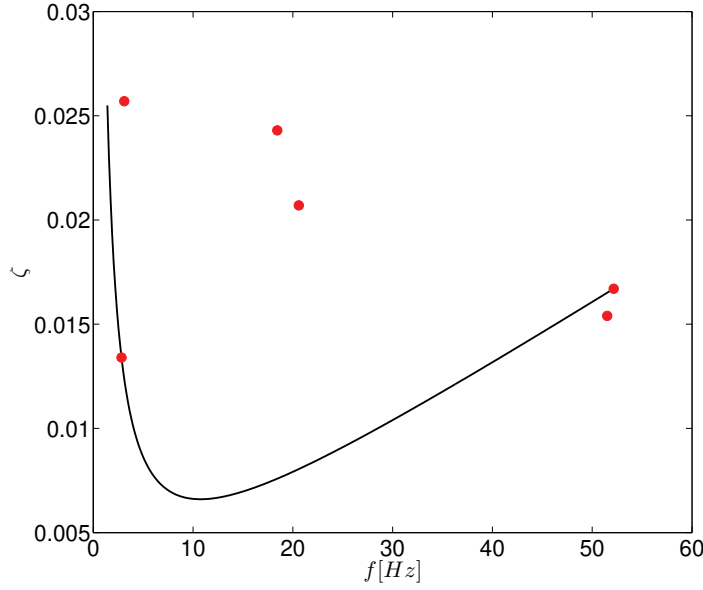


Figure 5.55: Rayleigh damping model included in the cantilever numerical models

of freedom = 1, eq.5.26. For the first bending mode of a cantilever with continuous mass and stiffness distribution the kinetically equivalent mass is 0.25 of the total mass. The total mass of the structure is $m = A \times h \times \rho = 4.51$ kg where A is the area of the cross-section $A = \pi(110^2 - 103.6^2)/4 = 1073.67$ mm². The instrumentation consists of 5 accelerometers and one force sensor besides the steel rings that hold the sensors on the structure. Ignoring the mass of the cables, $M_{p,1} = 0.25 \times (4.51 \times 10^{-3} + 6 \times 210 \times 10^{-6}) = 1.44 \times 10^{-3}$ t or 1.44 kg.

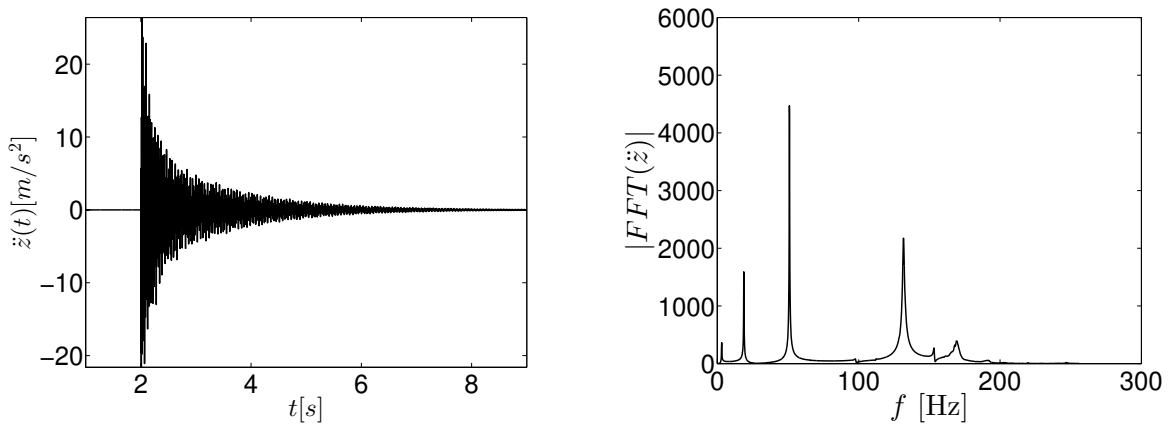
$$M_{p,r} = \{\phi_r\}^T [M] \{\phi_r\} \quad (5.26)$$

In this example, the effective modal mass in case of the first mode in each direction (y and z) including the instrumentation will be considered when estimating C_c . The contribution of higher modes will be considered later by performing model updating and uncertainty quantification. $\omega_{E,1}$ is the measured natural frequency of the mode 1 z-direction, $\omega_{E,1} = 2 \times \pi \times 2.9 = 18.22$. The critical damping is $C_c = 2 \times 1.44 \times 18.22 \approx 52.5$ N×s/m. For the second mode y-direction $\omega_{E,2} = 2 \times \pi \times 3.1 = 19.4$ rad/s. The critical damping is $C_c = 2 \times 1.44 \times 19.4 \approx 55.8$ N×s/m. For simplification purposes C_c will be considered 55 N×s/m for the both modes. The damping force without considering the cable is $F_\zeta = -C\dot{u}$ where $C = \zeta \times C_r$.

The total damping force including the cables effect $F_c = F_{\zeta,w} + F_\zeta = -C_d\dot{u} - C\dot{u} = -(C_d + C)\dot{u}$. Assuming that the estimated damping ratio ζ_E from the measurement includes the effect of the interaction between the cables and the structure, then it is possible to write that $(C_d + C) = \zeta_E \times C_r$. As a result:

$$C_d = \zeta_E \times C_r - C = (\zeta_E - \zeta) \times C_r \quad (5.27)$$

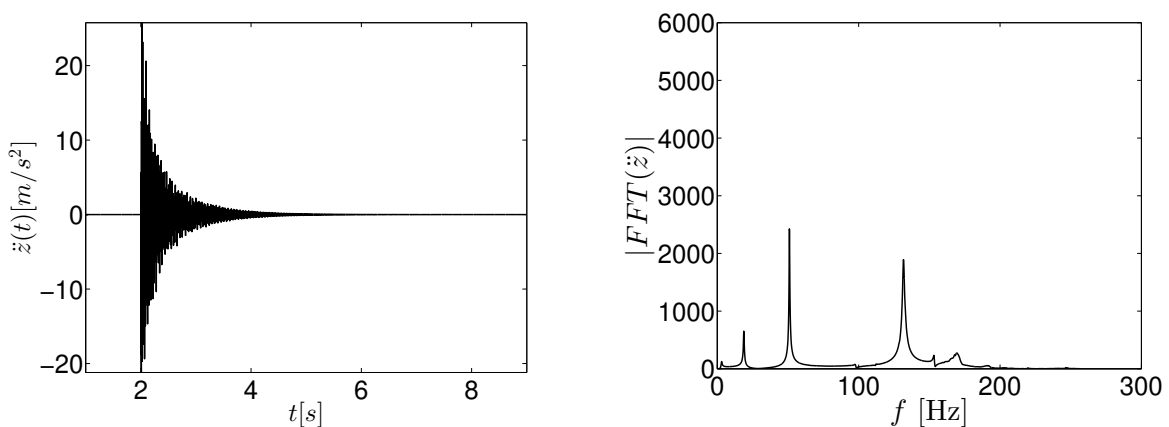
Since the Rayleigh damping model in figure 5.55 gives low damping value for the second mode, it was assumed that $\zeta = 0.1 \times \zeta_E \approx 0.1 \times 0.03 = 0.003$, $C_d \approx 0.9 \times 0.03 \times 55 = 1.485 \text{ N}\times\text{s}/\text{m} \approx 0.0015 \text{ N}\times\text{s}/\text{mm}$. In order to include the uncertainty when estimating M_p and ζ_E , the range $C_d = [0.0001\text{--}0.01] \text{ N}\times\text{s}/\text{mm}$ was considered in the next steps.



(a) Simulated acceleration time history

(b) |FFT| shows the simulated response of the structure in frequency domain

Figure 5.56: Simulated dynamic structural response at the top of the cantilever due to the excitation in figure 5.51, case 1, using the numerical model $G_{M,1}$



(a) Simulated acceleration time history

(b) |FFT| shows the simulated response of the structure in frequency domain

Figure 5.57: Simulated dynamic structural response at the top of the cantilever due to the excitation in figure 5.51, case 1, using the numerical model $G_{M,2}$

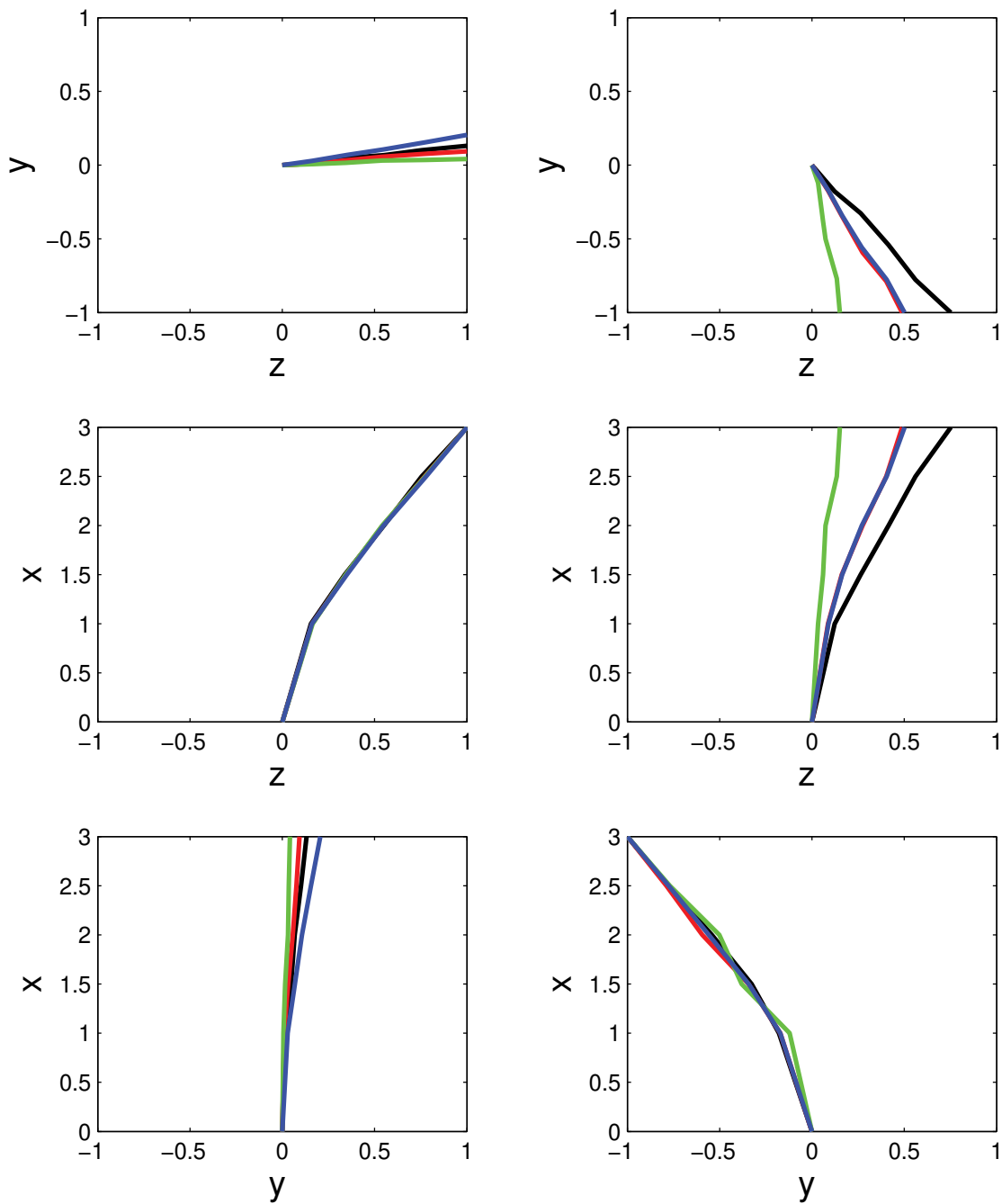
Table 5.18: Natural frequencies and damping ratios obtained using the numerical model $G_{M,1}$ by analyzing numerical response using the SSI method

		1	2	3	4	5	6
case 1	f Hz	3.01	3.05	18.50	18.81	50.68	51.06
	ζ [%]	3.18	3.31	0.55	0.51	0.20	0.22
case 2	f Hz	2.99	3.08	18.49	18.80	50.68	51.05
	ζ [%]	3.25	3.70	0.55	0.52	0.20	0.22
case 3	f Hz	2.97	3.04	18.47	18.79	50.67	51.04
	ζ [%]	3.23	3.18	0.55	0.52	0.20	0.22
case 4	f Hz	2.96	3.01	18.46	18.78	50.66	51.04
	ζ [%]	3.28	3.33	0.55	0.51	0.20	0.22

Table 5.19: Natural frequencies and damping ratios obtained using the numerical model $G_{M,2}$ by analyzing numerical response using the SSI method

		1	2	3	4	5	6
case 1	f Hz	2.92	3.02	18.51	18.80	50.68	51.05
	ζ [%]	14.41	9.69	1.70	1.43	0.44	0.45
case 2	f Hz	2.97	3.01	18.50	18.79	50.68	51.05
	ζ [%]	7.45	6.27	1.09	0.97	0.32	0.34
case 3	f Hz	2.96	3.01	18.48	18.78	50.67	51.04
	ζ [%]	4.85	4.66	0.82	0.75	0.26	0.28
case 4	f Hz	2.96	3.01	18.46	18.78	50.66	51.04
	ζ [%]	3.28	3.33	0.55	0.51	0.20	0.22

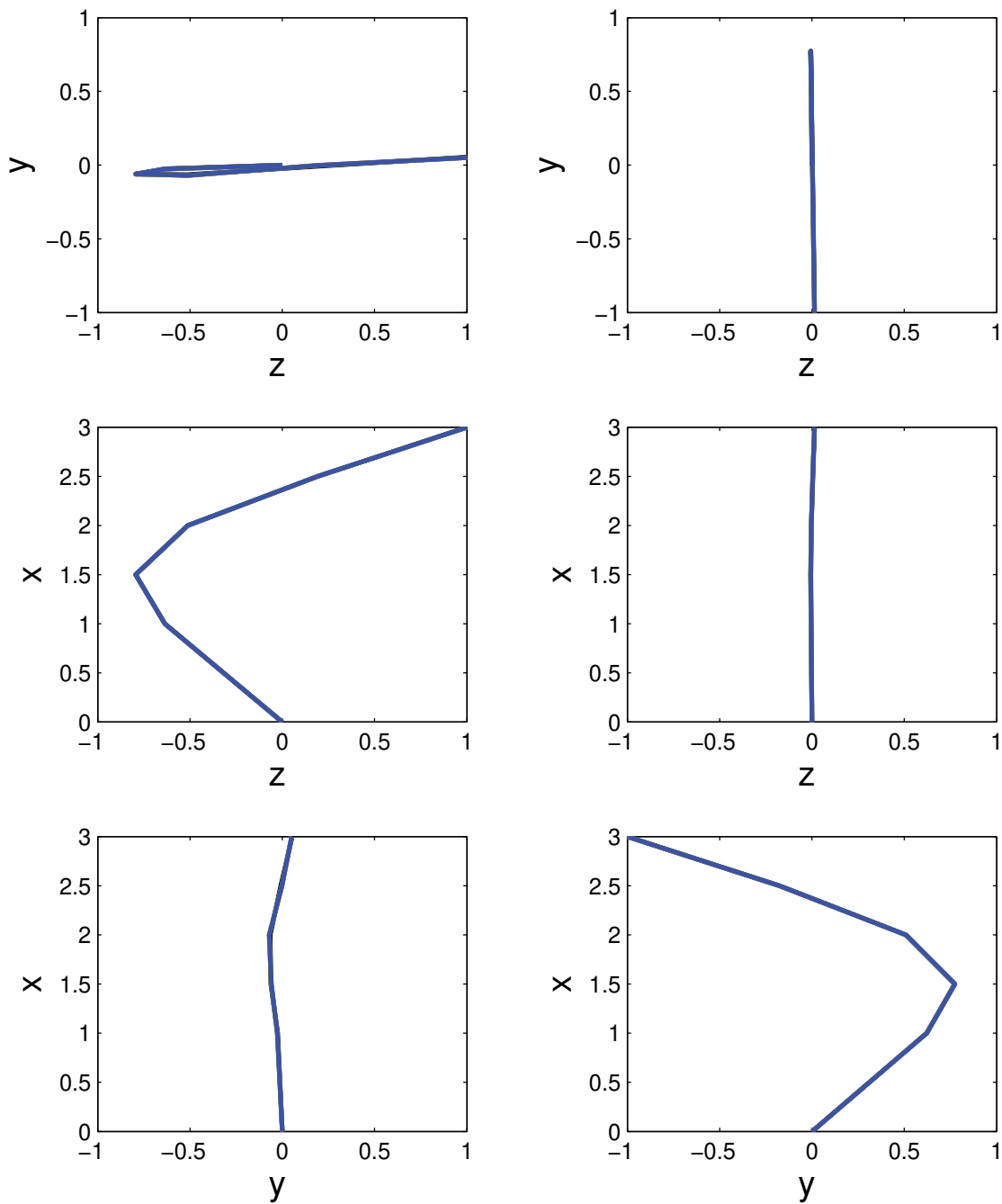
In order to estimate the quality of the developed numerical models $G_{M,1}$ and $G_{M,2}$ compared to the experimental model G_E the energy of the acceleration signals was calculated for all damage cases given the initial input parameters for the model $G_{M,1}$ in table 5.20 and for the model $G_{M,2}$ in table 5.21. The results in figures 5.64 show that the influence of the stiffness of the cables on the structural response is small compared to the damping effect in figure 5.65. However, both models show agreement with the experimental results in case of the first three damage cases. The reason for the disagreement related to damage case 4 may be because of the inaccurate or insufficient asymmetry model. The Q_V values in tables 5.22 and 5.23 were calculated considering the first three damage cases. The results show that considering the damping effect of the cables provides a better numerical model in case of damage detection.



(a) mode shape 1

(b) mode shape 2

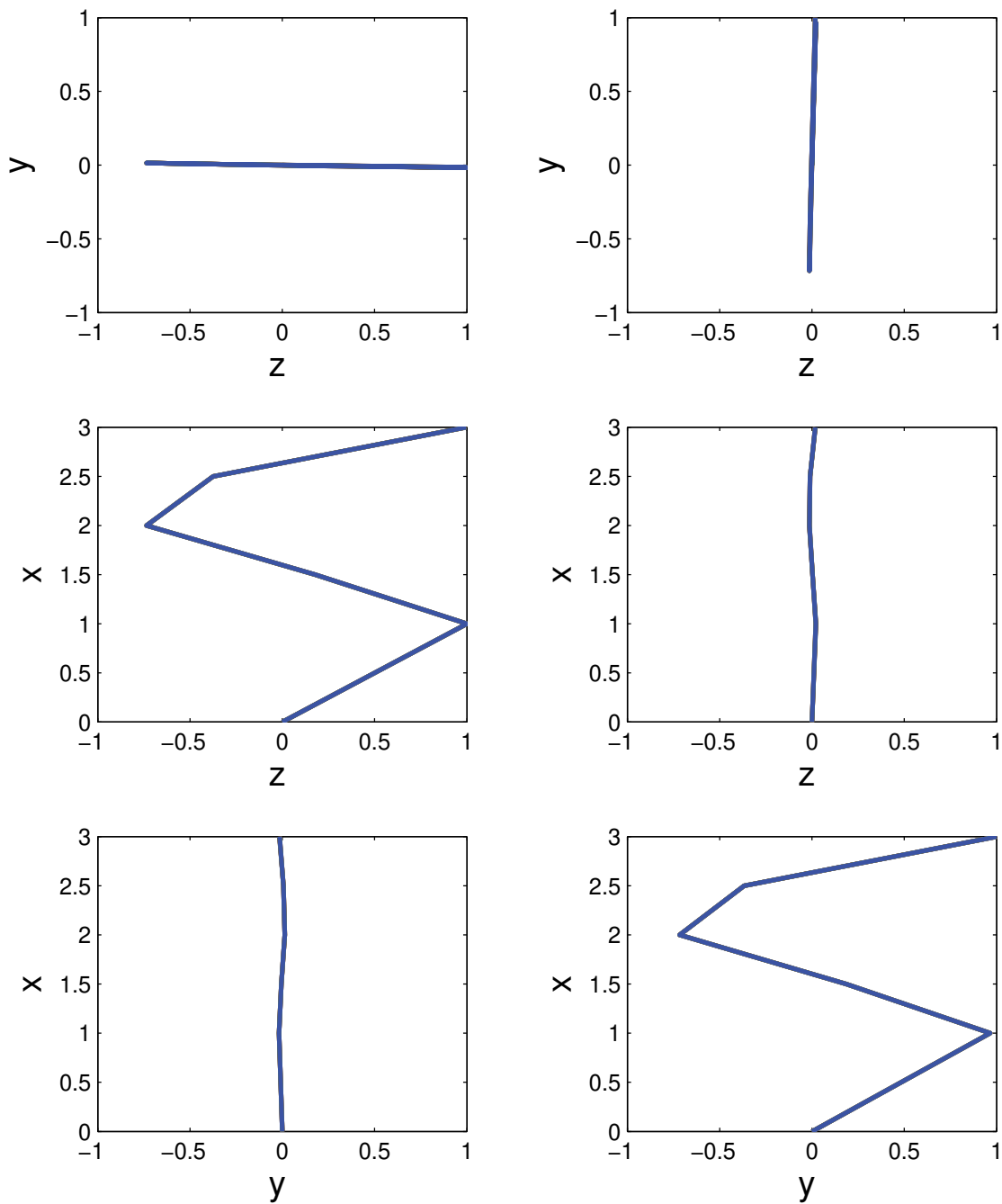
Figure 5.58: Mode shapes 1 and 2 and scaled to unit modal displacement obtained using the numerical model $G_{M,1}$ by analyzing numerical response using the SSI method. θ_1^g : black, θ_2^g : red, θ_3^g : green, θ_4^g : blue



(a) mode shape 3

(b) mode shape 4

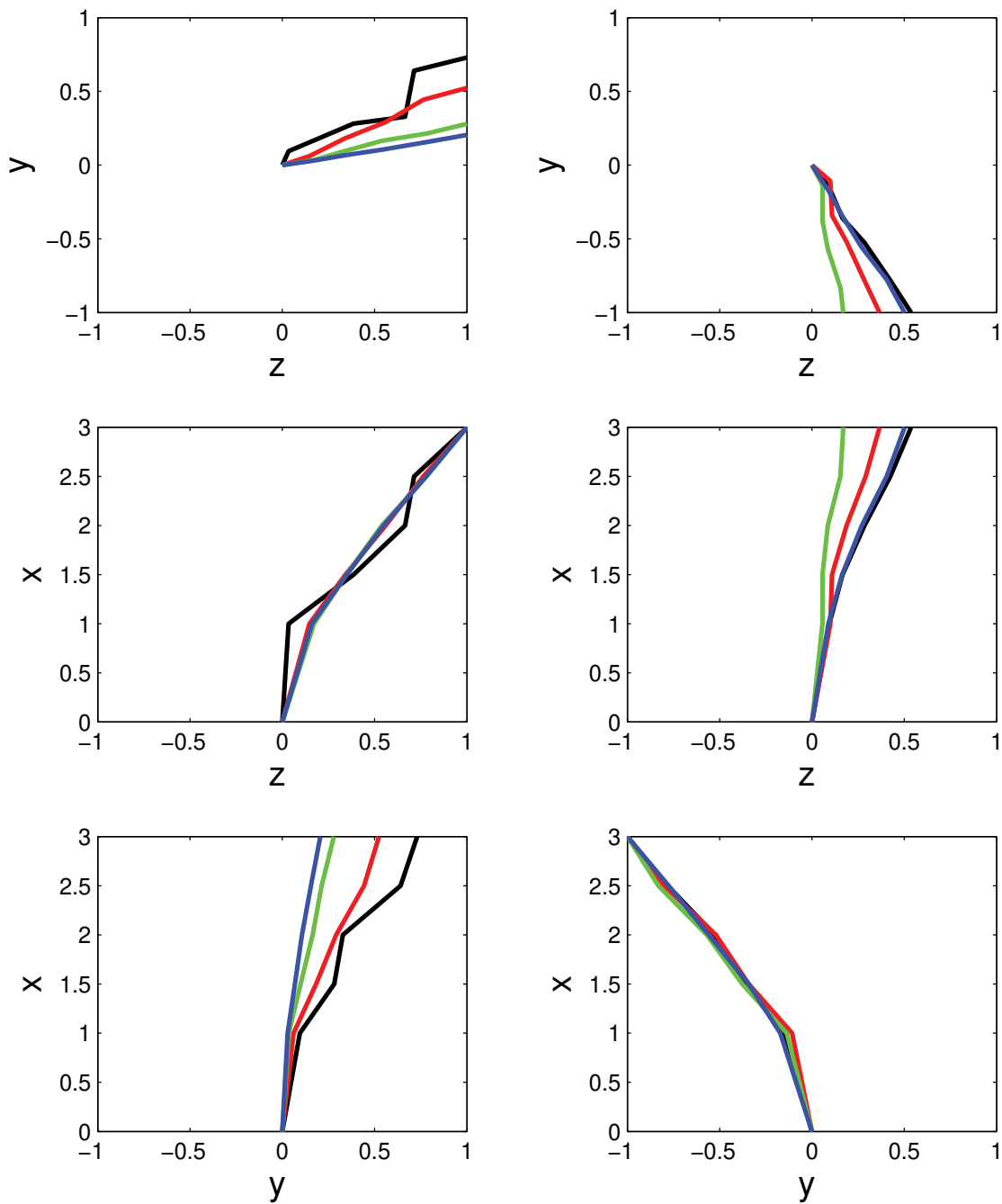
Figure 5.59: Mode shapes 3 and 4 and scaled to unit modal displacement obtained using the numerical model $G_{M,1}$ by analyzing numerical response using the SSI method. θ_1^g : black, θ_2^g : red, θ_3^g : green, θ_4^g : blue



(a) mode shape 5

(b) mode shape 6

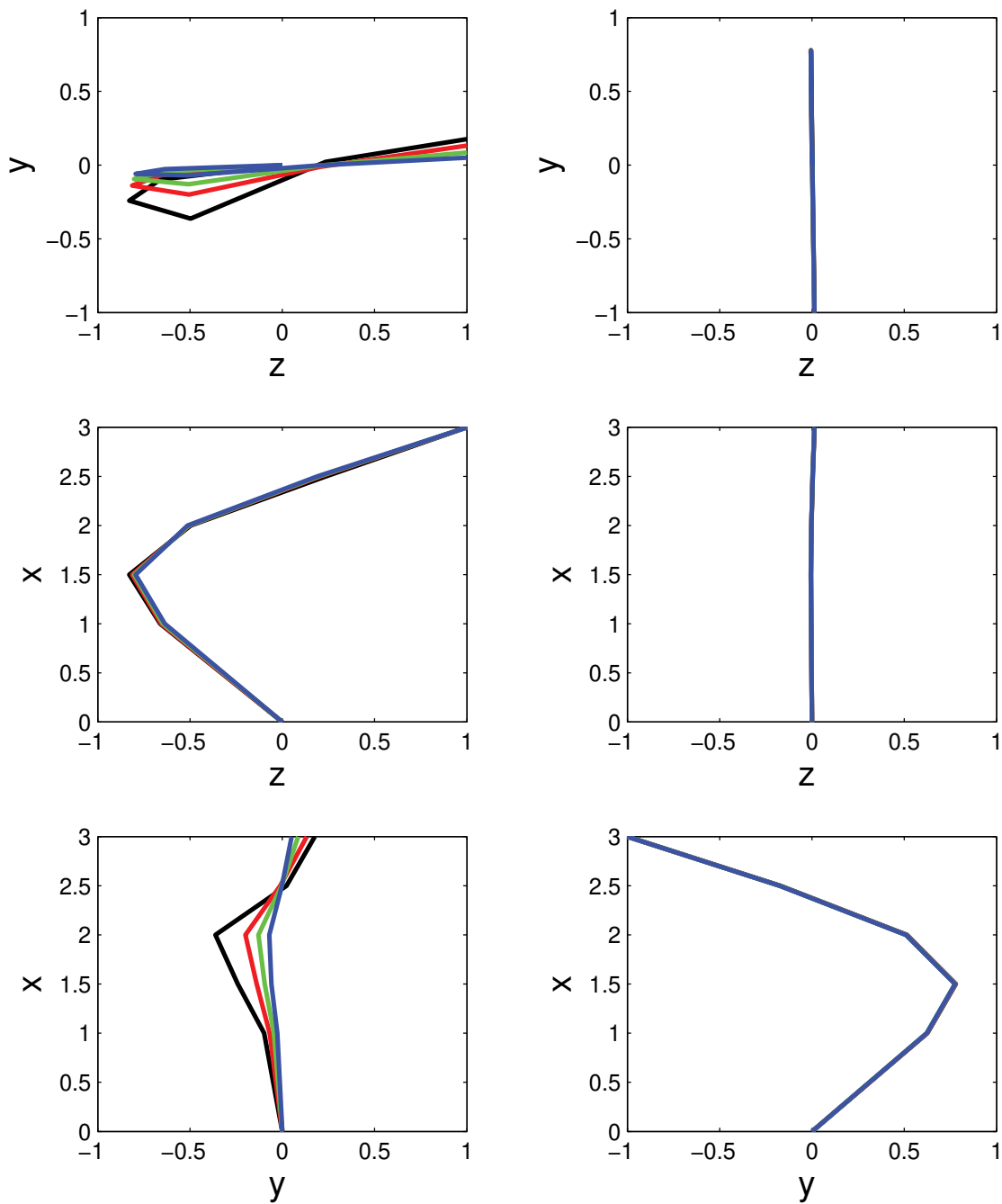
Figure 5.60: Mode shapes 5 and 6 and scaled to unit modal displacement obtained using the numerical model $G_{M,1}$ by analyzing numerical response using the SSI method. θ_1^g : black, θ_2^g : red, θ_3^g : green, θ_4^g : blue



(a) mode shape 1

(b) mode shape 2

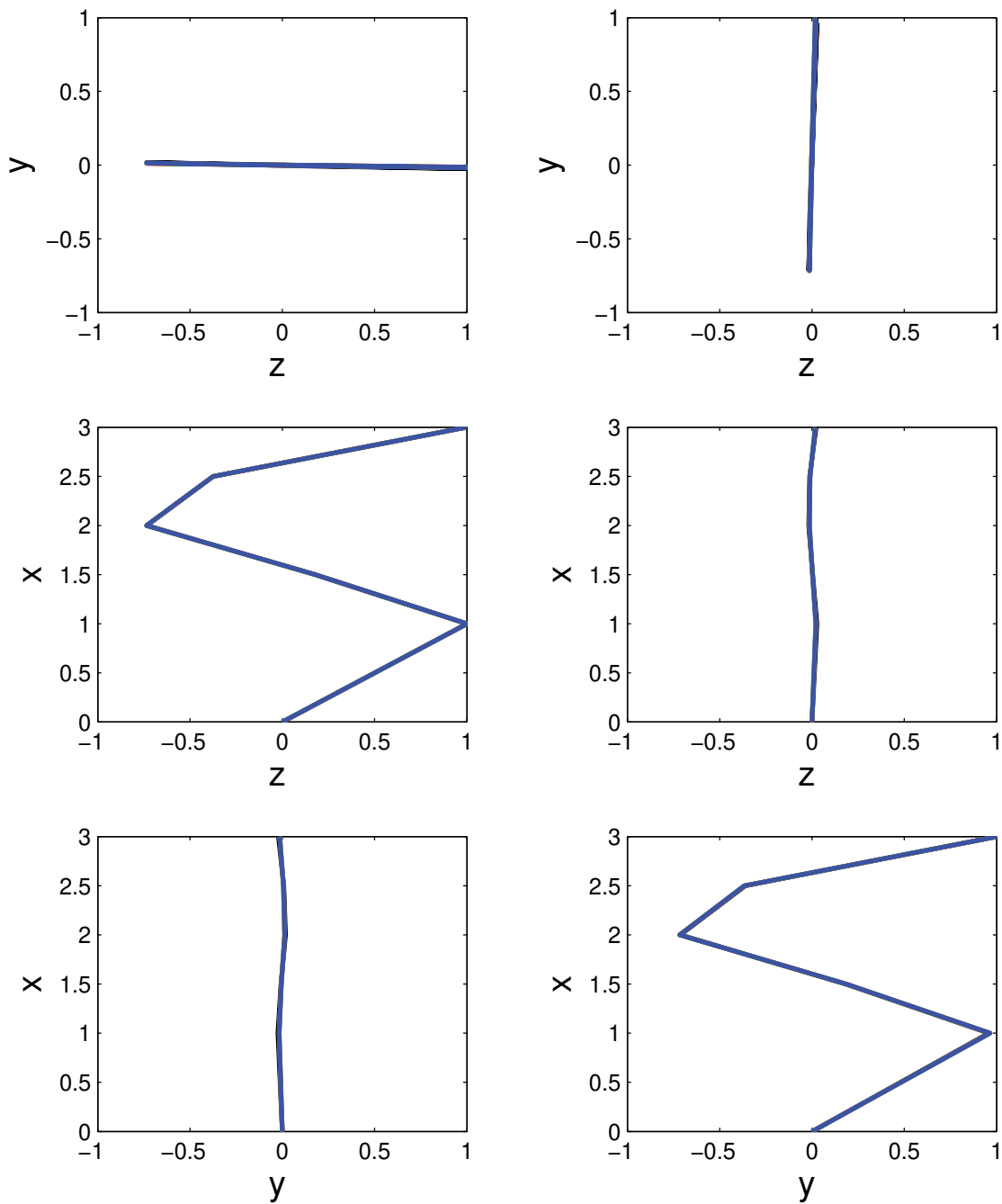
Figure 5.61: Mode shapes 1 and 2 and scaled to unit modal displacement obtained using the numerical model $G_{M,2}$ by analyzing numerical response using the SSI method. θ_1^g : black, θ_2^g : red, θ_3^g : green, θ_4^g : blue



(a) mode shape 3

(b) mode shape 4

Figure 5.62: Mode shapes 3 and 4 and scaled to unit modal displacement obtained using the numerical model $G_{M,2}$ by analyzing numerical response using the SSI method. θ_1^g : black, θ_2^g : red, θ_3^g : green, θ_4^g : blue



(a) mode shape 5

(b) mode shape 6

Figure 5.63: Mode shapes 5 and 6 and scaled to unit modal displacement obtained using the numerical model $G_{M,2}$ by analyzing numerical response using the SSI method. θ_1^g : black, θ_2^g : red, θ_3^g : green, θ_4^g : blue

Table 5.20: The input parameters of $G_{M,1}$ used to calculate Q_V

θ^g [kg]	$F_{w,1}$ [N]	$F_{w,2}$ [N]	$E_{p,1}$ [N/mm ²]	$E_{p,2}$ [N/mm ²]	F_y/F_z	E_c [N/mm ²]
0	15	15	3000	4000	0.5	45
0.5	10	10	3000	4000	0.5	30
1	5	5	3000	4000	0.5	15
1.5	0	0	3000	4000	0.5	0

Table 5.21: The input parameters of $G_{M,2}$ used to calculate Q_V

θ^g kg	$F_{w,1}$ [N]	$F_{w,2}$ [N]	$E_{p,1}$ [N/mm ²]	$E_{p,2}$ [N/mm ²]	F_y/F_z	$C_{d,z}$ [N×s/mm]	$C_{d,y}$ [N×s/mm]
0	15	15	3000	4000	0.5	0.01	0.01
0.5	10	10	3000	4000	0.5	0.008	0.008
1	5	5	3000	4000	0.5	0.002	0.002
1.5	0	0	3000	4000	0.5	0	0

Table 5.22: The quality of the numerical model $G_{M,1}$ compared to the experimental model G_E

x [m]	$Q_{V,i}(y)$	$Q_{V,i}(z)$
3	0.00	0.74
2.5	1.00	0.96
2	1.00	1.00
1.5	0.99	0.93
1	0.00	1.00
Q_V	0.76	

Table 5.23: The quality of the numerical model $G_{M,2}$ compared to the experimental model G_E

x [m]	$Q_{V,i}(y)$	$Q_{V,i}(z)$
3	0.99	0.95
2.5	0.99	0.96
2	0.98	0.98
1.5	1.00	0.97
1	0.99	0.98
Q_V	0.98	

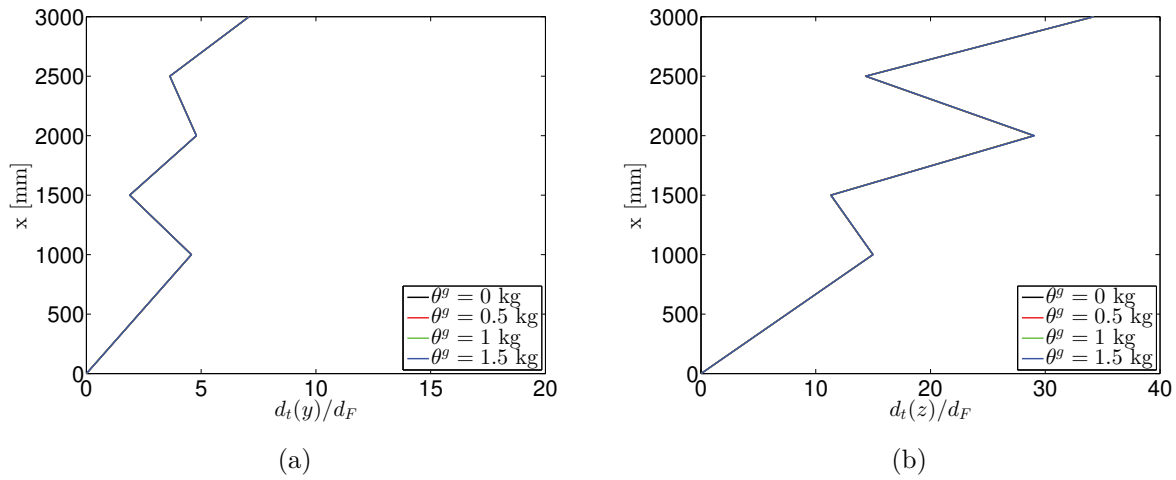


Figure 5.64: d_t/d_F under the same excitation using the first model $G_{M,1}$

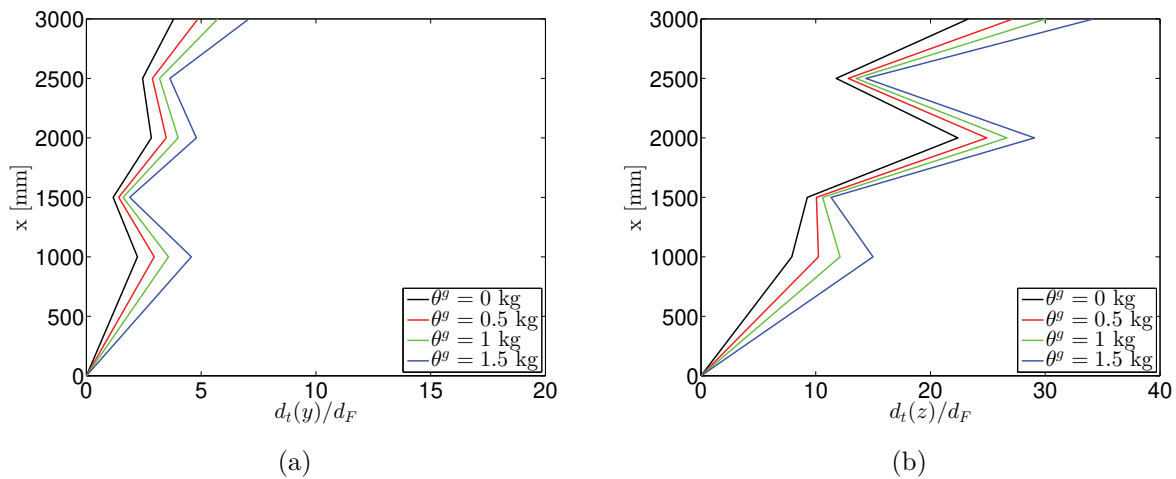


Figure 5.65: d_t/d_F under the same excitation using the second model $G_{M,2}$

5.2.5 Design of Experiments

Since it was observed that cables might have a damping effect and based on the results of the SDOF example, figure 3.14, impulse excitation was chosen to investigate the cable's effect. The cumulative signal energy d of the acceleration time histories $[\ddot{u}(t)] = [\ddot{y}(t), \ddot{z}(t)]$ were used as an output structural response to detect damage. The variation of the structural response due to uncertainty in the mass of the sensor was omitted since it was possible to measure it in the laboratory.

For both developed numerical models $G_{M,1}$ and $G_{M,2}$, the uncertainty in the elastic modulus of the cantilever E_p was considered. The influence of the asymmetry of the variation of the structural response was investigated by including the force F_y as a random variable. In the

Table 5.24: The statistical properties of the prior density functions of the input parameters of the developed numerical model $G_{M,1}$

	$F_{w,1}$ [N]	$F_{w,2}$ [N]	$E_{p,1}$ [N/mm ²]	$E_{p,2}$ [N/mm ²]	E_c [N/mm ²]	F_y/F_z
μ	15	15	3500	3500	15	0.5
Max	20.19	20.19	4712	4712	28	2.23
Min	9.81	9.81	2288	2288	2	-1.232
COV	0.2	0.2	0.2	0.2	0.5	2

case of the first model $G_{M,1}$, the uncertainty in the elastic modulus of the cables E_C was considered. In the second model $G_{M,2}$, the uncertainty in the properties of the cables as dampers was considered. The studied uncertainty was introduced in the numerical model by assigning probabilistic models based on the uniform distribution to the chosen parameters, table 5.24 and table 5.25.

Similar to what was applied in the previous section, the time history of the impulse excitation F_z for damage case 1 (no damage: $\theta_1^g = 0$), which was recorded during the laboratory modal test and shown in figure 5.51, was applied after applying F_w and performing the initial transient analysis. The energy of noise signal d_γ due to ambient vibration excitation γ_F was considered $0.05 \times d_{t,min}$. d_γ was chosen based on the response of the structure without excitation. As a result, $\bar{d} = d_t - d_\gamma = 0.95 \times d_{t,min}$. Uncertainty ϵ due to instrumentation, initial conditions and sensor quality was considered as a normally distributed uncertainty with zero mean and standard deviation $\sigma_\epsilon = 0.05\bar{d}$, eq. (5.28). In this example, σ_ϵ was assumed. However, it can be increased if other factors influence the response.

$$\epsilon \sim \mathcal{N}(0, \sigma_\epsilon^2) \quad (5.28)$$

Table 5.25: The statistical properties of the prior density functions of the input parameters of the developed numerical model $G_{M,2}$. $C_{d,y,1}$, $C_{d,y,2}$, $C_{d,z,1}$ and $C_{d,z,2}$ are given in N×s/mm

	$F_{w,1}$ [N]	$F_{w,2}$ [N]	$E_{p,1}$ [N/mm ²]	$E_{p,2}$ [N/mm ²]	$C_{d,y,1}$	$C_{d,y,2}$	$C_{d,z,1}$	$C_{d,z,2}$	F_y/F_z
μ	15	15	3500	3500	0.004	0.004	0.004	0.004	0.5
Max	20.19	20.19	4712	4712	0.0075	0.0075	0.0075	0.0075	2.23
Min	9.81	9.81	2288	2288	0.0005	0.0005	0.0005	0.0005	-1.232
COV	0.2	0.2	0.2	0.2	0.5	0.5	0.5	0.5	2

A Latin hypercube sampling method was used to generate $N = 1000$ samples to investigate the variation of the response d due to the input parameters $\{\theta\}$. The size of the sample was

chosen as a trade off between the required computational time and quality of the Meta-models that were developed in the next step to solve more samples. The structural response $\ddot{u}(t) = [\ddot{y}(t), \ddot{z}(t)]$ for damage case 1 ($\theta^g = 0$) was computed for each sample. The cumulative signal energy values $\{d\}$ of the acceleration time histories $\ddot{u}(t)$ were computed based on eq. (3.5). For all samples, the initial conditions $u(0) = \dot{u}(0) = 0$ and a constant excitation F_z were applied.

5.2.6 Sensitivity analysis

The sensitivity analysis method described in section 3.4 was used to obtain information about the contribution of $\{\theta\}$ to the outputs $\{d\}$. Meta-models $\{d\}$ were developed to perform the sensitivity analysis. The data sets which include $N = 1000$ samples calculated in the previous subsection were used. The statistical properties of the residuals were examined to ensure that they satisfy the requirements described in section 3.4.4. The Total-effect index sT values were calculated using $[d]$ for both models $G_{M,1}$ and $G_{M,2}$. Figure 5.66 shows the results of the applied sensitivity analysis.

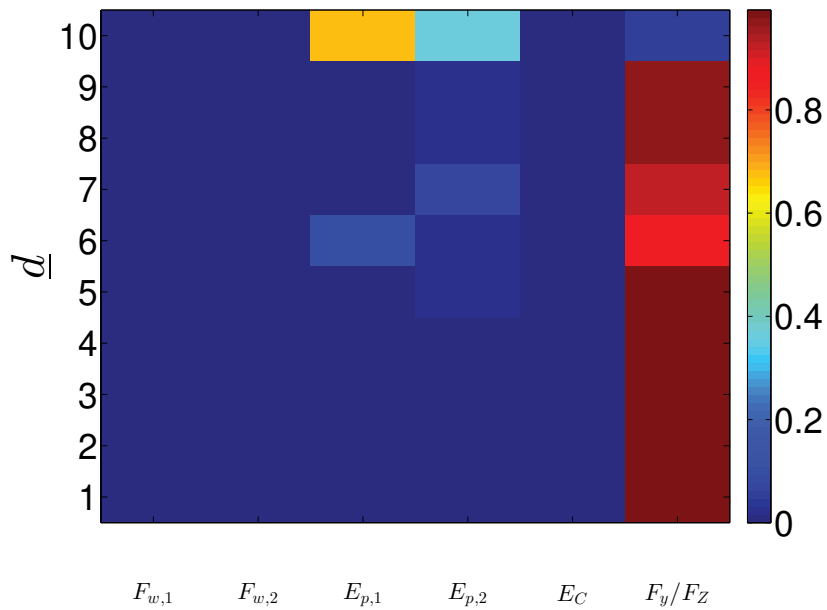
In case of the first model $G_{M,1}$ the Total-effect index sT values show that the studied structural response is sensitive to F_y , $E_{p,1}$ and $E_{p,2}$. This means that the asymmetry of the structure influences the studied response more than the studied damage.

In case of the second model $G_{M,2}$, the Total-effect index sT values show that the studied structural response is sensitive to F_y , $E_{p,1}$, $E_{p,2}$ and the damping constant $C_{d,y}$. Since $C_{d,y}$ is a part of the studied damage model, it is expected that if the second model $G_{M,2}$ is chosen to evaluate the performance of the inspection method, damage will be detected faster than if the first model $G_{M,1}$ is chosen. The quality of the DOE models considering $G_{M,1}$ and $G_{M,2}$ can be obtained based on the eq.(5.29).

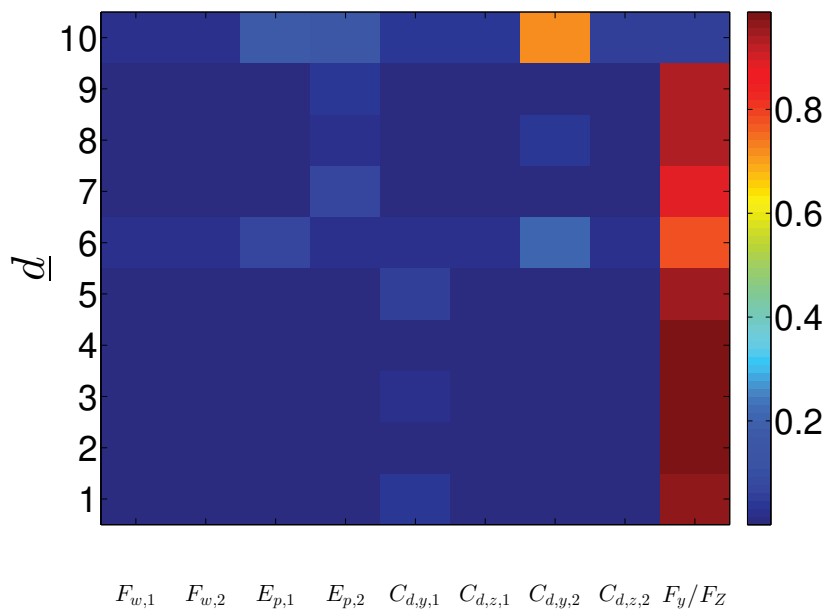
$$Q_{DOE} = \begin{cases} \frac{sT(F_{w,1}, F_{w,2}, E_C)}{sT(\{\theta\}|G_{M,1})} = \frac{0.06}{10.2} \approx 0 & \text{for } G_{M,1} \\ \frac{sT(F_{w,1}, F_{w,2}, C_{d,y,1}, C_{d,y,2}, C_{d,z,1}, C_{d,z,2})}{sT(\{\theta\}|G_{M,2})} = \frac{1.52}{10.6} \approx 0.15 & \text{for } G_{M,2} \end{cases} \quad (5.29)$$

5.2.7 Model updating

Meta-models $\{\hat{d}\} = f(\{\hat{\theta}\})$ were developed for model updating. In case of the first model $G_{M,1}$, three parameters were considered to be important $\{\hat{\theta}\} \equiv \{E_{p,1}, E_{p,2}, F_y/F_z\}$. In case of the second model $G_{M,2}$, five parameters were considered to be important $\{\hat{\theta}\} \equiv \{E_{p,1}, E_{p,2}, C_{d,y1}, C_{d,y2}, F_y/F_z\}$. Uniform distribution-based prior probability density functions, given in table 5.24 and table 5.25, were assigned to the input parameters that should be updated.



(a) $sT_{i,j}$ calculated using $G_{M,1}$



(b) $sT_{i,j}$ calculated using $G_{M,2}$

Figure 5.66: Total-effect index $sT_{i,j}$ calculated using the numerical models $G_{M,1}$ and $G_{M,2}$. Channel numbers from 1 to 5 are in y direction, and 6 to 10 are in z direction.

Applying the Bayesian updating approach explained before in section 3.5, the posterior density functions $p(\{\theta\}|\{\bar{d}\})$ of the parameters $\{\hat{\theta}\}$ were computed in case of both numerical models,

figures 5.67, 5.68. The statistical properties of the posterior density functions of the input parameters for each numerical model are presented in tables 5.26, 5.27.

In case of the first numerical model $G_{M,1}$, applying model updating produces a significant difference between $E_{p,1}$ and $E_{p,2}$ to represent the influence of the asymmetry of the structure on the studied structural response. In case of the second numerical model $G_{M,2}$ the influence of the asymmetry of the structure was maintained by increasing F_y/F_z and the difference between $E_{p,1}$ and $E_{p,2}$.

In order to evaluate the quality of the measurements for each numerical model, the index Q_M given in eq. (3.47) was computed. In case of $G_{M,1}$, the parameter related to damage which was E_c in this example was not updated. Therefore, $Q_{M,1} = 0$. In case of $G_{M,2}$, only 2 parameters of 6 related to damage were updated. They are: $C_{d,y1}$ and $C_{d,y2}$. Therefore, $Q_{M,2}$ can be calculated as follows:

$$Q_{M,2} = 1 - \frac{1}{6} \left(\frac{\sigma_{C_{d,y1}|\bar{d}}}{\sigma_{C_{d,y1}}} + \frac{\sigma_{C_{d,y2}|\bar{d}}}{\sigma_{C_{d,y2}}} \right) = 1 - \frac{1}{6} \left(\frac{7 \times 10^{-5}}{5 \times 10^{-4}} + \frac{2 \times 10^{-5}}{5 \times 10^{-4}} \right) = 0.3 \quad (5.30)$$

5.2.8 Assessment of the inspection method

The developed method in section 3.6.2 was applied. Damage $\theta_i^g \in [0 \text{ } 90\%] \times 15 \text{ [N]}$ was used to calculate the response $d_i(\theta_i^g)$ with an interval $\Delta\theta^g = 0.015 \times 15$. Based on eq. (3.63), if (PFP=0.05) and for n=10 output (channels), N=196. The number of samples for each damage step $\Delta\theta^g$ was increased until $POD(\theta_i^g)$ converged. The investigation shows that $N = 1000$ samples for each damage step are sufficient to obtain constant POD curves.

Table 5.26: The statistical properties of the posterior density functions of the input parameters calculated using $G_{M,1}$

	$E_{p,1}$ [N/mm ²]	$E_{p,2}$ [N/mm ²]	F_y/F_z
μ	7100	2575.6	0.25
σ	27.4	41.3	0.008

Table 5.27: The statistical properties of the posterior density functions of the input parameters calculated using $G_{M,2}$

	$E_{p,1}$ [N/mm ²]	$E_{p,2}$ [N/mm ²]	$C_{d,y,1}$ [N×s/mm]	$C_{d,w,y,2}$ [N×s/mm]	F_y/F_z
μ	8520.5	6549.3	0.0018	0.0019	0.40
σ	141.3	104.2	7×10^{-5}	2×10^{-5}	0.011

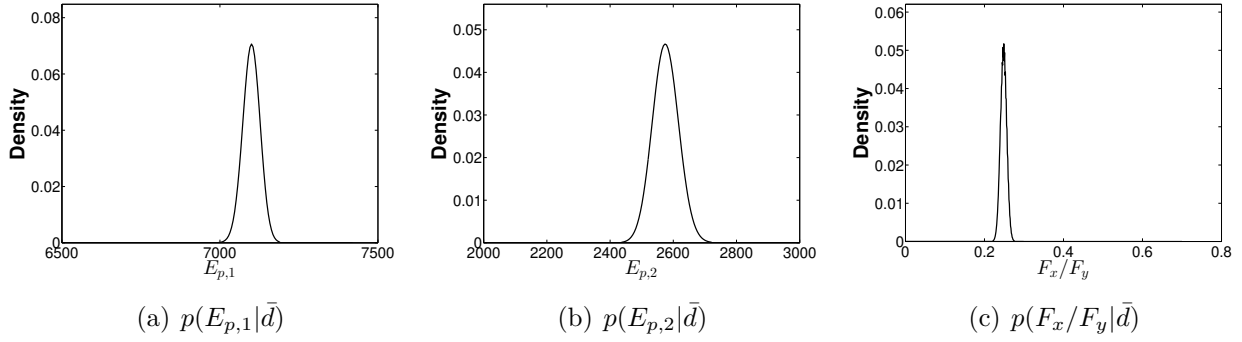


Figure 5.67: Posterior density functions of the updated input parameters using $\{\bar{d}, G_{M,1}\}$

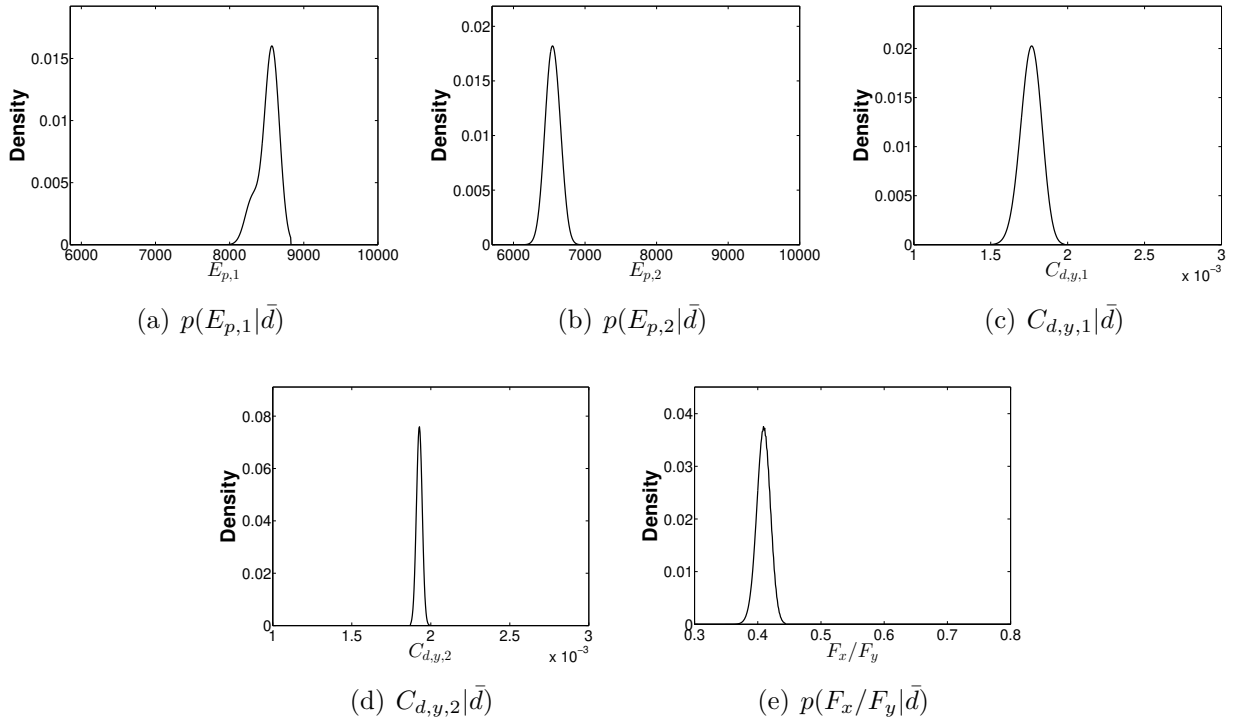


Figure 5.68: Posterior density functions of the updated input parameters using $\{\bar{d}, G_{M,2}\}$

In case of $G_{M,1}$, damage was increased by reducing F_w and E_c based on eq. (5.23) as follows:

$$\forall \theta_{\Delta i}^g, \theta_{\Delta i+1}^g : \theta_{\Delta i+1}^g = \theta_{\Delta i}^g + \Delta \theta^g \Rightarrow F_{w,\Delta i+1} = F_{w,\Delta i} - 0.015 \times 15, E_{C,\Delta i+1} = 3.125 \times F_{w,\Delta i+1} + \epsilon_{E_c} \quad (5.31)$$

where $F_{w,\Delta i}$ refers to the cable forces after reducing it by $0.015 \times 15 \times i$ where $i = 1, 2, \dots$. ϵ_{E_c} refers to the uncertainty of E_c which is given in table 5.24.

In case of $G_{M,2}$, damage was increased by reducing F_w , $C_{d,y}$ and $C_{d,z}$ as follows:

$$\forall \theta_{\Delta i}^g, \theta_{\Delta i+1}^g : \theta_{\Delta i+1}^g = \theta_{\Delta i}^g + \Delta \theta^g \Rightarrow F_{w, \Delta i+1} = F_{w, \Delta i} - 0.015 \times 15, C_{d, \Delta i+1} = C_{d, \Delta i} - 0.015 \times C_{d, 0} + \epsilon_{C_d} \quad (5.32)$$

where $C_{d, \Delta i}$ refers to the damping constant of the cable after reducing it by $0.015 \times C_{d, 0} \times i$ where $i = 1, 2, \dots$. $C_{d, 0}$ refers to the initial value of the damping constant corresponded with damage case 1 (no damage) after model updating. $C_{d, 0}$ value is given in table 5.27. ϵ_{C_d} refers to the uncertainty of $C_{d, 0}$ after model updating. Figure 5.68 shows that the posterior density functions $p(C_d | \bar{d})$ have a distribution shape close to the normal distribution. Therefore $\epsilon_{C_d} \sim \mathcal{N}(0, \sigma_{\epsilon_{C_d} | \bar{d}}^2)$. $\sigma_{\epsilon_{C_d} | \bar{d}}$ values are given in table 5.27.

Figures 5.69 and 5.70 show that the reliability of the studied inspection method depends on the chosen numerical model. Based on the problem definition given in eq. (5.20), in case of $G_{M,1}$, the smallest damage that can not be missed is $\theta^g \approx 7$ N. However, in case of $G_{M,2}$, the smallest damage that can not be missed is $\theta^g \approx 0.22$ N.

The inspection method was evaluated at $\theta^g = 0.5$ N by computing the index Q_D using eq. (3.61). It was found that $Q_D(G_{M,1}) = 0$ and $Q_D(G_{M,2}) = 1$.

The developed method in section 3.6.2 was applied to calculate the probability of damage detection using experimental data. 10 samples were used for damage case. The result is presented in figure 5.71. The results show that detecting damage is faster than what $G_{M,1}$ show. However, it is not possible to compare the results directly to $G_{M,2}$ results since smaller damage size interval in case of experiments is required.

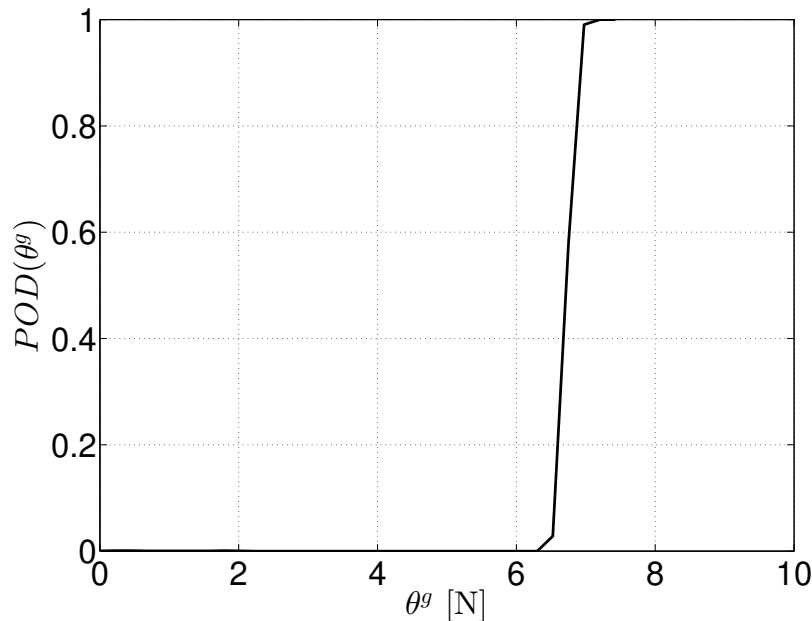


Figure 5.69: $POD(\theta^g)$ curve using $G_{M,1}$

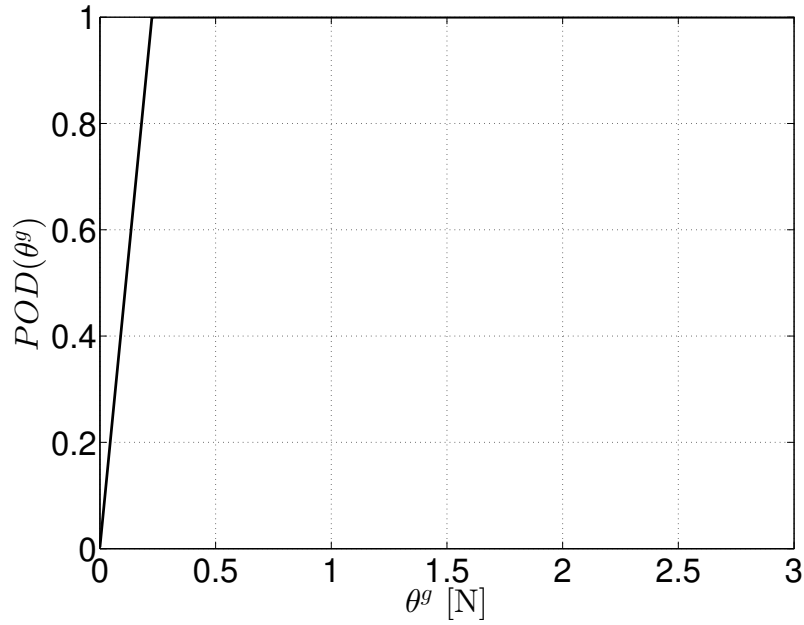


Figure 5.70: $POD(\theta^g)$ curve using $G_{M,2}$

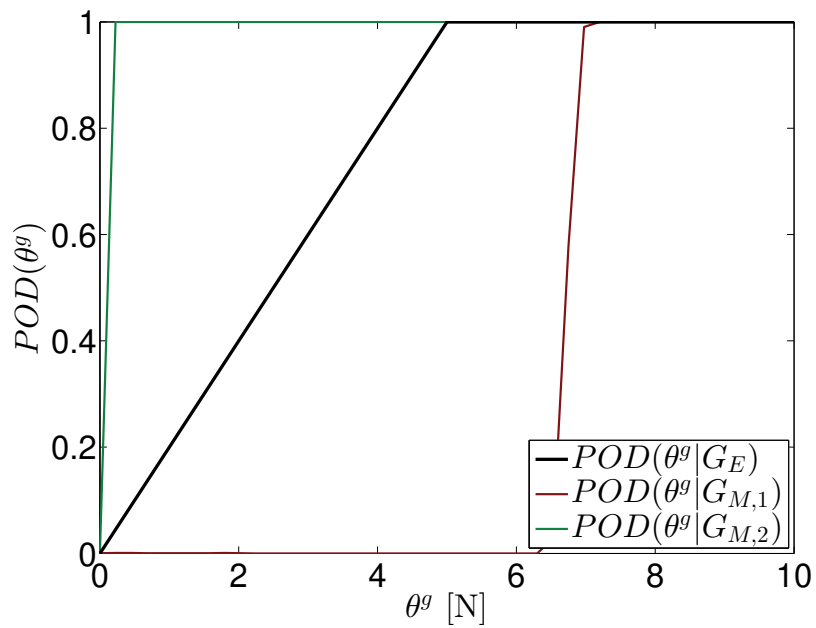


Figure 5.71: Comparison between $POD(\theta^g)$ curves obtained G_E , $G_{M,1}$ and $G_{M,1}$

5.2.9 Conclusion

In this example, the performance of a vibration-based inspection method to detect damage in a cantilever structure was tested. Two damage models were considered. The following results can be pointed out:

- The reliability of the inspection method depends on the defined damage model.
- All phenomena which might influence the response of the structure and could cause false alarm should be investigated. For example, the asymmetry and nonlinear behavior.
- The quality of the assessment of the performance of the inspection method is independent of the representation of the phenomena considered in the developed models. Q_D quantifies the reliability of an inspection method. The accuracy of the computed Q_D quantifies the quality of the reliability assessment method, and this depends on the accuracy of Q_V , Q_{DOE} , and Q_M as well.
- Sufficient damage size interval is required to evaluate the performance of the chosen inspection accurately.

Chapter 6

Reference Object: Pole

6.1 Introduction

In many engineering disciplines, such as mechanical engineering, producing large amounts of standardized products provides the opportunity to apply a well-defined reliability assessment procedure which is based on inspecting a large number of samples that emulate a real structure or a part of it. Strict statistical restrictions related to the test conditions, for example, the number of samples, damage size interval, the number of repetition can be precisely followed. In civil engineering discipline, each structure is a unique product. Therefore, in most cases applying a traditional reliability assessment procedure is not possible. However, there are some rare cases where civil engineering standardized products are produced in large amounts. In this chapter, one of these rare cases is presented.

The main objective of this application is to investigate the performance of an inspection method for damage detection in identical structures. Poles used for electricity cables or light poles, provide the opportunity to investigate the variability of many nearly identical structures.

The influence of choosing different experimental models G_E on the reliability of the inspection method for damage detection is investigated taking into account two test setups.

The test setups and the modal parameters obtained from experiments are presented. The numerical model is used to perform a statistical study and to calculate the probability of damage detection.

6.2 Problem definition and test setup

A series of poles that will be used to carry the catenary system of a new railway line was chosen for this investigation. Since sets of the poles were designed and manufactured to be identical,

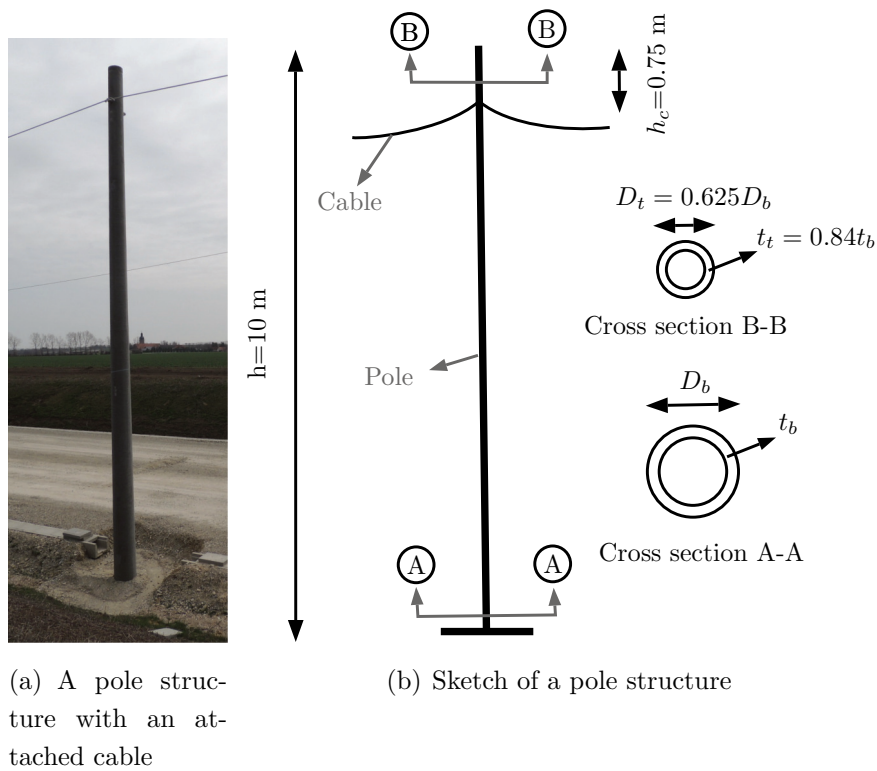


Figure 6.1: One of the studied pole structure and a sketch shows cross sections

they proved to be the perfect candidates for repeated experimentation. Their location along a railway construction site also provided convenient access to a large number of them in close proximity.

While the structural system is rather simple (a cantilever), the fact that there is a large number of identical poles allows for types of investigations that are usually not possible for most civil engineering structures. Each pole considered in this study was of the same type (same material, reinforcement, and intended use) and is 10 m tall including the foundation, figure 6.1. During the production process each pole was pre-stressed by applying a tension force F_{ps} on the reinforcement before casting concrete. The tension was released and transferred to the concrete as compression after the concrete cured.

Dynamic measurements were collected using uniaxial accelerometers. A test system was constructed to attach the sensors on each pole quickly and to ensure that the measurement locations remained the same relative to the top of the structure. Ribbons were placed on each side of a wooden plate to create two lines of sensors perpendicular to each other. Small wooden blocks were placed along the ribbons at a distance of 0.75 m that conformed to the shape of the pole and had small steel plates fixed to them. The accelerometers were fastened to a separate set of steel plates of the same size with high strength magnets on the opposite side. Elastic bands were wrapped around the pole and fixed to the wooden blocks to keep them securely fastened to the structure. The sensor magnet assembly could then be quickly fixed to

and removed from the pole at each measurement location. Environmental conditions, such as wind and temperature, could not be controlled since the measurements were taken outside on site. However, the temperature was measured during each test. Generally, temperature varied between 20° and 25° C. Although no wind speed measurement was performed, it was observed that often the wind speed in the last two days was higher than the wind speed in the first two days. A total of 26 poles were investigated over the course of four days. At that time the construction site was not finished only cables with different sag/tension were attached to the poles, and no catenary was installed.

According to the orientation of the accelerometers, the coordinate system was defined as follows: z: vertical, x and y: horizontal. The sensors were placed to construct almost 45° according to the cables, figure 6.2.

Two setups of the accelerometers were used, table 6.1,: one reference and five roving sensors per setup and measurement direction. This totaled in 11 components in each direction with a reasonably dense vertical grid over the top 7.5 m of the pole, figure 6.3. Four different excitations were used: sweep sine shaker in x-direction applied to the top of the pole, ambient, hammer in y-direction applied close to 2.5 m measured from the base of the pole (about 2 m above the ground level), and Gaussian white noise from the shaker in x-direction applied to the top of the pole.

In this study, the influence of the cables on the structural response was investigated similar to the cantilever example in chapter 5. Therefore, the focus was only on the results obtained from the hammer excitation. The primary goal was to obtain the minimum damage size that can be missed considering different experimental models G_E and two sensor setups (S_1 and S_2 in table 6.1).

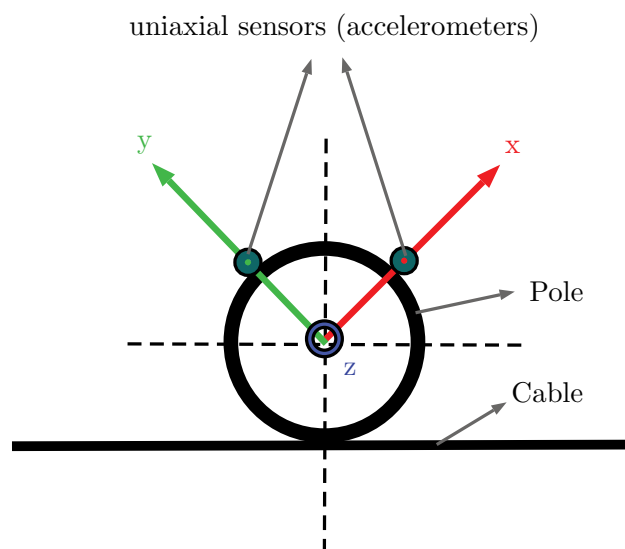
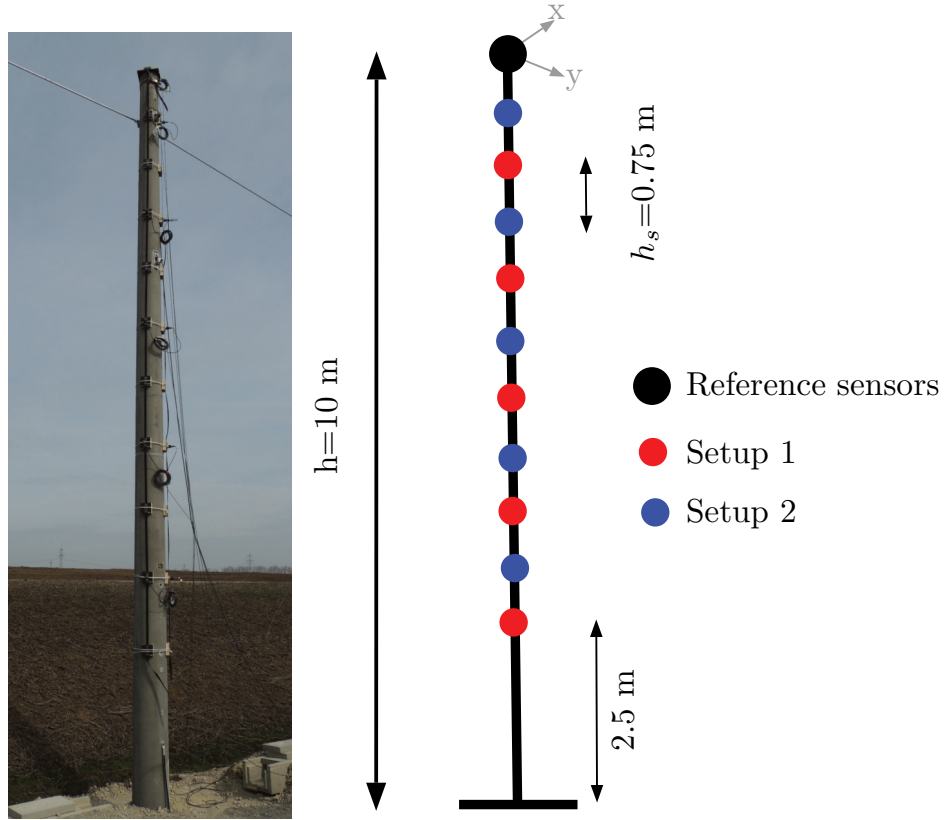


Figure 6.2: Top view of the sensor location



(a) Test system constructed on a pole (b) Sketch shows the sensors locations in both test setups

Figure 6.3: Developed test system used to perform dynamic measurements on the studied structure

Table 6.1: Sensor locations for each test setup measured from the base of the pole

Setup	Sensor Nr.					
	1	2	3	4	5	6 Ref.
S_1	2.5	4	5.5	7	8.5	10 [m]
S_2	3.25	4.75	6.25	7.75	9.25	10 [m]

$$\forall \theta^g : POD(\theta^g + \Delta\theta^g) = 1 \text{ and } POD(\theta^g - \Delta\theta^g) < 1 \text{ and } PFP \leq 0.05 \text{ given } G_{E,ip}, S_{is} \quad (6.1)$$

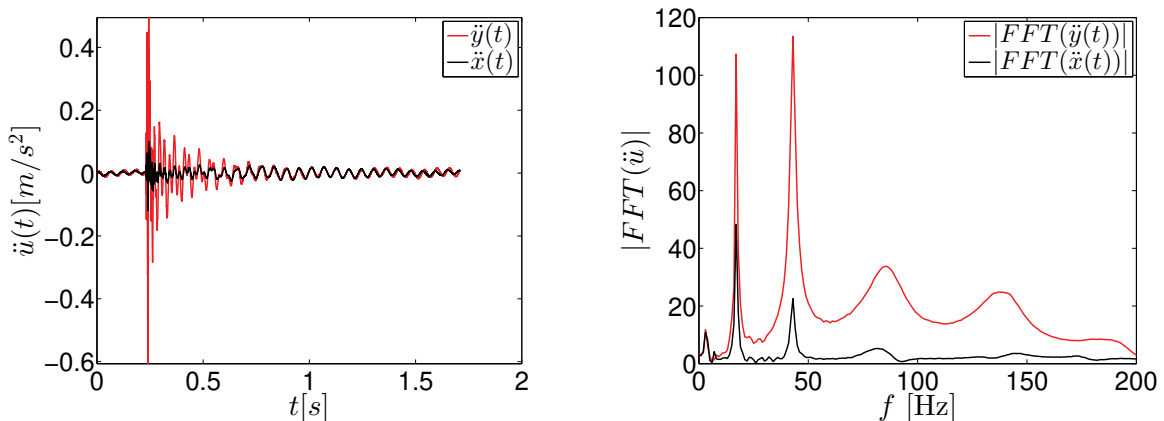
where $ip = 1, 2, \dots, 26$ refers to the chosen pole and $is = 1, 2$ refers to the chosen setup.

6.3 Test results

The acceleration time histories from each excitation and pole were combined between the two setups and used to identify the dynamic properties of each pole using the procedure explained in appendix C where the stochastic subspace identification (SSI) method was used to obtain the modal parameters, which are summarized in table 6.2 by their occurrence and statistical properties. Eight modes were consistently identified on the poles, figures 6.5 – 6.8. 16 poles were analyzed to get the statistical properties. For each pole, several tests were performed. The mean values of the frequencies and modal damping for each pole and for each mode were computed from different tests. Finally, the mean value of the means and the standard deviation of the means of the modal parameters were calculated and presented in table 6.2 for the 16 poles. In some tests, especially under impulse excitation, it was not possible to obtain all 8 modes.

The results show that structures assumed to be identical show considerable variation in their dynamic parameters. It was found that uncertainty in the damping ratios was more significant than the uncertainty in frequencies. The uncertainty of the mode shapes increases in case of higher modes.

The signal energy \bar{d}_t of the recorded acceleration signals was calculated for each applied impulse and for each setup in x and y direction based on eq. (3.5), figure 6.9 and 6.10. The results show that although the excitation force was applied in y direction, the values of the signal energy in x direction $\bar{d}_t(x)$ in many cases may reach about 50 % of the signal energy values in y direction $\bar{d}_t(y)$, $\bar{d}_t(x) \approx 0.5\bar{d}_t(y)$. The asymmetry of the system caused by cables or other factors can be the reason of obtaining these results.



(a) Time history of the acceleration measured at the top of the pole Nr.262-26 (b) |FFT| shows the response of the structure in frequency domain

Figure 6.4: Structural response at the top of the pole Nr.262-28 under an impulse excitation

Table 6.2: Statistical properties of the natural frequencies and modal damping ratios extracted from measurements obtained from 16 poles

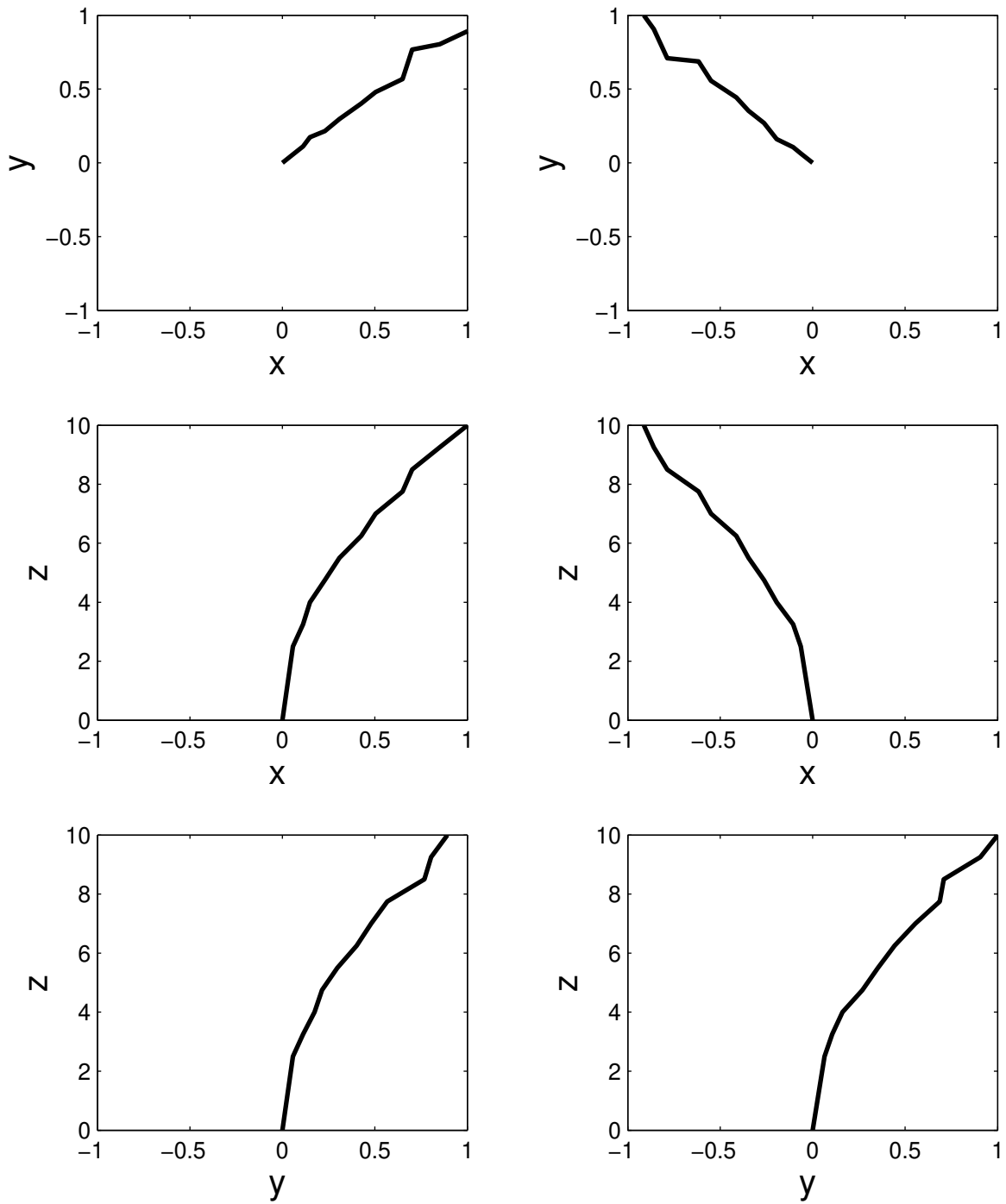
	1	2	3	4	5	6	7	8
μ_f [Hz]	3.476	3.912	17.480	17.601	45.634	45.203	87.465	87.958
σ_f	0.069	0.082	0.519	0.303	0.948	0.993	1.274	1.038
COV	0.020	0.021	0.030	0.017	0.021	0.022	0.015	0.012
μ_ζ %	0.595	5.173	2.043	0.768	2.099	2.235	3.666	3.662
σ_ζ	0.268	2.370	0.821	0.250	1.055	0.729	0.452	0.677
COV	0.450	0.458	0.402	0.325	0.503	0.326	0.123	0.185

6.4 Numerical model

Two finite element models were developed to investigate the influence of the cables on the studied structure, figure 6.11. A shell element type was used to model the pole, and a beam element type was used to model the reinforcement bars. The cables were modeled in the first numerical model G_{MR} , figure 6.11 (a), which is considered as a reference model. In the second numerical model G_M , figure 6.11 (b), the cables were replaced by a mass point equivalent to the mass of the cables. The influence of the stiffness of the cables was ignored in G_M . Checking the quality of G_M compared to G_{MR} in case of damage detection can show if the stiffness of the cables influences the assessment of the performance of the chosen inspection method. Moreover, replacing the cables with a mass point reduces the computational time of about 40 %.

Based on the construction plans of the pole and the cables provided by the manufacturer, it was possible to obtain all the inputs related to the geometrical and the material properties as well as the pre-stress force F_{ps} . Ten cross sections were used to consider the variation of the cross-section of the pole from the base to the top. The variation of the cross section was considered to be linear along the height of the pole.

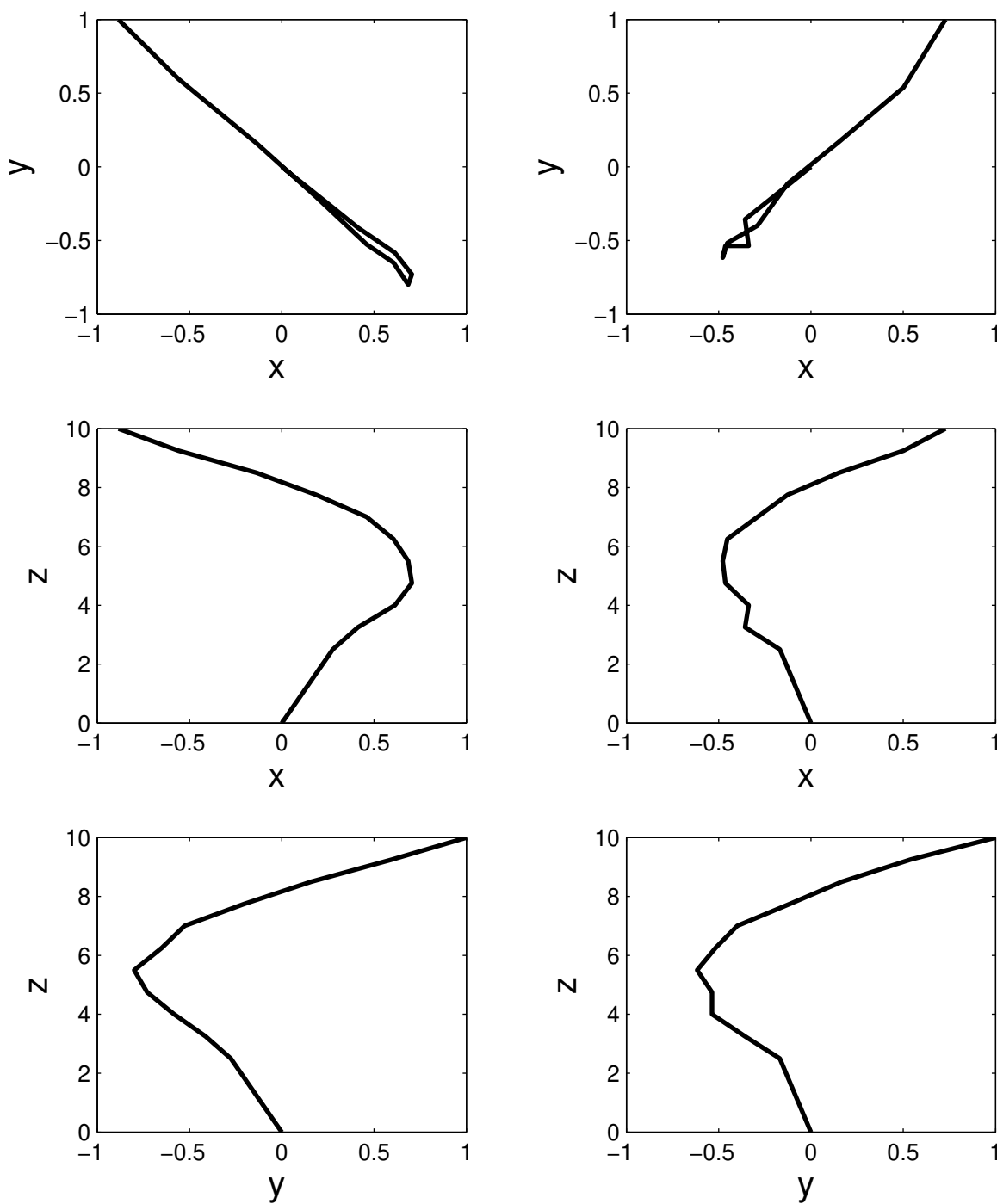
Since the results of the modal tests show that mode 2 has high damping ratios, it is expected that the cables have a damping effect. Therefore, two viscous dampers were added to the model. The first damper, which has a constant $C_{d,1}$, was oriented perpendicular to the cables and the second damper, which has a constant $C_{d,2}$, was oriented in the direction of the cables. The dampers were attached to the pole model in the same node where the cables attached to the pole in the reference model G_{MR} . If the pole behaves similar to the PVC cantilever which was studied in the previous chapter, it can be expected that damage influences both the first and second modes more than the higher modes. This means if measurements don't capture both first modes, damage may be detected late, or even the inspection method could not be reliable to detect the required damage size.



(a) mode shape 1

(b) mode shape 2

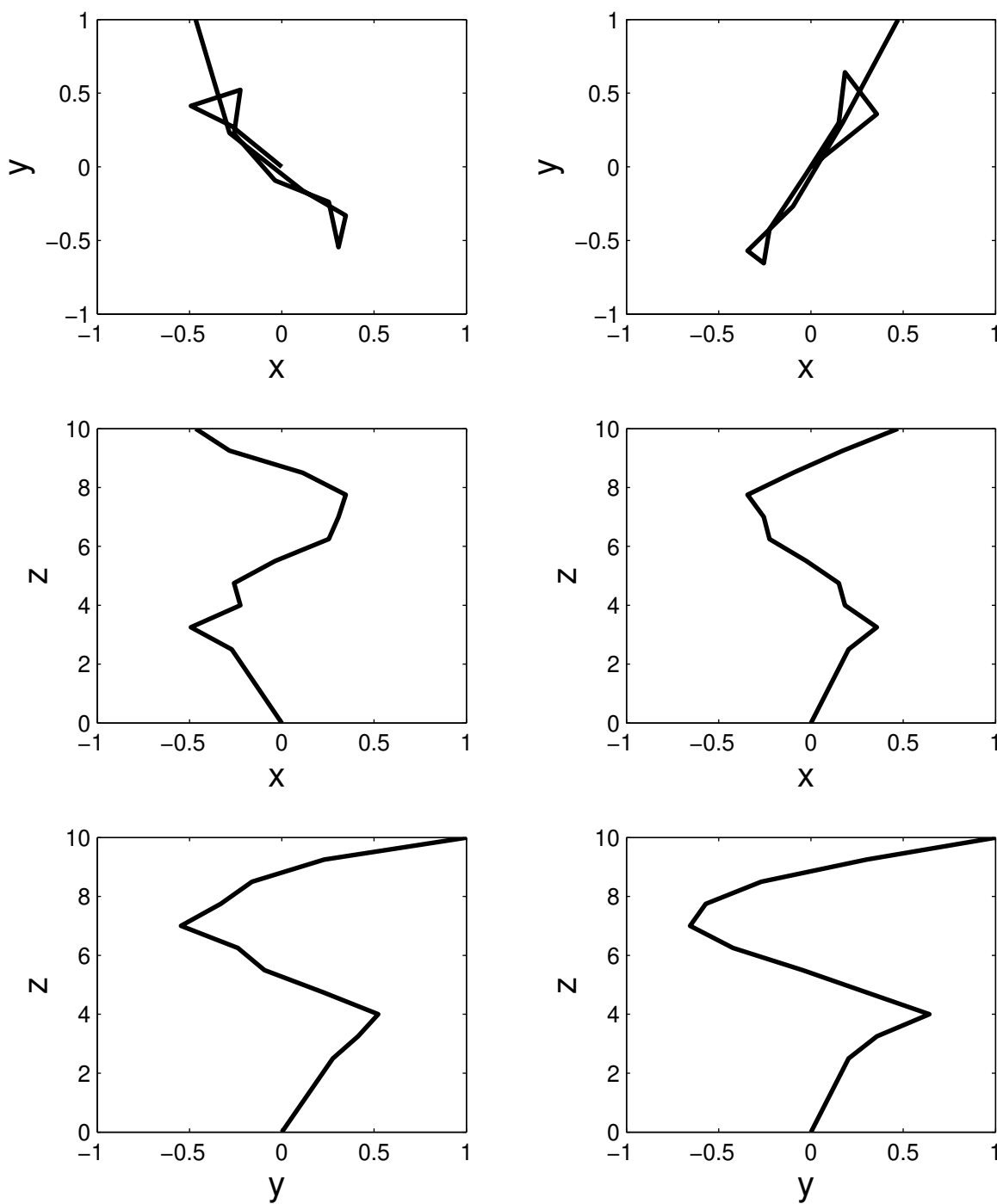
Figure 6.5: Mode shapes 1 and 2 extracted from experimental data



(a) mode shape 3

(b) mode shape 4

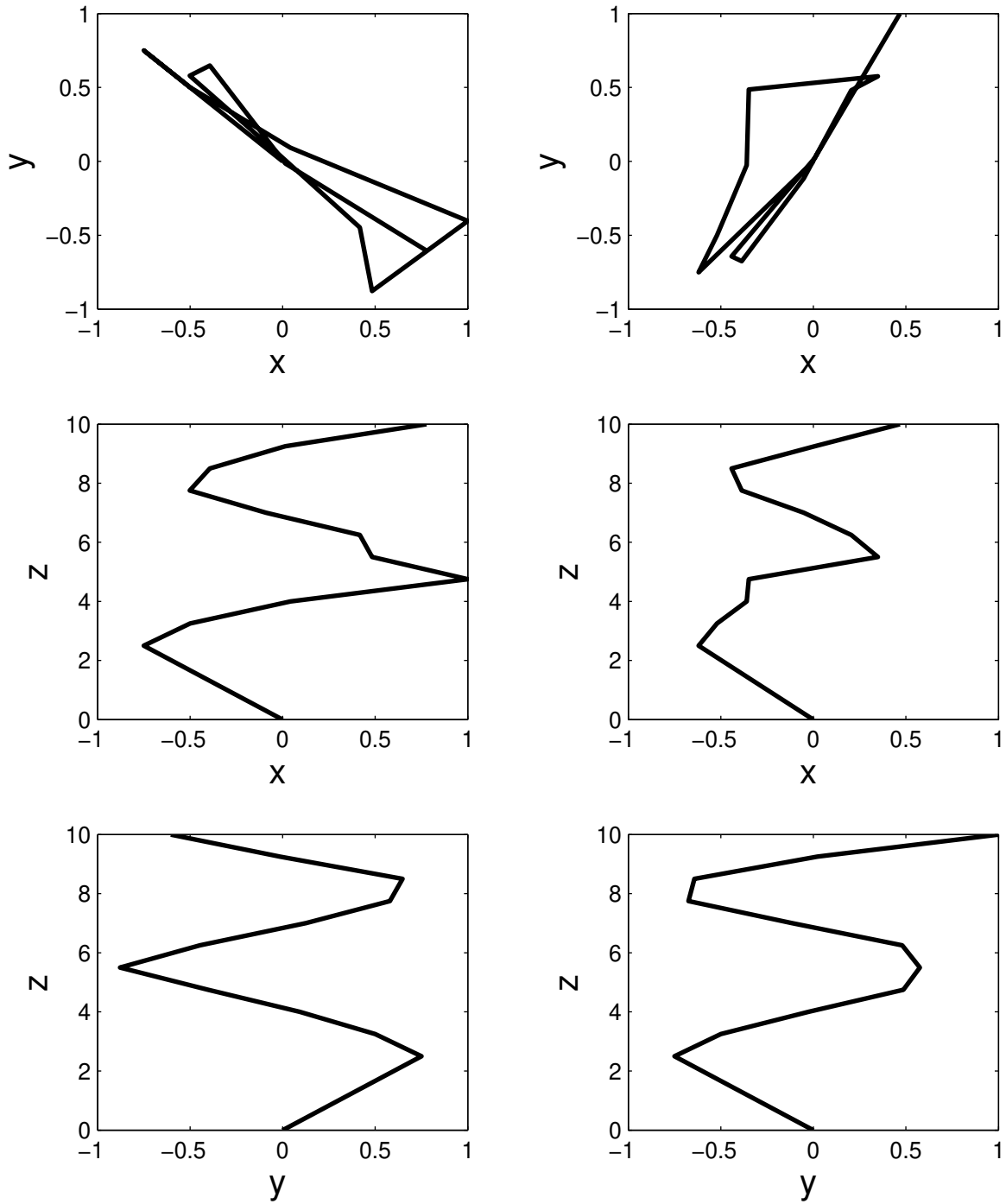
Figure 6.6: Mode shapes 3 and 4 extracted from experimental data



(a) mode shape 5

(b) mode shape 6

Figure 6.7: Mode shapes 5 and 6 extracted from experimental data



(a) mode shape 7

(b) mode shape 8

Figure 6.8: Mode shapes 7 and 8 extracted from experimental data

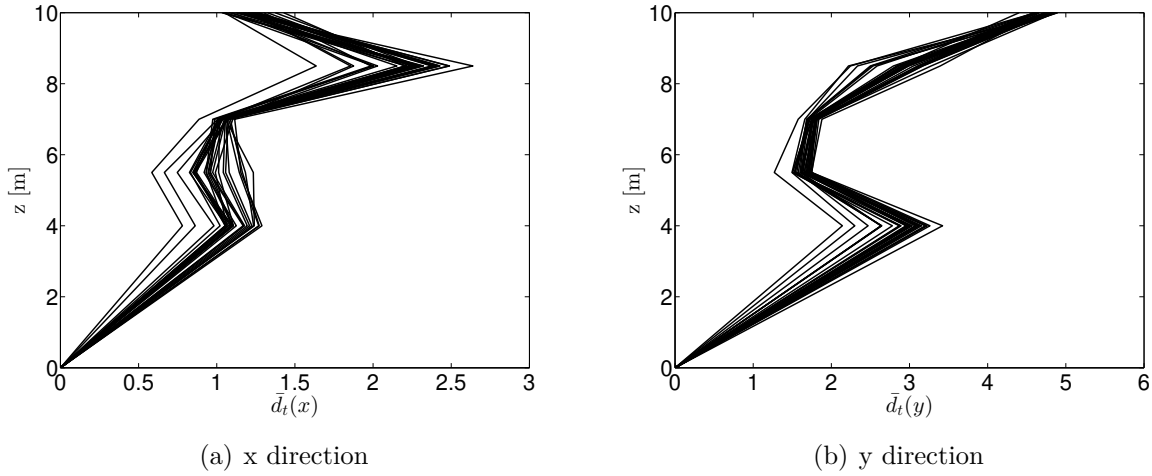


Figure 6.9: \bar{d}_t under 30 impulse excitation setup 1, pole Nr.262-28

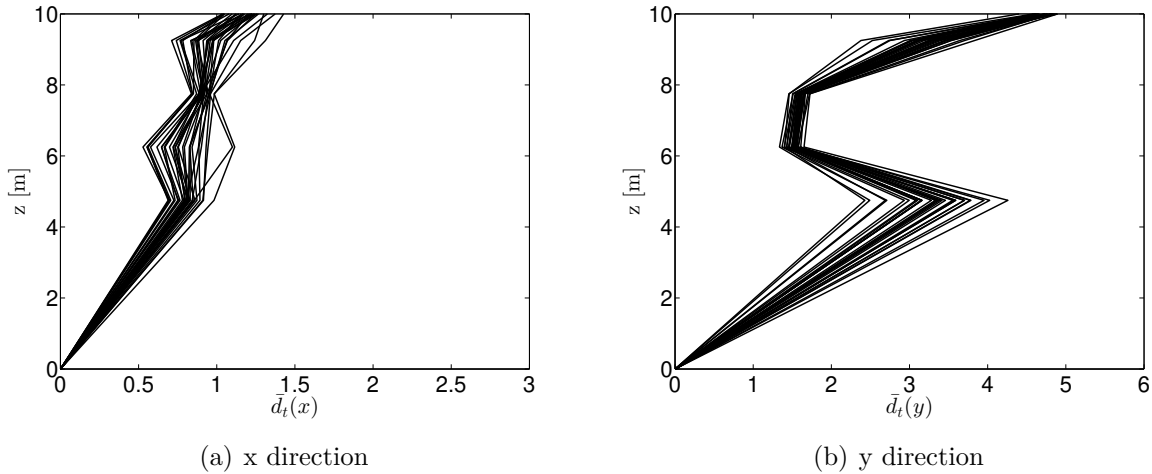


Figure 6.10: \bar{d}_t under 30 impulse excitation setup 2, pole Nr.262-28

The initial values of $C_{d,1}$ and $C_{d,2}$ can be estimated similar to the cantilever example in the previous chapter. The kinetically equivalent mass in case of the first mode $M_{p,1}$ in both directions was approximated here as 25% of the total mass using the simplified assumption of a constant mass distribution. Including the mass of the cables M_c , $M_{p,1} \approx 0.35$ t. $\omega_{E,1} \approx 2 \times \pi \times 3.5 = 22$ rad/s. The critical damping is $C_c \approx 2 \times 350 \times 22 \approx 15400$ N×s/m. It was assumed that $C_d \approx 0.1 \times 15400 = 1540$ N×s/m = 1.54 N×s/mm. In order to include the uncertainty when estimating the effective modal mass from the first mode without considering the higher modes, and the uncertainty of ζ_E the range $C_d = [1-20]$ N×s/mm was considered in the next steps.

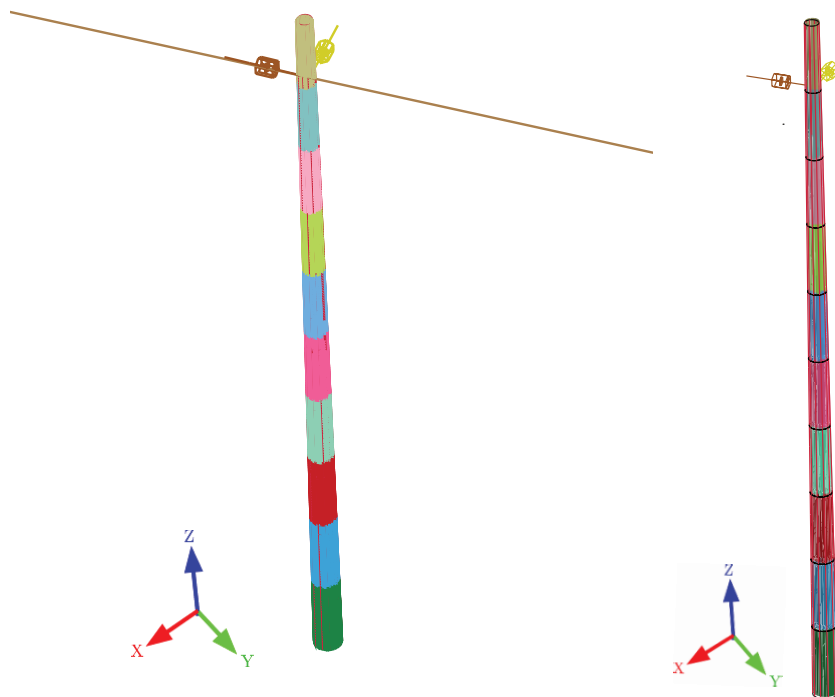
The shell elements were meshed to smaller elements with a maximum size of (40×40) mm². The reinforcement bar beam elements were meshed in a way that the start and the end of each

beam element are coupled to two edge nodes of a shell element. The beam elements of the cables in the reference model G_{MR} were meshed to 500 mm size elements.

Since the sensors were rotated about 45° from the cables, the global numerical models G_{MR} and G_M were rotated 45° about the z-axis. As a result, the computed acceleration signals in x and y-direction can be compared to the measurements directly.

The pole was fixed to the base until 50 cm high before adding the soil which may cover from $L_p = 0$ to 1 m of the lower part of the pole. The variation of L_p is because that the railway was still under construction.

To include the influence of the force F_p on the dynamic response of the structure, a transient analysis was performed after applying F_p to the reinforcement bars as an axial load along their length. The self-weight was included as well to obtain the influence of the mass of the cables on the structure. To avoid the vibration of the structure during the performed analysis, a large damping value was assigned to the model by increasing α in the Rayleigh damping model as shown in figure 6.12. Moreover, after applying the loads, a sufficient duration was considered (1 second) until the response of the model was damped to zero. As a result, the dynamic influence



(a) Numerical model of the studied pole with cables G_{MR} (b) Numerical model of the studied pole G_M . Cables were replaced by a mass point

Figure 6.11: Numerical models developed for evaluating the performance of the studied inspection method

of the applied loads was prevented. After that, the time history of the impulse excitation was applied at the node which represents the location where impulse force was applied on the site. In this stage, the mean values of the modal damping ratios extracted from measurements and presented in table 6.2 was used to develop the Rayleigh damping model, eq. (5.5), with $\alpha = 2.47$ and $\beta = 1.25e-04$. Since no input impulse excitation was measured, the impulse force presented in the previous chapter for in figure 5.51 was applied after amplifying its amplitude 10 times. The frequency rate was chosen as $\Delta f = 4096$ Hz. The computed structural response of the pole is presented in figures 6.14 and 6.15. In the case of G_{MR} , the noise was observed after applying the impulse. This means that smaller time step Δt may be required. The computed acceleration signals under the applied impulse excitation were used for system identification applying the SSI method following the procedure explained in appendix C considering the values of the input parameters for damage case 1 presented in table 6.5 for G_{MR} and 6.6 for G_M . Tables 6.3 and 6.4 show the obtained frequencies and damping ratios from the simulated results. Figures 6.16 – 6.18 and 6.19 – 6.21 show the extracted mode shapes. The results show that it was not possible to obtain the first 2 mode shapes in case of G_{MR} and the first 3 mode shapes in case G_M . Several reasons can be behind not capturing the missing mode shapes. For example, high damping ratios, weak system identification analysis and/or lack of computed experiment. Improving the results may require performing better data processing and/or more computed experiments. Obtaining a precise explanation requires more investigation.

For calculating the quality of the numerical model G_M compared to the reference model G_{MR} for damage detection, five damage cases were studied. Damage was introduced in G_M by reducing the mass of the cables and the damping constants of the dampers as shown in table 6.6. Damage was introduced in G_{MR} by reducing the diameter of the cables and the constants of the dampers as shown in table 6.5. The signal energy d_t of the acceleration signals was calculated in x and y directions based on eq. (3.5) for each damage case under the same applied impulse, figures 6.22 and 6.23. The agreement between the developed numerical model G_M and the reference model G_{MR} was computed applying eq (3.3) taking into account the studied damage model and the applied excitation. The results are presented in table 6.7. The values of Q_V show that the stiffness of the cables has a local effect on the response of the node close where the cables are attached to the pole, otherwise, no influence on the response of the other pole nodes was observed. Since the mean value, $Q_V \approx 1$, the evaluation process of the chosen inspection method for damage detection is expected to remain valid although the stiffness of the cables was omitted.

6.5 Design of experiments

Since it was observed that cables might have a damping effect and based on the results of the SDOF example, figure 3.14, impulse excitation was chosen to investigate the cable's effect. The

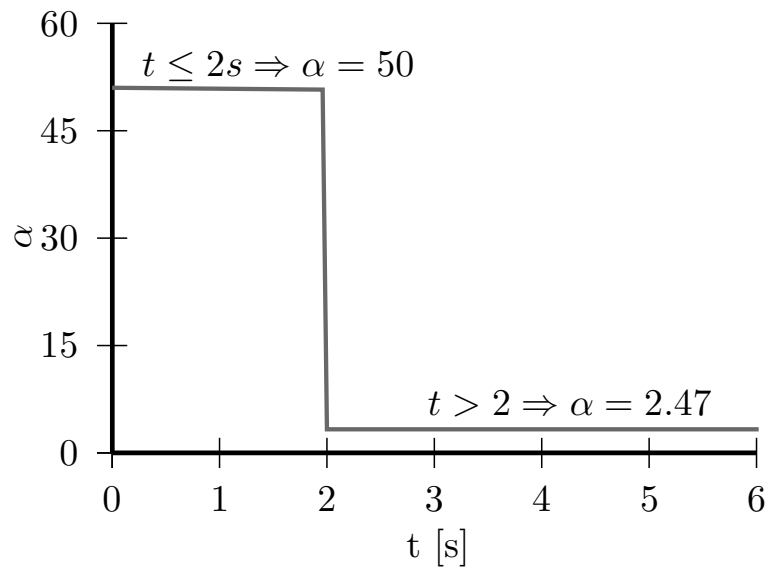


Figure 6.12: The contribution of the mass of the structure in the Rayleigh damping model during performing transient analysis

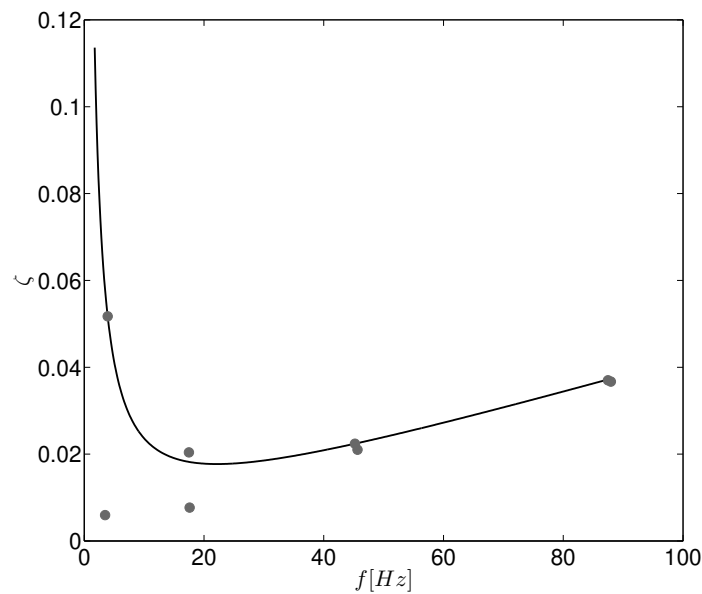


Figure 6.13: Rayleigh damping model included in the pole numerical models

Table 6.3: The natural frequencies and modal damping ratios extracted from the simulated test using G_{MR}

	1	2	3	4	5	6	7	8
f [Hz]			16.97	17.2	45.07	45.25	85.17	85.31
ζ %			5.96	6.21	0.62	0.72	0.36	0.31

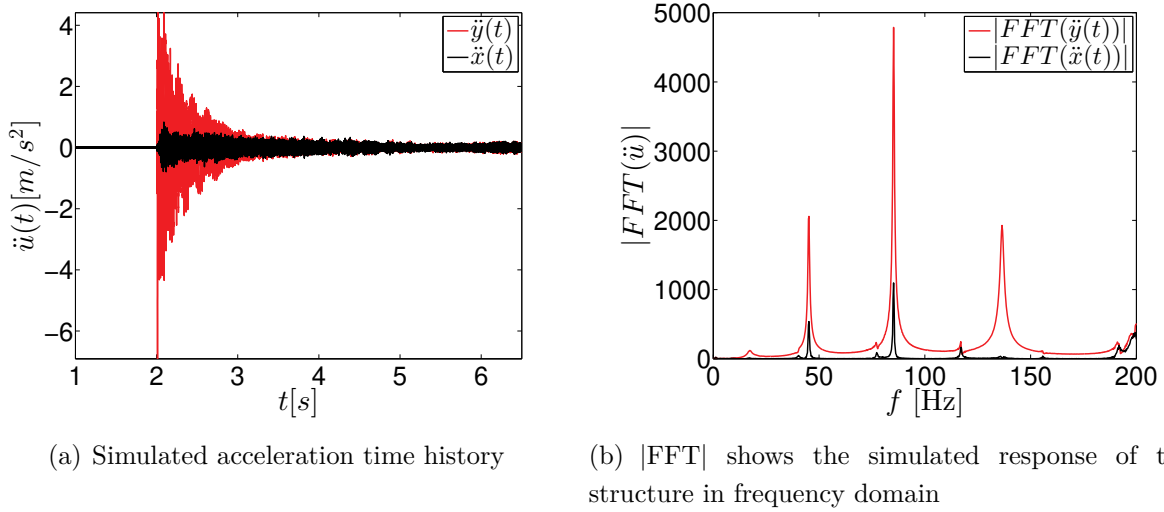


Figure 6.14: Simulated dynamic structural response at the top of the pole due to the excitation in figure 5.51, damage case 1, using the numerical model G_{MR}

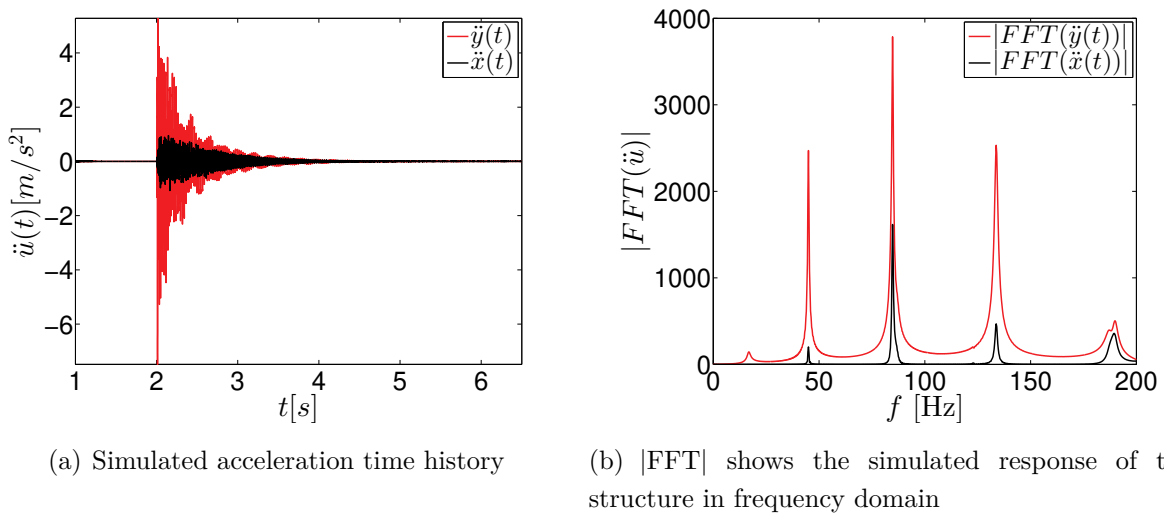
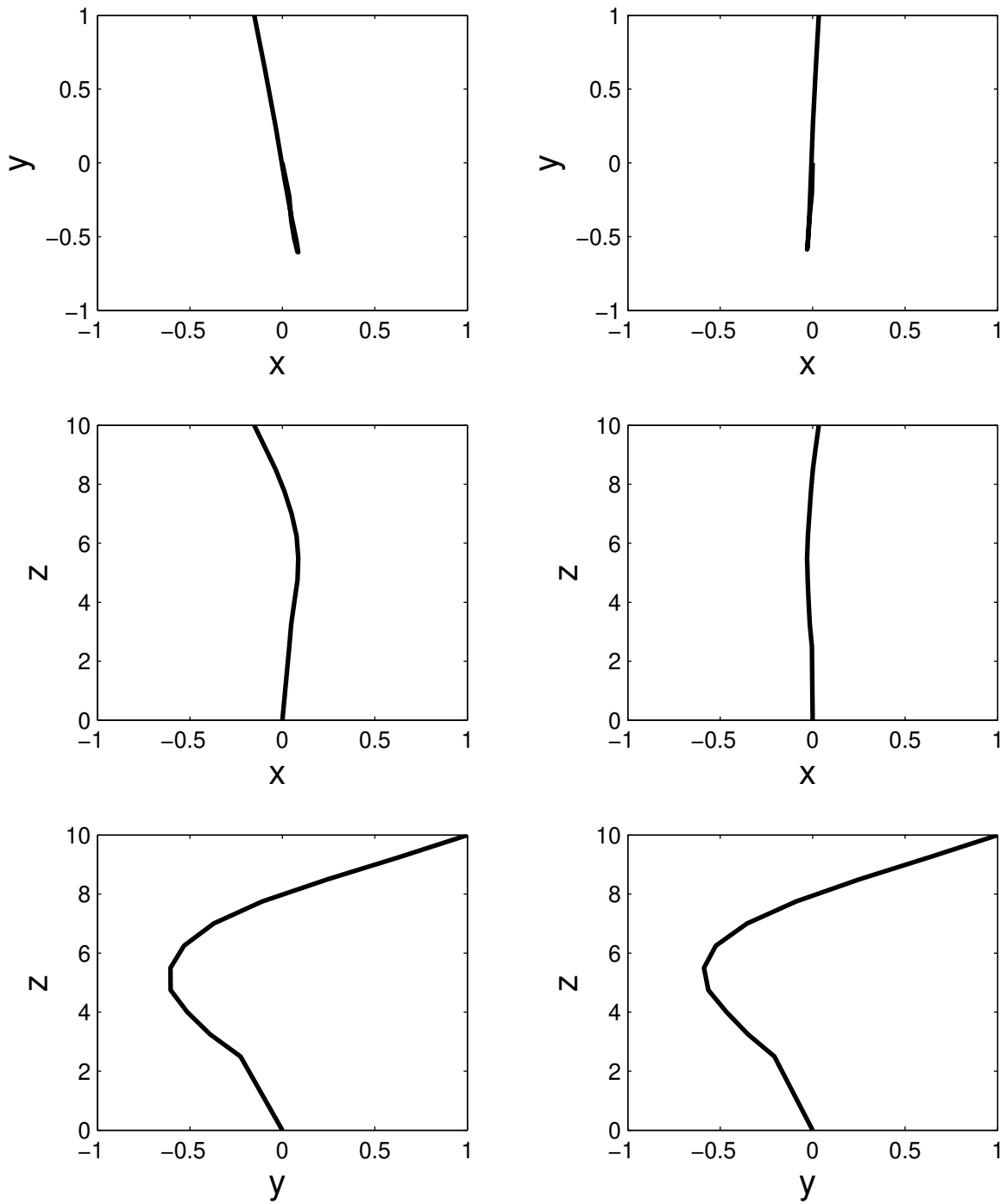


Figure 6.15: Simulated dynamic structural response at the top of the pole due to the excitation in figure 5.51, damage case 1, using the numerical model G_M

Table 6.4: The natural frequencies and modal damping ratios extracted from the simulated test using G_M

	1	2	3	4	5	6	7	8
f [Hz]				16.79	44.94	45.02	84.58	84.79
$\zeta\%$				4.69	0.567	0.589	0.757	0.332

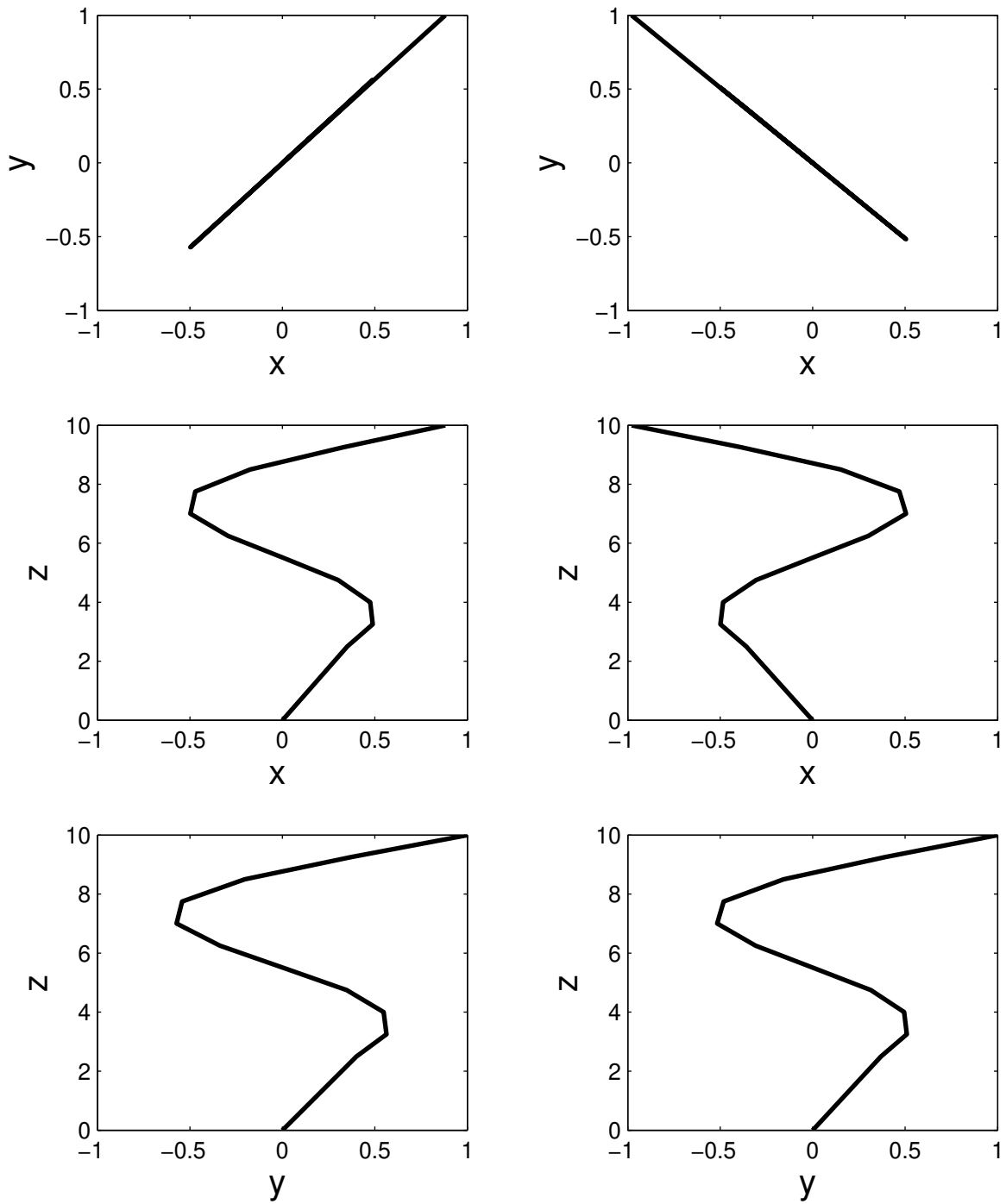
cumulative signal energy d of the acceleration time histories $[\ddot{u}(t)] = [\ddot{x}(t), \ddot{y}(t)]$ were used as an



(a) mode shape 3

(b) mode shape 4

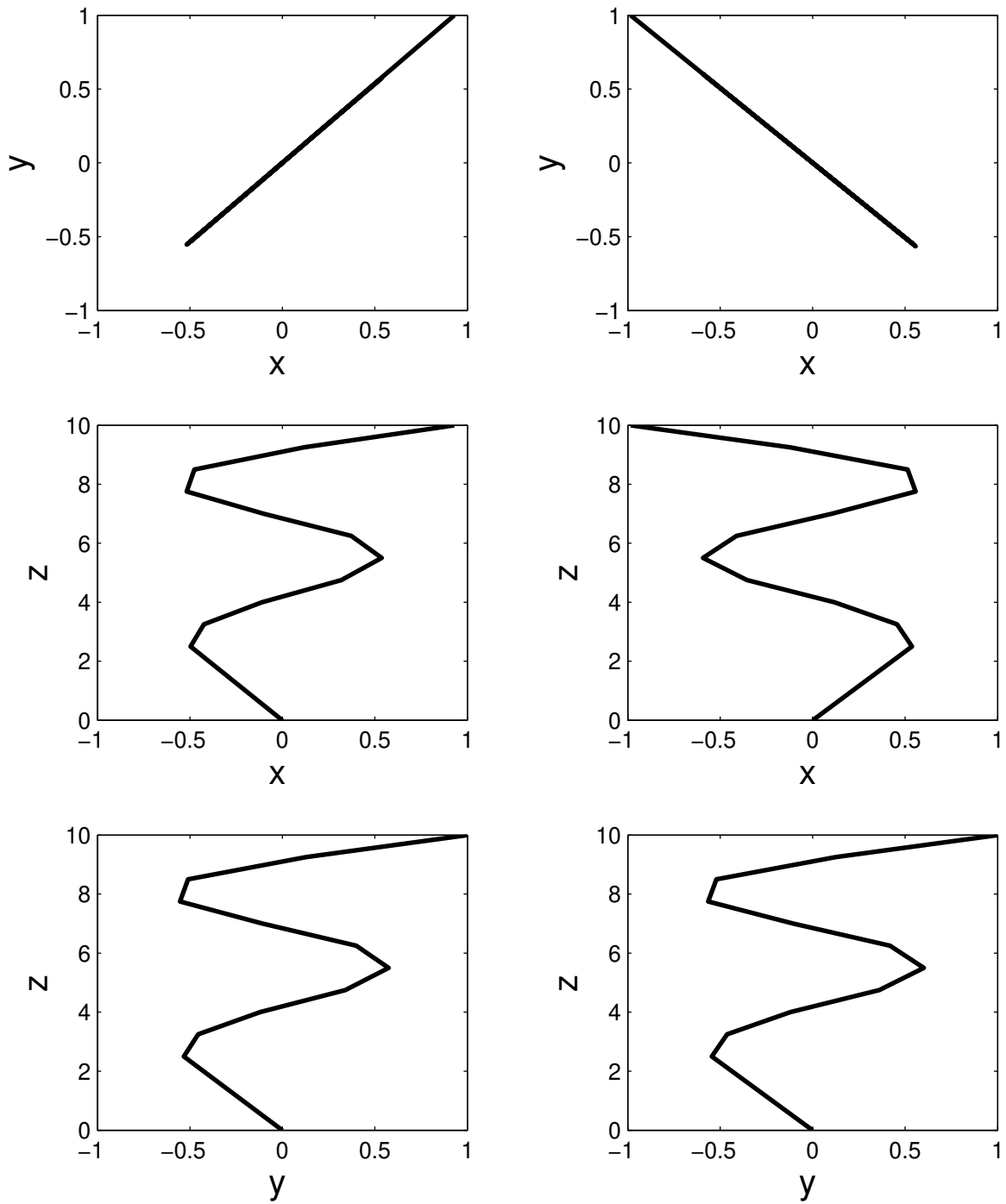
Figure 6.16: Mode shapes 3 and 4 extracted from the simulated test using G_{MR}



(a) mode shape 5

(b) mode shape 6

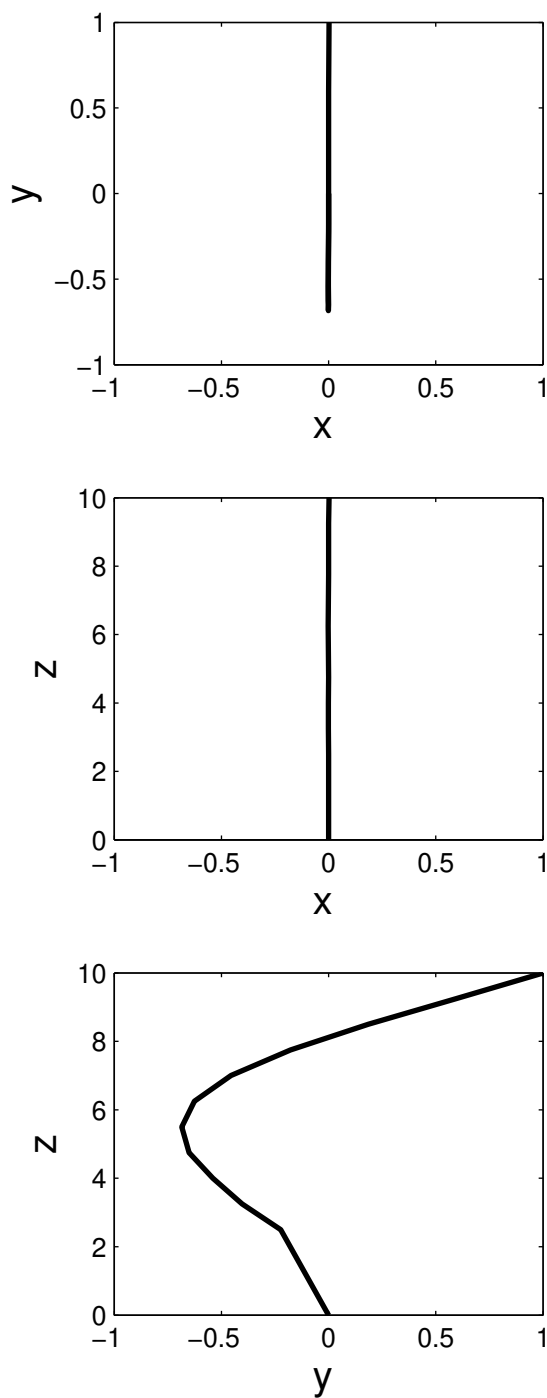
Figure 6.17: Mode shapes 5 and 6 extracted from the simulated test using G_{MR}



(a) mode shape 7

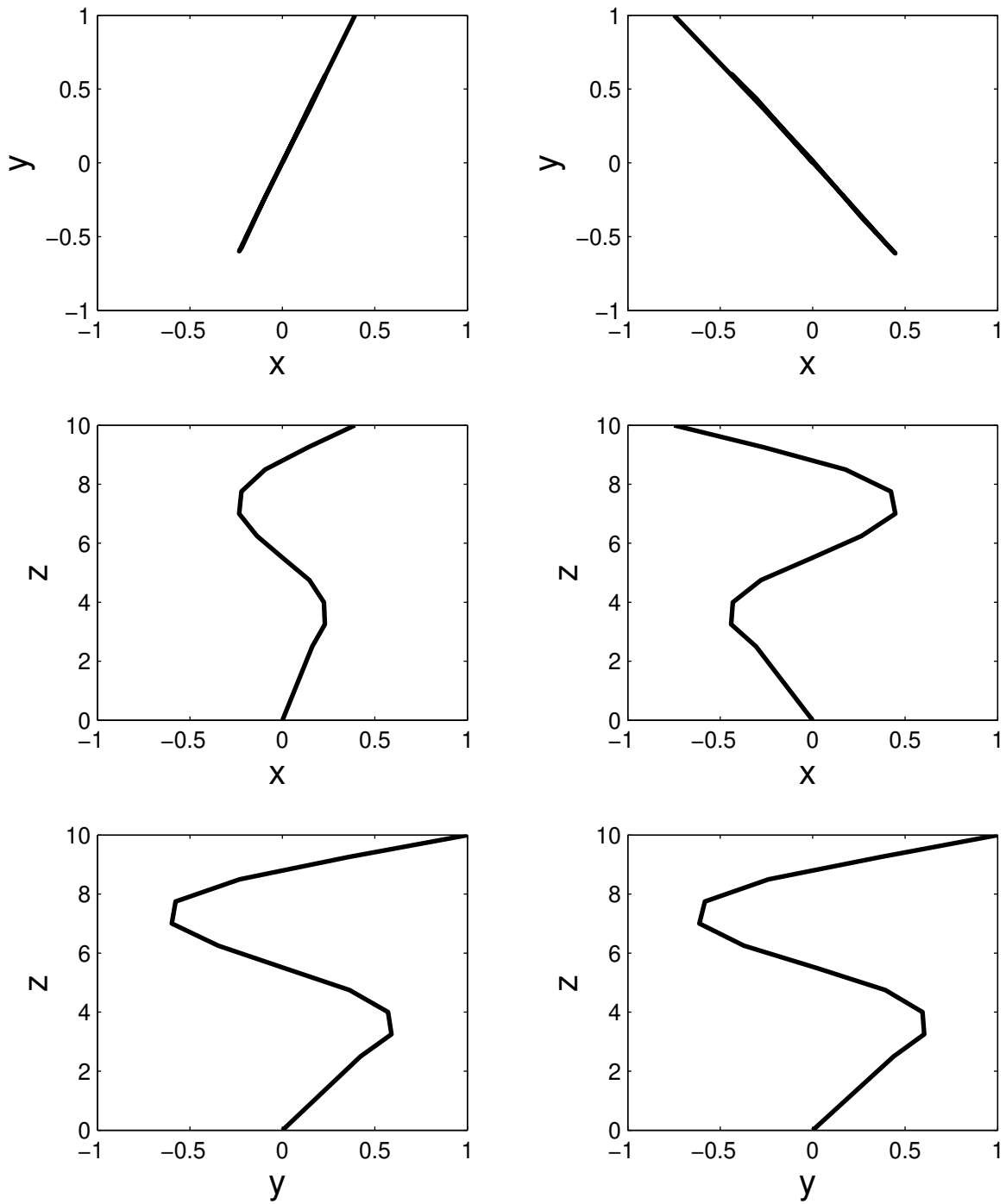
(b) mode shape 8

Figure 6.18: Mode shapes 7 and 8 extracted from the simulated test using G_{MR}



(a) mode shape 4

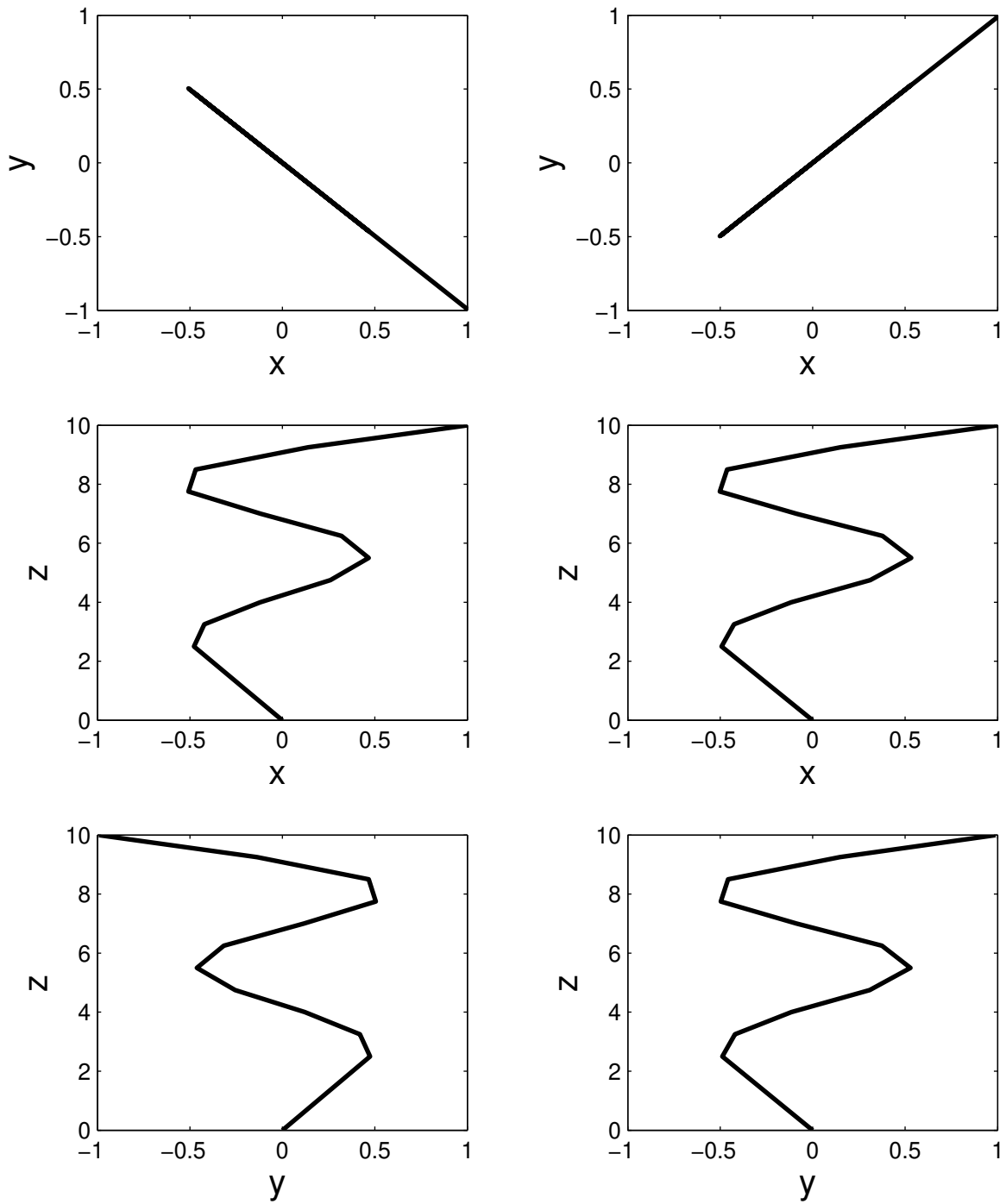
Figure 6.19: Mode shape 4 extracted from the simulated test using G_M



(a) mode shape 5

(b) mode shape 6

Figure 6.20: Mode shapes 5 and 6 extracted from the simulated test using G_M



(a) mode shape 7

(b) mode shape 8

Figure 6.21: Mode shapes 7 and 8 extracted from the simulated test using G_M

Table 6.5: The input parameters of G_{MR} used to calculate Q_V

Damage case	θ^g %	d_c	$C_{d,1}$ [N×s/mm]	$C_{d,2}$ [N×s/mm]	F_y/F_z	$10 - L_p$ [m]
1	0.00	1.000 d_c	10	10	0.0	9.5
2	0.25	0.875 d_c	8	8	0.0	9.5
3	0.50	0.750 d_c	6	6	0.0	9.5
4	0.75	0.625 d_c	4	4	0.0	9.5
5	1.00	0.500 d_c	2	2	0.0	9.5

Table 6.6: The input parameters of G_M used to calculate Q_V

Damage case	θ^g %	d_c	$C_{d,1}$ [N×s/mm]	$C_{d,2}$ [N×s/mm]	F_y/F_z	$10 - L_p$ [m]
1	0.00	1.000 M_c	10	10	0.0	9.5
2	0.25	0.767 M_c	8	8	0.0	9.5
3	0.50	0.564 M_c	6	6	0.0	9.5
4	0.75	0.391 M_c	4	4	0.0	9.5
5	1.00	0.255 M_c	2	2	0.0	9.5

Table 6.7: The quality of the numerical model G_M compared to the reference model G_{MR}

z [m]	$Q_V(x)$	$Q_V(y)$
10.0	1.00	1.00
9.25	0.91	0.83
8.50	0.99	0.99
7.75	1.00	1.00
7.00	1.00	1.00
6.25	1.00	1.00
5.50	1.00	1.00
4.75	1.00	1.00
4.00	1.00	1.00
Q_V	0.98	

output structural response to detect damage. The uncertainty of the input parameters that were obtained from the construction plans of the pole and the cables provided by the manufacturer was omitted, for example, the pre-stress force F_p , the wall thickness of the pole, the concrete and reinforcement properties. As a result, in this example, the uncertainty of the parameters, which were not measured either provided by the manufacturer and may influence the damage

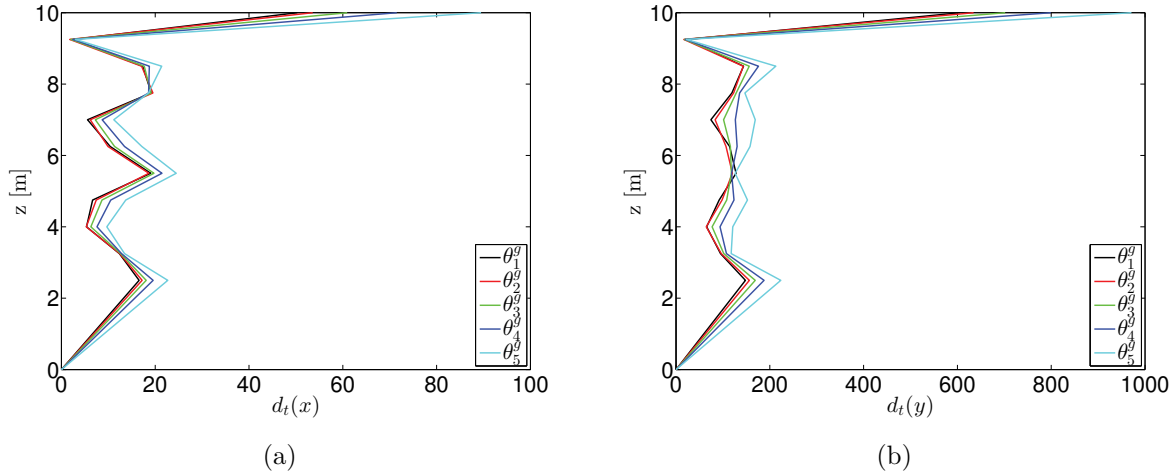


Figure 6.22: d_t under the same excitation using the reference model G_{MR}

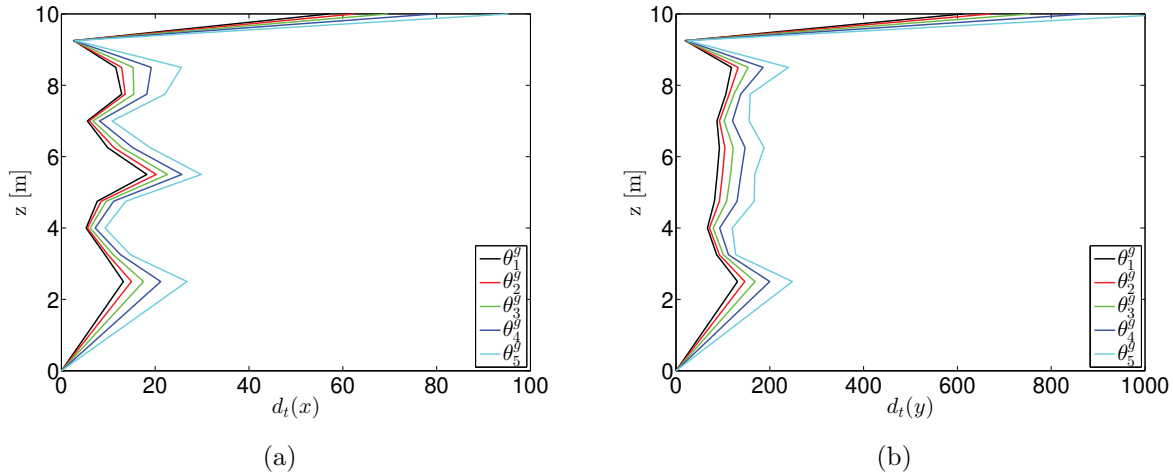


Figure 6.23: d_t under the same excitation using the model G_M

detection process, were considered. Similar to the cantilever results in the previous chapter, the natural frequencies of the studied poles obtained from the model tests show that the system is asymmetric. Moreover, since the impulse excitations were applied by hand, it is expected that the excitation may not be applied in y-direction correctly. Therefore, an additional force component in x-direction was considered.

In order to consider the variation of L_P related to the lower part of the pole, different sets of nodes were defined to represent different boundary conditions at the basement. The first set considers that all degrees of freedom of the nodes located at $z=0$ m are fixed. The last node set considers that all degrees of freedom of the nodes located between $0 \leq z \leq 1$ are fixed. In general, for a set A that contains $j = 1, 2, \dots, k$ nodes (n_j), that have 6 degrees of freedom, it is possible to write:

$$\forall n_j \in A : 0 \leq z(n_j) \leq L_p \Rightarrow DOF_l(n_j) = 0 | l = 1, 2, \dots, 6 \tag{6.2}$$

Table 6.8 presents the statistical properties assigned to the damper constants, the excitation amplitude in x and y-direction, the mass of the cables as a part of the studied damage model and length of the pole.

A Latin hypercube sampling method was used to generate $N = 1000$ samples to investigate the variation of the response d due to the input parameters $\{\theta\}$. The size of the sample was chosen as a trade off between the required computational time and quality of the Meta-models that were developed in the next step to solve more samples. The structural response $\ddot{u}(t) = [\ddot{x}(t), \ddot{y}(t)]$ for damage case 1 ($\theta^g = 0$) was computed for each sample. The cumulative signal energy values $\{d\}$ of the acceleration time histories $\ddot{u}(t)$ were computed based on eq. (3.5). For all samples, the initial conditions $u(0) = \dot{u}(0) = 0$.

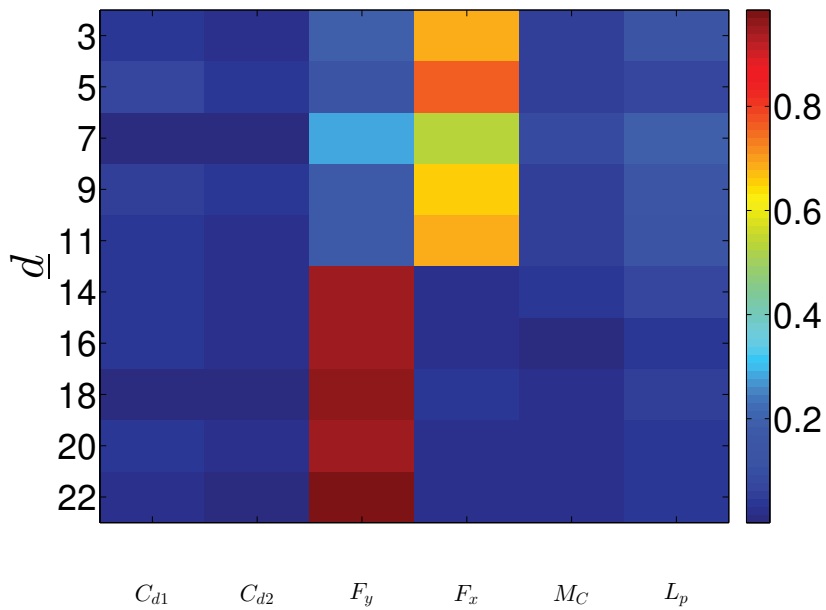
6.6 Sensitivity analysis

The sensitivity analysis method described in section 3.4 was used to obtain information about the contribution of $\{\theta\}$ to the outputs $\{d\}$. Meta-models $\{d\}$ were developed to perform the sensitivity analysis. The data sets which include $N = 1000$ samples calculated in the previous subsection were used. The statistical properties of the residuals were examined to ensure that they satisfy the requirements described in section 3.4.4. The Total-effect index sT values were calculated using $[d]$. Figure 6.24 shows the results of the applied sensitivity analysis.

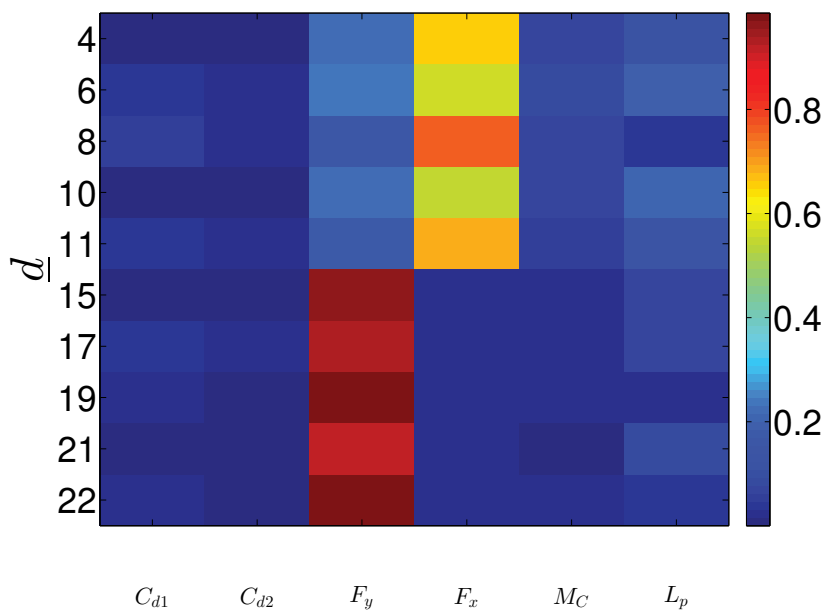
The results show that the amplitude of the excitation F_y influences the studied structural response in the x-direction. The large structural response in x-direction indicates that F_x , which can be caused by the asymmetry of the structure or the imperfection of the application of F_y , is large. As a result, the probability of damage detection may depend on the asymmetry model introduced in the numerical model.

Table 6.8: The statistical properties of the prior density functions of the input parameters of the developed numerical model G_M

	$C_{d,1}$ [N×s/mm]	$C_{d,2}$ [N×s/mm]	F_y [N]	F_x [N]	Mc [t]	$10 - L_p$ [m]
μ	7	7	20	5.0	0.055	8.5
Max	13	13	37.3	9,3	0.010	10
Min	0.95	0.95	2.7	0.67	0.0074	7
COV	0.5	0.5	0.5	0.5	0.5	0.1



(a) Setup 1: S_1



(b) Setup 2: S_2

Figure 6.24: Total-effect index $sT_{i,j}$ calculated for the two setups given in table 6.1. Channel numbers from 1 to 11 are in x direction, 12 to 22 are in y direction. 11 is x reference and 22 is y reference at the top of the pole

The Total-effect index sT show that the influence of the cable should be considered as a damper and as a mass point. Moreover, the variation of the L_p has to be taken into account otherwise false alarm is expected.

Based on eq.(6.3), the quality of the DOE models can be obtained. $Q_{DOE}(S_1) = 0.09$ and $Q_{DOE}(S_2) = 0.07$.

$$Q_{DOE} = \frac{sT(C_{d,1}, C_{d,2}, M_c)}{sT(\{\theta\})} \quad (6.3)$$

6.7 Model updating

Meta-models $\{\hat{d}\} = f(\{\hat{\theta}\})$ were developed for model updating. In this example, the geometrical and material properties of the cables are given in the construction plan. Therefore, the uncertainty in the mass of the cable was not considered. All other inputs were considered to be important $\{\hat{\theta}\} \equiv \{\theta \setminus M_c\}$. The statistical properties of the prior density functions are based on the uniform distribution, table 6.8 . Applying the Bayesian updating approach explained before in section 3.5, the posterior density functions $p(\{\theta\}|\{\bar{d}\})$ of the parameters were computed considering each setup separately. Since the input impulse excitation was not measured during the test, it should be included as an unknown parameter. As a result, if N impulse responses are used to update the model, $3+2 \times N$ input parameters have to be updated. They are three common input parameters $C_{d,1}, C_{d,2}, L_p$ and two parameters $F_{y,im}, F_{x,im}$ for each input impulse im . It is important to mention that after applying an impulse, the response of the structure decayed to its static state before applying the next impulse.

In this study, for each pole, three independent impulse responses were used to update the model. As a result, 9 parameters were included.

Since each input excitation was identical and no repetition was applied, it is not possible to ensure that the noise was at its minimum level. To estimate the noise energy d_γ , the cumulative energy of each impulse was computed for each Δt . Since the shape of the cumulative energy of an impulse without noise is known, the noise energy can be estimated approximately as shown in figure 6.25 and eq. (6.4). As a result, $\bar{d} = d_t - d_\gamma$. The procedure was applied to all measurement data and all poles. Two examples for estimating d_γ from real measurements are presented in figure 6.26. Uncertainty ϵ due to instrumentation, initial conditions and sensor quality was considered as a normally distributed uncertainty with zero mean and standard deviation $\sigma_\epsilon = 0.2\bar{d}$. This value is reasonable because of the influence of the wind on the instrumentation system. The statistical properties of the posterior density functions of the updated input parameters are presented in tables 6.9, 6.10.

In order to evaluate the quality of the measurements for each setup S_1 and S_2 , the index Q_M

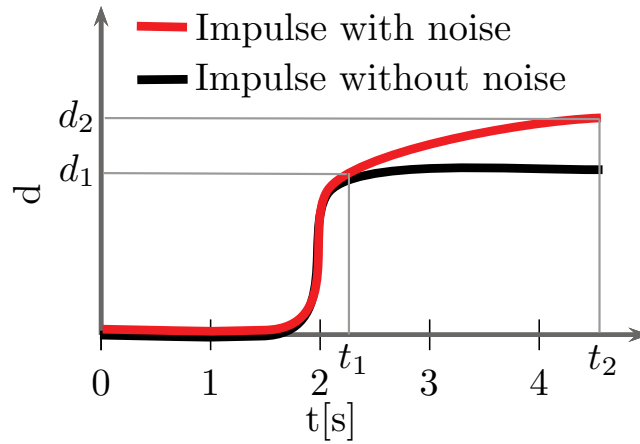


Figure 6.25: Estimation of the noise energy d_γ in an impulse response d_t

given in eq. (3.47) was computed. The results are shown in tables 6.9 and 6.10. The results show that although low design of experiments quality values $Q_{DOE} < 10\%$ were obtained, it was possible to obtain $Q_M > 90\%$. This is because of using three independent impulse responses to update the system, $N_{\bar{d}} = 3$.

$$d_\gamma = d_2(t_2) - d_1(t_1) \tag{6.4}$$

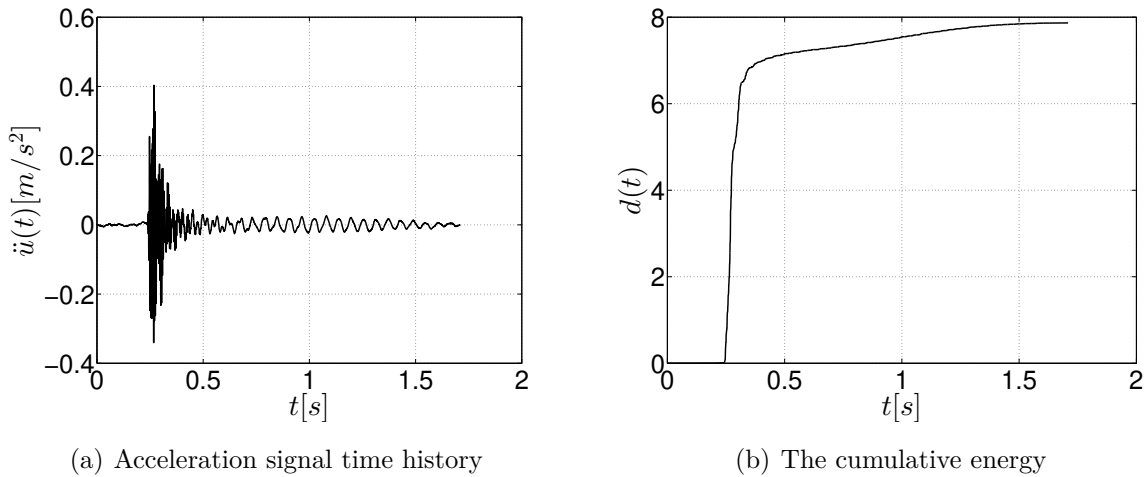


Figure 6.26: Acceleration signal time history with about 10% noise

An example of the posterior of the updated parameters is shown in figure 6.28 in case of S_1 and in figure 6.29 in case of S_2 for pole number 9 (239-25). The updated amplitudes of the excitations in x and y directions of the three applied impulses are shown in figure 6.30 and figure 6.31.

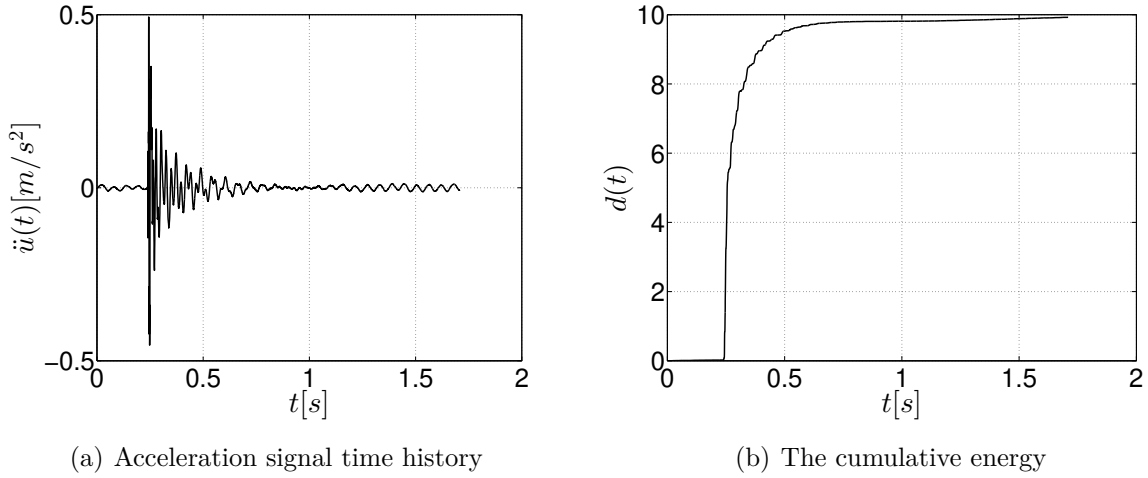


Figure 6.27: Acceleration signal time history with about 2% noise

6.8 Assessment of the inspection method

The developed method in section 3.6.2 was applied. Damage $\theta_i^g \in [0 \text{ } 50\%] \times M_c$ [ton] was used to calculate the response $d_i(\theta_i^g)$ with an interval $\Delta\theta^g = 0.015 \times M_c$. Based on eq. (3.63), (PFP=0.05) and for $n=22$ output (channels), $N=430$. The number of samples for each damage step $\Delta\theta^g$ was increased until $POD(\theta_i^g)$ converged. The investigation shows that $N = 2000$ samples for each damage step are sufficient to obtain converged POD curves.

Damage was introduced in G_M by reducing M_c and C_d as follows:

$$\forall \theta_{\Delta i}^g, \theta_{\Delta i+1}^g : \theta_{\Delta i+1}^g = \theta_{\Delta i}^g + \Delta\theta^g \Rightarrow M_{c,\Delta i+1} = M_{c,\Delta i} - 0.015 \times M_{c,0}, C_{d,\Delta i+1} = C_{d,\Delta i} - 0.015 \times C_{d,0} + \epsilon_{C_d} \quad (6.5)$$

where $M_{c,\Delta i}$ refers to the mass of the cable after reducing it by $0.015 \times M_{c,0} \times i$ where $i = 1, 2, \dots$. $M_{c,0}$ refers to the initial value of the mass of the cable. $C_{d,\Delta i}$ refers to the damping constant of the cable after reducing it by $0.015 \times C_{d,0} \times i$ where $i = 1, 2, \dots$. $C_{d,0}$ refers to the initial value of the damping constant corresponded with damage case 1 (no damage) after model updating. $C_{d,0}$ value is given in table 6.9 and table 6.10 for each pole. ϵ_{C_d} refers to the uncertainty of $C_{d,0}$ after model updating. Figures 6.28 and 6.29 show that the posterior density functions $p(C_d|\bar{d})$ have a distribution shape close to the normal distribution. Therefore $\epsilon_{C_d} \sim \mathcal{N}(0, \sigma_{\epsilon_{C_d}|\bar{d}}^2)$. $\sigma_{\epsilon_{C_d}|\bar{d}}$ values are given in table 6.9 and table 6.10 for each pole.

Figures 6.32 and 6.33 show that the reliability of the studied inspection method depends on the chosen experimental model and the test setup. Table 6.11 shows the minimum damage size that can be missed. The results show that applying setup 2; damage can be detected faster than applying setup 1.

Table 6.9: The statistical properties of the posterior density functions of the common input parameters. Pole 1–13. $C_{d,1}$ and $C_{d,2}$ are given in [N×s/mm]

Pole Nr.	S_1					S_2			
		$C_{d,1}$	$C_{d,2}$	L_p [m]	Q_M	$C_{d,1}$	$C_{d,2}$	L_p [m]	Q_M
1	μ	8.76	19.82	1.00		12.84	15.56	0.48	
	σ	0.252	0.159	0.014	97%	0.168	0.174	0.038	98%
2	μ	6.29	2.64	0.00		15.81	4.80	0.67	
	σ	0.649	0.268	0.015	93%	0.240	0.530	0.029	94%
3	μ	13.92	8.46	1.00		9.90	2.38	0.88	
	σ	0.288	0.412	0.004	95%	0.329	0.164	0.024	96%
4	μ	17.41	8.28	0.04		13.90	16.68	0.52	
	σ	0.138	0.507	0.006	95%	0.234	0.211	0.021	97%
5	μ	17.14	12.11	0.71		13.66	15.78	0.13	
	σ	0.152	0.226	0.052	97%	0.132	0.261	0.030	97%
6	μ	7.90	8.01	0.00		16.56	2.77	0.34	
	σ	0.526	0.490	0.010	93%	0.273	0.203	0.011	97%
7	μ	13.44	16.77	0.42		15.97	15.59	0.01	
	σ	0.139	0.181	0.047	98%	0.103	0.061	0.017	99%
8	μ	9.46	8.94	0.23		5.28	7.88	0.46	
	σ	0.784	0.632	0.057	90%	0.94	0.55	0.03	89%
9	μ	16.60	15.95	0.24		15.64	15.81	0.43	
	σ	0.050	0.206	0.026	98%	0.137	0.169	0.031	98%
10	μ	16.91	14.57	0.89		14.87	14.74	0.25	
	σ	0.099	0.197	0.026	98%	0.035	0.188	0.039	98%
11	μ	16.82	15.23	0.67		16.68	12.39	0.24	
	σ	0.109	0.121	0.034	98%	0.035	0.197	0.027	98%
12	μ	14.59	13.30	0.39		13.01	15.74	0.13	
	σ	0.196	0.283	0.048	97%	0.153	0.245	0.040	97%
13	μ	17.77	14.20	0.55		16.95	12.18	0.13	
	σ	0.122	0.240	0.028	97%	0.191	0.330	0.022	96%

The inspection method was evaluated at $\theta^g = 0.002$ [ton] or $\theta^g = 2$ kg by computing the index Q_D using eq. (3.61).

Table 6.10: The statistical properties of the posterior density functions of the common input parameters. Pole 14–26. $C_{d,1}$ and $C_{d,2}$ are given in [N×s/mm]

Pole Nr.		S_1				S_2			
		$C_{d,1}$	$C_{d,2}$	L_p [m]	Q_M	$C_{d,1}$	$C_{d,2}$	L_p [m]	Q_M
14	μ	10.65	1.93	0.01		10.48	4.20	0.47	
	σ	0.615	0.318	0.023	93%	0.536	0.093	0.042	95%
15	μ	11.52	5.04	0.09		15.10	13.13	0.58	
	σ	0.439	0.328	0.019	94%	0.247	0.336	0.023	96%
16	μ	17.71	5.21	0.84		14.88	6.67	0.23	
	σ	0.205	0.733	0.040	93%	0.232	0.543	0.021	94%
17	μ	11.98	7.36	0.71		9.65	15.09	0.46	
	σ	0.505	0.544	0.045	92%	0.707	0.535	0.039	91%
18	μ	11.27	14.45	0.25		17.49	17.54	0.88	
	σ	0.459	0.402	0.033	94%	0.121	0.163	0.017	98%
19	μ	11.55	11.33	0.06		15.01	12.80	0.47	
	σ	0.460	0.771	0.026	91%	0.101	0.252	0.031	97%
20	μ	6.03	7.88	0.00		15.95	15.92	0.60	
	σ	0.617	0.495	0.009	92%	0.149	0.162	0.027	98%
21	μ	16.67	6.40	0.58		12.08	17.60	0.70	
	σ	0.199	0.388	0.036	96%	0.218	0.142	0.023	97%
22	μ	17.04	9.42	0.03		14.74	15.13	0.40	
	σ	0.142	0.480	0.014	96%	0.161	0.207	0.037	97%
23	μ	10.36	4.79	0.98		13.08	12.21	0.00	
	σ	0.433	0.521	0.027	93%	0.243	0.203	0.019	97%
24	μ	14.38	16.29	0.46		12.68	20.69	0.77	
	σ	0.166	0.191	0.048	97%	0.126	0.081	0.013	99%
25	μ	17.22	12.15	0.49		14.96	11.05	0.34	
	σ	0.022	0.048	0.081	99%	0.111	0.340	0.028	97%
26	μ	13.84	16.15	0.68		14.61	15.63	0.12	
	σ	0.207	0.148	0.026	97%	0.075	0.229	0.031	98%

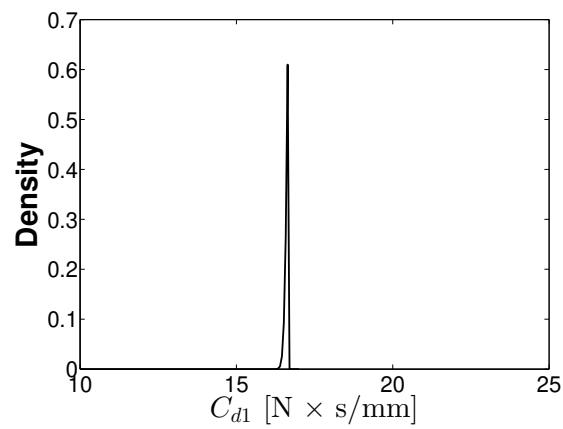
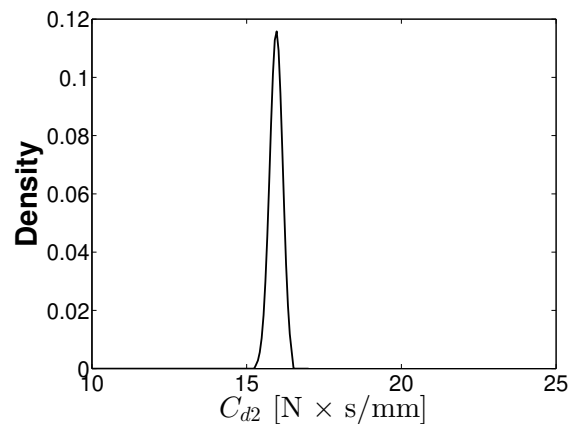
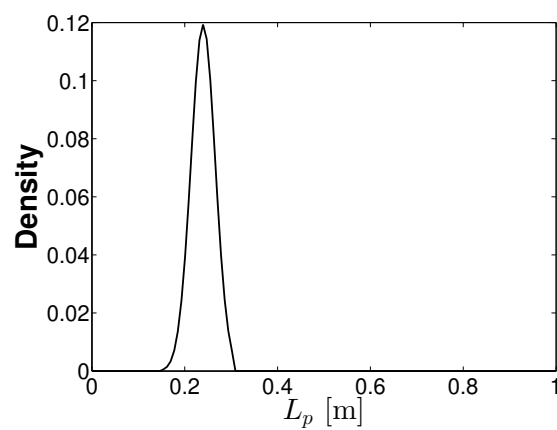
(a) $p(C_{d1}|\bar{d})$ (b) $p(C_{d2}|\bar{d})$ (c) $p(L_p|\bar{d})$

Figure 6.28: Posterior density functions of the updated input parameters using \bar{d} from pole Nr. 9 (239-25), Setup S_1

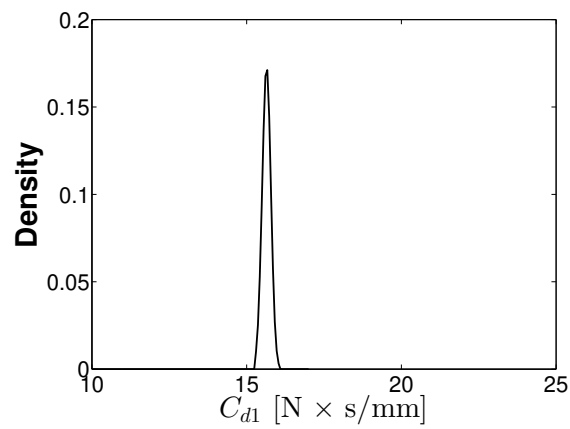
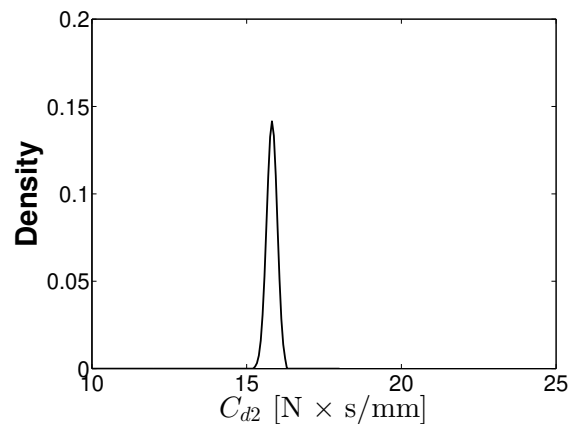
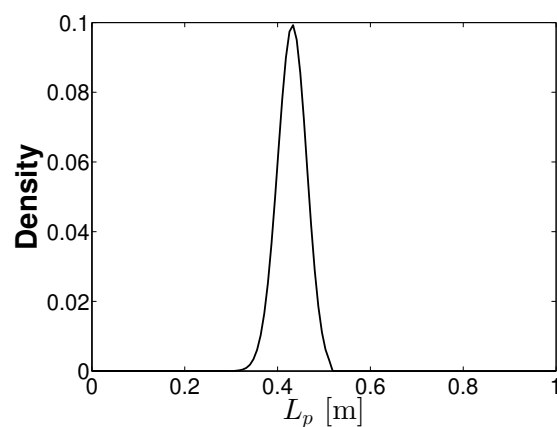
(a) $p(C_{d1}|\bar{d})$ (b) $p(C_{d2}|\bar{d})$ (c) $p(L_p|\bar{d})$

Figure 6.29: Posterior density functions of the updated input parameters using \bar{d} from pole Nr. 9 (239-25), Setup S_2

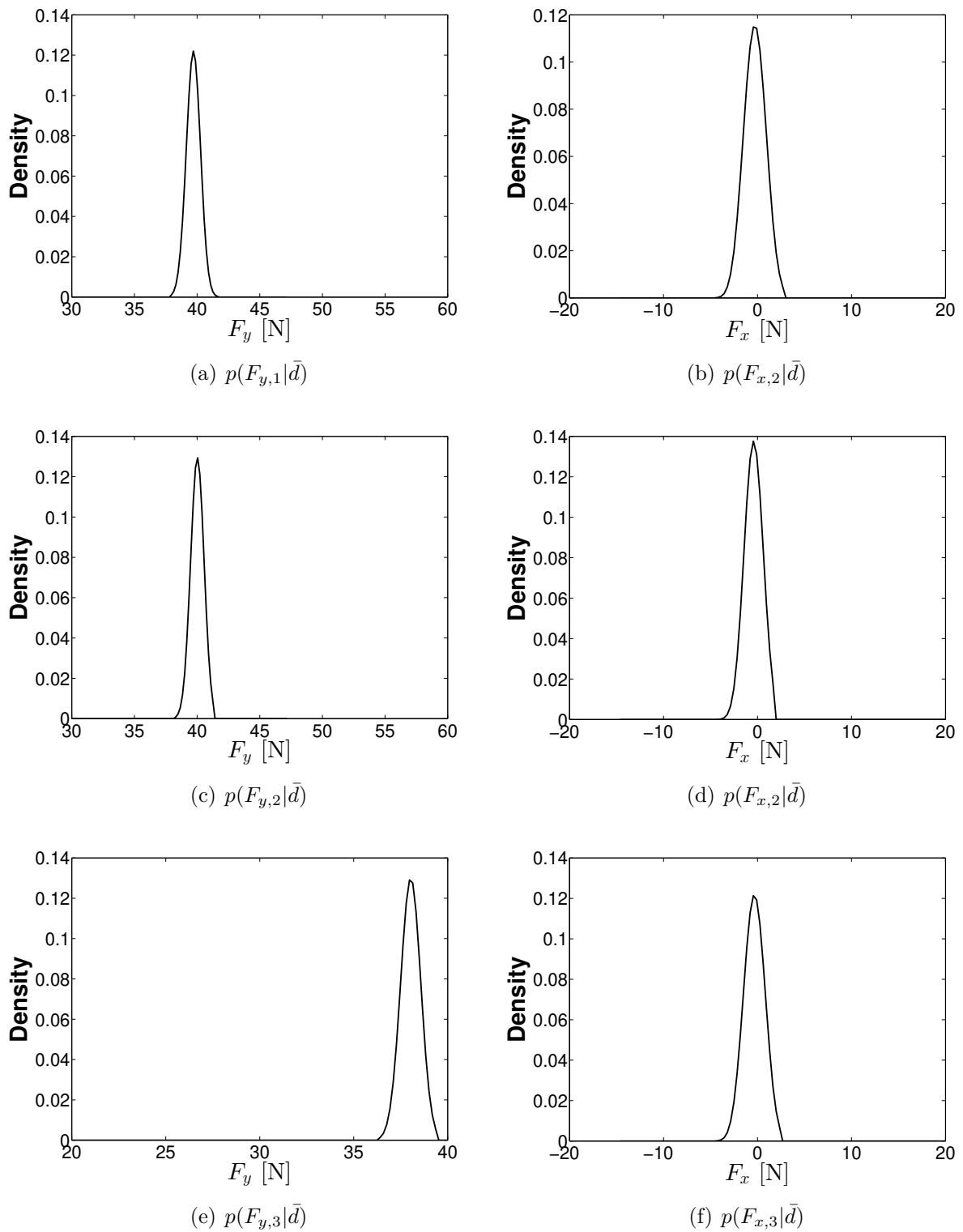


Figure 6.30: Posterior density functions of the updated impulse excitation amplitudes in x and y directions, S_1

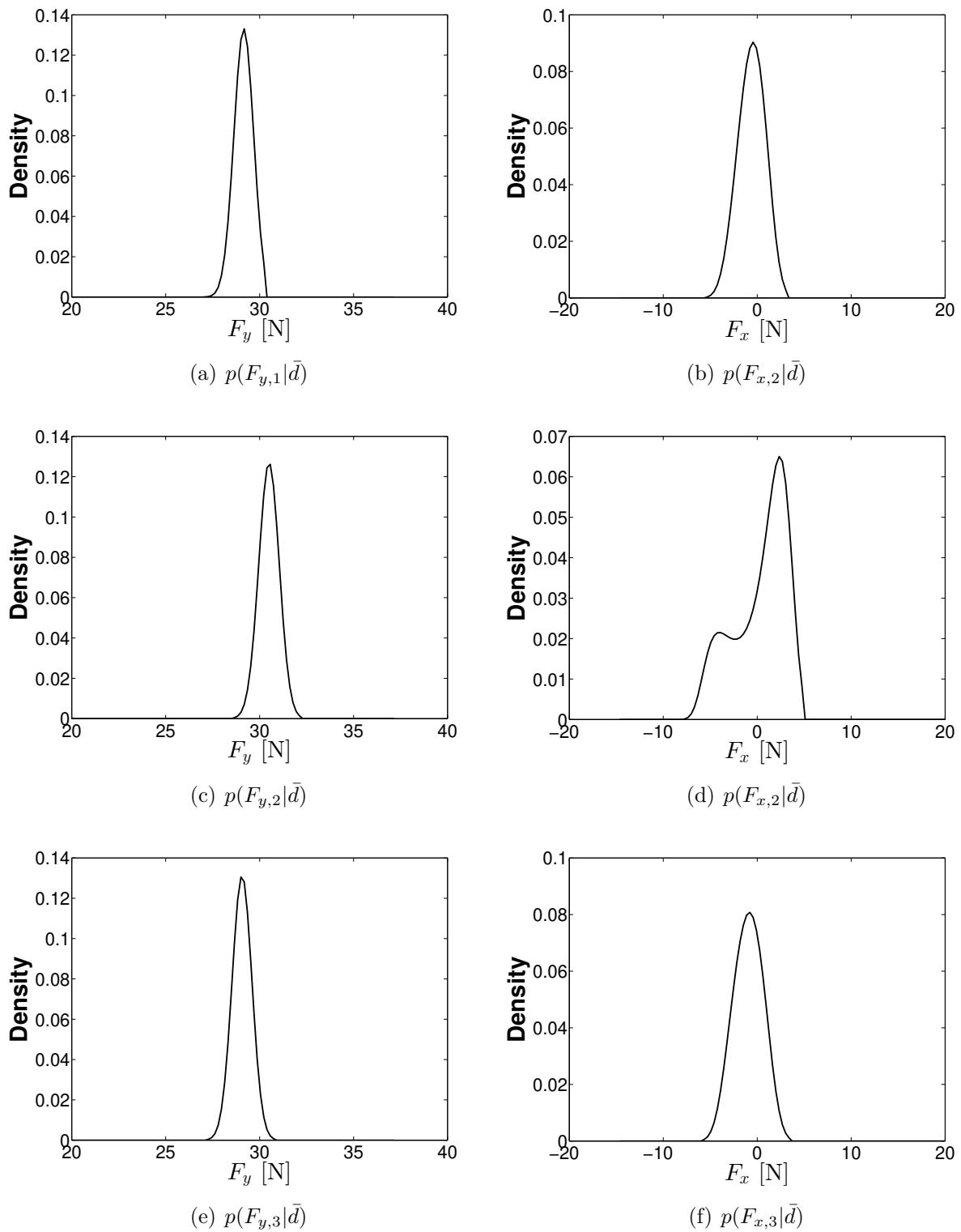


Figure 6.31: Posterior density functions of the updated impulse excitation amplitudes in x and y directions, S_2

Table 6.11: The minimum damage size that can be missed based on the problem definition in eq. (6.1)

S_1				S_2			
Pole Nr.	θ^g [kg]	Pole Nr.	θ^g [kg]	Pole Nr.	θ^g [kg]	Pole Nr.	θ^g [kg]
1	8.3	14	5.0	1	2.5	1	5.0
2	6.6	15	5.8	2	4.1	2	3.3
3	4.1	16	5.0	3	3.3	3	3.3
4	2.5	17	5.8	4	2.5	4	6.6
5	1.7	18	6.6	5	2.5	5	1.7
6	5.8	19	7.4	6	2.5	6	2.5
7	1.7	20	9.1	7	1.7	7	1.7
8	11.6	21	4.1	8	6.6	8	3.3
9	1.7	22	2.5	9	1.7	9	1.7
10	1.7	23	5.0	10	1.7	10	3.3
11	1.7	24	2.5	11	1.7	11	2.5
12	2.5	25	1.7	12	3.3	12	3.3
13	2.5	26	2.5	13	3.3	13	2.5

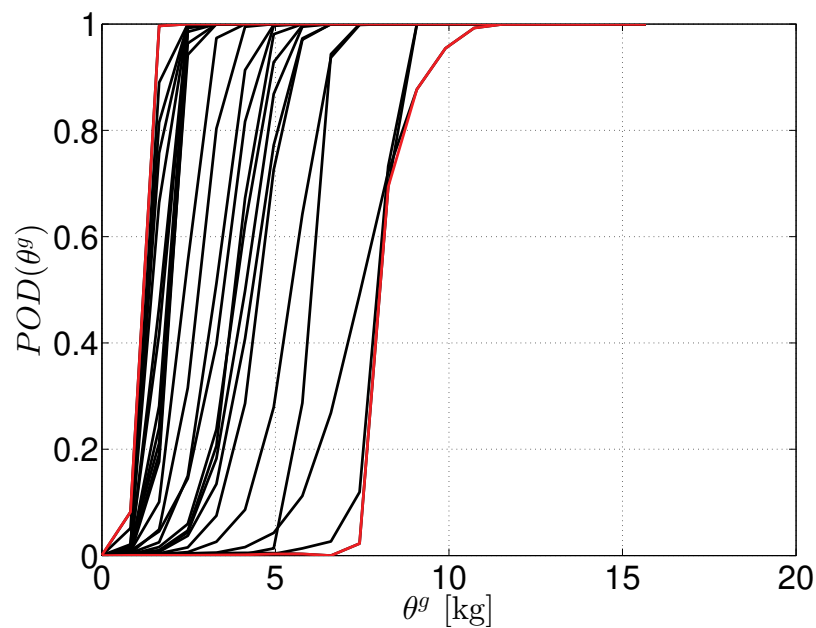
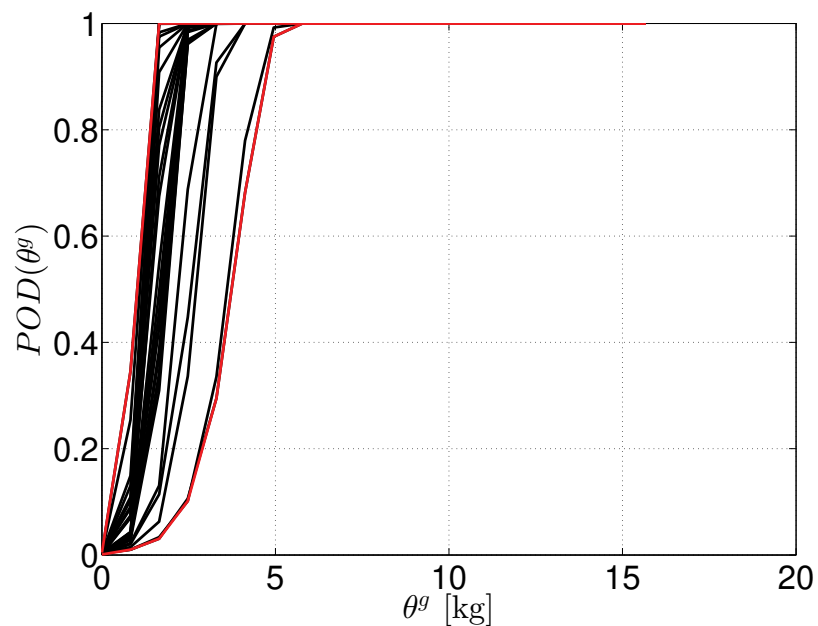


Figure 6.32: $POD(\theta^g)$ using G_M and different 26 pole experimental model, S_1 . Red: maximum and minimum curves value

Table 6.12: The index Q_D computed based on eq. (3.61) for $\theta^g = 0.002$ [t] or $\theta^g = 2$ kg

S_1				S_2			
Pole Nr.	POD(θ^g)	Pole Nr.	POD(θ^g)	Pole Nr.	POD(θ^g)	Pole Nr.	POD(θ^g)
1	0%	14	10%	1	75%	1	28%
2	2%	15	4%	2	20%	2	66%
3	18%	16	3%	3	41%	3	92%
4	58%	17	1%	4	90%	4	7%
5	83%	18	0%	5	89%	5	95%
6	3%	19	0%	6	68%	6	77%
7	88%	20	0%	7	100%	7	99%
8	0%	21	33%	8	7%	8	71%
9	94%	22	59%	9	100%	9	98%
10	73%	23	9%	10	99%	10	64%
11	100%	24	64%	11	100%	11	84%
12	71%	25	91%	12	65%	12	68%
13	57%	26	61%	13	73%	13	86%

**Figure 6.33:** $POD(\theta^g)$ using G_M and different 26 pole experimental model, S_2 . Red: maximum and minimum curves value

6.9 Conclusion

In this example, the performance of a vibration-based inspection method to detect damage in identical structures was tested. 26 poles as G_E and two setups were considered. The following results can be pointed out:

- The reliability of the inspection method depends on the chosen design of experiments and the physical model.
- A numerical reference model G_{MR} can be used to evaluate the quality of the developed numerical model G_M which could reduce the computational effort significantly.
- The probability of detection could be used to evaluate the quality of the measurements in case of damage detection.

Chapter 7

Discussion

7.1 Introduction

Based on what was presented about state of the art, chapter 2, many types of damage can be represented by many numerical and physical damage models which can be used if the reliability of an inspection method should be evaluated. Therefore, it is important to mention that the goal of this work was not to present and to test all damage models but to develop a general framework which can provide an argument for choosing a specific model against others.

It can be challenging to develop a single inspection method that provides all damage identification levels for all types of damage. Therefore, the developed strategy in this work started with a problem definition to select specific damage in a specific structure to be detected.

The strategy developed in this work evaluates the assessment procedure followed to check the reliability of the inspection method and shows which partial model should be improved if the desired damage size is not detected. If the quality of the partial models cannot be improved, the inspection method is considered unreliable, and an alternative inspection method should be selected.

It is possible to decouple the problem to a more significant number of partial models, for example, a damage model, material model, excitation model, etc. The advantage of the decoupling procedure is that it is possible to switch any partial model and keep other partial models without any modification to evaluate the influence of this change on the performance of the inspection method. For example, many numerical models can be tested keeping the same DOE, experimental data, and the damage indicator.

On the other hand, developing several damage models to represent a specific damage type can lead to a coupling problem with the global numerical model of the structure. For example, coupling a multidimensional damage numerical model to a unidimensional global numerical model and vice versa.

In the next section, the results obtained from the numerical and the experimental studies are discussed to specify the limitations of the developed strategy and to introduce improvements that may enhance the reliability of the studied inspection method.

7.2 Quality assessment: Limitation and improvement

7.2.1 Assessment procedure

The general purpose of the quality assessment in this work was not to develop the best model. However, the goal was to provide knowledge about the relative quality between a currently used model and a reference model which was assumed to be the best model. Moreover, this study did not give evidence that there was a unique optimal model.

The assessment principle is based on decoupling a global model into several partial models and evaluating each of these partial models at each step of the re-coupling procedure. An ideal assessment procedure may be to decouple the global model into an infinite number of partial models and then to assess each one before re-coupling them. Based on that, the ideal quality of assessment method was represented by a circle with the unit radius. Each point of this circle represents the maximum quality of a partial model. In this work, only the quality of the four essential partial models were investigated: numerical models, the design of experiments, measurements, and damage indicators. If the studied partial models are equally important, then the circle can be divided into four equal quarters by placing the quality of the studied partial models on the circle with an angle interval of 90° . This quality representation helps to compare different partial models and different inspection methods for detecting a specific damage type.

7.2.2 Assessment results

The procedure described above was applied to the studied examples in this work. Table 7.1 presents the partial models that were switched to explore their influence on the reliability of the inspection method. In the SDOF example, the excitation properties as a part of the DOE model were evaluated using the sensitivity analysis to illustrate their influence on the studied damage model, figure 3.14. The damage indicator was tested with and without considering model updating.

In the case of the three-DOF frame structure, damage scenarios as a part of the numerical model were investigated. Different excitation properties as a part of the DOE model were tested.

Table 7.1: An overview of the comparison of the studied partial model in each example

Example	Partial models			
	G_M	DOE	g	f
SDOF		X		X
3DOF	X	X		
Frame		X		X
PVC	X			
Poles	X	X	X	

In case of the steel frame structure different DOE models including the excitation properties (frequency and location), sensor number were evaluated in case of damage detection. Different damping models were introduced in the damage indicator model to obtain their influence on the reliability of the inspection method. In case of the PVC cantilever example, two numerical models were developed to explore the changes in the reliability of the inspection method if those models were chosen.

Experiments from identical physical models were used to investigate their influence on the reliability of the inspection method. Two numerical models were developed to explore the influence of the cable stiffness on the assessment procedure. Two test setups as a part of the DOE model were evaluated.

Figure 7.1 illustrates the quality of the partial models of the SDOF system example represented inside the ideal assessment circle. The SDOF system example can be the best and maybe the only case where an ideal design of experiment can be obtained. In all other examples presented in this work, it was not possible to reach more than $Q_{DOE} \geq 0.75$ based on the optimal DOE definition used in this work. The example pointed out that the reliability of the chosen inspection method to detect the defined damage size depends on measurements. Therefore, if the reliability of the inspection method should be improved, the quality of measurements should be improved by conducting more experiments or using a better sensor quality, etc.

In real civil engineering structures, an ideal design of experiments may not be applicable as the three degrees of freedom system studied in this work showed. As a result, more experiments were needed to gain information about other parameters which are unrelated to the chosen damage type but influenced the outputs significantly, figure 7.2.

The chosen DOE can be improved by performing more experiments or changing the type and the properties of the excitations. Another solution is to design an inverse experiment that considers damping ratios and masses as desired inputs and stiffness as undesired inputs. In this case, it is possible to prove that the variation of the studied response is not due the variation of damping ratios or the masses. As a result, the variation of the chosen response can be explained

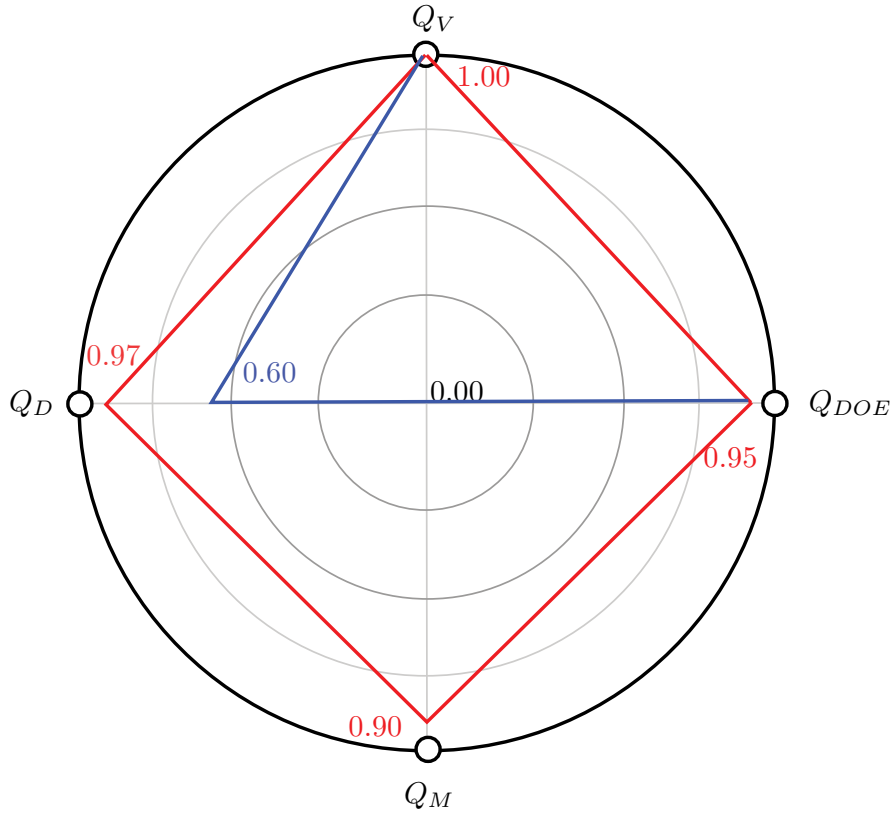


Figure 7.1: Partial models quality of the SDOF system example (red: with model updating, blue: without model updating)

by the variation of the stiffness. For example, if $[M]$ and $[C]$ are the mass and damping matrices of the structure and $[K_i]$ is the stiffness matrix for damage case i and $[K_{i+1}]$ is the stiffness matrix for damage case $i+1$, damage related to the stiffness changes $\theta^g = \Delta[K] = [K_{i+1}] - [K_i]$ can be detected as follows:

$$\forall \theta_i^g, \theta_{i+1}^g : \theta_i^g \neq \theta_j^g \text{ if } [M]|d(\theta_i^g) = [M]|d(\theta_{i+1}^g) \text{ and } [C]|d(\theta_i^g) = [C]|d(\theta_{i+1}^g) \rightarrow [K_i] \neq [K_{i+1}] \quad (7.1)$$

The investigation introduced in eq. (7.1) can be improved by including the damage pattern $DP(\theta^g)$ concept. If $DP(\Delta[M])$ and $DP(\Delta[C])$ represent the response patterns due to the change of mass and the response patterns due to the change of damping, respectively, it is possible to write:

$$\forall \theta_i^g, \theta_{i+1}^g : \theta_i^g \neq \theta_{i+1}^g \text{ if } DP(\theta^g) \neq DP(\Delta[M]) \text{ and } DP(\theta^g) \neq DP(\Delta[C]) \rightarrow [K_i] \neq [K_{i+1}] \quad (7.2)$$

Eq. (7.2) can be coupled to eq. (3.15) to improve the design of experiments by finding the best sensor location for damage detection and for preventing false alarm. If $DP(\Delta\theta)$ is the response patterns due the variation of the input parameters which are not related to damage, $\{\theta\} \setminus \theta^g$,

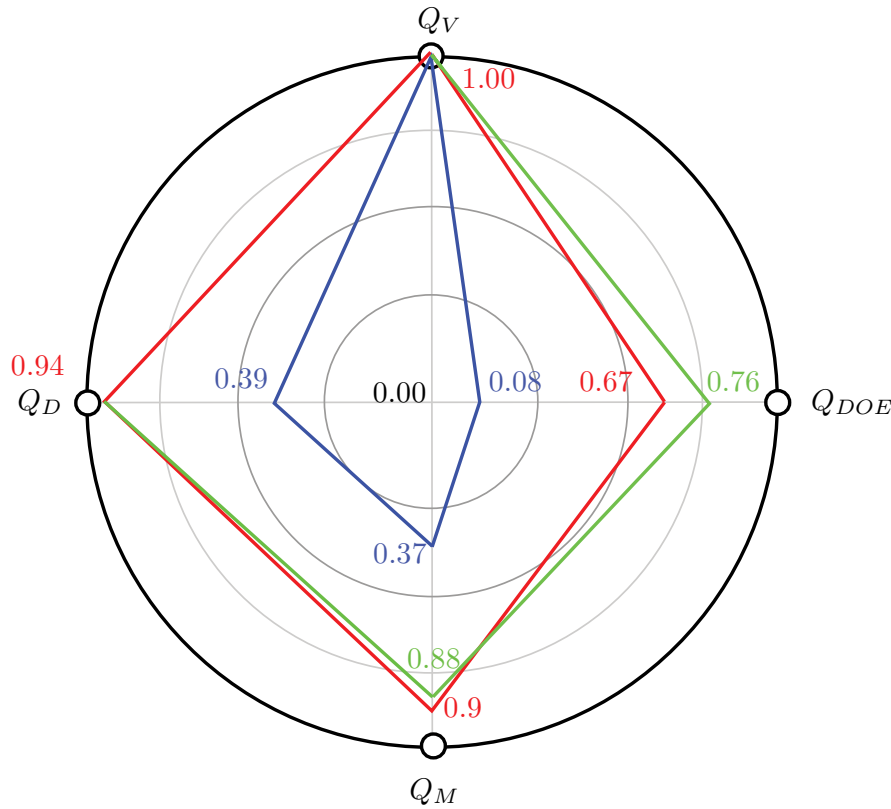


Figure 7.2: Partial models quality of the 3DOFs system example: red line is if damage was at the top k_1 or middle story k_2 and blue line if damage was at the ground story k_3

the DOE model can be improved as follows:

$$\forall x \subseteq \Omega : \arg \max_x [Q_V(d(x), \bar{d}(x)), sT(\theta^g, d(x))], DP(\theta^g) \neq DP(\Delta\theta) \quad (7.3)$$

In the third example- steel frame structure, it was meant to develop a numerical model independently of the chosen DOE model. However, the results in table 5.9 indicate that Q_V depends on the chosen DOE model which includes the sensor positions, sensors number and the excitation properties, figure 7.3. Damage development is a critical point that was investigated by introducing different damping models in the damage indicator model, section 5.1.5.

The relationship between G_M and DOE can be used to improve the quality of the numerical model G_M for damage detection by applying eq. (3.14), eq. (3.15) and eq. (3.16) in section 3.4.1. In this case, the best excitation properties and sensor positions that lead to better POD can be selected based on the results in table 5.9 and figure 5.28. For example, given that $Q_{V,th}$ and sT_{th} are predefined threshold values for Q_V and sT , if only the sensors $\{u_{opt}\} \subseteq \{u\}$, where the structural response satisfies $Q_V > Q_{V,th} = 0.6$ and $st(\theta^g) > sT_{th} > 0.0$, were only chosen, eq. (7.4), the quality of the numerical model for damage detection can be improved to the values shown in table 7.2. Moreover, the results of the applied sensitivity analysis show that exciting the structure in z direction (out of plan) can improve the probability of damage detection and

reduce the false alarm.

$$\forall \{u_{opt}\} \subseteq \{u\} : Q_V(d(x), \bar{d}(x)) > 0.6 \cap sT(\theta^g, d(x)) > 0 \quad (7.4)$$

Table 7.2: Quality of the numerical model compared to the physical model for different DOE given that d is the signal energy after applying eq. (7.4)

	20 Hz y	20 Hz x	30 Hz y	30 Hz x	60 Hz y	60 Hz x	170 Hz y	170 Hz x
Q_V	0.78	0.81	0.83	0.82	0.76	0.81	0.95	0.61

The results obtained from the cantilever example in chapter 5, figure 7.4, and the reference object (pole) in chapter 6, figure 7.5, agree with the investigation results shown in figure 3.14 from the SDOF example. If the damage model includes only the stiffness of the cables, the damage indicator obtained under an impulse excitation is not sensitive to damage, figure 5.69, table 6.7. If the damping influence was included, the reliability of the inspection method improved significantly, figures 5.70, 6.32 and 6.33.

The results from the pole example in chapter 6 show that if the cable damping was not activated during the experiments, the damage would be detected late. This means if the model updating results using experiments from a model $G_{E,i}$ gave larger damping constant C_d than a model $G_{E,j}$, damage was detected using model $G_{E,i}$ faster than using model $G_{E,j}$, eq. (7.5). As a result, it is possible to evaluate the quality of the experiments for detecting the studied damage type based on the value C_d obtained from the posterior density functions. Also, the results indicate that the asymmetry of the structure can influence the reliability of the inspection method. Therefore, more investigation should be done to develop an appropriate asymmetry model that leads to accurate inspection method assessment.

$$\forall i, j : C_d|G_{E,i} > C_d|G_{E,j} \Rightarrow POD(\theta^g|G_{E,i}) > POD(\theta_j^g|G_{E,j}) \quad (7.5)$$

The reliability of the inspection methods used in this work for the experimental studies in chapter 5 and 6 are based on the developed damage model including damping. If the damping models introduced in damage indicator model behave differently, it is expected to obtain different POD curves. Therefore, more experiments and studies to investigate the relationship between damping and the damage indicator model are required.

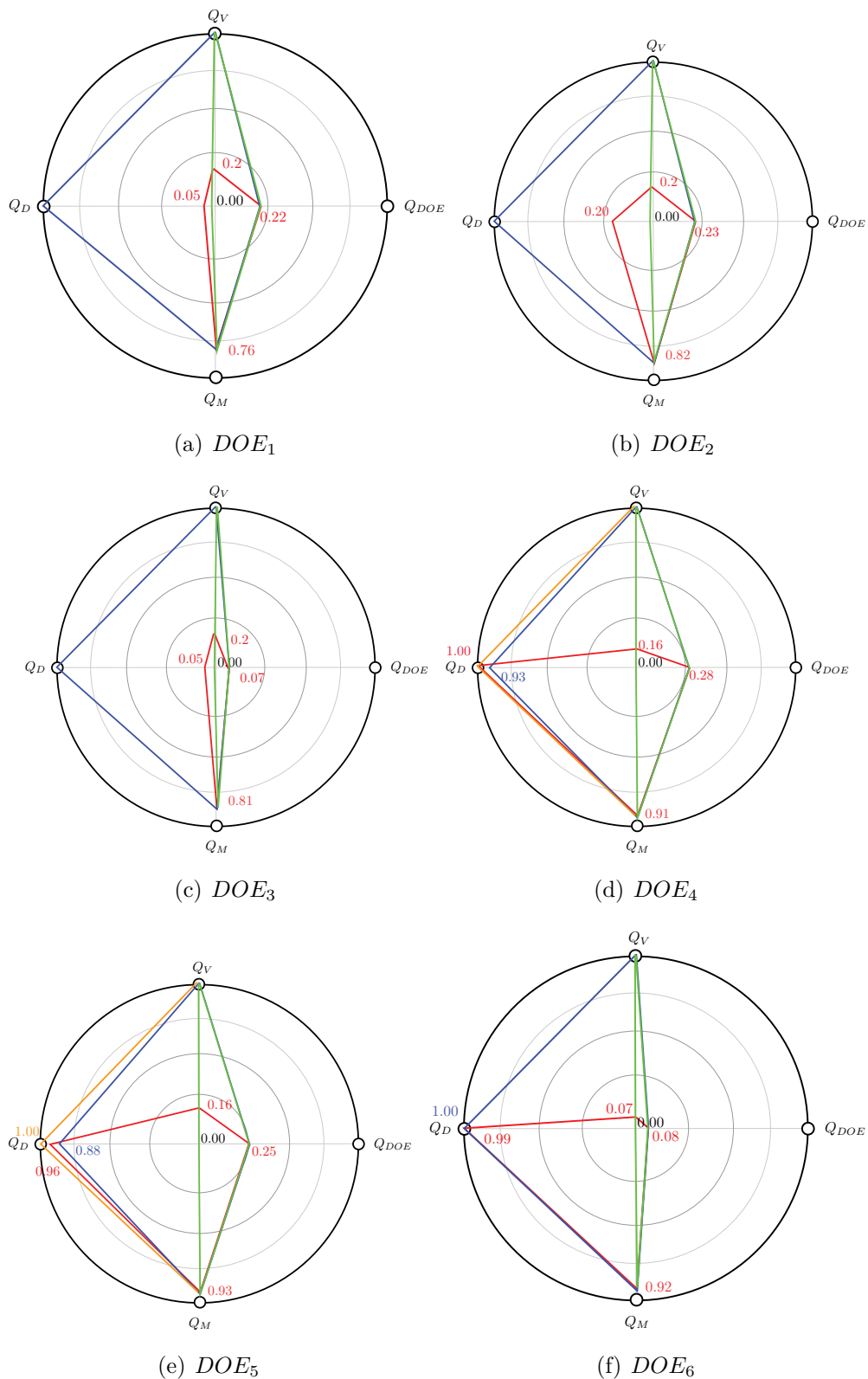


Figure 7.3: Partial models quality of the studied one span steel frame structure considering different DOE models and damping models (red: no damping influence, blue: linear damping model, green: slow damping changes (parabolic), orange: fast damping model changes (parabolic) (covered by blue in some figures))

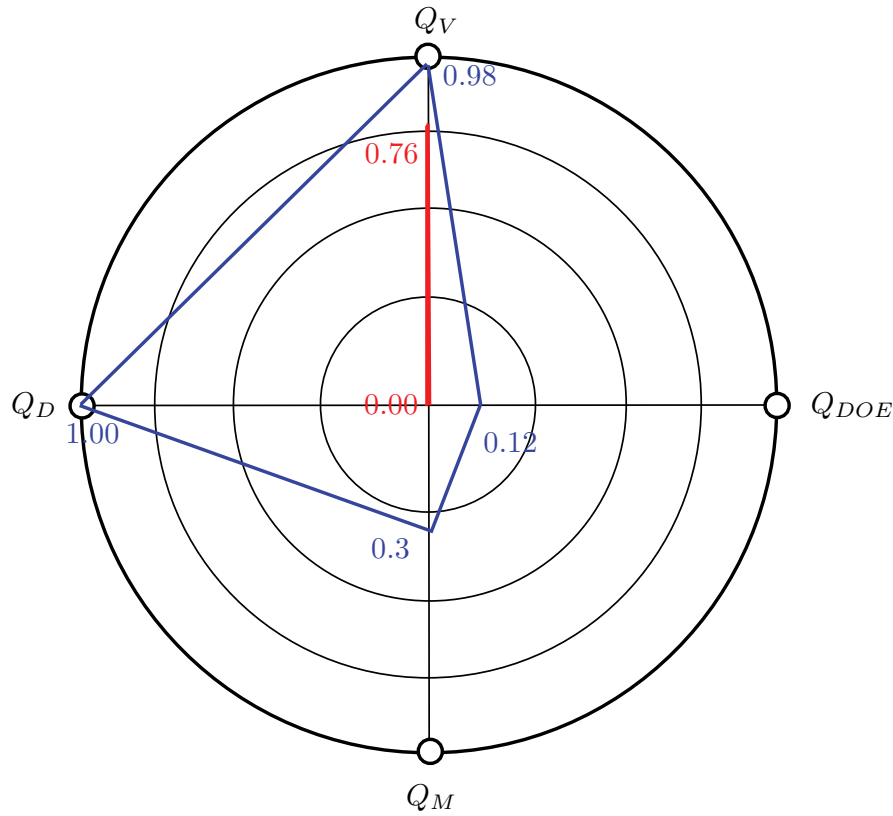


Figure 7.4: Partial models quality of the PVC cantilever example: red line is if the numerical model $G_{M,1}$ was chosen and blue line is if the numerical model $G_{M,2}$ was chosen

7.3 Conclusion

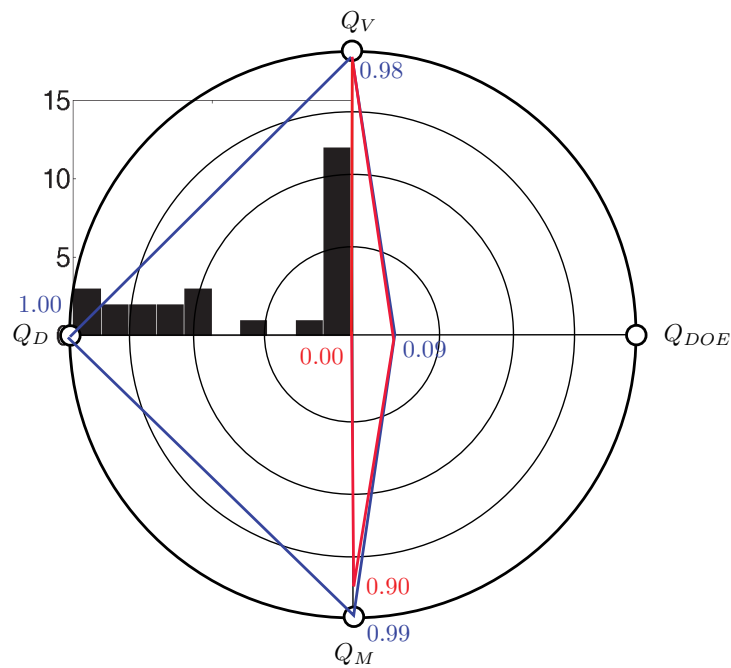
The potential relationship between the quality of the developed models and the reliability of an inspection method for damage detection considering the influence of different types of uncertainty can be concluded as follows:

$G_M : \{\theta\}, \theta^g \rightarrow d(\theta^g, \{\theta\})$: Low Q_V value \Rightarrow inaccurate assessment of the inspection method. Damage will be detected faster or slower than in case of experiments.

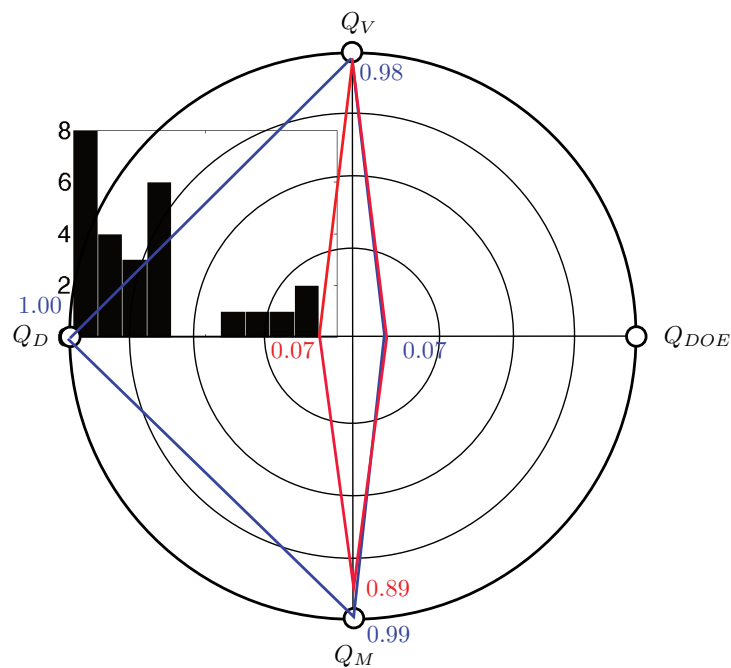
$DOE : \{\hat{\theta}\} \subseteq \{\theta\} \rightarrow F, [U], \dots$: Low Q_{DOE} value \Rightarrow false alarm due to the variation of the input parameters which are not related to damage is expected. As a solution to avoid false alarm, a unique damage pattern can be developed as a part of the DOE model.

$g_E : G_E, DOE, \gamma_F, \theta_E^g \rightarrow \bar{d}$: Low Q_M value \Rightarrow measurements do not provide enough information about damage. As a result, lower POD value is expected

$f : \theta^g \rightarrow d(\theta^g, \epsilon)$: Low Q_D value \Rightarrow unreliable inspection method (low POD value or/and high FPF value).



(a) Test setup 1



(b) Test setup 2

Figure 7.5: Partial models quality of the studied pole structure considering two test setups and 26 experimental model G_E . The histograms show the distribution of the 26 pole samples based on Q_D . Red: the minimum values of the quality indexes, blue: the maximum values of the quality indexes

In the chosen vibration based inspection method, applying forced vibration tests by choosing the appropriate excitation properties that lead to a structural response which is sensitive to the studied damage can help to detect small damage sizes that global inspection method may not detect. Moreover, likelihood functions and damage indicators based on the measured signal energy showed promising results in the case of model updating and damage detection.

Performing primary modal tests and applying system identification to extract the modal parameters of the system provide valuable information that can help to develop a high-quality numerical model (high Q_V value). This leads to an accurate assessment of the studied inspection method.

Chapter 8

Conclusion and Outlook

The current work proposed a model-based strategy to assess and improve the performance of inspection methods for detecting a specific target damage size. The developed strategy is a probabilistic framework which combines several general methods to obtain information about the relationship between utilized models and the reliability of an inspection method.

To simplify the studied global problem, a decoupling procedure was followed to obtain several models before coupling them again. The decoupling principle is based on classifying the studied issues into different groups as follows:

1. The numerical model which contains the developed numerical models of a studied structure and a chosen damage model.
2. The design of experiments which includes a procedure that should be followed to excite a structure and acquire its response. The goal of a chosen design of the experiment is to obtain sufficient information about the variation of a structural response due to damage taking into account different types of uncertainty.
3. The measurements which should provide information to reduce uncertainty and to improve the reliability of a studied inspection method.
4. The damage indicator which represents a relationship between damage size and a chosen structural response of a studied structure.

The developed strategy is based on quantifying the quality of each partial model before computing the reliability of a chosen inspection method. The assessment procedure provides information that should be considered if the improvement of the performance of the chosen inspection method is required. Indexes were used to represent the quality of models which were coupled in a specific manner.

First, after choosing a studied structure, the desired damage type, and a size that should be detected, numerical models of the structure and damage should be developed, and an inspection method should be selected. In the next step, the input parameters and output response should be defined to develop a design of experiment to investigate the relationship between the variation of the outputs and the variation of the input parameters. The quality of the numerical model is quantified using an index Q_V which represents the agreement between the variation of the response of the numerical model of the studied structural and the response of the experimental model due to damage. Low Q_V value lead to inaccurate inspection method assessment.

The coupling between the numerical model and the chosen design of the experiment is accomplished by assigning probabilistic models to the input parameters uncertainty and selecting a sampling method to generate a sufficient number of samples that leads to obtaining the statistical properties of the outputs uncertainty. The primary objective of a chosen design of the experiment is to obtain a significant contribution of desired input parameters which help to detect damage and prevent the influence of undesired input parameters which lead to a false alarm. Therefore, a sensitivity analysis has to be performed to estimate the contribution of each input parameter to each output. The quality of a chosen design of the experiment is quantified using an index Q_{DOE} which is based on the results of the sensitivity analysis. If the low Q_{DOE} value is obtained, a high probability of false alarm should be expected.

Measurements were obtained by performing tests on a physical model based on a chosen design of the experiment. Measurements can provide additional information about the behavior of a structure which can reduce the considered uncertainty. The index Q_M quantifies a quality of measurements based on the uncertainty of desired input parameters before and after taking into account measurements. Considering measurements inside the developed strategy was achieved by using a Bayesian updating approach. Measurements were coupled to the system by assigning a likelihood function to measurements and prior density functions to the input parameters. If the low Q_M value is obtained, measurements do not provide enough information about the critical parameters.

In the next step, a response of the updated numerical model due to damage covering a required range of damage sizes is used to develop a damage size-damage indicator relationship. This relationship is necessary to assess the reliability of a chosen inspection method using the probability of damage detection and the probability of false alarm (false positive). A POD method was developed in this work. The reliability of a chosen inspection method for detecting a specific damage type and size is quantified by an index Q_D which combines both the POD and PFA. The inspection method is not reliable if the low Q_D value is obtained.

Since the efficiency was considered, a Meta-modeling approach was followed to reduce the computational effort and to reduce the complexity of the numerical models. Meta-models are employed to replace complex models to achieve the following goals:

1. Performing sensitivity analysis to obtain the contribution of the considered input parameters to the chosen outputs and to select the important parameters;
2. Applying a model updating procedure to reduce the uncertainty of the important input parameters.

The quality of the developed Meta-models was evaluated by checking the statistical requirements of the residuals. Many methods can be used to develop a Meta-model based on a studied problem. In this work, Meta-models based on polynomial equations were used. The least squares method was applied to obtain the regression coefficients. To improve the quality of the developed Meta-models, a strategy was developed and presented to choose the appropriate terms to obtain optimal or suboptimal Meta-models. Although the advantage of using the Meta-models was significant if a sensitivity analysis and a model updating procedure were performed, the quality of Meta-models should be evaluated by testing basic assumptions related to the statistical properties of the residuals. Otherwise, using low-quality Meta-models may lead to critical errors.

A vibration-based inspection method was applied to numerical and experimental examples to illustrate the application of the developed framework. First, a single degree of freedom system was employed to explain each step of the strategy in detail if a stiffness degradation damage type should be detected. The analytical solution was used to calculate a structural response to avoid a numerical error. As a result, the uncertainty of each step of the strategy can be investigated without influencing the numerical error. Moreover, the influence of choosing a specific excitation type, as a part of a chosen design of the experiment, on obtaining information about desired input parameters was presented.

Second, three degrees of freedom system was used to illustrate the influence of the damage location on the reliability of an inspection method. For this reason, damage at different locations and multi-damage scenarios were studied. A principle of damage patterns was presented to distinguish between the studied scenarios. Damage patterns were developed based on a chosen response of the studied structure due to damage. The chosen inspection method is reliable if the desired damage size was detected with a high probability of detection and low probability of false alarm considering a unique damage patterns set for each scenario.

In the third example, damage in a single-span-one-story steel structure was investigated. The frame was constructed using steel cubes elements connected to each other by bolts. Using these cubes brings complexity to numerical models because of the non-uniform cross-section and connection conditions between cubes. Damage was introduced to the experimental model by replacing the cubes at both ends of the beam by 3D hinges. A shaker was connected to the structure using magnets to produce harmonic excitations. The reliability of the inspection method was investigated taking into account the influence of different damping models and DOE

models which include the number of the sensors, the excitation frequency and the direction of the excitation.

In the fourth example, a cantilever structure made from Polyvinyl chloride (PVC) was studied. A particular damage type was modeled by applying a tension force using adjustable weights to the structure. Two numerical models were developed to represent the structure and the chosen damage. The goal of the example was to illustrate the influence of the developed models on the reliability of the chosen inspection method.

In the fifth example, the performance of a chosen inspection method for damage detection in a pole structure was evaluated considering 26 different experimental models and two test setups.

The results show that improving numerical models, choosing appropriate excitations which lead to a structural response sensitive to damage, updating the uncertainty of essential parameters and choosing appropriate damage indicators can improve the reliability of a chosen inspection method by detecting a specified damage target earlier. These results of this study indicate that there is a significant relationship between the quality of the studied partial models and the reliability of the inspection method for damage detection.

An optimal DOE provided information about desired input parameters that help to detect damage and prevented the influence of undesired input parameters that can lead to a false alarm. However, if some undesired parameters influenced the selected outputs, then they turn to be essential inputs and experiments should provide sufficient information about those parameters otherwise high probability of false alarm should be expected.

The studied partial models may not always be independent. Choosing an optimal DOE was based on defining the inputs and the outputs of the numerical model. The quality of measurements is based on one side on the quality of the chosen DOE and in the other side on measurements uncertainty due to white noise, environmental conditions, quality of the sensors, etc. The quality of damage indicators was influenced by the updated uncertainty after considering measurements. Moreover, the reliability of the chosen inspection methods is based on the desired damage size that should be detected. The method provides a base to choose, evaluate, and compare chosen partial models for a specific damage detection problem.

Many relevant topics should be considered in future studies. For example, the influence of choosing different probabilistic models of uncertainty as coupling models on the quality of the studied partial models and the reliability of inspection methods for damage detection requires more investigation. Moreover, an efficient strategy should be developed to obtain optimal or suboptimal designs of experiments for damage detection and model identification. The decoupling and the assessment procedure used in this work provided the first step to decouple the current studied partials models to finer partial models to improve the evaluation process.

Many other helpful methods which were not mentioned here can be appropriately included to improve the quality of the assessment introduced by the current strategy. For example, the

reliability of an inspection method was based on a chosen threshold to distinguish between noise and damage signal. As a result, threshold optimization has to be a topic for future research as a factor to improve the reliability of the chosen inspection method.

Defining prior probability density functions and extracting the dynamic properties from a dynamic response of a studied structure require user experience in most cases. As a result, uncertainty caused by a human decision should not be ignored for future studies.

The results show that a validation process should be developed. Comparing natural frequencies and mode shapes was not sufficient to obtain a conclusion about the quality of the numerical model. One possible solution is to use the concept of damage patterns developed in this work to validate a model in case of damage detection.

Moreover, a strategy to improve the studied partial models should be developed. The strategy can be based on performing a sensitivity analysis to obtain information about the most critical partial model which has a significant influence on the reliability of the chosen inspection method.

References

- Frederick A. Just Agosto. *Damage detection based on the geometric interpretation of the eigenvalue problem*. PhD thesis, Faculty of the Virginia Polytechnic Institute and State University, 1997.
- Hamid Ahmadian, John Mottershead, and Michael I. Friswell. Damage location indicators from substructure mode shapes. *Inverse Problems in Engineering*, 8(4):309–323, 2000.
- Charles Annis and Luca Gandossi. *ENIQ TGR Technical Document - Influence of Sample Size and Other Factors on Hit/Miss Probability of Detection Curves (ENIQ report N. 47)*. Number 47. Publications Office of the European Union, 2012.
- J.V. Araújo dos Santos, C.M. Mota Soares, C.a. Mota Soares, and N.M.M. Maia. Structural damage identification in laminated structures using FRF data. *Composite Structures*, 67(2): 239–249, February 2005.
- Ivan Argatov and Eric A. Butcher. On the separation of internal and boundary damage in slender bars using longitudinal vibration frequencies and equivalent linearization of damaged bolted joint response. *Journal of Sound and Vibration*, 330(13):3245–3256, June 2011.
- Michèle Basseville. Model-based statistical signal processing for change and damage detection. In Christian Boller, Fou Kuo Chang, and Yozo Fujino, editors, *Encyclopedia of Structural Health Monitoring*, number 36, chapter 36, pages –. John Wiley & Sons, Ltd., 2009.
- Michèle Basseville, Laurent Mevel, Antonio Vecchio, Bart Peeters, and Herman Van der Auweraer. Output-Only Subspace-Based Damage Detection - Application to a Reticular Structure. *Structural Health Monitoring*, 2(2):161–168, June 2003.
- Michèle Basseville, Albert Benveniste, Maurice Goursat, and Laurent Mevel. Subspace-Based Algorithms for Structural Identification, Damage Detection, and Sensor Data Fusion. *EURASIP Journal on Advances in Signal Processing*, 2007(1):069136, 2007.
- Ali Bastani, Hamidreza Amindavar, Mahnaz Shamshirsaz, and Naserodin Sepehry. Adaptive Linear Prediction Damage Detection Technique in Structural Health Monitoring. *Mechanics of Advanced Materials and Structures*, 19(6):492–498, September 2012.

- Alan P. Berens. *NDE Reliability Data Analysis - Metals Handbook*, volume 17. Nondestructive Evaluation and Quality Control, ASM International, 9 edition, 1989.
- Alan P. Berens and Peter W. Hovey. *Evaluation of NDE reliability characterization*, volume I. Dayton: Air Force Wright-Aeronautical Laboratory, Wright-Patterson Air Force Base, 1981.
- Maximilian Billmaier and Christian Bucher. System identification based on selective sensitivity analysis: A case-study. *Journal of Sound and Vibration*, 332(11):2627–2642, 2013.
- Emanuel Bombasaro. *Investigation of different vortex shedding models based on sensibility and probability method to evolve probabilistic models*. PhD thesis, Vienna University of Technology, 2011.
- Kittipong Boonlong. Vibration-Based Damage Detection in Beams by Cooperative Coevolutionary Genetic Algorithm. *Advances in Mechanical Engineering*, 2014, 2014.
- G. E. P. Box and R. Draper. *Empirical Model- Building with Response Surfaces*. Wiley Series in Probability and Statistics, New York, 1 edition, 1987.
- G.E.P. Box and K.B. Wilson. On the experimental attainment of optimum conditions. *Journal of the Royal Statistical Society*, 13(1):1–45, 1951.
- Christian Bucher and Thomas Most. A comparison of approximate response functions in structural reliability analysis. *Probabilistic Engineering Mechanics*, 23(2-3):154–163, 2008.
- M. Chandrashekar and Ranjan Ganguli. Uncertainty handling in structural damage detection using fuzzy logic and probabilistic simulation. *Mechanical Systems and Signal Processing*, 23(2):384–404, February 2009.
- Ming-Hui Chen and Joseph G. Ibrahim. Power prior distributions for regression models, 2000.
- Fook Choon Choi, Jianchun Li, Bijan Samali, and Keith Crews. An experimental study on damage detection of structures using a timber beam. *Journal of Mechanical Science and Technology*, 21(6):903–907, June 2007.
- Anil K. Chopra. *Dynamics of Structures: Theory and Applications to Earthquake Engineering*. Civil Engineering and Engineer. Prentice Hall, 2012. ISBN 9780132858038. URL <https://books.google.de/books?id=3cctkgEACAAJ>.
- Suleyman Korhan Ciloglu. *The impact of uncertainty in operational modal analysis for structural identification of constructed systems*. PhD thesis, Drexel University, 2006.
- Hugh W. Coleman and W. Glenn Steele. *Experimentation, validation, and uncertainty analysis for engineers*. John Wiley & Sons, 3 edition, 2009.

- Amanda L. Cundy. *Use of response surface metamodels in damage identification of dynamic structures*. PhD thesis, Virginia Polytechnic Institute and State University, 2003.
- Ulrike Dackermann. *Vibration-Based Damage Identification Methods for Civil Engineering Structures Using Artificial Neural Networks*. PhD thesis, University of Technology Sydney, 2010.
- Oliver R. de Lautour and Piotr Omenzetter. Damage classification and estimation in experimental structures using time series analysis and pattern recognition. *Mechanical Systems and Signal Processing*, 24(5):1556–1569, July 2010.
- Maher Deeb and Volkmar Zabel. The Reliability of Model-Based NDT in Civil Engineering Using Vibration-Based Inspection Method Including Models Coupling Quality. *Open Access e-journal of Nondestructive Testing*, 19(5), 2014.
- Wu Di. *Vibration-based Structural Assessment with Damage-Detection-Oriented Models*. PhD thesis, Hong Kong Polytechnic University, 2004.
- Scott W. Doebling, Charles R. Farrar, Michael B. Prime, and Daniel W. Shevitz. *Damage identification and health monitoring of structural and mechanical systems from changes in their vibration characteristics: a literature review*. Los Alamos National Laboratory report LA 13070- MS, 1996.
- Michael Havbro Faber. Risk and safety in civil engineering. *Lecture Notes. Swiss Federal Institute of Technology*, 2007.
- Sheng-En Fang and Ricardo Perera. Damage identification by response surface based model updating using D-optimal design. *Mechanical Systems and Signal Processing*, 25(2):717–733, February 2011.
- X. Fang, H. Luo, and J. Tang. Structural damage detection using neural network with learning rate improvement. *Computers & Structures*, 83(25-26):2150–2161, September 2005.
- Alexander Forrester, András Sóbester, and Andy Keane. *Engineering Design via Surrogate Modelling: A Practical Guide*. John Wiley & Sons, Ltd, 2008.
- Michael I. Friswell, J.E.T. Penny, and S.D. Garvey. Parameter subset selection in damage location. *Inverse Problems in Engineering*, 5(3):189–215, 1997.
- Toni Fröbel. *Data coupled civil engineering applications: Modeling and quality assessment methods*. PhD thesis, Bauhaus-Universität Weimar, 2012.
- Michael L. Fugate, Hoon Sohn, and Charles R. Farrar. Vibration-based damage detection using statistical process control. *Mechanical Systems and Signal Processing*, 2001.

- Masatoshi Futakawa, Takashi Naoe, Hiroyuki Kogawa, and Yujiro Ikeda. Damage Diagnostic of Localized Impact Erosion by Measuring Acoustic Vibration. *Journal of Nuclear Science and Technology*, 41(11):1059–1064, November 2004.
- Luca Gandossi and Charles Annis. *ENIQ TGR Technical Document - Probability of Detection Curves: derivation and uses for Risk-Informed In-Service Inspection Applications*. Number 41. Publications Office of the European Union, 2010.
- Andrew Gelma, John Carlin, Hal Stern, and David Rubin. *Bayesian Data Analysis Second Edition*. Chapman & Hall/CRC, Boca Raton, 2004.
- E.R. Generazio. Design of experiments for validating probability of detection capability of NDT systems and for qualification of inspectors. *Materials Evaluation*, (June), 2009.
- George A. Georgiou. *Probability of Detection (POD) curves: derivation, applications and limitations - Research Report 454*. Jacobi Consulting Limited, Health and Safety Executive, 2006.
- Valentina Golubović-Bugarski and Drago Blagojević. An Approach to Damage Detection In A Beam Like Structures From Experimentally Measured FRF Data. *International Journal of Engineering*, pages 296–305, 2010.
- Robert M. Gray. Entropy and Information Theory. *New York*, 17(1994):306, 2009.
- Yan Guo, Kai Yang, and Adel Alaeddini. A Truncated Logistic Regression Model in Probability of Detection Evaluation. *Quality Engineering*, 23(4):365–377, October 2011.
- Amir Ardalan Mosavi Khandan Haghighi. *Vibration-based Damage Detection and Health Monitoring of Bridges*. PhD thesis, North Carolina State University, 2010.
- K. He and W.D. Zhu. A vibration-based structural damage detection method and its applications to engineering structures. *International Journal of Smart and Nano Materials*, 2(3):194–218, September 2011.
- Joshua Hegenderfer, Sez Atamturktur, and Austin Gillen. Topics in Modal Analysis II, Volume 6. 6, 2012.
- Richard G. Hills and Timothy G. Trucano. Statistical validation of engineering and scientific models: Background. *Sandia National Laboratories, SAND99-1256*, (May), 1999.
- Nilson Roberto Inocente-junior and Nazih Mechbal. Real-time structural damage detection using parity residue analysis. *ABCM Symposium Series in Mechatronics*, 4:325–334, 2010.
- Shuichi Jimbo, Antonino Morassi, Gen Nakamura, and Kenji Shirota. A non-destructive method for damage detection in steel-concrete structures based on finite eigendata. *Inverse Problems in Science and Engineering*, 20(2):233–270, 2012.

- Ghada Karaki. *Assessment of coupled models of bridges considering time-dependent vehicular loading*. PhD thesis, Bauhaus-Universität Weimar, 2011.
- Holger Keitel. *Bewertungsmethoden für die Prognosequalität von Kriechmodellen des Betons*. PhD thesis, Bauhaus-Universität Weimar, 2011.
- N. T. Khiem. Crack detection for structure based on the dynamic stiffness model and the inverse problem of vibration. *Inverse Problems in Science and Engineering*, 14(1):85–96, January 2006.
- Anne S. Kiremidjian, Erik G. Straser, Teresa Meng, Kincho Law, and Hoon Sohn. Title: Structural damage monitoring for civil structures. In *in Structural Health Monitoring Current Status and Perspectives*, Fu-Kuo Chang, ed., Technomic Publishing Co, pages 371–382, 1997.
- J.S. Knopp, J.C. Aldrin, E. Lindgren, and C. Annis. Investigation of a Model-Assisted Approach to Probability of Detection Evaluation (Preprint). In *Proceedings of 33rd Annual Review of Progress in Quantitative Nondestructive Evaluation (QNDE)*, 2006.
- M. Kögl, S. Hnourlebaus, and L. Gaul. Finite element simulation of non-destructive damage detection with higher harmonics. *NDT & E International*, 37(3):195–205, April 2004.
- Steven J. Kranock. *Real-time structural damage detection using model-based observers*. PhD thesis, University of Colorado, 2000.
- K. Krishnan Nair and Anne S. Kiremidjian. Time Series Based Structural Damage Detection Algorithm Using Gaussian Mixtures Modeling. *Journal of Dynamic Systems, Measurement, and Control*, 129(3):285, 2007.
- Rathish P. Kumar, T. Oshima, S. Mikami, Y. Miyamori, and T. Yamazaki. Damage identification in a lightly reinforced concrete beam based on changes in the power spectral density. *Structure and Infrastructure Engineering: Maintenance, Management, Life-Cycle Design and Performance*, 8(8):715–727, 2012.
- H.F. Lam and C.T. Ng. A probabilistic method for the detection of obstructed cracks of beam-type structures using spatial wavelet transform. *Probabilistic Engineering Mechanics*, 23(2-3):237–245, April 2008.
- T. Lauwagie, H. Sol, and E. Dascotte. Damage identification in beams using inverse methods. In *International Conference on Noise and Vibration Engineering*, 2002. URL <http://past.isma-isaac.be/isma2002/>.
- S.S. Law, T.H.T. Chan, and D. Wu. Efficient numerical model for the damage detection of large scale structure. *Engineering Structures*, 23:436–451, 2001.

- Daniel P. Loucks, Eelco van Beek, Jerry R. Stedinger, Jozef P.M. Dijkman, and Monique T. Villars. *Water resources systems planning and management. An introduction to methods, models and applications*. Studies and reports in hydrology. UNESCO Publishing / WL - Delft Hydraulics, 2005.
- LSTC. LS-DYNA Keyword User's Manual. Technical Report August, LIVERMORE SOFTWARE TECHNOLOGY CORPORATION, 2012.
- J. Maeck and Guido De Roeck. Damage Detection on a Prestressed Concrete Bridge and RC Beams Using Dynamic System Identification. *Key Engineering Materials*, 167-168:320–327, 1999.
- C. Mandache, M. Khan, A. Fahr, and M. Yanishevsky. Numerical modelling as a cost-reduction tool for probability of detection of bolt hole eddy current testing. *Nondestructive Testing and Evaluation*, 26(1):57–66, March 2011.
- Arnold R. Marder. Replication microscopy techniques for NDE. *ASM Handbook.*, 17, 1989.
- Steven G. Mattson and Sudhakar M. Pandit. Statistical moments of autoregressive model residuals for damage localisation. *Mechanical Systems and Signal Processing*, 20(3):627–645, April 2006.
- V. Meruane and W. Heylen. Damage Detection with Parallel Genetic Algorithms and Operational Modes. *Structural Health Monitoring*, 9(6):481–496, March 2010.
- MIL-HDBK-1823A. Nondestructive evaluation system reliability assessment. Technical report, Department of Defense Handbook, December 2009.
- Thomas Most. Assessment of structural simulation models by estimating uncertainties due to model selection and model simplification, 2011.
- Thomas Most and Christian Bucher. Probabilistic analysis of concrete cracking using neural networks and random fields. *Probabilistic Engineering Mechanics*, 22(2):219–229, 2007.
- Ch. Müller, M. Elagin, M. Scharmach, C. Bellon, G-R. Jaenisch, S. Bär, B. Redmer, J. Goebbels, U. Ewert, U. Zscherpel, R. Boehm, G. Brekow, A. Erhard, T. Heckel, U. Tessaro, and D. Tschardtke. *Reliability of nondestructive testing (NDT) of the copper canister seal weld-R-06-08*. Svensk Kärnbränslehantering AB (SKB), 2006.
- Raymond H. Myers, Douglas C. Montgomery, and Christine M. Anderson-Cook. *Response Surface Methodology: Process and Product Optimization Using Designed Experiments, 3rd Edition*. Wiley Series in Probability and Statistics, 2009.

- K. Krishnan Nair, Anne S. Kiremidjian, and Kincho H. Law. Time series-based damage detection and localization algorithm with application to the ASCE benchmark structure. *Journal of Sound and Vibration*, 291(1-2):349–368, March 2006.
- Mourad Nasser. *Quality Assessment of Dynamic Soil-Structure Interaction Models Using Energy Measures*. PhD thesis, Bauhaus-Universität Weimar, 2012.
- C.T. Ng, M. Veidt, and H.F. Lam. Probabilistic Damage Characterisation in Beams using Guided Waves. *Procedia Engineering*, 14:490–497, January 2011.
- Susanne Nikulla. *Quality assessment of kinematical models by means of global and goal-oriented error estimation techniques*. PhD thesis, Bauhaus-Universität Weimar, 2012.
- Wieslaw Ostachowicz and Marek Krawczuk. Modeling for Detection of Degraded Zones in Metallic and Composite Structures. In Christian Boller, Fou Kuo Chang, and Yozo Fujino, editors, *Encyclopedia of Structural Health Monitoring*. John Wiley & Sons, Ltd, 2009.
- Christian P. Robert. Simulation of truncated normal variables. *Statistics and Computing*, 5(2):121–125, 1995.
- Costas Papadimitriou and Geert Lombaert. The effect of prediction error correlation on optimal sensor placement in structural dynamics. *Mechanical Systems and Signal Processing*, 28:105–127, 2012.
- Chiwoo Park, Jiong Tang, and Yu Ding. Aggressive Data Reduction for Damage Detection in Structural Health Monitoring. 9(1), 2010.
- Ricardo Perera and Antonio Ruiz. A multistage FE updating procedure for damage identification in large-scale structures based on multiobjective evolutionary optimization. *Mechanical Systems and Signal Processing*, 22(4):970–991, May 2008.
- Ricardo Perera, Sheng-En Fang, and C. Huerta. Structural crack detection without updated baseline model by single and multiobjective optimization. *Mechanical Systems and Signal Processing*, 23(3):752–768, April 2009.
- Clovis Petrin, Charles Annis, and Sharon I. Vukelich. A recommended methodology for quantifying NDE/NDI based on aircraft engine experience. *AGARD Lecture Series*, 1993.
- P. Srinivasa Rao and Ch. Ratnama. Damage Identification of Welded Structures Using Time Series Models and Exponentially Weighted Moving Average Control Charts. *Jordan Journal of Mechanical and Industrial Engineering*, 4(6):701–710, 2010.
- C.P. Ratcliffe. Damage detection using a modified Laplacian operator on mode shape data. *Journal of Sound and Vibration*, 204:505–517, 1997.

- Marvin Rausand and Arnljot Høyland. *System Reliability Theory: Models, Statistical Methods, and Applications*. Wiley Series in Probability and Statistics - Applied Probability and Statistics Section. Wiley, 2004.
- John O. Rawlings, Sastry G. Pantula, and David A. Dickey. *Applied Regression Analysis: A Research Tool*. Springer-Verlag New York, 2 edition, 1998.
- Degalhal Mallikarjuna Reddy and Seetharaman Swarnamani. Application of the FRF curvature energy damage detection method to plate like structures. *World Journal of Modelling and Simulation*, 8(2):147–153, 2012.
- Markus Christian Reuter. *Multikriterielle Bewertungsmethode für die Prognosequalität von Komplexen Ingenieurmodellen*. PhD thesis, Bauhaus-Universität Weimar, 2012.
- Edwin Reynders. system identification methods for (operational) modal analysis: Review and comparison. *Archives of Computational Methods in Engineering*, 19-1:51–124, 2012.
- Edwin Reynders, Mattias Schevenels, and Guido De Roeck. MACEC 3.3: A Matlab Toolbox for Experimental and Operational Modal Analysis, Report BWM-2014-06. Technical Report July, Faculty of Engineering, Department of Civil Engineering, Structural Mechanics Section, 2014.
- Ward D. Rummel and George A. Matzkanin. *Nondestructive evaluation (NDE) capabilities data book*. Nondestructive Testing Information Analysis Center (NTIAC), 3 edition, 1997.
- Anders Rytter. *Vibrational based inspection of civil engineering structures*. PhD thesis, 1993.
- Andrea Saltelli, Marco Ratto, Terry Andres, Francesca Campolongo, Jessica Cariboni, Debora Gatelli, Michaela Saisana, and Stefano Tarantola. *Global Sensitivity Analysis. The Primer*. John Wiley & Sons, Ltd, Chichester, UK, December 2007.
- Jing Shi, Xiangjun Xu, Jialai Wang, and Gong Li. Beam damage detection using computer vision technology. *Nondestructive Testing and Evaluation*, 25(3):189–204, September 2010.
- Hoi Wai Shih. *Damage assessment in structures using vibration characteristics*. PhD thesis, Queensland University of Technology, 2009.
- Ellen Simoen, Babak Moaveni, Joel P. Conte, ASCE Member, and Geert Lombaert. Uncertainty Quantification in the Assessment of Progressive Damage in a 7-Story Full-Scale Building Slice. *Journal of Engineering*, 2013.
- Ripudaman Singh. Three decades of NDI reliability assessment. Technical Report May, 2000.
- Jean-Jacques Sinou. *A review of damage detection and health monitoring of mechanical systems from changes in the measurement of linear and non-linear vibrations*. 2009.

- Hoon Sohn. *A Bayesian probabilistic approach to damage detection for civil structures*. PhD thesis, Stanford University, 1998.
- Hoon Sohn and Kincho H. Law. Bayesian probabilistic damage detection of a reinforced-concrete bridge column. *Earthquake Engineering and Structural Dynamics*, 29(8), 2000.
- Wieslaw J. Staszewski and Keith Worden. Signal processing for damage detection. In Christian Boller, Fou Kuo Chang, and Yozo Fujino, editors, *Encyclopedia of Structural Health Monitoring*, number 21, chapter 21, pages –. John Wiley & Sons, Ltd., 2009.
- Tadeusz Stepinski, Tadeusz Uhl, and Wieslaw Staszewski. *Advanced Structural Damage Detection: From Theory to Engineering Applications*. 2013.
- M. M. Reda Taha. Wavelet Transform for Structural Health Monitoring: A Compendium of Uses and Features. *Structural Health Monitoring*, 5(3):267–295, September 2006.
- Ben H. Thacker, Scott W. Doebling, Francois M. Hemez, Mark C. Anderson, Jason E. Pepin, and Edward A. Rodriguez. *Concepts of Model Verification and Validation*. Oct 2004.
- R. Bruce Thompson, Lisa H. Brasche, D. Forsyth, E. Lindgren, P. Swindell, and W. Winfree. Recent advances in model-assisted probability of detection. *in 4th European-American Workshop on the Reliability of NDE, Berlin, Germany*, pages 23–26, 2009.
- A. Tomaszewska. Influence of statistical errors on damage detection based on structural flexibility and mode shape curvature. *Computers & Structures*, 88(3-4):154–164, February 2010.
- Transportation Research Board. Transportation Research Circular E-C107: Control of Cracking in Concrete: State of the Art. Technical Report October, Transportation Research Board, Washington, DC 20001, 2006.
- A. Turon, P.P. Camanho, J. Costa, and C.G. Dávila. A damage model for the simulation of delamination in advanced composites under variable-mode loading. *Mechanics of Materials*, 38(11):1072–1089, November 2006.
- M. Uchida, K. Yoshida, Y.G. Nakagawa, A.J. Allen, and A.D. Whapham. Application of positron annihilation to fatigue and plastic damage detection in SA508 and type 304 steels. *Nondestructive Testing and Evaluation*, 7(1-6):83–91, 1992.
- Yujue Wang. *A non-destructive damage detection method for reinforced concrete structures based on modal strain energy*. PhD thesis, University of Technology, Sydney, 2010.
- Falk K. Wittel, Ferenc Kun, and Hans J. Herrmann. Particle models: Simulation of damage and fracture in composites using a discrete element approach. *Damage and its Evolution in Fiber Composite Materials: Simulation and Non-Destructive Evaluation*, (3):1–18, 2006.

- John D. Wood. Guide to Nondestructive Evaluation Techniques. 17:49–51, 1989.
- Keith Worden and Michael I. Friswell. Modal-vibration-based damage identification. In *Health San Francisco*, pages 1–37. 2009.
- Keith Worden and G. Manson. Damage identification using multivariate statistics: kernel discriminant analysis. *Inverse Problems in Engineering*, 8(1):25–46, 2000.
- J.R. Wu and Q.S. Li. Structural parameter identification and damage detection for a steel structure using a two-stage finite element model updating method. *Journal of Constructional Steel Research*, 62(3):231–239, March 2006.
- A.-M. Yan, G. Kerschen, P. De Boe, and J.-C. Golinval. Structural damage diagnosis under varying environmental conditions-part I: a linear analysis. *Mechanical Systems and Signal Processing*, 19:847–864, 2005.
- Ai-Min Yan and Jean-Claude Golinval. Null subspace-based damage detection of structures using vibration measurements. *Mechanical Systems and Signal Processing*, 20(3):611–626, April 2006.
- Y.J. Yan, L. Cheng, Z.Y. Wu, and L.H. Yam. Development in vibration-based structural damage detection technique. *Mechanical Systems and Signal Processing*, 21(5):2198–2211, July 2007.
- Ruigen Yao and Shamim N. Pakzad. Autoregressive statistical pattern recognition algorithms for damage detection in civil structures. *Mechanical Systems and Signal Processing*, 31: 355–368, August 2012.
- Shu Yao, Jun Teng, Yiqing Xiao, and Feng Xu. Detection of the support damage of spatial steel structures under earthquakes based on shaking table test. *Theoretical and Applied Mechanics Letters*, 1(3):031002, 2011.
- Ka-Veng Yuen. *Bayesian methods for structural dynamics and civil engineering*. John Wiley & Sons, 2010.
- Ka-Veng Yuen, James L. Beck, and Lambros S. Katafygiotis. Unified probabilistic approach for model updating and damage detection. *Journal of Applied Mechanics-Transactions of the ASME*, 73(4):555–564, 2006.
- Volkmar Zabel. *Applications of wavelet analysis in system identification*. PhD thesis, Bauhaus-Universität Weimar, 2002.
- Kun Zhang, Hui Li, Zhongdong Duan, and S.S. Law. A probabilistic damage identification approach for structures with uncertainties under unknown input. *Mechanical Systems and Signal Processing*, 25(4):1126–1145, May 2011.

- Q.W. Zhang. Statistical damage identification for bridges using ambient vibration data. *Computers & Structures*, 85(7-8):476–485, April 2007.
- Wensong Zhou, Zhanjun Wu, and Laurent Mevel. Vibration-based Damage Detection to the Composite Tank Filled with Fluid. *Structural Health Monitoring*, 9(5):433–445, February 2010.
- X. Q. Zhu, S.S. Law, and M. Jayawardhan. Experimental study on Statistical Damage Detection of RC Structures based on Wavelet Packet Analysis. *Journal of Physics: Conference Series*, 305:012107, July 2011.

Appendix A

MATLAB Implementations

A.1 Bayesian Model updating

```
% This file was created by Maher Deeb 2014
% This updating procedure is recommended if Meta-models are used
function []=D_Model_Bayesian_Updating_MD2TL(mean_x, Range_x, Y_exp, Std_model_meas)

%%%%%%%%%%%%%%%%%%%%%%%%%%%%%%%%%%%%%%%%%%%%%%%%%%%%%%%%%%%%%%%%%%%%%%%%
%%%%%%%%%%%%%%%%%%%%%%%%%%%%%%%%%%%%%%%%%%%%%%%%%%%%%%%%%%%%%%%%%%%%%%%%
% Inputs:
% mean_x: row vector the mean values of the input parameters [1xN_{\theta}]
% Range_x: row vector [1xN_{\theta}], it was defined as
%Range_x=max_x-mean_x=mean_x-min_x=(max_x-min_x)/2
%Y_exp: [N_{\bar{d}}, N_{test}] Matrix contains the measured structural
%response i=1:N_{\bar{d}} at
%each test j=1:N_{test}
%Std_model_meas:[N_{\bar{d}}, N_{test}] Matrix contains the standard
%deviation of the total uncertainty= measurement uncertainty+uncertainty
%because of \theta variation + uncertainty due to using Meta-models
%%%%%%%%%%%%%%%%%%%%%%%%%%%%%%%%%%%%%%%%%%%%%%%%%%%%%%%%%%%%%%%%%%%%%%%%
%%%%%%%%%%%%%%%%%%%%%%%%%%%%%%%%%%%%%%%%%%%%%%%%%%%%%%%%%%%%%%%%%%%%%%%%
% the outputs (posteriors) will be saved to a file
%%%%%%%%%%%%%%%%%%%%%%%%%%%%%%%%%%%%%%%%%%%%%%%%%%%%%%%%%%%%%%%%%%%%%%%%
%%%%%%%%%%%%%%%%%%%%%%%%%%%%%%%%%%%%%%%%%%%%%%%%%%%%%%%%%%%%%%%%%%%%%%%%
rpi=1; % Integer: the number of repeating the updating procedure.
%the goal is to be sure that the process is robust if similar posteriors
%were obtained.
while rpi<2
    fprintf('\n ...Model Updating.... started..');
    init_error=1e+5;
    d_prev_error=0;
```

```
%double: error between the calculated and measured structural response.
% it is optional to use. I used it later to monitor the output of the
% Meta-models since Meta-model results can contain some errors
tic % start to calculate the computing time
Nx=2000; % Integer: define the number of samples that
%will be used at each updating step
% Nx should be large enough to obtain constant posteriors but caution
% with computing time and effort
par_i=length(mean_x);
% Integer: the number of parameters that should be updated
[x,pdf_x]=prior_dist(Nx,mean_x,Range_x,'unif');
% this function provide samples giving that
% the prior are obtained from uniform dist. functions.
%x and pdf_x are matrices [Nx,N_{\theta}]
% if other distribution is required then x, pdf_x can be provided
% manually or using the function "sampling-from-Posterior"

xx1=x;
save('temp_posterior','xx1','pdf_x')
%temporary posteriors will be saved at each updating step
%when the next updating step starts, the updated parameters in the previous
%step will be taken into account by loading the file and sampling from it
P(\theta_{i+1}|\bar{d},\theta_{i})

i121=0;

for i0=1:5 % number of loops of applying P(\theta_{i+1}|\bar{d},\theta_{i})
    i_main=1; %counter
    i_repeat=0;
    % Logic value between 0 and 1: if 0 the next parameter will be updated
    %if 1 the current parameter will be updated again by setting all
    %other parameters to their initial distributions. The goal is to
    %search for the most important parameter that reduce the error the
    %most and update this parameter first. This procedure has no
    %influence if a numerical model was used to update the parameters
    %however, in case of using Meta-models, this procedure can lead to
    %better results.
    while i_main<par_i+1
        k=0; % counter
        load('tempop_posterior') % applying P(\theta_{i+1}|\bar{d},\theta_{i})
        for il=1:par_i % start updating the parameter il
            x(:,il)=sampling-from-Posterior(xx1(:,il),pdf_x(:,il),Nx);
            % This function provide Nx samples from any given
            % distribution. In this work, it was used to sample from
            % the computed posterior.
            %Note: in this level any other sampling methods can be used
            %like MCMC or similar but if the updating procedure takes long
```

```

%time it could be interrupted because of license problems
%if someone else is using the same matlab tool box
for ij=1:Nx
    pdf_xxx(ij,i1)=pdf_x(find(xx1(:,i1)<=x(ij,i1),1,'last'),i1);
    % This is important for the next step when the
    % likelihood of the parameter x_{i1}
    %at its value x_i has to be calculated.
end
end

pdf_x_Pos(:,i_main)=pdf_x(:,i_main);
% give the initial value of the posterior

for x_i=mean_x(i_main)-0.5*Range_x(i_main):Range_x(i_main)/(Nx*1):...
    mean_x(i_main)+0.5*Range_x(i_main)-Range_x(i_main)/(1*Nx)
    %in this loop the likelihood will be calculated at each
    %value x_{i1}=x_i inside the range [min_x,max_x]. Nx is
    %important for the quality of the updated dist.
    k=k+1;
    x_plot(k,i_main)=x_i; % this is only for plotting purpose later
    %% prepare the matrices for calculating the likelihood at value x_{i1}=x_i
    x_a=x;
    pdf_x_a=pdf_xxx;
    x_a(:,i_main)=ones(Nx,1)*x_i;
    if x_i<min(x(:,i_main)) || x_i>max(x(:,i_main))
        %% if x_{i1}=x_i out of the range [min_x,max_x],
        %then the likelihood is 0 and no computation is necessary
        pdf_x_a(:,i_main)=ones(Nx,1).*0;
    else
        pdf_x_a(:,i_main)=ones(Nx,1).*...
            pdf_x(find(xx1(:,i_main)<=x_i,1,'last')...
                ,i_main);
    end
end
L_y_x_i=1;
% initial value of the product (P(\bar{d}|\theta)*P(\theta))
for ptheta=1:par_i
    %calculate prod.P(\theta)
    L_y_x_i=L_y_x_i.*pdf_x_a(:,ptheta);
end
%%
if L_y_x_i>0
    y_post_model=zeros(Nx,length(Y_exp(:,1)),length(Y_exp(:,1)));
    %initial value of the model output
    for N_test=1:length(Y_exp(1,:)) %number of tests
        for j=1:length(Y_exp(:,1)) %number of the outputs
            y_post_model(:,j,N_test)=f(x_a);
            % introduce your model here. It is recommended

```

```

% to use Meta-models otherwise it takes look
% time to be calculated
L_y_x_i=L_y_x_i.*(normpdf(Y_exp(j,N_test),...
    y_post_model(:,j,N_test),...
    (Std_model_meas(j,N_test).^2).^0.5));
%calculate the
%product(P(\bar{d}|\theta)*P(\theta)) based on
%a likelihood function obtained from normal
%dist. In general any function can be used
end
end
end
L_y_x(k,i_main)=sum(L_y_x_i);
% the final product(P(\bar{d}|\theta)*P(\theta)) at x_i for
% different combinations of x\ x_i
end
pdf_x_Pos(:,i_main)=L_y_x(:,i_main)./sum(L_y_x(:,i_main));
% get the normalized posterior
pdf_x(:,i_main)=pdf_x_Pos(:,i_main);
xx1(:,i_main)=x_plot(:,i_main);
clear L_y_x y_post_model1
i121=i121+1;
for i10=1:par_i
    x_max_lik(i0,i10)=sum(xx1(:,i10).*pdf_x(:,i10));
    %calculate the mean value from the posteriors
end
end
%% the updating procedure is finished.
%from here only the robustness of the
%Meta-models will be checked to ensure the
% quality of the updating results. This can be ignored if other
% the numerical model model is used for example.
for N_test=1:length(Y_exp(1,:))
    for j=1:length(Y_exp(:,1))
        y_post_model1(j,N_test)=f(x_max_lik);
        % introduce your Meta-model here
    end
end
% end
end
figure(999)
plot(i121,sum(sum((Y_exp-y_post_model1).^2)),'--o')
%plot the error ( this plot should show that the
%error converges to 0 otherwise large error
%due to using Meta-models should be expected)
hold on
%% a procedure to search for the most important
%parameter and accept\reject the posterior
%(important only in case of using Meta-models)

```



```

    if i_main>0
        if i0==0
            if abs(sum(sum((Y_exp-y_post_model1).^2)))-...
                init_error<d_prev_error && i_repeat==0
                [x_i, pdf_x_i]=prior_dist(Nx, mean_x, Range_x, 'unif');
                xx1(:,1:i_main)=x_i(:,1:i_main);
                pdf_x(:,1:i_main)=pdf_x_i(:,1:i_main);
                if d_prev_error<0 || i_main>1
                    i_main=i_main-1;
                    i_repeat=1;
                end
                d_prev_error=abs(sum(sum((Y_exp-y_post_model1).^2)))-init_error;
                save('temop_posterior','xx1','pdf_x')
            else
                save('temop_posterior','xx1','pdf_x')
                i_repeat=0;
                init_error=min(abs(sum(sum((Y_exp-y_post_model1).^2))), init_error)
            end
        else
            if (abs(sum(sum((Y_exp-y_post_model1).^2))<prev_error)
                init_error=abs(sum(sum((Y_exp-y_post_model1).^2)));
                save('temop_posterior','xx1','pdf_x')
            end
        end
        end
        end
        end
        i_main=i_main+1;
    end
    if (init_error<0.0001)
        break
    end
end
hold off
toc % to compute the calculation time

%% plot the posterior
load('temop_posterior')
x_plot=xx1;
pdf_x_Pos=pdf_x;
for i_main=1:par_i
    sorted_data=sortrows([x_plot(:,i_main) pdf_x_Pos(:,i_main)],1);
    x_sort(:,i_main)=sorted_data(:,1);
    pdf_x_Pos(:,i_main)=sorted_data(:,2);
    pdf_x_Pos_mean_i(mean_i,1,i_main)=...
        x_sort(find(pdf_x_Pos(:,i_main))==...
            max(pdf_x_Pos(:,i_main)),1,'first'),i_main);
    pdf_x_Pos_mean_i(mean_i,2,i_main)=max(pdf_x_Pos(:,i_main));
end
end

```

```

Nx=length(pdf_x_Pos(:,1));
%% save the updating results
save(['Model_Bayesian_Updating_results-' int2str(rpi)]...
     , 'x_sort', 'pdf_x_Pos', 'x', 'pdf_x', 'range_x', 'x_max_lik')

for i_main=1:par_i
    figure1=figure(i_main+667);
    set(figure1, 'Position', [0 0 840 700])
    axes1 = axes('Parent',figure1,'FontSize',24,'FontWeight','bold');
    plot(xx1(:,i_main),pdf_x(:,i_main),'Parent',axes1,...
         'LineWidth',2.5,'LineStyle','--','Color',[0 0 0]);
    hold on
    plot(x_sort(:,i_main),pdf_x_Pos(:,i_main),'Parent',axes1,'LineWidth',2.5,...
         'Color',[0.5 0.5 0.5]);
    ylabel({'Density'},'FontWeight','bold','FontSize',30);
    xlim([min(x_sort(:,i_main)) max(x_sort(:,i_main))])
    ylim([0 inf])
end
fprintf('\n ...Model Updating.... done..');
rpi=rpi+1;
pause
close all
end
end

```

A.2 Sampling from a uniform distribution function

```

function[x,pdf_x]=prior_dist(Nx,mean_x,Range_x,dist_perior)
par_i=length(mean_x);
samplesA=lhsdesign(Nx,par_i,'criterion','correlation')-0.5;
x=zeros(Nx,par_i);
for i=1:Nx
    for j=1:length(mean_x)
        x(i,j) = mean_x(j)+1*Range_x(j)*samplesA(i,j);
    end
end
pdf_x=zeros(Nx,par_i);
norm_all=ones(par_i,1);
for i=1:length(mean_x)
    if(strcmp(dist_perior(i,:), 'unif')==1)
        pdf_x(:,i) = unifpdf(x(:,i),mean_x(i)-Range_x(i)/2,mean_x(i)+Range_x(i)/2);
    end
    norm_all(i)=sum(pdf_x(:,i));
    pdf_x(:,i)=(pdf_x(:,i)./norm_all(i));
end
end

```

end

A.3 Sampling from any distribution function using the inverse method

```
function[X_f, pdf_f]=sampling_from_Posterior(x, pdf_x, Nx)
%This method id called 'The Inversive Method' and it can be found easily in the literature
%"Drawing a Sample from a Given Distribution", Dhiren Ghosh and Andrew Vogt, Section on Sur
cdf_x = cumsum(pdf_x);
cdf_x(1)=0;
cdf_x(end)=1;

for i=1:Nx
    U = rand(1,1);
    X_f(i,1) = x(sum(cdf_x<=U));
    pdf_f(i,1)=pdf_x(find(x<=X_f(i,1),1,'last'));
end
end
```

A.4 Probability of detection

```
%This file was created by Maher Deeb 2014
%Probability of damage detection POD
function[]=POD_basic_method(Yd,damage_size,damage_pattern)
%%%%%%%%%%%%%%%%%%%%%%%%%%%%%%%%%%%%%%%%%%%%%%%%%%%%%%%%%%%%%%%%%%%%%%%%
%%%%%%%%%%%%%%%%%%%%%%%%%%%%%%%%%%%%%%%%%%%%%%%%%%%%%%%%%%%%%%%%%%%%%%%%
%inputs:
%Yd: is a 4 dimensions array which includes the structural response due
%damage.
%Yd(sample Number,test Number ,Number related to the
%size of the damage,DOF Number)
%damage_pattern: =1 if the studied structural response increases by increasing
%damage. =-1 if the studied structural response decreases by increasing
%damage. = 0 if the studied structural response is not sensitive to damage
%damage_size: is a vector contains the size of the studied damage which
%increases the from the minimum damage size to the maximum damage size
%with a certain interval
Nx=length(Yd(:,1,1,1));
%search for the threshold
for j=1:length(Yd(1, :,1,1))
    for k=1:length(Yd(1,1,1, :))
        if damage_pattern(k, j)>0
```



```

end
POD=1-POD;
POD_95=1-POD_95;
%save the results
save('POD','damage_size','POD','POD_95','damage_pattern')
%Plot the POD and POD95
figure(1)
plot(damage_size,POD)
hold on
plot(damage_size,POD_95,'r')
hold off
end

```

A.5 Developing Meta-models and selecting their terms

```

%This file was created by Maher Deeb 2013
% developing Meta-models and optimizing their terms
function[chosen_terms,beta_linear,R2_linear,R2_normal,res_i,cov_res_i]=...
    A_meta_model_generation(x,y,degree,interaction,N)
%%%%%%%%%%%%%%%%%%%%%%%%%%%%%%%%%%%%%%%%%%%%%%%%%%%%%%%%%%%%%%%%%%%%%%%%
%%%%%%%%%%%%%%%%%%%%%%%%%%%%%%%%%%%%%%%%%%%%%%%%%%%%%%%%%%%%%%%%%%%%%%%%
%Inputs:
%x: a matrix [N_sample,N_{\theta}]. The columns refer to the number of the
%input parameters and the rows refer to the size of the samples.
%y: is a matrix [N_sample,N_{\bar{d}}]. The columns refer to the number of the
%outputs and the rows refer to the size of the samples.
%y=f(x) which is obtained from solving the numerical model N_sample times
%degree: the maximum degree of the polynomial equation. if degree=2 then x
%and x^2 will be considered.
%interaction: the maximum degree of the terms interaction. e.g. if
%interaction=2, then the terms x1 x2 x3 x1x2 x1x3 x2x3 will be considered
%N: size of the sample
%outputs:
%chosen_terms: is a matrix contains integers related to the term order
%beta_linear: regression coefficients of each term
%R2_linear: if close to 1 then the assumption of the
%linearity between the terms and the outputs is correct (good Meta-model)
%R2_normal: if close to 1 then the residual is normally distributed (good Meta-model)
%cov_res_i: if close to 0 then the error is random (good Meta-model)
%res_i: the residual

%%%%%%%%%%%%%%%%%%%%%%%%%%%%%%%%%%%%%%%%%%%%%%%%%%%%%%%%%%%%%%%%%%%%%%%%
%%%%%%%%%%%%%%%%%%%%%%%%%%%%%%%%%%%%%%%%%%%%%%%%%%%%%%%%%%%%%%%%%%%%%%%%
%generate the terms based on the given maximum degree of the polynomial
x_total=[x];

```

```

for i=2:degree
    x_total=[x_total x.^i];
end
m=0;
mul=ones(N,1);
N1=length(x_total(1,:));

function[terms_no]=get_number_of_terms(N1,interaction)
    terms_no=0;
    for i=1:interaction
        terms_no=terms_no+factorial(N1)/(factorial(i)*factorial(N1-i));
    end
end
function[combinations_full_total,terms]=get_the_used_term...
(N1,interaction,N,x_total)
combinations_full_total=zeros(N,get_number_of_terms(N1,interaction));
%generate the interaction between the terms
terms=zeros(1,interaction);
for i=1:interaction
    c = combnk(1:length(x_total(1,:)),i);
    for j=1:length(c(:,1))
        m=m+1;
        for k=1:length(c(1,:))
            mul=mul.*x_total(:,c(j,k));
            terms(m,k)=c(j,k);
        end
        combinations_full_total(:,m)=mul;
        mul=ones(N,1);
    end
end
end
[combinations_full_total,terms]=get_the_used_term(N1,interaction,N,x_total);
%calculate the correlation between each term and the output data
clearvars -except combinations_full_total terms N y R2_linear_tol ...
R2_normal_tol cov_res_i_tol
k=0;
for i=1:length(combinations_full_total(1,:))
    k=k+1;
    clc
    step_1=100-round(100*(length(combinations_full_total(1,:))...
        -k)/length(combinations_full_total(1,:)));
    combinations_full=combinations_full_total(:,k);
    chosen_terms=terms(k,:);
    X1_linear = [ones(N,1) combinations_full];
    [beta_linear] = regress(y,X1_linear);
    beta_linear_mult=prod(beta_linear);
    if (beta_linear_mult==0)

```

```

        combinations_full_total(:,k)=[];
        terms(k,:)=[];
        k=k-1;
    else
        y_linear = beta_linear(1)*ones(N,1);
        for ii=1:length(combinations_full(1,:))
            y_linear = y_linear + beta_linear(ii+1)*combinations_full(1:N,ii);
        end
        R2_linear(k) = (corr(y,y_linear))^2;
        y_linear=[];
    end
end
end
% sort the terms based on the correlation. First term show the maximum
% correlation
combinations_full_total_sorted=[R2_linear',combinations_full_total'];
combinations_full_total_sorted1=(sortrows(combinations_full_total_sorted,-1))';
combinations_full_total_sorted1(1,:)=[];
terms_sorted=[R2_linear',terms];
terms_sorted1=sortrows(terms_sorted,-1);
terms_sorted1(:,1)=[];
combinations_full_total=combinations_full_total_sorted1;
terms=terms_sorted1;
%+++++
%+++++
%+++++
clearvars -except combinations_full_total terms N y...
    R2_linear_tol R2_normal_tol cov_res_i_tol
k=0;
%start to build the model: combine the terms and ignore the terms that do
%not improve the Meta-model
R2_linear=[];
for i=1:length(combinations_full_total(1,:))
    clc
    step_2=100-round(100*(length(combinations_full_total(1,:))-k)...
        /length(combinations_full_total(1,:)))
    k=k+1;
    combinations_full=combinations_full_total(:,1:k);
    chosen_terms=terms(1:k,:);
    X1_linear = [ones(N,1) combinations_full];
    [beta_linear,conf_Ints,res_i,rint,stats] = regress(y,X1_linear);
    beta_linear_mult=prod(beta_linear);
    %+++++
    %the last step if still the last term does not work
    if (k==length(combinations_full_total(1,:)) && beta_linear_mult==0)
        combinations_full=combinations_full_total(:,1:k-1);
        chosen_terms=terms(1:k-1,:);
        X1_linear = [ones(N,1) combinations_full];
    end
end
end

```

```

[beta_linear, conf_Ints, res_i, rint, stats] = regress(y, X1_linear);
y_linear_1 = beta_linear(1)*ones(N,1);
for ii=1:length(combinations_full(1,:))
    y_linear_1 = y_linear_1 + beta_linear(ii+1)*combinations_full(1:N,ii);
end
% cross validation of the error (residual)
res_standardized=res_i;
res_standardized=sort(res_standardized);
res_standardized_domy=randn(N,1);
res_standardized_domy=sort(res_standardized_domy);
% is the error normal distributed
R2_normal = (corr(res_standardized,res_standardized_domy))^2;
%check the linearty of the data
R2_linear = (corr(y,y_linear))^2
%check if the error is random
cov_res_i=cov(res_i(2:end),res_i(1:end-1));
end
%+++++
y_linear_1 = beta_linear(1)*ones(N,1);
for ii=1:length(combinations_full(1,:))
    y_linear_1 = y_linear_1 + beta_linear(ii+1)*combinations_full(1:N,ii);
end
R2_linear_help(k) = (corr(y,y_linear_1))^2;
if (beta_linear_mult==0 || R2_linear_help(max(k-1,1))>R2_linear_help(k))
    combinations_full_total(:,k)=[];
    terms(k,:)=[];
    k=k-1;
else
    y_linear = beta_linear(1)*ones(N,1);
    for ii=1:length(combinations_full(1,:))
        y_linear = y_linear + beta_linear(ii+1)*combinations_full(1:N,ii);
    end
    % cross validation of the error (residual)
    res_standardized=res_i;
    res_standardized=sort(res_standardized);
    res_standardized_domy=randn(N,1);
    res_standardized_domy=sort(res_standardized_domy);
    % is the error normal distributed (R2_normal=1 then yes)
    R2_normal = (corr(res_standardized,res_standardized_domy))^2;
    %check the linearty of the data (R2_linear=1
    %then the assumption is correct)
    R2_linear = (corr(y,y_linear))^2
    %check if the error is random (cov_res_i=0 then yes)
    cov_res_i=cov(res_i(2:end),res_i(1:end-1));
end
end
%+++++

```



```
%+++++  
end
```

Appendix B

Finite Element models (LS DYNA reduced input)

B.1 Steel frame structure

```
## LS-DYNA Keyword file created by LS-PrePost(R) V4.3 (Beta) - 27Jul2015(09:00)
## Created on Nov-02-2015 (12:06:48)
*KEYWORD MEMORY=500000000 NCPU=1
*TITLE
##
LS-DYNA keyword deck by LS-PrePost
*CONTROL_IMPLICIT_DYNAMICS
##      imass      gamma      beta      tdybir      tdydth      tdybur      irate
          1          0.5          0.25          0.01.00000E281.00000E28          0
*CONTROL_IMPLICIT_GENERAL
##      imflag      dt0      imform      nsbs      igs      cnstn      form      zero_v
          1 0.0019531          2          1          2          0          0          0
*CONTROL_TERMINATION
##      endtim      endcyc      dtmin      endeng      endmas
          5.0          0          0.0          0.01.000000E8
*DATABASE_NODOUT
##      dt      binary      lcur      ioopt      option1      option2
 0.0019531          0          0          1          0.0          0
*DATABASE_HISTORY_NODE_SET
##      id1      id2      id3      id4      id5      id6      id7      id8
          269          0          0          0          0          0          0          0
*BOUNDARY_SPC_SET
```

```

$#      nsid      cid      dofx      dofz      dofrx      dofry      dofrz
      196         0         1         1         1         1         1
*LOAD_NODE_POINT
$#      nid      dof      lcid      sf      cid      m1      m2      m3
      13730      2         1      100.0      0         0         0         0
*PART
$#                                           title
LSHELL1
$#      pid      secid      mid      eosid      hgid      grav      adpopt      tmid
      1         2         2         0         0         0         0         0
*SECTION_SHELL_TITLE
hinge plate
$#      secid      elform      shrf      nip      propt      qr/irid      icomp      setyp
      2         2         1.0      5         1.0         0         0         1
$#      t1      t2      t3      t4      nloc      marea      idof      edgset
      25.0     25.0     25.0     25.0     0.0         0.0         0.0         0
*MAT_ELASTIC_TITLE
hinge
$#      mid      ro      e      pr      da      db      not used
      27.83000E-9  177000.00.30000001  0.0      0.0         0
*PART
$#                                           title
LSHELL2
$#      pid      secid      mid      eosid      hgid      grav      adpopt      tmid
      2         2         2         0         0         0         0         0
*PART
$#                                           title
4
$#      pid      secid      mid      eosid      hgid      grav      adpopt      tmid
      3         4         4         0         0         0         0         0
*SECTION_SHELL_TITLE
stiffers
$#      secid      elform      shrf      nip      propt      qr/irid      icomp      setyp
      4         2         1.0      4         1.0         0         0         1
$#      t1      t2      t3      t4      nloc      marea      idof      edgset
      6.0      6.0      6.0      6.0      0.0         0.0         0.0         0
*MAT_ELASTIC_TITLE
stiffers
$#      mid      ro      e      pr      da      db      not used

```

47.83000E-9 177000.00.30000001 0.0 0.0 0

*PART

\$# title

4

\$#	pid	secid	mid	eosid	hgid	grav	adpopt	tmid
	4	4	4	0	0	0	0	0

*PART

\$# title

4

\$#	pid	secid	mid	eosid	hgid	grav	adpopt	tmid
	5	4	4	0	0	0	0	0

*PART

\$# title

4

\$#	pid	secid	mid	eosid	hgid	grav	adpopt	tmid
	6	4	4	0	0	0	0	0

*PART

\$# title

LSHELL7

\$#	pid	secid	mid	eosid	hgid	grav	adpopt	tmid
	7	1	1	0	0	0	0	0

*SECTION_SHELL_TITLE

cube

\$#	secid	elform	shrf	nip	propt	qr/irid	icom	setyp
	1	2	1.0	4	1.0	0	0	1

\$#	t1	t2	t3	t4	nloc	mare	idof	edgset
	6.0	6.0	6.0	6.0	0.0	0.0	0.0	0

*MAT_ELASTIC_TITLE

steel_cube

\$#	mid	ro	e	pr	da	db	not used
	17.83000E-9	179000.00	.30000001		0.0	0.0	0

*PART

\$# title

LSHELL8

\$#	pid	secid	mid	eosid	hgid	grav	adpopt	tmid
	8	1	1	0	0	0	0	0

*PART

\$# title

LSHELL9

```
##      pid      secid      mid      eosid      hgid      grav      adpopt      tmid
      9          1          1          0          0          0          0          0
*PART
##
LSHELL10
##      pid      secid      mid      eosid      hgid      grav      adpopt      tmid
      10         1          1          0          0          0          0          0
*PART
##
LSHELL11
##      pid      secid      mid      eosid      hgid      grav      adpopt      tmid
      11         1          1          0          0          0          0          0
*PART
##
LSHELL12
##      pid      secid      mid      eosid      hgid      grav      adpopt      tmid
      12         1          1          0          0          0          0          0
*PART
##
LSHELL13
##      pid      secid      mid      eosid      hgid      grav      adpopt      tmid
      13         1          1          0          0          0          0          0
*PART
##
LSHELL14
##      pid      secid      mid      eosid      hgid      grav      adpopt      tmid
      14         1          1          0          0          0          0          0
*PART
##
LSHELL15
##      pid      secid      mid      eosid      hgid      grav      adpopt      tmid
      15         1          1          0          0          0          0          0
*PART
##
LSHELL16
##      pid      secid      mid      eosid      hgid      grav      adpopt      tmid
      16         1          1          0          0          0          0          0
*PART
##
```

LSHELL17

##	pid	secid	mid	eosid	hgid	grav	adpopt	tmid
	17	1	1	0	0	0	0	0

*PART

title

LSHELL18

##	pid	secid	mid	eosid	hgid	grav	adpopt	tmid
	18	1	1	0	0	0	0	0

*PART

title

LSHELL19

##	pid	secid	mid	eosid	hgid	grav	adpopt	tmid
	19	1	1	0	0	0	0	0

*PART

title

LSHELL20

##	pid	secid	mid	eosid	hgid	grav	adpopt	tmid
	20	1	1	0	0	0	0	0

*PART

title

LSHELL21

##	pid	secid	mid	eosid	hgid	grav	adpopt	tmid
	21	1	1	0	0	0	0	0

*PART

title

LSHELL22

##	pid	secid	mid	eosid	hgid	grav	adpopt	tmid
	22	1	1	0	0	0	0	0

*PART

title

LSHELL23

##	pid	secid	mid	eosid	hgid	grav	adpopt	tmid
	23	1	1	0	0	0	0	0

*PART

title

LSHELL24

##	pid	secid	mid	eosid	hgid	grav	adpopt	tmid
	24	1	1	0	0	0	0	0

*PART

```
## title
LSHELL25
## pid secid mid eosid hgid grav adpopt tmid
    25      1    1     0     0     0     0     0
*PART
## title
LSHELL26
## pid secid mid eosid hgid grav adpopt tmid
    26      1    1     0     0     0     0     0
*PART
## title
LSHELL27
## pid secid mid eosid hgid grav adpopt tmid
    27      1    1     0     0     0     0     0
*PART
## title
LSHELL28
## pid secid mid eosid hgid grav adpopt tmid
    28      1    1     0     0     0     0     0
*PART
## title
LSHELL29
## pid secid mid eosid hgid grav adpopt tmid
    29      1    1     0     0     0     0     0
*PART
## title
LSHELL30
## pid secid mid eosid hgid grav adpopt tmid
    30      1    1     0     0     0     0     0
*PART
## title
LSHELL31
## pid secid mid eosid hgid grav adpopt tmid
    31      1    1     0     0     0     0     0
*PART
## title
LSHELL32
## pid secid mid eosid hgid grav adpopt tmid
    32      1    1     0     0     0     0     0
```

*PART

\$# title

LSHELL33

\$#	pid	secid	mid	eosid	hgid	grav	adpopt	tmid
	33	1	1	0	0	0	0	0

*PART

\$# title

LSHELL34

\$#	pid	secid	mid	eosid	hgid	grav	adpopt	tmid
	34	1	1	0	0	0	0	0

*PART

\$# title

LSHELL35

\$#	pid	secid	mid	eosid	hgid	grav	adpopt	tmid
	35	1	1	0	0	0	0	0

*PART

\$# title

LSHELL36

\$#	pid	secid	mid	eosid	hgid	grav	adpopt	tmid
	36	1	1	0	0	0	0	0

*PART

\$# title

LSHELL37

\$#	pid	secid	mid	eosid	hgid	grav	adpopt	tmid
	37	1	1	0	0	0	0	0

*PART

\$# title

LSHELL38

\$#	pid	secid	mid	eosid	hgid	grav	adpopt	tmid
	38	1	1	0	0	0	0	0

*PART

\$# title

LSHELL39

\$#	pid	secid	mid	eosid	hgid	grav	adpopt	tmid
	39	1	1	0	0	0	0	0

*PART

\$# title

LSHELL40

\$#	pid	secid	mid	eosid	hgid	grav	adpopt	tmid
-----	-----	-------	-----	-------	------	------	--------	------


```

    40      1      1      0      0      0      0      0
*PART
$#                                     title
LSHELL41
$#  pid  secid  mid  eosid  hgid  grav  adpopt  tmid
    41      1      1      0      0      0      0      0
*PART
$#                                     title
LSHELL42
$#  pid  secid  mid  eosid  hgid  grav  adpopt  tmid
    42      1      1      0      0      0      0      0
*PART
$#                                     title
LSHELL43
$#  pid  secid  mid  eosid  hgid  grav  adpopt  tmid
    43      1      1      0      0      0      0      0
*PART
$#                                     title
LSHELL44
$#  pid  secid  mid  eosid  hgid  grav  adpopt  tmid
    44      1      1      0      0      0      0      0
*PART
$#                                     title
LSHELL45
$#  pid  secid  mid  eosid  hgid  grav  adpopt  tmid
    45      1      1      0      0      0      0      0
*PART
$#                                     title
LSHELL46
$#  pid  secid  mid  eosid  hgid  grav  adpopt  tmid
    46      1      1      0      0      0      0      0
*PART
$#                                     title
LSHELL47
$#  pid  secid  mid  eosid  hgid  grav  adpopt  tmid
    47      1      1      0      0      0      0      0
*PART
$#                                     title
LSHELL48
```

```
##      pid      secid      mid      eosid      hgid      grav      adpopt      tmid
      48          1          1          0          0          0          0          0
*PART
##
LSHELL49
##      pid      secid      mid      eosid      hgid      grav      adpopt      tmid
      49          1          1          0          0          0          0          0
*PART
##
LSHELL50
##      pid      secid      mid      eosid      hgid      grav      adpopt      tmid
      50          1          1          0          0          0          0          0
*PART
##
LSHELL51
##      pid      secid      mid      eosid      hgid      grav      adpopt      tmid
      51          1          1          0          0          0          0          0
*PART
##
LSHELL52
##      pid      secid      mid      eosid      hgid      grav      adpopt      tmid
      52          1          1          0          0          0          0          0
*PART
##
LSHELL53
##      pid      secid      mid      eosid      hgid      grav      adpopt      tmid
      53          1          1          0          0          0          0          0
*PART
##
LSHELL54
##      pid      secid      mid      eosid      hgid      grav      adpopt      tmid
      54          1          1          0          0          0          0          0
*PART
##
LSHELL55
##      pid      secid      mid      eosid      hgid      grav      adpopt      tmid
      55          1          1          0          0          0          0          0
*PART
##
```

LSHELL56

\$#	pid	secid	mid	eosid	hgid	grav	adpopt	tmid
	56	1	1	0	0	0	0	0

*PART

\$# title

LSHELL57

\$#	pid	secid	mid	eosid	hgid	grav	adpopt	tmid
	57	1	1	0	0	0	0	0

*PART

\$# title

LSHELL58

\$#	pid	secid	mid	eosid	hgid	grav	adpopt	tmid
	58	1	1	0	0	0	0	0

*PART

\$# title

LSHELL59

\$#	pid	secid	mid	eosid	hgid	grav	adpopt	tmid
	59	1	1	0	0	0	0	0

*PART

\$# title

LSHELL60

\$#	pid	secid	mid	eosid	hgid	grav	adpopt	tmid
	60	1	1	0	0	0	0	0

*PART

\$# title

LSHELL61

\$#	pid	secid	mid	eosid	hgid	grav	adpopt	tmid
	61	1	1	0	0	0	0	0

*PART

\$# title

LSHELL62

\$#	pid	secid	mid	eosid	hgid	grav	adpopt	tmid
	62	1	1	0	0	0	0	0

*PART

\$# title

LSHELL63

\$#	pid	secid	mid	eosid	hgid	grav	adpopt	tmid
	63	1	1	0	0	0	0	0

*PART

```

$# title
LSHELL64
$# pid secid mid eosid hgid grav adpopt tmid
    64    1    1    0    0    0    0    0
*PART
$# title
LSHELL65
$# pid secid mid eosid hgid grav adpopt tmid
    65    1    1    0    0    0    0    0
*PART
$# title
LSHELL66
$# pid secid mid eosid hgid grav adpopt tmid
    66    1    1    0    0    0    0    0
*PART
$# title
Beam67
$# pid secid mid eosid hgid grav adpopt tmid
    67    3    3    0    0    0    0    0
*SECTION_BEAM_TITLE
shaker
$# secid elform shrf qr/irid cst scoor nsm
    3     1    1.0    2     0    0.0    0.0
$# ts1 ts2 tt1 tt2 nsloc ntloc
    1.0 1.0 1.0 1.0 0.0 0.0
*MAT_RIGID_TITLE
shaker
$# mid ro e pr n couple m alias
    31.0000E-15 227000.00.30000001 0.0 0.0 0.0
$# cmo con1 con2
    0.0 0 0
$#lco or a1 a2 a3 v1 v2 v3
    0.0 0.0 0.0 0.0 0.0 0.0
*PART
$# title
stiffers1
$# pid secid mid eosid hgid grav adpopt tmid
    68    4    4    0    0    0    0    0
*PART

```

```
## title
stiffer_2
## pid secid mid eosid hgid grav adpopt tmid
    69    4    5    0    0    0    0    0
*MAT_ELASTIC_TITLE
stiffers_in_case 2
## mid ro e pr da db not used
    57.83000E-9 177000.00.30000001 0.0 0.0 0
*PART
## title
stiffer_3
## pid secid mid eosid hgid grav adpopt tmid
    70    4    4    0    0    0    0    0
*PART
## title
Stiffer_4
## pid secid mid eosid hgid grav adpopt tmid
    71    4    5    0    0    0    0    0
*PART
## title
hinge_2_1
## pid secid mid eosid hgid grav adpopt tmid
    72    2    2    0    0    0    0    0
*PART
## title
hinge_2_1
## pid secid mid eosid hgid grav adpopt tmid
    73    2    2    0    0    0    0    0
*PART
## title
## pid secid mid eosid hgid grav adpopt tmid
    74    1    1    0    0    0    0    0
*PART
## title
## pid secid mid eosid hgid grav adpopt tmid
    75    1    1    0    0    0    0    0
*DEFINE_CURVE
```

```

$#   lcid     sidr     sfa     sfo     offa     offo     dattyp     lcint
      1       0       1.0     1.0     0.0     0.0         0         0
$#
*SET_PART_LIST
$#   sid     da1     da2     da3     da4     solver
      1     0.0     0.0     0.0     0.0MECH
$#   pid1     pid2     pid3     pid4     pid5     pid6     pid7     pid8
      1       2       3       4       5       6       9      10
     11     12     13     14     15     16     17     18
     19     20     21     22     23     24     25     26
     27     28     29     30     31     32     33     34
     35     36     37     38     39     40     41     42
     43     44     46     49     50     51     52     53
     54     55     56     57     58     59     60     61
     62     63     64     65     66     67       0       0
*CONSTRAINED_NODE_SET
$#   nsid     dof     tf
      1     71.00000E20
*DAMPING_GLOBAL
$#   lcid     valdmp     stx     sty     stz     srx     sry     srz
      0     0.4587     0.0     0.0     0.0     0.0     0.0     0.0
*DAMPING_PART_STIFFNESS_SET
$#   psid     coef
      13.36213E-6
*ELEMENT_SHELL
$#   eid     pid     n1     n2     n3     n4     n5     n6     n7     n8
*ELEMENT_BEAM
$#   eid     pid     n1     n2     n3     rt1     rr1     rt2     rr2     local
     72127     67    13730    82565    11693     0       0       0       0       2
*ELEMENT_MASS
$#   eid     nid     mass     pid
     82565    13730     0.0031     0
*NODE
$#   nid     x     y     z     tc     rc
*END

```

B.2 Cantilever PVC with cables

LS-DYNA Keyword file created by LS-PrePost(R) V4.3 (Beta) - 27Jul2015(09:00)

Created on Dec-02-2015 (16:58:09)

*KEYWORD MEMORY=500000000 NCPU=1

*PARAMETER

##	prmr1	val1	prmr2	val2	prmr3	val3	prmr4	val4
R par_1	6							
R par_2	4							
R par_3	3000							
R par_4	4000							
R par_5	-10							
R par_6	5							
R par_7	5							

*TITLE

title

LS-DYNA keyword deck by LS-PrePost

*CONTROL_IMPLICIT_DYNAMICS

##	imass	gamma	beta	tdybir	tdydth	tdybur	irate
	1	0.5	0.25	0.01.00000E28	1.00000E28		0

*CONTROL_IMPLICIT_GENERAL

##	imflag	dt0	imform	nsbs	igs	cnstn	form	zero_v
	02.44100E-4		2	1	1	0	0	0

*CONTROL_TERMINATION

##	endtim	endcyc	dtmin	endeng	endmas
	9.0	0	0.0	0.01.000000E8	

*DATABASE_NODOUT

##	dt	binary	lcur	ioopt	option1	option2
	2.44141E-4	1	0	1	0.0	0

*DATABASE_BINARY_D3PLOT

##	dt	lcdt	beam	npltc	psetid
	0.01	0	0	0	0

ioopt

0

*DATABASE_HISTORY_NODE_SET

##	id1	id2	id3	id4	id5	id6	id7	id8
	7	0	0	0	0	0	0	0

*BOUNDARY_SPC_SET

##	nsid	cid	dofx	dofy	dofz	dofrx	dofry	dofrz
----	------	-----	------	------	------	-------	-------	-------

```

      1      0      1      1      1      1      1      1
*SET_NODE_LIST_TITLE
NODESET(SPC) 1
$#   sid      da1      da2      da3      da4      solver
      1      0.0      0.0      0.0      0.0MECH
$#   nid1      nid2      nid3      nid4      nid5      nid6      nid7      nid8
      1      3      4      5      6      7      8      9
      10      11      12      13      0      0      0      0
*BOUNDARY_SPC_SET
$#   nsid      cid      dofx      dofy      dofz      dofrx      dofry      dofrz
      4      1      0      1      1      0      0      0
*SET_NODE_LIST
$#   sid      da1      da2      da3      da4      solver
      4      0.0      0.0      0.0      0.0MECH
$#   nid1      nid2      nid3      nid4      nid5      nid6      nid7      nid8
      1228      0      0      0      0      0      0      0
*BOUNDARY_SPC_SET
$#   nsid      cid      dofx      dofy      dofz      dofrx      dofry      dofrz
      5      2      0      1      1      0      0      0
*SET_NODE_LIST
$#   sid      da1      da2      da3      da4      solver
      5      0.0      0.0      0.0      0.0MECH
$#   nid1      nid2      nid3      nid4      nid5      nid6      nid7      nid8
      1227      0      0      0      0      0      0      0
*LOAD_NODE_POINT
$#   nid      dof      lcid      sf      cid      m1      m2      m3
      1228      1      1&par_1      1      1      0      0      0
      1227      1      1&par_2      2      2      0      0      0
      722      2      2&par_5      0      0      0      0      0
      1197      1      2&par_6      0      0      0      0      0
*PART
$#                                          title
LSHELL1
$#   pid      secid      mid      eosid      hgid      grav      adpopt      tmid
      1      1      4      0      0      0      0      0
*SECTION_SHELL_TITLE
PVC
$#   secid      elform      shrf      nip      propt      qr/irid      icomp      setyp
      1      2      1.0      5      1.0      0      0      1

```



```

$#      t1      t2      t3      t4      nloc      marea      idof      edgset
        3.2      3.2      3.2      3.2      0.0      0.0      0.0      0
*MAT_ELASTIC_TITLE
PVC_half_pipe
$#      mid      ro      e      pr      da      db      not used
        41.39000E-9&par_4      0.40000001      0.0      0.0      0
*PART
$#
cable_right
$#      pid      secid      mid      eosid      hgid      grav      adpopt      tmid
        2      2      3      0      0      0      0      0
*SECTION_BEAM_TITLE
rubber
$#      secid      elform      shrf      qr/irid      cst      scoor      nsm
        2      6      1.0      2      0      0.0      0.0
$#      vol      iner      cid      ca      offset      rrcon      srcon      trcon
        100.0      0.0      0      20.0      0.0      0.0      0.0      0.0
*MAT_CABLE_DISCRETE_BEAM_TITLE
rubber_right
$#      mid      ro      e      lcid      f0      tmaxf0      tramp      iread
        31.10000E-9&par_7      0      0.0      0.0      0.0      0
*PART
$#
half_pipe
$#      pid      secid      mid      eosid      hgid      grav      adpopt      tmid
        3      1      1      0      0      0      0      0
*MAT_ELASTIC_TITLE
PVC
$#      mid      ro      e      pr      da      db      not used
        11.39000E-9&par_3      0.40000001      0.0      0.0      0
*PART
$#
cable_left
$#      pid      secid      mid      eosid      hgid      grav      adpopt      tmid
        4      2      5      0      0      0      0      0
*MAT_CABLE_DISCRETE_BEAM_TITLE
rubber_left
$#      mid      ro      e      lcid      f0      tmaxf0      tramp      iread
        51.10000E-9&par_7      0      0.0      0.0      0.0      0

```

*MAT_ELASTIC_TITLE

rubber_not_used

\$#	mid	ro	e	pr	da	db	not used
	21.10000E-9		500.00	.49000001	0.0	0.0	0

*DEFINE_COORDINATE_SYSTEM_TITLE

cable_direction

\$#	cid	xo	yo	zo	x1	y1	z1
	1-53.399685	-0.1832911	2970.4487		-1000.0	0.0	4200.0

\$#	xp	yp	zp
	-1000.0	0.0	3200.0

*DEFINE_COORDINATE_SYSTEM_TITLE

cable_direction_2

\$#	cid	xo	yo	zo	x1	y1	z1
	2 53.4000026	.5396E-15	2970.0		1000.0	0.0	4200.0

\$#	xp	yp	zp
	1000.0	0.0	3200.0

*DEFINE_CURVE

\$#	lcid	sidr	sfa	sfo	offa	offo	dattyp	lcint
	1	0	1.0	1.0	0.0	0.0	0	0
\$#		a1		o1				
		0.0		0.0				
		1.0		1.0				
		10.0		1.0				

*DEFINE_CURVE

\$#	lcid	sidr	sfa	sfo	offa	offo	dattyp	lcint
	2	0	1.0	1.0	0.0	0.0	0	0
\$#		a1		o1				
		2.0		0.0				
		2.00024414		0.46030399				
		2.00048828		0.835998				
		2.00073242		1.19890499				
		2.00097656		1.53562903				
		2.0012207		1.832165				
		2.00146484		2.0726819				
		2.00170898		2.24561095				
		2.00195313		2.30832791				
		2.00219727		2.26083398				
		2.00244141		2.128093				
		2.00268555		1.93994105				


```

    1230    1229         0         0         0         0         0         0
*SET_NODE_LIST
$#   sid     da1     da2     da3     da4  solver
     7     0.0     0.0     0.0     0.0MECH
$#   nid1    nid2    nid3    nid4    nid5    nid6    nid7    nid8
     236    690    724    755    721     0     0     0
*SET_PART_LIST
$#   sid     da1     da2     da3     da4  solver
     1     0.0     0.0     0.0     0.0MECH
$#   pid1    pid2    pid3    pid4    pid5    pid6    pid7    pid8
     1     2       0       0       0       0     0     0
*DAMPING_GLOBAL
$#   lcid    valdmp    stx     sty     stz     srx     sry     srz
     3     0.0     0.0     0.0     0.0     0.0     0.0     0.0
*DAMPING_PART_STIFFNESS
$#   pid     coef
     11.30000E-5
*ELEMENT_SHELL
$#   eid     pid     n1     n2     n3     n4     n5     n6     n7     n8
*ELEMENT_BEAM
$#   eid     pid     n1     n2     n3     rt1    rr1    rt2    rr2    local
     1117    2     246    1228    5     0     0     0     0     2
     1118    4     126    1227    5     0     0     0     0     2
*ELEMENT_MASS
$#   eid     nid     mass     pid
     1111    721    2.100000e-004    1
     1112    755    2.100000e-004    1
     1113    724    2.100000e-004    1
     1114    690    2.100000e-004    1
     1115    236    2.100000e-004    1
     1116    722    2.100000e-004    1
*NODE
$#   nid           x           y           z           tc           rc
*END

```

B.3 Cantilever PVC with dampers

LS-DYNA Keyword file created by LS-PrePost(R) V4.3 (Beta) - 27Jul2015(09:00)

Created on Dec-03-2015 (15:03:53)

*KEYWORD MEMORY=500000000 NCPU=1

*PARAMETER

##	prmr1	val1	prmr2	val2	prmr3	val3	prmr4	val4
R par_1	6							
R par_2	4							
R par_3	3000							
R par_4	4000							
R par_5	1							
R par_6	1							
R par_7	1							
R par_8	1							
R par_9	1							
R par_10	1							
R par_11	1							
R par_12	1							

*TITLE

##

title

LS-DYNA keyword deck by LS-PrePost

*CONTROL_IMPLICIT_DYNAMICS

##	imass	gamma	beta	tdybir	tdydtb	tdybur	irate
	1	0.5	0.25	0.01.00000E28	1.00000E28		0

*CONTROL_IMPLICIT_GENERAL

##	imflag	dt0	imform	nsbs	igs	cnstn	form	zero_v
	02.44100E-4		2	1	1	0	0	0

*CONTROL_TERMINATION

##	endtim	endcyc	dtmin	endeng	endmas
	9.0	0	0.0	0.01.000000E8	

*CONTROL_TIMESTEP

##	dtinit	tssf	isdo	tslimt	dt2ms	lctm	erode	ms1st
	0.00.89999998		0	0.0	0.0	0	0	0
##	dt2msf	dt2mslc	imscl	unused	unused	rmscl		
	0.0	0	0			0.0		

*DATABASE_NODOUT

##	dt	binary	lcur	ioopt	option1	option2
	2.44141E-4	1	0	1	0.0	0

*DATABASE_BINARY_D3PLOT

##	dt	lcdt	beam	npltc	psetid
	0.01	0	0	0	0

##	ioopt
	0

*DATABASE_HISTORY_NODE_SET

##	id1	id2	id3	id4	id5	id6	id7	id8
	7	0	0	0	0	0	0	0

*BOUNDARY_SPC_SET

##	nsid	cid	dofx	dofy	dofz	dofrx	dofry	dofrz
	1	0	1	1	1	1	1	1

*SET_NODE_LIST_TITLE

NODESET(SPC) 1

##	sid	da1	da2	da3	da4	solver
	1	0.0	0.0	0.0	0.0	0.0MECH

##	nid1	nid2	nid3	nid4	nid5	nid6	nid7	nid8
	1	3	4	5	6	7	8	9
	10	11	12	13	0	0	0	0

*BOUNDARY_SPC_SET

##	nsid	cid	dofx	dofy	dofz	dofrx	dofry	dofrz
	9	0	1	1	1	1	1	1

*SET_NODE_LIST

##	sid	da1	da2	da3	da4	solver
	9	0.0	0.0	0.0	0.0	0.0MECH

##	nid1	nid2	nid3	nid4	nid5	nid6	nid7	nid8
	1236	1235	1234	1233	0	0	0	0

*LOAD_NODE_POINT

##	nid	dof	lcid	sf	cid	m1	m2	m3
	246	1	1&par_1		0	0	0	0
	126	1	1&par_2		0	0	0	0
	722	2	2&par_5		0	0	0	0
	1197	1	2&par_6		0	0	0	0
	246	3	1&par_11		0	0	0	0
	126	3	1&par_12		0	0	0	0

*PART

##								title
----	--	--	--	--	--	--	--	-------

LSHELL1

##	pid	secid	mid	eosid	hgid	grav	adpopt	tmid
	1	1	4	0	0	0	0	0

*SECTION_SHELL_TITLE

PVC

##	secid	elform	shrf	nip	propt	qr/irid	icomp	setyp
	1	2	1.0	5	1.0	0	0	1
##	t1	t2	t3	t4	nloc	marea	idof	edgset
	3.2	3.2	3.2	3.2	0.0	0.0	0.0	0

*MAT_ELASTIC_TITLE

PVC_half_pipe

##	mid	ro	e	pr	da	db	not used
	41.39000E-9	par_4	0.40000001		0.0	0.0	0

*PART

##	title
	cable_right

cable_right

##	pid	secid	mid	eosid	hgid	grav	adpopt	tmid
	2	2	3	0	0	0	0	0

*SECTION_BEAM_TITLE

rubber

##	secid	elform	shrf	qr/irid	cst	scoor	nsm	
	2	6	1.0	2	0	0.0	0.0	
##	vol	iner	cid	ca	offset	rrcon	srcon	trcon
	100.0	0.0	0	20.0	0.0	0.0	0.0	0.0

*MAT_CABLE_DISCRETE_BEAM_TITLE

rubber_right

##	mid	ro	e	lcid	f0	tmaxf0	tramp	iread
	31.10000E-9		5.0	0	0.0	0.0	0.0	0

*PART

##	title
	half_pipe

half_pipe

##	pid	secid	mid	eosid	hgid	grav	adpopt	tmid
	3	1	1	0	0	0	0	0

*MAT_ELASTIC_TITLE

PVC

##	mid	ro	e	pr	da	db	not used
	11.39000E-9	par_3	0.40000001		0.0	0.0	0

*PART

##	title
	cable_left

cable_left

##	pid	secid	mid	eosid	hgid	grav	adpopt	tmid
	4	2	5	0	0	0	0	0

*MAT_CABLE_DISCRETE_BEAM_TITLE

rubber_left

\$#	mid	ro	e	lcid	f0	tmaxf0	tramp	iread
	51.10000E-9		5.0	0	0.0	0.0	0.0	0

*PART

\$#								title
								spring_x

spring_x

\$#	pid	secid	mid	eosid	hgid	grav	adpopt	tmid
	5	5	8	0	0	0	0	0

*SECTION_DISCRETE_TITLE

spring

\$#	secid	dro	kd	v0	cl	fd
	5	0	0.0	0.0	0.0	0.0

\$#	cdl	tdl
	0.0	0.0

*MAT_SPRING_ELASTIC_TITLE

spring__x

\$#	mid	k
	8	10.0

*PART

\$#								title
								spring_y

spring_y

\$#	pid	secid	mid	eosid	hgid	grav	adpopt	tmid
	6	5	9	0	0	0	0	0

*MAT_SPRING_ELASTIC_TITLE

Spring_y

\$#	mid	k
	9	5.0

*PART

\$#								title
								damping_x

damping_x

\$#	pid	secid	mid	eosid	hgid	grav	adpopt	tmid
	7	3	6	0	0	0	0	0

*SECTION_DISCRETE_TITLE

Damper_1

\$#	secid	dro	kd	v0	cl	fd
	3	0	0.0	0.0	0.0	0.0

\$#	cdl	tdl
	0.0	0.0

*MAT_DAMPER_VISCOUS_TITLE

Damper_x_1

```

$#      mid      dc
        6      &par_7

```

*PART

```

$#                                           title
Damping_y
$#      pid      secid      mid      eosid      hgid      grav      adpopt      tmid
        8         3         7         0         0         0         0         0

```

*MAT_DAMPER_VISCOUS_TITLE

Damper_y_1

```

$#      mid      dc
        7      &par_9

```

*SECTION_DISCRETE_TITLE

Damper_2

```

$#      secid      dro      kd      v0      cl      fd
        4         0      0.0      0.0      0.0      0.0

```

```

$#      cdl      tdl
        0.0      0.0

```

*MAT_ELASTIC_TITLE

rubber_not_used

```

$#      mid      ro      e      pr      da      db      not used
        21.10000E-9      500.00.49000001      0.0      0.0      0

```

*MAT_DAMPER_VISCOUS_TITLE

Damper_x_2

```

$#      mid      dc
        10      &par_8

```

*MAT_DAMPER_VISCOUS_TITLE

Damper_y_2

```

$#      mid      dc
        11      &par_10

```

*DEFINE_COORDINATE_SYSTEM_TITLE

cable_direction

```

$#      cid      xo      yo      zo      xl      yl      zl
        1-53.399685-0.1832911 2970.4487      -1000.0      0.0      4200.0

```

```

$#      xp      yp      zp
        -1000.0      0.0      3200.0

```

*DEFINE_COORDINATE_SYSTEM_TITLE

cable_direction_2

```

$#      cid      xo      yo      zo      xl      yl      zl
      2 53.4000026.5396E-15 2970.0 1000.0 0.0 4200.0
$#      xp      yp      zp
      1000.0 0.0 3200.0
*DEFINE_CURVE
$#      lcid      sidr      sfa      sfo      offa      offo      dattyp      lcint
      1          0          1.0      1.0      0.0      0.0          0          0
$#              a1              o1
              0.0              0.0
              1.0              1.0
              10.0             1.0
*DEFINE_CURVE
$#      lcid      sidr      sfa      sfo      offa      offo      dattyp      lcint
      2          0          1.0      1.0      0.0      0.0          0          0
$#              a1              o1
              2.0              0.0
      2.00024414          0.46030399
      2.00048828          0.835998
      2.00073242          1.19890499
      2.00097656          1.53562903
      2.0012207          1.832165
      2.00146484          2.0726819
      2.00170898          2.24561095
      2.00195313          2.30832791
      2.00219727          2.26083398
      2.00244141          2.128093
      2.00268555          1.93994105
      2.00292969          1.726825
      2.00317383          1.52345097
      2.00341797          1.32494795
      2.00366211          1.15323699
      2.00390625          0.98761499
      2.00415039          0.82747298
      2.00439453          0.65515298
      2.00463867          0.50962502
      2.00488281          0.37505701
      2.00512695          0.255712
      2.00537109          0.0
      2.00561523          0.0

```

```

                2.00585938                0.0
*DEFINE_CURVE_TITLE
damping
$#   lcid      sidr      sfa      sfo      offa      offo      dattyp      lcint
      3         0        1.0      1.0      0.0      0.0         0         0
$#
      a1         o1
      0.0        50.0
      2.0        50.0
      2.00001001      1.20000005
      10.0         1.20000005
*SET_NODE_LIST_TITLE
NODESET(SPC) 2
$#   sid      da1      da2      da3      da4      solver
      2        0.0      0.0      0.0      0.0MECH
$#   nid1     nid2     nid3     nid4     nid5     nid6     nid7     nid8
      1228    1227      0        0        0        0        0        0
*SET_NODE_LIST_TITLE
NODESET(SPC) 3
$#   sid      da1      da2      da3      da4      solver
      3        0.0      0.0      0.0      0.0MECH
$#   nid1     nid2     nid3     nid4     nid5     nid6     nid7     nid8
      1228    1227      0        0        0        0        0        0
*SET_NODE_LIST
$#   sid      da1      da2      da3      da4      solver
      4        0.0      0.0      0.0      0.0MECH
$#   nid1     nid2     nid3     nid4     nid5     nid6     nid7     nid8
      1228      0        0        0        0        0        0        0
*SET_NODE_LIST
$#   sid      da1      da2      da3      da4      solver
      5        0.0      0.0      0.0      0.0MECH
$#   nid1     nid2     nid3     nid4     nid5     nid6     nid7     nid8
      1227      0        0        0        0        0        0        0
*SET_NODE_LIST_TITLE
NODESET(SPC) 6
$#   sid      da1      da2      da3      da4      solver
      6        0.0      0.0      0.0      0.0MECH
$#   nid1     nid2     nid3     nid4     nid5     nid6     nid7     nid8
      1230    1229      0        0        0        0        0        0
*SET_NODE_LIST

```

```

$#   sid      da1      da2      da3      da4      solver
      7        0.0      0.0      0.0      0.0MECH
$#   nid1     nid2     nid3     nid4     nid5     nid6     nid7     nid8
      236      690      724      755      721      0        0        0
*SET_NODE_LIST
$#   sid      da1      da2      da3      da4      solver
      8        0.0      0.0      0.0      0.0MECH
$#   nid1     nid2     nid3     nid4     nid5     nid6     nid7     nid8
      1231     1232      0        0        0        0        0        0
*SET_PART_LIST
$#   sid      da1      da2      da3      da4      solver
      1        0.0      0.0      0.0      0.0MECH
$#   pid1     pid2     pid3     pid4     pid5     pid6     pid7     pid8
      1        2        0        0        0        0        0        0
*DAMPING_GLOBAL
$#   lcid     valdmp      stx      sty      stz      srx      sry      srz
      3        0.0      0.0      0.0      0.0      0.0      0.0      0.0
*DAMPING_PART_STIFFNESS
$#   pid      coef
      11.30000E-5
*ELEMENT_SHELL
$#   eid      pid      n1      n2      n3      n4      n5      n6      n7      n8

*ELEMENT_DISCRETE
$#   eid      pid      n1      n2      vid      s      pf      offset
      1121      7      246     1236      0      1.0     0      0.0
      1122      7      126     1233      0      1.0     0      0.0
      1123      8      126     1234      0      1.0     0      0.0
      1124      8      246     1235      0      1.0     0      0.0
*ELEMENT_MASS
$#   eid      nid      mass      pid
      1111      721     2.100000e-004      1
      1112      755     2.100000e-004      1
      1113      724     2.100000e-004      1
      1114      690     2.100000e-004      1
      1115      236     2.100000e-004      1
      1116      722     2.100000e-004      1
*NODE
$#   nid      x      y      z      tc      rc

```

*END

B.4 Pole

LS-DYNA Keyword file created by LS-PrePost(R) V4.3 (Beta) - 27Jul2015(09:00)

Created on Jan-07-2016 (18:12:26)

*KEYWORD MEMORY=500000000

*TITLE

title

LS-DYNA keyword deck by LS-PrePost

*CONTROL_IMPLICIT_GENERAL

##	imflag	dt0	imform	nsbs	igs	cnstn	form	zero_v
		02.44100E-4	2	1	2	0	0	0

*CONTROL_TERMINATION

##	endtim	endcyc	dtmin	endeng	endmas
	6.5	0	0.0	0.01.000000E8	

*DATABASE_NODOUT

##	dt	binary	lcur	ioopt	option1	option2
	2.44141E-4	0	0	1	0.0	0

*DATABASE_HISTORY_NODE_SET

##	id1	id2	id3	id4	id5	id6	id7	id8
	8	0	0	0	0	0	0	0

*BOUNDARY_SPC_SET

##	nsid	cid	dofx	dofy	dofz	dofrx	dofry	dofrz
	3	0	1	1	1	1	1	1

*SET_NODE_LIST

##	sid	da1	da2	da3	da4	solver
	3	0.0	0.0	0.0	0.0MECH	

##	nid1	nid2	nid3	nid4	nid5	nid6	nid7	nid8

*BOUNDARY_SPC_SET

##	nsid	cid	dofx	dofy	dofz	dofrx	dofry	dofrz
	7	0	1	1	1	1	1	1

*SET_NODE_LIST

##	sid	da1	da2	da3	da4	solver
	7	0.0	0.0	0.0	0.0MECH	

##	nid1	nid2	nid3	nid4	nid5	nid6	nid7	nid8
	8649	8648	0	0	0	0	0	0


```

$#      pid      secid      mid      eosid      hgid      grav      adpopt      tmid
      11         1         2         0         0         0         0         0
*SECTION_BEAM_TITLE
reinforcement
$#      secid      elform      shrf      qr/irid      cst      scoor      nsm
      1         3         1.0         5         0         0.0         0.0
$#      a         rampt      stress
      201.0         0.0         0.0
*MAT_ELASTIC_TITLE
Reinforcement
$#      mid      ro      e      pr      da      db      not used
      27.83000E-9  193000.00.30000001      0.0      0.0      0
*PART
$#                                          title
LSHELL52
$#      pid      secid      mid      eosid      hgid      grav      adpopt      tmid
      52         2         1         0         0         0         0         0
*SECTION_SHELL_TITLE
t_52
$#      secid      elform      shrf      nip      propt      qr/irid      icomp      setyp
      2         2         1.0         5         1.0         0         0         1
$#      t1      t2      t3      t4      nloc      marea      idof      edgset
      52.0      52.0      52.0      52.0      0.0      0.0      0.0      0
*MAT_ELASTIC_TITLE
Concrete
$#      mid      ro      e      pr      da      db      not used
      12.35000E-9  42240.0      0.2      0.0      0.0      0
*PART
$#                                          title
LSHELL53
$#      pid      secid      mid      eosid      hgid      grav      adpopt      tmid
      53         3         1         0         0         0         0         0
*SECTION_SHELL_TITLE
t_53
$#      secid      elform      shrf      nip      propt      qr/irid      icomp      setyp
      3         2         1.0         5         1.0         0         0         1
$#      t1      t2      t3      t4      nloc      marea      idof      edgset
      53.0      53.0      53.0      53.0      0.0      0.0      0.0      0
*PART

```

```

$#                                     title
LSHELL54
$#   pid   secid   mid   eosid   hgid   grav   adpopt   tmid
      54     4     1     0     0     0     0     0
*SECTION_SHELL_TITLE
t_54
$#   secid   elform   shrf   nip   propt   qr/irid   icompl   setyp
      4       2     1.0     5     1.0     0     0     1
$#   t1     t2     t3     t4   nloc   marea   idof   edgset
      54.0   54.0   54.0   54.0   0.0     0.0     0.0     0
*PART
$#                                     title
LSHELL55
$#   pid   secid   mid   eosid   hgid   grav   adpopt   tmid
      55     5     1     0     0     0     0     0
*SECTION_SHELL_TITLE
t_55
$#   secid   elform   shrf   nip   propt   qr/irid   icompl   setyp
      5       2     1.0     5     1.0     0     0     1
$#   t1     t2     t3     t4   nloc   marea   idof   edgset
      55.0   55.0   55.0   55.0   0.0     0.0     0.0     0
*PART
$#                                     title
LSHELL56
$#   pid   secid   mid   eosid   hgid   grav   adpopt   tmid
      56     6     1     0     0     0     0     0
*SECTION_SHELL_TITLE
t_56
$#   secid   elform   shrf   nip   propt   qr/irid   icompl   setyp
      6       2     1.0     5     1.0     0     0     1
$#   t1     t2     t3     t4   nloc   marea   idof   edgset
      56.0   56.0   56.0   56.0   0.0     0.0     0.0     0
*PART
$#                                     title
LSHELL57
$#   pid   secid   mid   eosid   hgid   grav   adpopt   tmid
      57     7     1     0     0     0     0     0
*SECTION_SHELL_TITLE
t_57

```



```

$#  secid  elform  shrf    nip    propt  qr/irid  icompl  setyp
      7      2      1.0     5      1.0     0        0        1
$#   t1     t2     t3     t4     nloc    marea    idof     edgset
      57.0   57.0   57.0   57.0    0.0     0.0     0.0     0
*PART
$#                                           title
LSHELL58
$#   pid    secid    mid    eosid    hgid    grav    adpopt    tmid
      58      8      1      0      0      0      0      0
*SECTION_SHELL_TITLE
t_58
$#  secid  elform  shrf    nip    propt  qr/irid  icompl  setyp
      8      2      1.0     5      1.0     0        0        1
$#   t1     t2     t3     t4     nloc    marea    idof     edgset
      58.0   58.0   58.0   58.0    0.0     0.0     0.0     0
*PART
$#                                           title
LSHELL59
$#   pid    secid    mid    eosid    hgid    grav    adpopt    tmid
      59      9      1      0      0      0      0      0
*SECTION_SHELL_TITLE
t_59
$#  secid  elform  shrf    nip    propt  qr/irid  icompl  setyp
      9      2      1.0     5      1.0     0        0        1
$#   t1     t2     t3     t4     nloc    marea    idof     edgset
      59.0   59.0   59.0   59.0    0.0     0.0     0.0     0
*PART
$#                                           title
LSHELL60
$#   pid    secid    mid    eosid    hgid    grav    adpopt    tmid
      60     10      1      0      0      0      0      0
*SECTION_SHELL_TITLE
t_60
$#  secid  elform  shrf    nip    propt  qr/irid  icompl  setyp
     10      2      1.0     5      1.0     0        0        1
$#   t1     t2     t3     t4     nloc    marea    idof     edgset
     60.0   60.0   60.0   60.0    0.0     0.0     0.0     0
*PART
$#                                           title

```

LSHELL61

\$#	pid	secid	mid	eosid	hgid	grav	adpopt	tmid
	61	11	1	0	0	0	0	0

*SECTION_SHELL_TITLE

t_61

\$#	secid	elform	shrf	nip	propt	qr/irid	icomp	setyp
	11	2	1.0	5	1.0	0	0	1

\$#	t1	t2	t3	t4	nloc	marea	idof	edgset
	61.0	61.0	61.0	61.0	0.0	0.0	0.0	0

*PART

\$#	title							
	damper_x							

damper_x

\$#	pid	secid	mid	eosid	hgid	grav	adpopt	tmid
	62	13	6	0	0	0	0	0

*SECTION_DISCRETE_TITLE

damper_x

\$#	secid	dro	kd	v0	cl	fd
	13	0	0.0	0.0	0.0	0.0

\$#	cdl	tdl
	0.0	0.0

*MAT_DAMPER_VISCOUS_TITLE

Damper_x

\$#	mid	dc
	6	2.0

*PART

\$#	title							
	damper_y							

damper_y

\$#	pid	secid	mid	eosid	hgid	grav	adpopt	tmid
	63	14	7	0	0	0	0	0

*SECTION_DISCRETE_TITLE

Damper_y

\$#	secid	dro	kd	v0	cl	fd
	14	0	0.0	0.0	0.0	0.0

\$#	cdl	tdl
	0.0	0.0

*MAT_DAMPER_VISCOUS_TITLE

Damper_y

\$#	mid	dc
	7	2.0

*MAT_CABLE_DISCRETE_BEAM_TITLE

cable

\$#	mid	ro	e	lcid	f0	tmaxf0	tramp	iread
	42.70000E-9	69000.0		0	0.0	0.0	0.0	0

*DEFINE_CURVE

\$#	lcid	sidr	sfa	sfo	offa	offo	dattyp	lcint
	1	0	1.0	1.0	0.0	0.0	0	0

\$#	a1	o1
	0.0	0.0
	1.0	1.0
	10.0	1.0

*DEFINE_CURVE_TITLE

damping

\$#	lcid	sidr	sfa	sfo	offa	offo	dattyp	lcint
	2	0	1.0	1.0	0.0	0.0	0	0

\$#	a1	o1
	0.0	20.0
	2.0	20.0
	2.00024414	2.47000003
	10.0	2.47000003

*DEFINE_CURVE_TITLE

impulse

\$#	lcid	sidr	sfa	sfo	offa	offo	dattyp	lcint
	3	0	1.0	1.0	0.0	0.0	0	0

\$#	a1	o1
	2.0	0.0
	2.00024414	0.46030399
	2.00048828	0.835998
	2.00073242	1.19890499
	2.00097656	1.53562903
	2.0012207	1.832165
	2.00146484	2.0726819
	2.00170898	2.24561095
	2.00195313	2.30832791
	2.00219727	2.26083398
	2.00244141	2.128093
	2.00268555	1.93994105
	2.00292969	1.726825
	2.00317383	1.52345097

2.00341797	1.32494795
2.00366211	1.15323699
2.00390625	0.98761499
2.00415039	0.82747298
2.00439453	0.65515298
2.00463867	0.50962502
2.00488281	0.37505701
2.00512695	0.255712
2.00537109	0.0
2.00561523	0.0
2.00585938	0.0

*SET_BEAM

\$# sid

1

\$#	k1	k2	k3	k4	k5	k6	k7	k8
-----	----	----	----	----	----	----	----	----

*SET_PART_LIST

\$#	sid	da1	da2	da3	da4	solver
-----	-----	-----	-----	-----	-----	--------

1	0.0	0.0	0.0	0.0	0.0	OMECH
---	-----	-----	-----	-----	-----	-------

\$#	pid1	pid2	pid3	pid4	pid5	pid6	pid7	pid8
-----	------	------	------	------	------	------	------	------

10	11	52	53	54	55	56	57
58	59	60	61	0	0	0	0

*SET_PART_LIST

\$#	sid	da1	da2	da3	da4	solver
-----	-----	-----	-----	-----	-----	--------

2	0.0	0.0	0.0	0.0	0.0	OMECH
---	-----	-----	-----	-----	-----	-------

\$#	pid1	pid2	pid3	pid4	pid5	pid6	pid7	pid8
-----	------	------	------	------	------	------	------	------

10	11	52	53	54	55	56	57
58	59	60	61	0	0	0	0

*SET_PART_LIST

\$#	sid	da1	da2	da3	da4	solver
-----	-----	-----	-----	-----	-----	--------

3	0.0	0.0	0.0	0.0	0.0	OMECH
---	-----	-----	-----	-----	-----	-------

\$#	pid1	pid2	pid3	pid4	pid5	pid6	pid7	pid8
-----	------	------	------	------	------	------	------	------

10	11	52	53	54	55	56	57
58	59	60	61	0	0	0	0

*DAMPING_GLOBAL

\$#	lcid	valdmp	stx	sty	stz	srx	sry	srz
-----	------	--------	-----	-----	-----	-----	-----	-----

2	0.0	0.0	0.0	0.0	0.0	0.0	0.0	0.0
---	-----	-----	-----	-----	-----	-----	-----	-----

*DAMPING_PART_STIFFNESS_SET

\$# psid coef

31.25000E-4

```
*ELEMENT_SHELL
```

```
$#  eid    pid    n1    n2    n3    n4    n5    n6    n7    n8
```

```
*ELEMENT_BEAM
```

```
$#  eid    pid    n1    n2    n3    rt1   rr1   rt2   rr2  local
```

```
*ELEMENT_DISCRETE
```

```
$#  eid    pid    n1    n2    vid    s    pf    offset
```

```
    8191    62    625    8648    0    1.0    0    0.0
```

```
    8192    63    625    8649    0    1.0    0    0.0
```

```
*NODE
```

```
$#  nid          x          y          z    tc    rc
```

```
*END
```

Appendix C

System identification

C.1 System identification by applying the Stochastic subspace identification (SSI) method using MACEC

Step 1: Open MACEC graphic user interface by typing macec in MATLAB

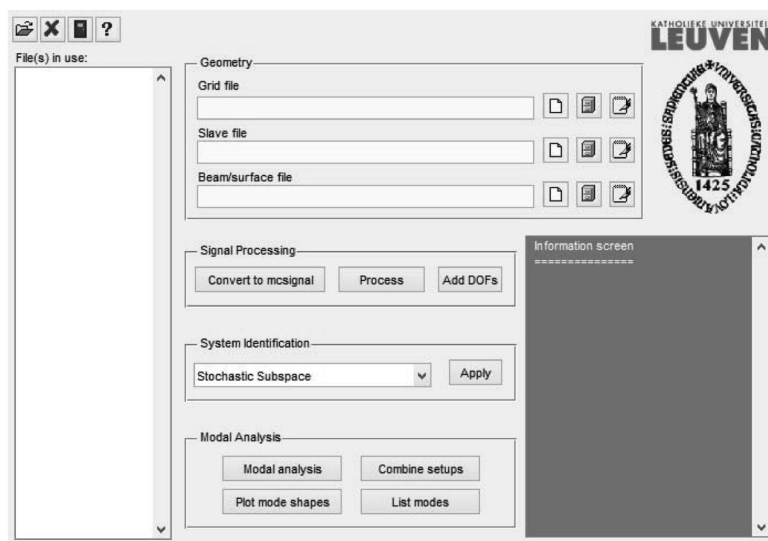


Figure C.1: Graphic user interface of MACEC

Step 2: Define the geometry of the measurement points as in table 6.1.

Step 3: Since no measurement at the base of the pole was acquired, the node 0 was assumed to be fixed and has null displacement. In MACEC this assumption can be fulfilled by defining a slave relationship between node 1 as a master node and node 0 as a slave node with null

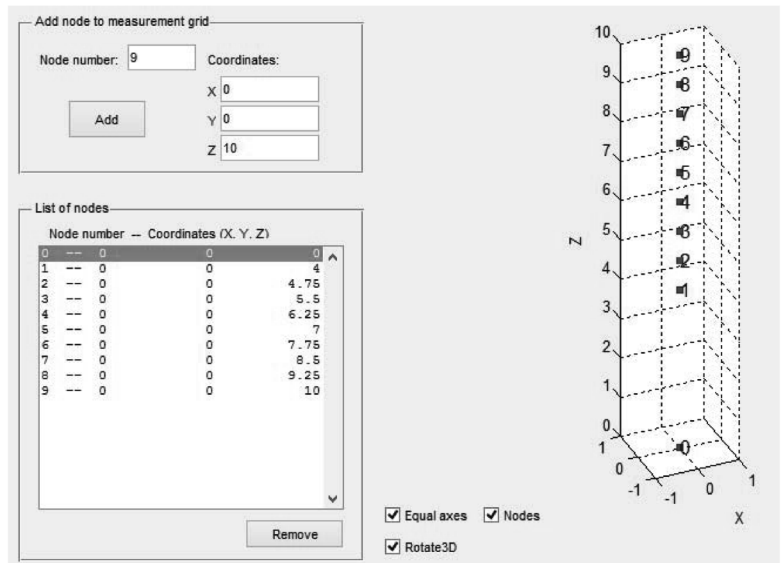


Figure C.2: Creating the grid file of the pole's geometry

amplitude for all DOF.

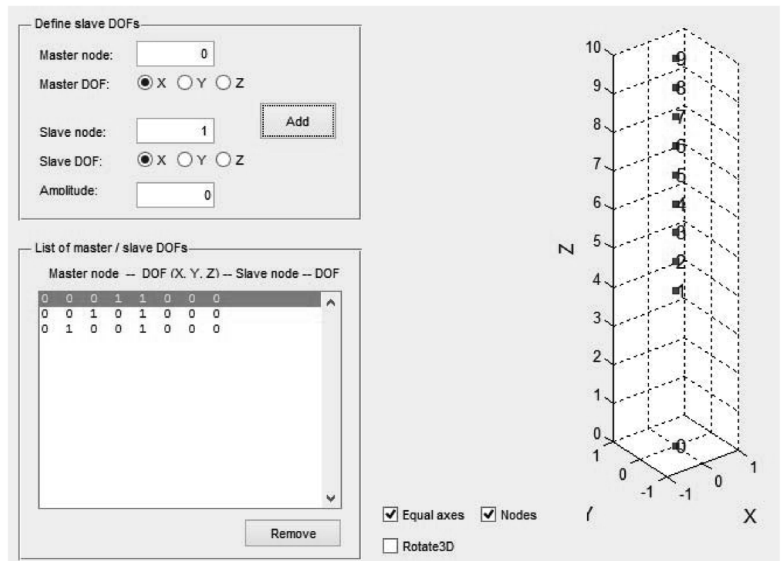


Figure C.3: Creating the slave file to fix the node 0 at z=0 m

Step 4: For mode plotting purpose, the node are connected together using beam elements.

Step 5: After loading the signal file which can be ASCII or MAT file type, that data should be converted to a MACEC signal. In this step, the frequency rate, units and type of the signals (acceleration) have to be defined. After converting the signal, the user is able to preview the signal of each channel and check its frequency content. Moreover, some basic processes can be applied to the signal, for example, removing the offset, deleting unwanted channels, etc.

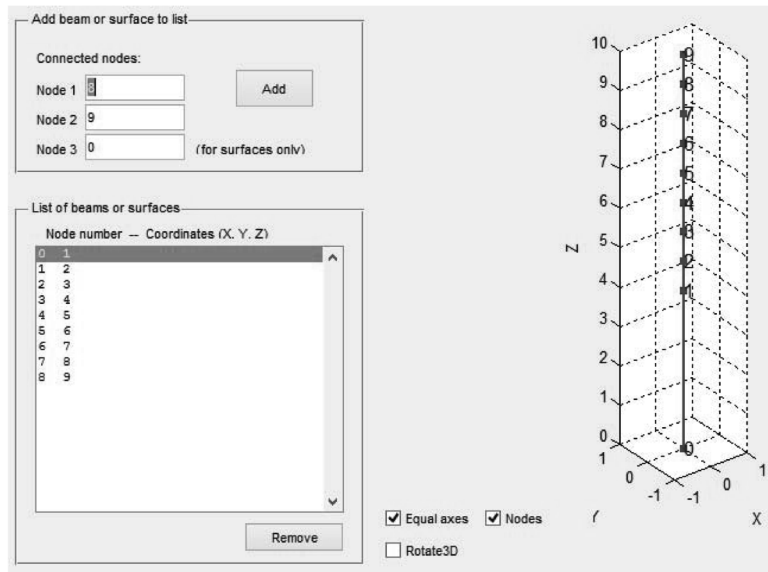


Figure C.4: Creating the beam file to link the measurement points

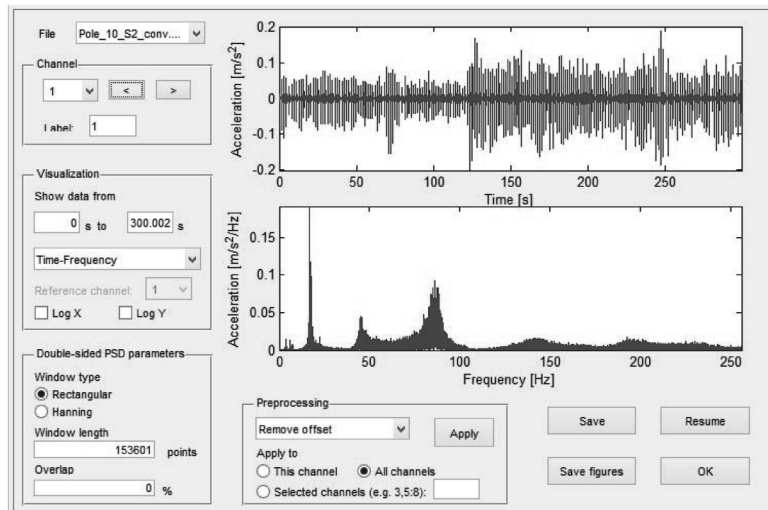


Figure C.5: Processing the acceleration signal

Step 6: Assign the channels of the measurement points to their relevant degrees of freedom defined before in the grid file the orientation of the sensor has been considered by defining the direction.

Step 7: Start system identification. MACEC provides several methods to determine the modal characteristics from the measurements. Since the input signal was not measured, the output-only methods have to be applied. In this work the Stochastic Subspace Identification method was applied. Two SSI methods can be applied: Reference-based data-driven stochastic subspace identification (SSI-data/ref) and Reference-based covariance-driven stochastic subspace identification (SSI-cov/ref). Both methods were tested here. The channel numbers 5 and 10 in both setups were given as references in x and y direction respectively. The expected system

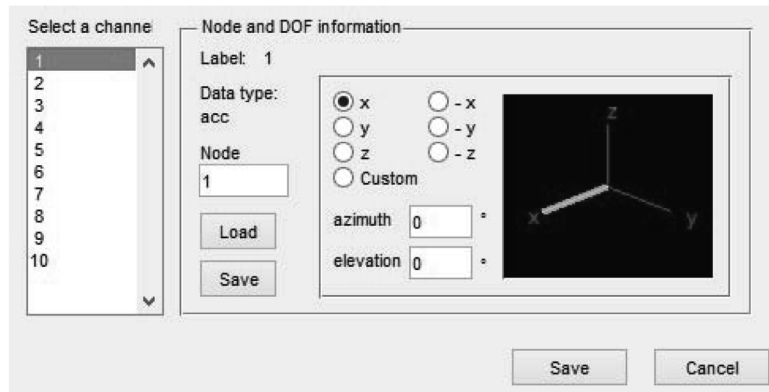


Figure C.6: Assigning the channels to their relevant degrees of freedom and directions

order, which should be two times the number of the expected modes, was given 40. After building the block Hankel matrix and calculating the QR decomposition and the Singular value decomposition (SVD), the real order of the system can be obtained by checking the nonzero peaks the singular value figure. The singular value figure shows the choosing the order equal to 150 should be enough to describe the system. After that the system matrices can be calculated. Choosing higher order can lead to many unphysical modes that should be eliminated manually in the next step. However, in order to separate the close modes, higher order may required. If SSI CD/ref method is applied, the number of the blocks to calculate the covariance is required. In this example, the number of the blocks was chosen 200 which is the given default value.

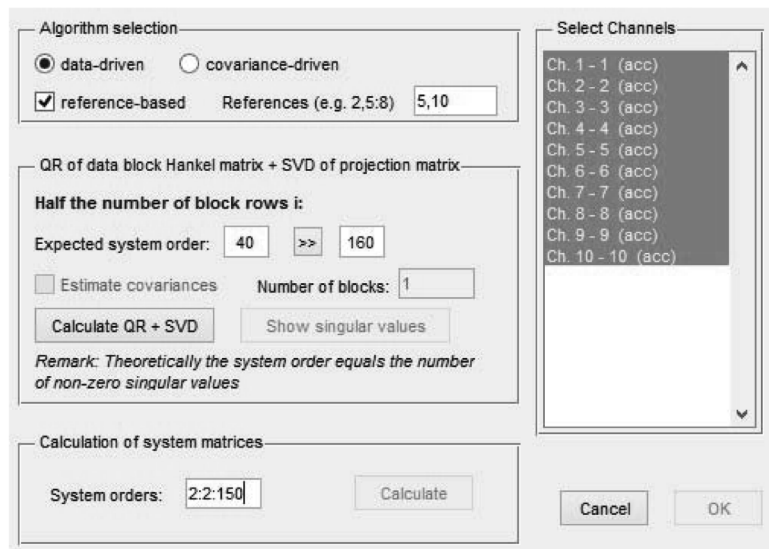


Figure C.7: Applying SSI methods

Step 8: Perform modal analysis to estimate the modal characteristics from the system matrices. The physical modes should be chosen from stabilization diagram. MACEC provides several useful parameters that help to validate the physical modes of the system. For example, the the modal phase collinearity (MPC), the Mean phase (MP) and Mean Phase Deviation (MPD).

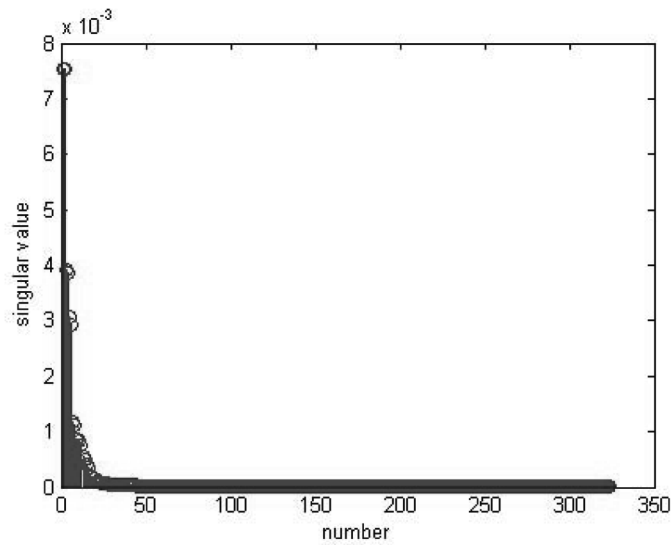


Figure C.8: Estimating the real order of the system by checking the singular value figure

Theoretically, if the mode is real, then MPC=1, MP=0 and MPD=0. However, some unphysical mode may satisfy these conditions. Therefore, checking the real and the imaginary part of the mode is necessary. In real modes, the the imaginary part is close to zero. It is important to mention that in each setup the same number of mode should be chosen to be coupled later.

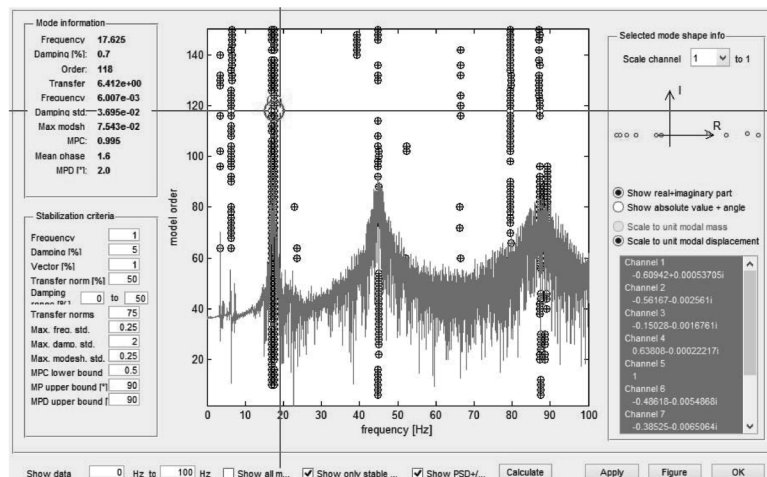


Figure C.9: Performing modal analysis

Step 9: combining the setup and plotting the mode shapes

Step 10: Listing the modes

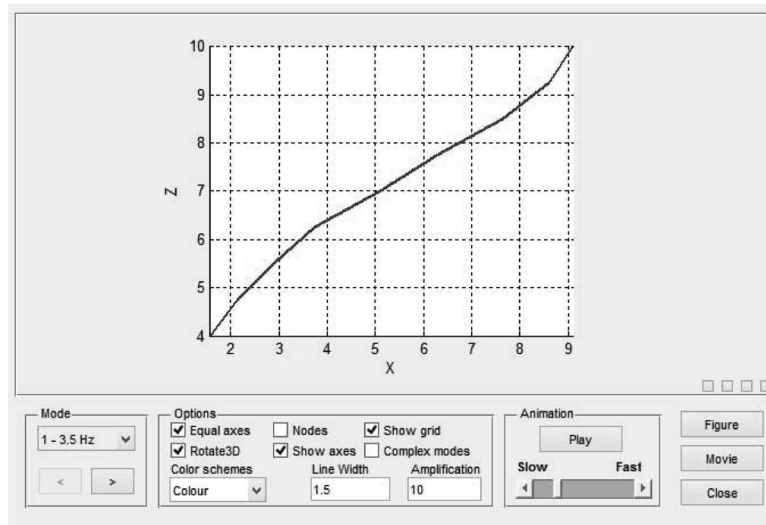


Figure C.10: Plotting mode shapes

Table C.1: The obtained frequencies and damping ratios from the experimental data applying SSI

Method/Setup	Mode	1	2	3	4	5	6	7	8
SSI DD/Ref S1	f [Hz]	3.47		16.85	17.61	44.69	44.91	87.21	88.27
	ζ %	0.40		1.66	0.89	3.12	2.79	3.95	4.10
SSI DD/Ref S2	f [Hz]	3.45		16.95	17.62	44.86	44.92	87.14	88.34
	ζ %	0.43		0.82	0.74	2.87	3.41	4.42	4.12
SSI CD/Ref S1	f [Hz]	3.47		16.89	17.61	44.73	44.80	87.13	88.33
	ζ %	0.30		1.45	0.88	3.06	3.54	4.36	4.01
SSI CD/Ref S2	f [Hz]	3.48		16.99	17.63	44.88	44.92	87.16	88.27
	ζ %	0.78		1.72	0.70	2.85	3.60	4.68	4.32
SSI DD	f [Hz]	3.46		16.90	17.62	44.78	44.91	87.18	88.31
	ζ %	0.41		1.24	0.81	3.00	3.10	4.19	4.11
SSI CD	f [Hz]	3.48		16.94	17.62	44.81	44.86	87.14	88.30
	ζ %	0.54		1.58	0.79	2.95	3.57	4.52	4.16